INVESTIGATING MECHANISMS OF FTLD-TDP PATHOGENESIS

A Dissertation

Presented to the Faculty of the Graduate School

of Cornell University

In Partial Fulfillment of the Requirements for the Degree of

Doctor of Philosophy

by

Owen Adam Brady

January 2014

INVESTIGATING MECHANISMS OF FTLD-TDP PATHOGENESIS

Owen Adam Brady, Ph.D.

Cornell University 2014

Frontotemporal lobar degeneration (FTLD) is a devastating dementia disorder that causes profound changes in personality, behavior, and language abilities. Major breakthroughs in the past decade have advanced the understanding of the molecular genetics and pathological mechanisms underlying this disease, in particular the most common subtype, FTLD-TDP. Several causative and risk modifying genes have been identified which implicate defects in protein degradation and RNA metabolism pathways. The work presented here can be split into two main projects. In the first, I examine the physical properties of TDP-43 aggregation, which is a hallmark of FTLD-TDP. Specifically, I characterize the role that phosphorylation plays in mediating the aggregation propensity of TDP-43 in a mammalian cell culture system. I further show that TDP-43 aggregates are cleared by the autophagy lysosome and ubiquitin proteasome systems, with the ubiquitin binding adaptor protein, p62/SQSTM1 facilitating this process. In the second project, I sought to characterize the recently identified FTLD-TDP risk factor, TMEM106B. Using cell culture model systems, I demonstrate that TMEM106B overexpression causes specific defects in lysosome size, morphology, and degradative capacity. I also ruled out the effect of a small coding variant associated with the TMEM106B risk allele when the proteins are highly expressed at the same level, indicating that increased TMEM106B levels are the likely cause of defects seen in certain cases of FTLD-TDP. I have also identified a putative

degradation pathway implicating lumenal lysosomal enzymes and a membrane bound intramembrane protease, SPPL2a, in the sequential proteolysis of TMEM106B. This pathway may represent a novel therapeutic target for controlling TMEM106B levels *in vivo*. Overall, my work has contributed significant findings to the field of FTLD-TDP related research and has increased the body of knowledge regarding the cellular and molecular mechanisms that contribute to this terrible disease.

BIOGRAPHICAL SKETCH

Owen Adam Brady was born on March 4, 1986 to parents Owen Edward Brady III and Barbara Schofield Brady. He grew up with his two older sisters Leah and Elizabeth in the bucolic northern New York town of Potsdam, where he enjoyed learning and playing outdoors.

While growing up, Adam attended summer science camps which marked the beginning of his interests in science and research. He attended Potsdam High School from 2000 to 2003 and the Clarkson School from 2003 to 2004. It was during these years that he solidified his desire to be a research scientist in biology. Starting in 2004, Adam attended the University of Delaware as a biology major and worked in the lab of Dr. Deni Galileo, where he studied glioma cell migration. He graduated in 2008 with a B.A. honors degree with distinction in in biology with a minor in biochemistry. While at UD, Adam met his future wife, Kellie Cox-Brady, whom he married while attending graduate school at Cornell University in the field of Biochemistry, Molecular, and Cell Biology. During his studies he worked in the lab of Dr. Fenghua Hu, studying aspects of neurodegeneration in the context of human disease. Adam greatly enjoyed his time at Cornell and in Ithaca and looks forward to his life's next steps in the D.C. area as a postdoc at the National Institutes of Health.

Dedicated to Kellie, Owen, Barbara, Leah, and Elizabeth

in memory of Helen Brady, Elizabeth Schofield, and Frank Rummel

ACKNOWLEDGEMENTS

I owe a great amount of thanks to the many people who made my success here at Cornell possible. First, I want to thank my advisor and mentor, Dr. Fenghua Hu. As her first graduate student, I had a unique experience playing a role in the establishment of a new lab. I thank her for challenging my abilities by teaching me the importance of asking the right scientific questions and how that should drive your approach to research. I also wish to thank my committee members Dr. Bill Brown and Dr. David Lin for their advice and guidance these past several years. Together, these people have helped me to grow tremendously as a scientist. Finally I wish to thank the rest of the PIs and support staff in the field of BMCB and the MBG department who have helped me in my research, especially the labs of Drs. Yuxin Mao, Marcus Smolka, Haiyuan Yu, and Tony Bretscher.

In my personal life, I owe a tremendous amount of credit to my wife, Kellie Cox-Brady. She has been my unwavering partner these last several years and given me the fortitude and confidence to pursue my goals here. She has been a constant in my life and I couldn't imagine having done this without her love and support. None of this would have been possible if it weren't for my parents who have unconditionally supported my academic goals and raised me to keep my mind open and fostered my love of learning. Thanks also go out to my sisters who have sent so much love and moral support to me. Finally, thanks to all of my many Cornell and Ithaca friends who have helped me keep my sense of humor all these years and made my time here such a pleasure.

TABLE OF CONTENTS

LIST OF FIGURES

LIST OF TABLES

CHAPTER 1

INTRODUCTION

1.1 Frontotemporal lobar degeneration

Frontotemporal lobar degeneration (FTLD) describes the neurodegenerative process that occurs in the prefrontal and anterior temporal cortex of the human brain, which causes a class of dementia disorders known as frontotemporal dementia (FTD)(1). Despite similar patterns of neurodegeneration, the molecular and genetic basis of FTLD is diverse. Furthermore, FTLD is commonly co-morbid with amyotrophic lateral sclerosis (ALS), which is characterized by degeneration of upper and lower motor neurons (2,3). Nevertheless, recent progress in the field has led to a new level of understanding of these complex disorders and common pathways that are disrupted in them have become evident. This chapter will provide an overview of the current knowledge regarding FTLD and its associated pathology.

1.1.1 Epidemiology

FTLD is the third leading cause of all dementia cases after Alzheimer's disease and vascular dementia and the second leading cause of presenile dementia, defined as cases with an age of onset earlier than 65 years (4,5). FTLD accounts for ~5-10% of all dementia cases (6). Estimates of FTLD prevalence based on multiple population based studies are approximately 10-20 per 100,000 with an incidence between 3.5-4.1 per 100,000 person-years in the 45-64 year age group (5,7-9). At least 50% of FTLD

cases are sporadic, meaning there is no family history, however FTLD is familial in approximately 35-50% of cases, which are usually inherited in an autosomal dominant pattern (10). FTLD is incurable and has a median disease duration of 6-8 years (11-13).

1.1.2 Clinical subtypes and symptoms

Generally, FTLD is characterized by profound changes in personality and social behavior and is frequently associated with deficits in interpreting and producing language. Clinically, it is divided into three subtypes: behavioral variant FTD (bvFTD), semantic dementia (SD), and progressive non-fluent aphasia (PNFA). Subtypes are defined by the predominant early symptoms; however, as the disease progresses there is often significant overlap in symptomology correlated with increased neurodegeneration in the affected brain regions (reviewed in (14,15)).

bvFTD is the most common subtype, accounting for approximately two thirds of FTLD diagnoses (16). bvFTD manifests with drastic changes in personality and anti-social behavior with impairments in executive function, blunting of emotional affect, loss of insight, and loss of empathy. It is also associated with changes in food preference and inability to control appetite as well the development of stereotyped and ritualized behaviors (17,18).

The other two subtypes of FTLD, SD and PNFA, primarily affect language abilities. SD is characterized by anomia, which consists of the loss of the ability to recall words and names. This is due to defects in conceptualizing categories including objects and faces. Less common words are not understood and the ability to associate

specific words with pictures or concepts is lost. Patients may repeat phrases and words without being aware of their meaning. Grammatical rules, non-verbal problem solving, and memory are frequently spared in SD during the early course of the disease (19,20). In cases of PNFA, by comparison, word meanings and object recognition abilities are relatively intact; however, patients have impairments in motor speech fluency and grammatical construction. Phonological aspects of language are affected, with patients exhibiting difficulty in producing the right sounds and ordering of words in spoken language (21,22).

1.2 Molecular pathology and genetics

The last decade has seen incredible progress in the understanding of the molecular pathology and genetic causes of FTLD. Current models of pathophysiology recognize four principle subtypes, defined by the predominant proteinacious inclusions observed in the brains of affected patients. Generally speaking, each subtype has specific known causal mutations which result in the observed phenotype; however, new genetic causes and risk modifying genes continue to be identified. (23), (reviewed in (15,24)). Table 1.1 provides a list of the current known causes and risk factors for various classes of FTLD and the major molecular pathology present in each case.

1.2.1 FTLD-Tau

The first type of FTLD to have a causative mutation linked to it was FTLD-Tau, characterized by inclusions of the microtubule associated protein tau encoded by

Table 1.1 Known genetic causes and risk factors for FTLD

Gene	Protein	Pathological subtype	Clinical phenotype	Protein functions	Locus
TARDBP	TDP-43	TDP-43	ALS[1]	mRNA Splicing and transcription, mRNA transport and stabilization, miRNA biogenesis, stress granule formation	1p36
MAPT	Microtubule associated protein Tau	Tau	FTD	Stability of axonal microtubules	17q21
Grn	Progranulin	TDP-43	FTD	Growth factor, pro/anti-inflammatory, cell migration, lysosomal functions?	17q21
Ubqln2	Ubiquilin 2	TDP-43	ALS, ALS-FTD, FTD[2]	Protein degradation (adaptor for UPS, autophagy)	Xp11
VCP	p97/Valosin-containing protein	TDP-43	IBMPFD (FTD), ALS	Protein degradation (adaptor for ERAD, UPS, and autophagy), membrane fusion	9p13
C9orf72	Chr.9 Open reading frame 72	TDP-43, UPS	ALS, FTD-ALS, FTD	unknown, related to DENN proteins	9p21
TMEM106B	TMEM106B	TDP-43	FTD, ALS[3]	Lysosomal membrane protein, lysosome morphology, function	7p21
CHM2B	Charged multivesicular body protein 2b	UPS	FTLD, ALS[4]	component of ESCRTIII complex, MVB biogenesis and autophagy-lysosome degradation	3p11
FUS	FUS/TLS	FUS	ALS, FTD-ALS, FTD	Splicing and transcription, DNA repair, maintenance of genome integrity	16p11
SQSTM1	p62/Sequesto-some1	TDP-43	FTD, FTD-ALS	Protein degradation (adaptor for UPS, autophagy), scaffold for NF-kB signaling	5q35
hnRNPA1	Heterogeneous nuclear ribonucleoprotein A1	TDP-43	IBMPFD (FTD), ALS	packing and transport of mRNA, interaction with splicing machinery	12q13
hnRNPA2/ B1	Heterogeneous nuclear ribonucleoprotein A2/B1	TDP-43	IBMPFD (FTD), ALS	packing and transport of mRNA, interaction with splicing machinery	7p15

Table adapted from ref.31.
[1] Mutations present in rare cases of FTLD
[2] Mainly associated with ALS, mutations in different protein region linked to FTLD
[3] Risk modifier for FTLD with Grn mutations, associated with cognitive impairment in ALS
[4] Mainly associated with FTLD

the gene *MAPT*. Approximately 45% of all FTLD cases belong to this molecular subtype (24). In 1998, mutations in *MAPT* were identified to cause FTLD-Tau (25). To date, over two dozen mutations in the *MAPT* gene have been identified, with most of them mapping to the C-terminal portion of tau, interfering with microtubule assembly and regulatory activity of the protein (26). Genetic variants in the tau kinase GSK-3β may also be associated with FTLD-Tau (27).

1.2.2 FTLD-TDP

Along with FTLD-Tau, the other major molecular subtype of FTLD, and the focus of this dissertation, is FTLD-TDP. Accounting for ~45% of all FTLD cases, FTLD-TDP is characterized by pathological inclusions of the multifunctional RNA binding protein, TDP-43 (24). Prior to the discovery of TDP-43 in FTLD, all non-tauopathy cases of FTLD were referred to as FTLD-U due to characteristic ubiquitinated protein inclusions seen in post-mortem patient brains (23). TDP-43 was identified in 2006 as the major ubiquitinated protein present in the inclusions of FTLD-U and ALS patients by two groups simultaneously (28,29).

In FTLD-TDP brains, TDP-43 is truncated from a 43 kDa protein into C-terminal fragments of ~35 and ~25 kDa. TDP-43 pathological inclusions are also extensively ubiquitinated, hyper-phosphorylated, and redistributed from the nucleus to the cytoplasm, although nuclear aggregation is also observed in many cases (23,30)(reviewed in (31)). While TDP-43 is the major pathological protein in FTLD-TDP brains, it is also present in the inclusions of many other neurodegenerative disorders, most prominently in ALS, in which it is present in ~97% of cases, both

hereditary and sporadic. The remaining 3% of ALS cases contain FUS or SOD1 inclusions and are generally negative for TDP-43 (32). Further, TDP-43 inclusions have been reported in post-mortem brains from patients with Alzheimer's disease, Huntington's disease, spinal cerebellar ataxia 3, and even some cases of FTLD-Tau (33-37). While, mutations in the gene for TDP-43, *TARDBP*, are known to be causative for a fraction of FTLD and many ALS cases, the fact that TDP-43 inclusions are observed in so many neurodegenerative diseases raises the possibility that TDP-43 inclusions may also be a consequence of, in addition to a cause of neurodegeneration and this idea is a matter of considerable debate. Proper regulation of TDP-43 levels appears to be critical as TDP-43 overexpression animal models in *C. elegans*, *Drosophila*, and mice exhibit neurodegenerative phenotypes (38-40). Conversely, too little TDP-43 may drive a toxic loss of function phenotype, as TDP-43 knockout mice are embryonic lethal (41,42).

TDP-43 is a 414 amino acid protein localized primarily to the nucleus, but with known roles both in the nucleus and in the cytoplasm. Major features include a bipartite nuclear localization signal (NLS) from amino acids 82-98, dual RNA recognition motifs (RRMs), which bind both UG rich RNA and TG rich DNA sequences. A nuclear export signal (NES) is located within the second RRM domain. Finally, the C-terminal region from amino acids 274 to 414 remains relatively unstructured and likely mediates various protein-protein interactions necessary for proper protein function. The C-terminal domain (CTD) also contains a small glutamine and asparagine (Q/N) rich prion-like domain which may account for the aggregation prone properties of TDP-43. The entire CTD is also very glycine rich and

intrinsically unstructured, further accounting for its aggregation prone properties. The vast majority of pathogenic mutations in TDP-43 occur in this CTD (reviewed in (31)). These features and their major functional roles are laid out in a schematic of the TDP-43 protein in Figure 1.1.

1.2.2.1 Physiological roles of TDP-43

TDP-43 has extensive known functions involved in RNA transcription, splicing, processing, transport, and metabolism. First discovered as a DNA binding protein to the transactive response (TAR) DNA of chromosomally integrated HIV-1, TDP-43 was shown to act as a transcriptional repressor (43). Its DNA binding and transcriptional repression activity has since been demonstrated for an endogenous human gene as well (44). One of the best characterized functions of TDP-43 is regulation of RNA splicing, dependent on the preferential binding of its RRM motifs to UG repeats in single stranded RNA. TDP-43 has been shown to specifically enhance or suppress splicing in a large number of transcripts. TDP-43 dependent exon skipping activity has been reported for cystic fibrosis transmembrane conductance regulator exon 9, apolipoprotein AII exon 3, eukaryotic translation termination factor 1, and retinoid x receptor gamma (45-47). Conversely, TDP-43 enhances splicing of other transcripts including BRCA1 and the polymerase delta interacting protein/S6 kinase 1 Aly/REF-like target (47,48). In total, TDP-43 is estimated to regulate the splicing of over 950 transcripts. TDP-43 also has an autoregulatory splicing role. One of the over 1,000 3'UTR binding targets of TDP-43 is its own transcript. When levels of TDP-43 are too high, it catalyzes a splicing event leading to the selection of an

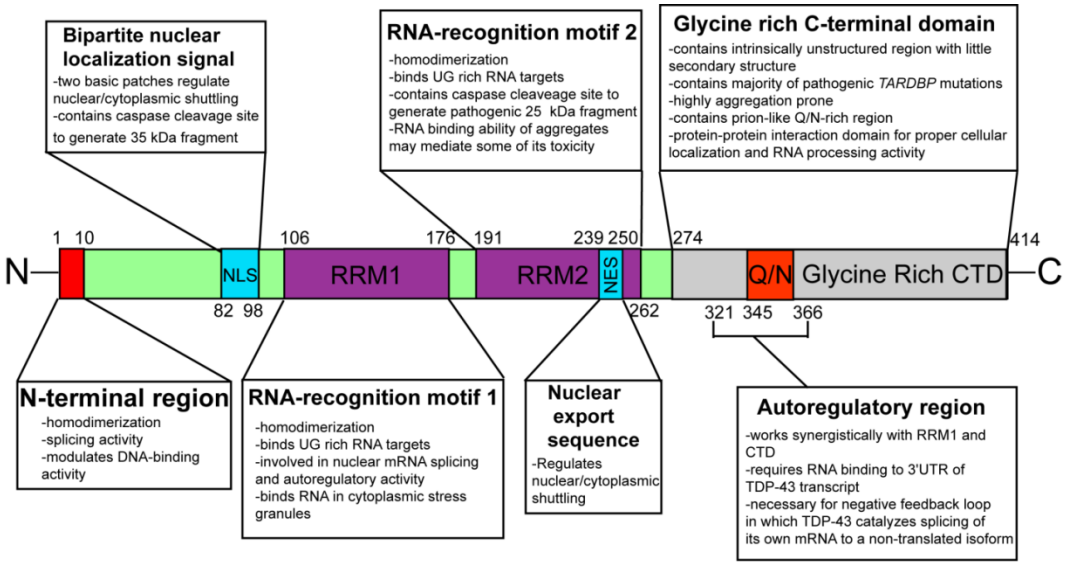

Figure 1.1: Schematic of TDP-43 domain structure, adapted from ref. 31. TDP-43 contains an N-terminal region required for many of its cellular functions. TDP-43 contains an NLS and NES essential for its functions in shuttling RNA species in and out of the nucleus. Loss of the NLS when TDP-43 is cleaved promotes cytosolic aggregation. RRM1 and RRM2 are essential for TDP-43's many regulatory roles governing RNA metabolism and transport and may be important in mediating TDP-43 toxicity in disease states. The C-terminal domain is intrinsically unstructured and contains a Q/N rich prion-like domain. These regions mediate TDP-43 aggregation into stress granules and toxic aggregates during disease pathogenesis. These regions are also important for TDP-43 functions and mediate numerous protein-protein interactions. Abbreviations: NLS, nuclear localization signal; NES, nuclear export signal; RRM, RNA recognition motif, Q/N, Glutamine/asparagine; UTR, untranslated region.

alternative, cryptic polyadenylation site. This has been proposed to result in less TDP-43 through the introduction of a premature stop codon resulting in non-sense mediated decay and/or nuclear retention of the TDP-43 transcript (49,50).

In addition to its splicing regulatory role, TDP-43 has been shown to bind the introns and 3'UTRs of numerous transcripts without affecting their splicing patterns. Recent, genome-wide studies of TDP-43 depleted mice performed by Polymenidou and colleagues demonstrated that TDP-43 binds to close to one third of the entire transcriptome, including over 6,000 brain enriched RNA targets (49). It is thought that this action may be essential for the long term stability of many of these transcripts, particularly those with introns >100kb, many of which are highly enriched in the brain.

TDP-43 has roles in binding other non mRNA targets in the nucleus as well. It has been demonstrated to bind to a variety of regulatory RNAs known as long non-coding RNAs (lncRNA), which are >200bp and may account for up to a fifth of the human genome (51). Two of these lncRNA TDP-43 targets include metastasis-associated lung adenocarcinoma transcript 1 (MALAT1) and nuclear-enriched autosomal transcript 1 (NEAT1) implicating potential roles in chromatin remodeling and cell-cycle progression (52). TDP-43 may also have roles in micro RNA (miRNA) biogenesis, as certain miRNAs have been reported by Burratti and colleagues, to be differentially up or down-regulated in response to reduced TDP-43 levels (53). Further, TDP-43 has been reported to bind both the Drosha microprocessor and Dicer complexes required for miRNA processing and maturation and these associations are dependent on its RRM domains and C-terminal tail (54-56) .

TDP-43 has both a nuclear localization and nuclear export signal. While the vast majority of TDP-43 resides in the nucleus at steady state, it can also dynamically shuttle various RNA targets between the nucleus and cytoplasm through its RRM domains (57). TDP-43 associates and traffics with various RNA containing granules in the cytosol such as P-bodies which contain RNA degradation machinery, stress granules which can sequester RNAs in times of cellular stress through interaction with aggregates of the prion like protein TIA-1, and transporting RNP granules which may facilitate proper localized translation of mRNA targets, for example at the synapse (58,59). A summary of TDP-43's many annotated roles is summarized in Figure 1.2.

1.2.2.2 Genetics of FTLD-TDP

The genetic causes of FTLD-TDP are varied and relatively complex compared to the other molecular classes of FTLD with more than a half dozen genes implicated as direct causes of or risk modifiers for disease progression. Mutations identified in 2004 in the gene encoding valosin containing protein (VCP) were found to result in a rare multisystem form of FTLD, known as inclusion body myopathy with Paget disease of bone and frontotemporal dementia (IBMPFD), which was later shown to contain TDP-43 inclusions (60,61). VCP is a member of the AAA ATPase family with many functional roles involved in ubiquitin dependent protein degradation through multiple pathways including endoplasmic reticulum associated degradation (ERAD), the ubiquitin proteasome system (UPS), and the autophagy-lysosome pathway (62). Further roles include mediating vesicle trafficking and homotypic membrane fusion events, mitotic events, and maintenance of genome stability (63,64).

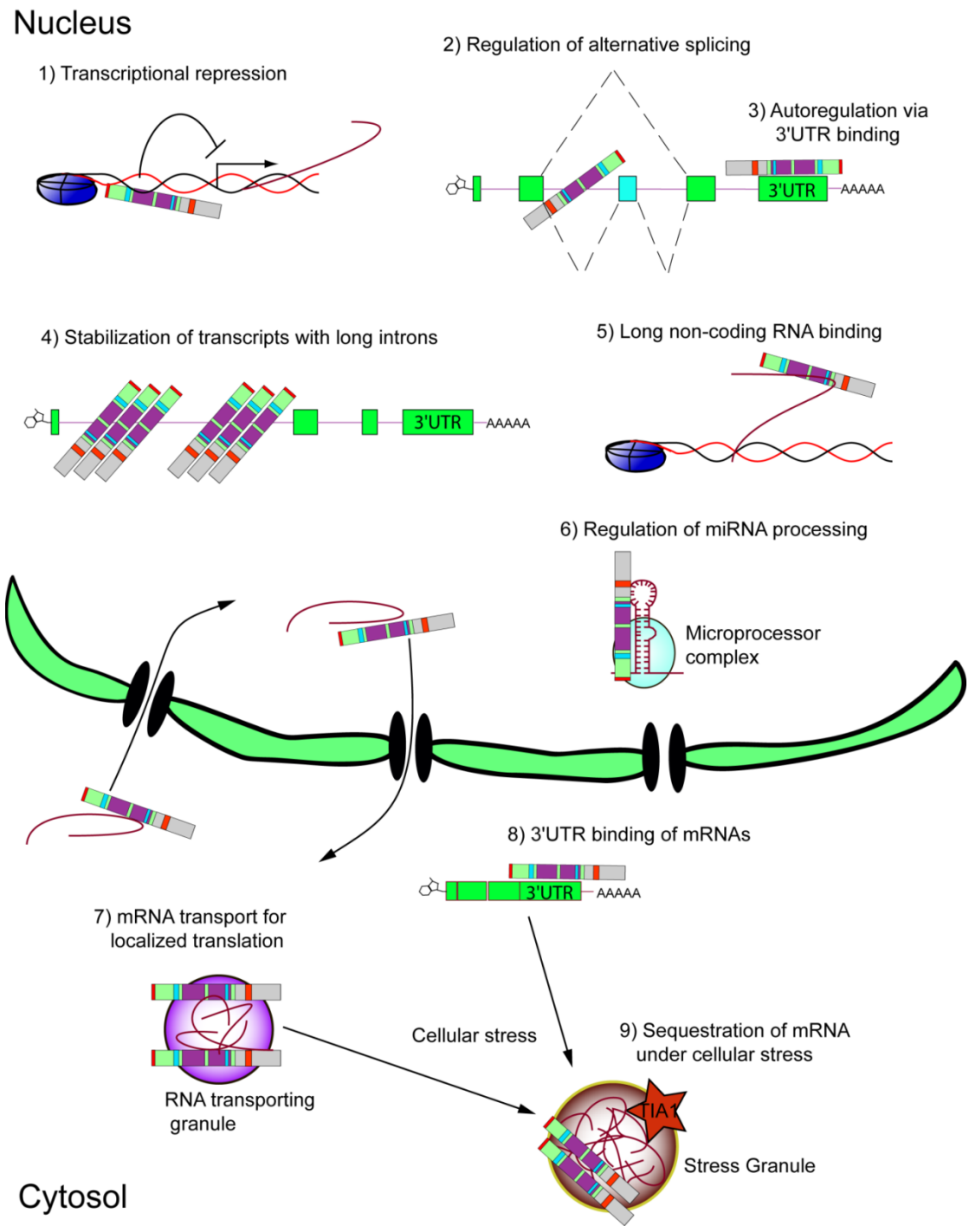
Nucleus
1) Transcriptional repression
2) Regulation of alternative splicing
3) Autoregulation via 3'UTR binding
3'UTR
AAAAA
4) Stabilization of transcripts with long introns
3'UTR
AAAAA
5) Long non-coding RNA binding
6) Regulation of miRNA processing
Microprocessor complex
8) 3'UTR binding of mRNAs
3'UTR
AAAAA
7) mRNA transport for localized translation
RNA transporting granule
Cellular stress
9) Sequestration of mRNA under cellular stress
TIA1
Stress Granule
Cytosol

Figure 1.2: Physiological functions of TDP-43, adapted from ref. 24. In the nucleus, evidence exists for TDP-43 binding single stranded DNA and regulating transcription (1) regulation of numerous mRNA alternative splicing events (2). TDP-43 controls the levels of numerous mRNAs, including its own transcript, through an autoregulatory mechanism in the 3'UTR (3). TDP-43 stabilizes mRNA species with long introns, which are highly enriched in the nervous system (4). TDP-43 is associated with several species of lncRNA (5) and is implicated in miRNA processing events (6). Cytosolic functions of TDP-43 include transport of mRNA for localized translation (7), particularly at synapses, 3' UTR binding of mature RNA (8), which may stabilize some transcripts and mediate sequestration into stress granules (9). Abbreviations: lncRNA, long non-coding RNA; miRNA, microRNA

Perhaps the most commonly mutated gene that causes a clinically "pure" FTLD-TDP phenotype is *GRN*, which encodes the multifunctional secreted growth factor progranulin (PGRN). This major finding was simultaneously reported by two independent research groups in 2006 (65,66). *GRN* mutations are responsible for an estimated 5-10% of total FTLD cases, 20% of familial FTLD cases, and 20% of familial and sporadic FTLD-TDP cases (67,68). The vast majority of disease causing *GRN* mutations result in premature stop codons, resulting in nonsense mediated decay of PGRN mRNA, however other causative mutations include certain missense mutations, splice site mutations, and mutations in the signal sequence resulting in impaired secretion (69-71). The net result of all of these mutations is reduced levels of active PGRN, resulting in an autosomal dominantly inherited haploinsufficiency.

The mechanism by which PGRN haploinsufficiency causes FTLD-TDP is poorly understood, but it has been suggested that loss of PGRN results in caspase dependent TDP-43 cleavage into the pathogenic 35 and 25 kDa fragments (30,72). PGRN is secreted as a pro-protein consisting of seven and a half granulin motifs, each of which contain a characteristic pattern of 12 disulfide bonded cysteine residues (73). Additionally, PGRN can be cleaved by multiple proteases including, elastase, proteinase-3, MMP-14, and ADAMTS-7, to yield individual granulin motifs each of which may be functionally distinct (73-77). PGRN cleavage can also be inhibited by the secretory leukocyte protease inhibitor (SLPI) and full length PGRN has been shown to be endocytosed into neurons by the trafficking receptor sortilin where it is targeted to lysosomes (74,78,79). Progranulin is secreted in large amounts in response to injury by immune cells such as microglia, suggesting that it may act on neurons in a

cell non-autonomous manner, although neurons do produce some PGRN as well (80,81). Individual granulins have been shown to mediate inflammatory events while full length PGRN has been shown to exert anti-inflammatory activity, potentially through antagonizing TNFR1 and TNFR2, although this latter point remains controversial (73,82,83). Finally, PGRN promotes cellular migration and acts as a survival signal by activating the AKT and ERK1/2 signaling pathways through an unknown mechanism (84,85).

Patients with FTLD-TDP caused by PGRN mutations may have vastly different clinical outcomes, even when presented with identical mutations, suggesting that other genes or environmental effects may be affecting disease progress (86). A genome wide association study (GWAS) by Van Deerlin and colleagues, published in 2010, identified single nucleotide polymorphisms in the *TMEM106B* gene as a risk factor for FTLD-TDP (87). These results were later replicated in further GWASs with different cohorts which showed that the major allele of TMEM106B is associated with worse outcome in patients with *GRN* mutations (88-91). In particular, the risk allele of TMEM106B was associated with a mean decrease in the age of onset of FTLD by 13 years. Additionally, the TMEM106B risk allele was associated with cognitive impairment in ALS patients and was also shown to be a risk factor for Alzheimer's disease (92-94). TMEM106B is a type II single pass transmembrane protein of unknown function (95). The TMEM106B risk allele may correlate with increased expression in patients, either through enhanced mRNA stability, differential response to a specific miRNA, through slower degradation kinetics due to a variant in a consensus glycosylation site, or some combination of these mechanisms (87,96,97).

There appears to be a correlation with decreased serum PGRN and mRNA levels in patients with the TMEM106B risk allele and increased expression of TMEM106B in cell culture models appears to raise the levels of intracellular PGRN (88,96,98). The relationship between *GRN* mutation status and TMEM106B mRNA levels remains controversial with some groups claiming TMEM106B mRNA is elevated while others say only the protein levels are affected and will be a matter of ongoing investigation.

1.2.3 FTLD-FUS

The second class of FTLD-U to be identified was FTLD-FUS, so named for the inclusions of the Fused in sarcoma protein (FUS). Mutations in FUS were co-discovered in 2009 as a cause of both FTLD and ALS and account for approximately 9% of total FTLD cases and less than 1% of total (5% of familial) ALS cases (24,99,100). Like TDP-43, FUS is an RNA binding protein with an aggregation prone, prion-like domain. It is involved in many of the same ontological cellular processes as TDP-43, including stabilization of long intron containing transcripts, binding of lncRNA, biogenesis of miRNA, transcriptional inhibition, mRNA transport, and stress granule formation. Additionally, FUS has roles associated with the general transcription machinery and in maintaining genome stability (24,101). Despite these similarities, there is little overlap in the RNA targets recognized by TDP-43 and FUS, suggesting that they play disparate roles within the cell (49,52,102).

1.2.4 FTLD-UPS

The final distinct molecular subtype of FTLD, is referred to as FTLD-UPS due to the presence of ubiquitinated inclusions. A single predominant pathological protein has yet to be identified for this subtype, if one exists (23). FTLD-UPS accounts for ~1% of all FTLD cases and is associated with familial mutations, best characterized by a Danish pedigree (24,103). FTLD-UPS is caused by mutations in the charged multivesicular body protein 2B (CHMP2B), a component of the endosomal sorting complex required for transport (ESCRT)-III complex. The ESCRT-III complex is a large multiprotein complex that serves to concentrate ubiquitinated cargoes for packaging into the intralumenal vesicles (ILVs) of late endosomes, also referred to as multivesicular bodies (MVBs), prior to fusion with lysosomes. The ESCRT-III complex also plays a role in recruiting deubiquitinating enzymes (DUBs) that remove ubiquitin moieties from cargo destined for degradation. Finally, the ESCRT-III complex recruits the AAA ATPase VPS4/Skd1, which disassembles the complex (reviewed in (104,105)).

1.2.5 FTLD is part of a clinico-pathological disease spectrum with ALS

There is significant overlap in terms of molecular pathology, disease mechanisms, and clinical presentation between patients with FTLD and ALS, particularly in those cases characterized by TDP-43 inclusions (reviewed in (15,24)). As many as 50% of FTLD and ALS patients share some symptoms of both diseases, while up to 15% of affected patients can be said to meet the clinical criteria of both diseases, hereafter referred to as FTLD-ALS (106-109). Hence, it is increasingly

recognized that FTLD and ALS may represent opposing sides of a disease spectrum. Nevertheless, different mutations in different genes have different propensities for causing either FTLD or ALS, with some causing clinically "pure" phenotypes, while others tend to have more mixed pathology. A summary of some of the more common causes of FTLD and ALS and their relative contributions to this disease spectrum are highlighted in Figure 1.3.

Several GWASs had previously demonstrated a major locus mapping to chromosome 9p21, associated with both FTLD and ALS (87,110-112). In 2011, two groups simultaneously reported the presence of expanded (~700-1,600 repeats) GGGGCC hexanucleoitde repeats within the first intron of the *C9ORF72* gene (113,114). Patients with these repeat expansions have particularly high incidences of co-morbidity with FTLD and ALS. This abnormality in *C9ORF72* is the single largest genetic contributing factor to FTLD and ALS identified, accounting for 10-30% of FTLD-TDP cases, 5-20% of sporadic ALS cases, 20-50% of familial ALS cases, and as much as 80% of FTLD-ALS cases (115-121). The C9ORF72 protein has an unknown function, but bioinformatic analysis reveals the presence of a DENN (differentially expressed in normal and neoplastic cells) domain, which are known to function as Rab-GEFs, suggesting a potential role in regulating membrane trafficking events (122).

Mutants in VCP cause IBMPFD, which includes features of Paget disease, FTLD, and ALS. Recently, mutations in two other RNA binding proteins in the same family as TDP-43, hnRNPA1 and hnRNPA2/B1, were also found to be causative of IBMPFD/ALS (123). Mutations in CHMP2B are most strongly associated with FTLD;

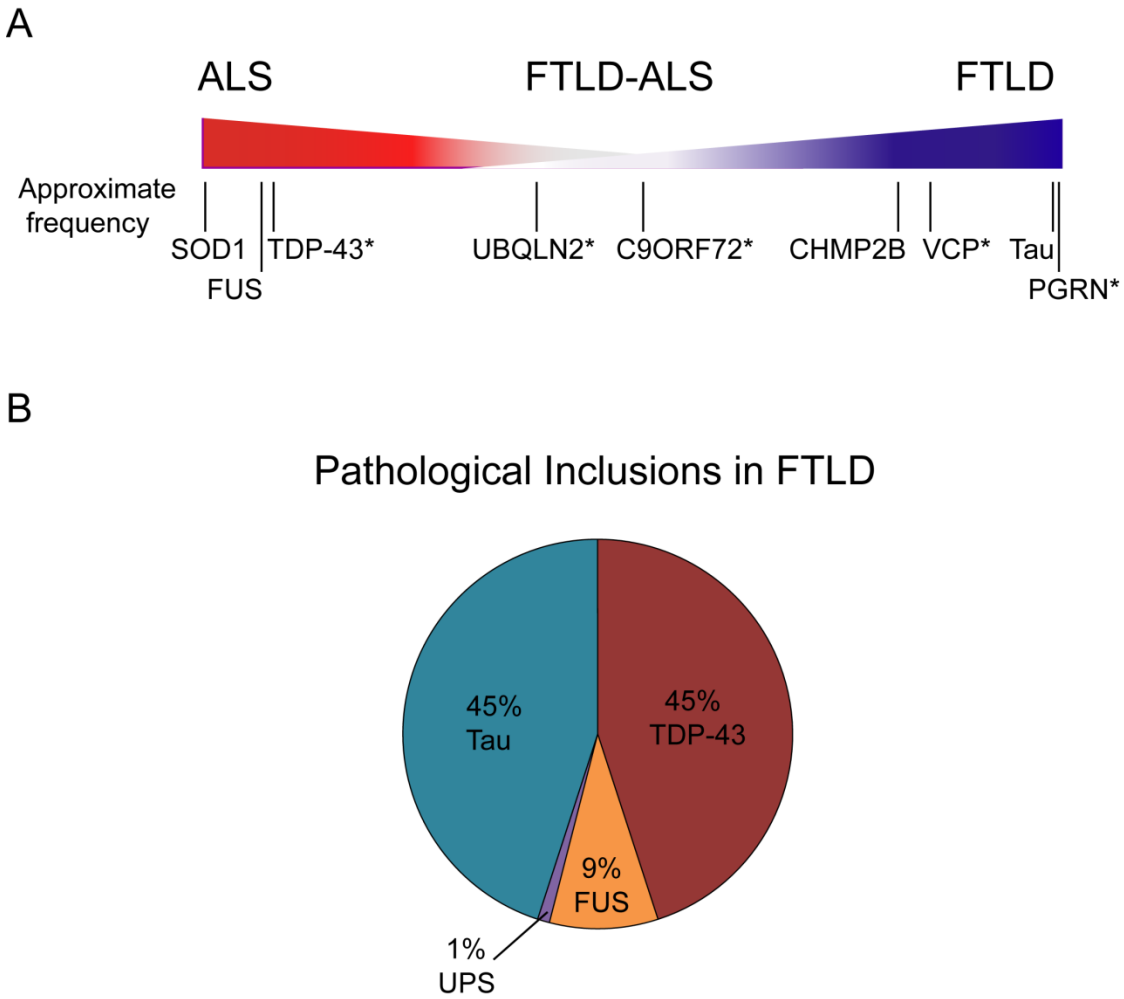

Figure 1.3: FTLD and ALS represent a disease continuum, adapted from ref. 24. (a) Certain mutations have propensities for one side of the continuum. Additionally, many mutations are capable of producing cases with clinical features of both diseases (FTLD-ALS). * indicates genetic causes of disease with TDP-43 proteinopathy. (b) Relative frequencies of the different pathological subtypes observed in FTLD. Note, that many of the genetic causes of FTLD-TDP and FTLD-FUS are also capable of causing ALS.

however, they can also cause ALS in some cases (124,125). Conversely, mutations in TDP-43 are nearly always linked to ALS, however, rare cases have been reported in which TDP-43 mutations cause FLTD-ALS or even pure FTLD (126-129). Two other proteins which are mutated in some cases of familial and sporadic ALS are the ubiquitin-binding adaptor proteins p62/SQSTM1 and ubiquilin 2 (UBQLN2). Like TDP-43, these can also cause FTLD-TDP in certain cases (130-132). In the case of UBQLN2, mutations that cause ALS are typically concentrated in its proline rich PXX domain, while FTLD-TDP causing mutations are located in other conserved regions of the protein (133).

1.3 Impaired proteostasis and RNA metabolism in FTLD-TDP

When reviewing the genetic causes and risk factors for FTLD, it is clear that pathways regulating protein homeostasis and various aspects of RNA homeostasis and metabolism are strikingly affected. It has been recognized for some time, that impaired proteostasis is a general feature of aging and neurodegeneration in particular, with post-mitotic neurons being particularly vulnerable to disruptions in protein degradation and quality control (134). The cell has two major pathways for the degradation of misfolded, aggregated, or otherwise unnecessary proteins: the ubiquitin proteasome system (UPS) and the autophagy-lysosome system. Furthermore, these two systems engage in a dynamic cross-talk with each other, and disruptions in one or both have far-reaching implications for the overall health of the cell (135). More recently, it has been realized that large-scale defects in RNA homeostasis are also implicated in a number of neurodegenerative disorders, most prominently FTLD and

ALS. Current models of neurodegeneration in FTLD and ALS hold that defects in any one of these major processes regulating protein and RNA homeostasis may drive further impairments in the other systems, causing a feedback loop of dysregulated protein and RNA processing, ultimately resulting in cell death (24,136). Figure 1.4 displays a cartoon schematic of the pathological conversion of TDP-43 in FTLD-TDP and the known causative mutations and risk factors which disrupt these critical processes in diseased neurons.

1.3.1 Proteostasis defects in the ubiquitin-proteasome and autophagy-lysosome systems

One of the hallmarks of FTLD-TDP is the aggregation of cleaved, ubiquitinated, and hyperphosphorylated TDP-43. It has been demonstrated that TDP-43 overexpression and TDP-43 aggregates are directly cytotoxic in a number of cell-based and animal models (38,39,137-140). In fact, aggregates of TDP-43 have been demonstrated to be cytotoxic even in yeast, which have no TDP-43 homolog. This toxicity is dependent on both the RNA binding and C-terminal aggregation prone regions of TDP-43 (141). TDP-43 aggregates are extensively ubiquitinated and removal by the 26S proteasome, with the aid of the chaperones Hsp70 and Hsp90, has been demonstrated to be one mechanism for removing these cytotoxic aggregates *in vitro* (139,142,143). The vast majority of ALS and to a lesser extent FTLD, disease linked TDP-43 mutations are concentrated in the aggregation prone C-terminal region and can enhance the aggregation propensity of TDP-43, further suggesting a potential gain of function toxicity caused by TDP-43 aggregation (144).

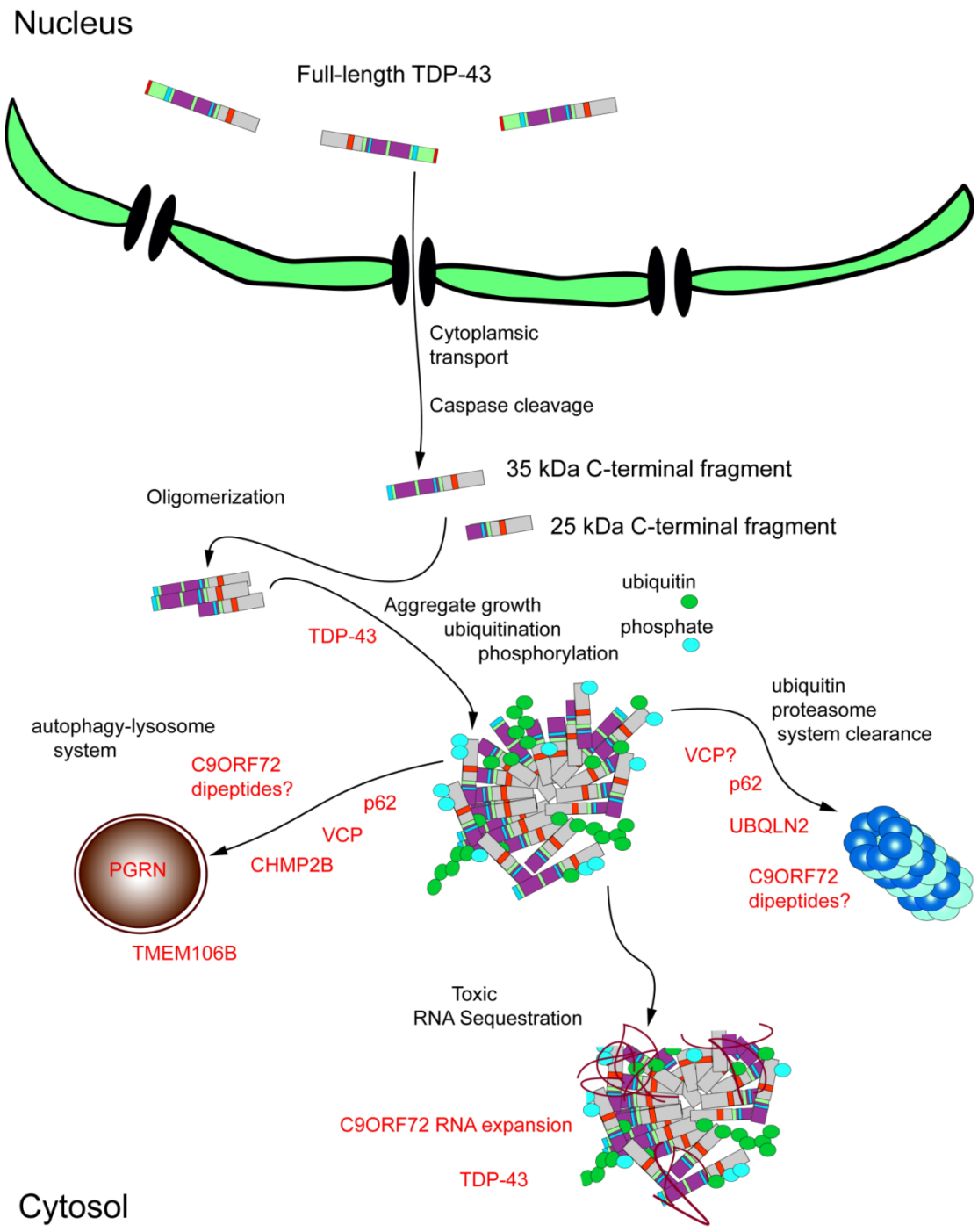
Nucleus
Full-length TDP-43
Cytoplamsic transport
Caspase cleavage
35 kDa C-terminal fragment
25 kDa C-terminal fragment
Oligomerization
TDP-43
Aggregate growth
ubiquitination
phosphorylation
ubiquitin
phosphate
autophagy-lysosome system
C9ORF72 dipeptides?
p62
VCP
CHMP2B
PGRN
TMEM106B
ubiquitin proteasome system clearance
VCP?
p62
UBQLN2
C9ORF72 dipeptides?
Toxic RNA Sequestration
C9ORF72 RNA expansion
TDP-43
Cytosol

Figure 1.4: Proposed sequence of events in pathological conversion of TDP-43 in FTLD-TDP, adapted from refs. 24, 31. The known FTLD-TDP genetic causes and risk factors and the pathways they disrupt are shown in red. Question marks indicate a role in that pathway, but insufficient evidence to conclude a causal effect on pathogenicity in disease states. Note, C9ORF72 RNA expansion disruption is thought to originate in the nucleus, but these cases also exhibit TDP-43 inclusions and likely cytosolic RNA disruption as well.

In addition to the UPS, the other major protein degradation mechanism in the cell is the autophagy-lysosome system, which is critical for the degradation and recycling of a large variety of protein substrates. Membrane proteins from the endocytic pathway destined for degradation are internalized into late endosomes, typically in a mono-ubiquitin dependent manner and are trafficked to the lysosomes, while bulk cytoplasmic degradation of large protein aggregates and organelles is mediated by sequestration of substrates within a double-membrane autophagic vacuole, which then fuses with lysosomes for degradation of its contents (145). The importance of functioning endo-lysosomal and autophagy-lysosome pathways in neuronal health is illustrated by the case of lysosomal storage disorders (LSDs). LSDs are a large group of ~50 metabolic disorders characterized by primary defects in lysosomal function, which are frequently associated with progressive neurodegenerative and dementia-like phenotypes (146,147). Not surprisingly, increasing evidence points to lysosomal dysfunction as playing a crucial role in the pathogenesis of many late-onset neurodegenerative diseases as well (146,148). The critical importance of autophagy in the maintenance of neuronal health was demonstrated in a seminal 2006 study, in which conditional, neuronal-specific, *ATG5*$^{-/-}$ mice were generated. The neurons of these mice are unable to complete the process of autophagosome formation which causes neurodegeneration by three weeks. Remarkably, these mice develop progressive behavioral and motor deficits accompanied by ubiquitinated protein inclusions within their neurons much like those seen in FTLD and ALS (149).

The proteins UBQLN2 and p62 are mutated in some cases of FTLD-TDP and ALS and belong to a class of ubiquitin binding adaptor proteins capable of binding ubiquitinated proteins and linking them to the proteasome for degradation (150). UBQLN2 can bind ubiquitinated proteins through its ubiquitin associated (UBA) domain and may bridge these substrates through direct binding to the proteasome through its ubiquitin like domain (UBL) (151). UBQLN2 disease linked mutations have been shown to impair ubiquitin mediated proteasomal degradation (132). Polymorphisms in the structurally similar protein, p62 have also been associated with FTLD-TDP and ALS and p62 positive inclusions are present in range of neurodegenerative conditions including Alzheimer's and Parkinson's diseases as well as FTLD-ALS caused by C9ORF72 repeat expansions (130,152,153). Recently, it was shown that p62 directly binds to TDP-43 in the brains of FTLD-TDP patients to facilitate the degradation of the 35 kDa fragment, and p62 binds to TDP-43 less efficiently in the brains of FTLD-TDP patients compared to non-diseased controls (154).

In addition to their roles in linking ubiquitinated proteins to the proteasome for degradation, the proteins UBQLN2 and p62 are also implicated in facilitating the autophagic degradation of ubiquitinated proteins. Overexpression of UBQLN2 protects cells from starvation-induced cell death, likely by promoting autophagic protein recycling and is observed within autophagic vacuoles and lysosomes via immunofluorescence and electron microscopy (155). The functionally and evolutionarily related protein, p62, has a similar domain architecture as UBQLN2, and likely mediates similar functions in both the UPS and autophagy pathways. The p62

protein contains an N-terminal PB1 domain, homologous to the UBL domain of UBQLN2, which mediates polymerization. In combination with its C-terminal UBA domain, p62 is thought to sequester ubiquitinated proteins into aggregates for autophagic clearance (150). Further, p62 contains a small domain known as the LC3-interacting region (LIR) that can directly bind to the autophagic membrane protein LC3 to facilitate aggregate removal (156). Cell culture studies show that p62 is capable of surrounding aggregated huntingtin and promoting its recruitment to autophagosomes and that depletion of p62 significantly increases cell death caused by these aggregates (157). Both UBQLN2 and p62 commonly co-localize with aggregates in diseased brains and have been shown to bind TDP-43, further highlighting the similar roles these two proteins have in maintaining cellular proteostasis at the intersection of the UPS and autophagy-lysosome pathways (150).

Another protein functionally linked with proteasome function, which is impaired in some cases of FTLD-TPD is VCP, which has two well documented roles related to proteasomal function. In ERAD, VCP, in cooperation with derlin-1 plays a role in extracting misfolded proteins from the endoplasmic reticulum (ER) for proteasome mediated degradation (158). Secondly, VCP has been shown to physically associate with multiple components of the UPS, including E3/E4 ubiquitin ligases, DUBs, and polyubiquitin (159). These associations are likely critical for its roles in mediating the ubiquitin-dependent degradation of numerous cytosolic proteins (62,160,161). It is important to note that there is little direct evidence that disease causing mutations in *VCP* specifically cause defects in the UPS, but considering the

extensive role VCP plays in this regard, it is conceivable that certain UPS functions may be subtly affected in disease states.

Like UBQLN2 and p62, VCP has annotated roles in both the UPS and autophagy-lysosome system, among others. Interestingly, there is much stronger evidence that disease causing VCP mutants impair the autophagy-lysosome system than the UPS. VCP plays an important role in the fusion of autophagosomes with lysosomes, with disease causing mutants leading to an accumulation of fusion-defective autophagosomes (162). In addition, autophagic dysfunction caused by VCP leads to the cytoplasmic accumulation of TDP-43 in cells and in mice, recapitulating one of the key pathological features of IBMPFD/ALS (163,164). A recent study used a proteomic approach to identify a VCP binding cofactor, UBXD1 which mediates the mono-ubiquitin dependent trafficking of caveolin-1 to lysosomes. The interaction between UBXD1 is abrogated by disease linked VCP mutants, while ERAD and UPS functions are preserved (165). These studies highlight the importance of VCP's roles in ubiquitin mediated membrane trafficking events in the endo-lysosomal and autophagy-lysosome pathway.

One of several potential pathogenic mechanisms by which C9ORF72 causes FTLD-ALS is through the unconventional translation of long, aggregating dipeptides in a process known as repeat-associated, RNA-encoded, non-ATG translation (RAN translation). RAN translation was first demonstrated in the case of the CAG repeat neurodegenerative disease, spinocerebellar ataxia type 8 in the *ATXN8* gene and results in a long polyglutamine peptide which is translated in a non-ATG dependent manner (166). RAN translation may be a common feature of a number of other

trinucleotide repeat diseases as well and may result in the buildup of toxic protein aggregates (167). Two recent reports demonstrate that dipeptides encoding Gly-Ala (GA), Gly-Pro (GP), and Gly-Arg (GR), are produced by the three reading frames of the GGGGCC repeats of *C9ORF72*, respectively (168,169). These dipeptide aggregates have been produced *in vitro* and are found in the neurons of patients with C9ORF72 repeat expansions. Furthermore, an anti-sense transcript is also purported to be produced, further increasing the repertoire of potentially toxic dipeptide aggregates that can be produced by GGGGCC repeat expansions (169). While the mechanism of dipeptide aggregate toxicity is poorly understood, one possibility is that massive amounts of abnormal aggregated protein may simply overwhelm the normal degradative capacity of the proteasome causing a generalized disruption of proteostasis and downstream toxicity.

Although its function is not known at this point, C9ORF72 itself may play a role in the autophagy-lysosome pathways. FTLD-TDP and ALS caused by C9ORF72 repeat expansions is associated with an approximately 50% reduction in the mRNA of both major isoforms of *C9ORF72*, suggesting haploinsufficiency as a potential disease mechanism (113,170). This mechanism is supported by a zebrafish model of ALS in which antisense knockdown of C9ORF72 levels causes neurodegeneration coupled with locomotor deficits (171). Since C9ORF72 contains a DENN domain, which has Rab-GEF activity and is highly associated with vesicular trafficking events, it is tempting to speculate that C9ORF72 may have an important role in late endosome or autophagosome trafficking to lysosomes, much like other known causes of FTLD and ALS (122,172). Finally, it should also be noted that the RAN associated dipeptides

seen in C9ORF72 repeat expansion carriers may similarly play a general role in disrupting autophagic clearance of proteins on a global level, although this remains hypothetical at this time.

The ESCRT-III component, CHMP2B is implicated in familial forms of FTLD-UPS and has a well described role in the trafficking of ubiquitinated membrane proteins into late endosomes/MVBs for eventual lysosomal degradation (173). Various splice site and nonsense mutations in the CHMP2B protein result in C-terminal truncations. These truncations remove an autoinhibitory domain from CHMP2B, causing it to constitutively bind late endosome membranes and thus the ESCRT-III complex cannot be disassembled by VPS4/Skd1. These mutations have been shown in cell culture models to prevent MVB and autophagosome fusion with lysosomes and result in an accumulation of p62 and ubiquitinated proteins (174-177). A recently described transgenic mouse model containing an intron 5-retention disease mutant exhibits progressive neurodegeneration and increased mortality, whereas loss of CHMP2B has no phenotype, suggesting a toxic gain of function in the endo-lysosomal pathway (178).

Mutations in the gene encoding PGRN invariably cause FTLD-TDP through a haploinsufficiency mechanism. PGRN is best known as a pleiotropic secreted growth factor with neurotrophic, cell migration, and pro- and anti-inflammatory functions (6). PGRN has not traditionally been ascribed a role in lysosomal function; however, several converging lines of evidence from recent studies have begun to hint at a potential role in this organelle. We have recently shown that sortilin promotes lysosomal trafficking of PGRN through its interaction with the extreme C-terminus of

full length PGRN (78,79). Furthermore, bioinformatic analysis reveals PGRN is transcriptionally co-regulated with a multitude of other lysosomal genes (179). PGRN, ranks among the top regulated targets by the Coordinated Lysosomal Expression and Regulation (CLEAR) network, under control by the master lysosomal transcription factor, TFEB (180). PGRN knockout mice exhibit tissue vacuolization, ubiquitinated protein inclusions, and accumulate the lysosomal waste byproduct, lipofuscin (181). Finally, a recent case report of siblings harboring homozygous PGRN mutations revealed diagnoses of neuronal ceroid lipofuscinosis (NCL), a much more severe and early onset neurodegenerative LSD (182). While the exact role of PGRN in lysosomes remains unknown, the available evidence points to a lysosomal function, which merits further investigation. The FTLD-TDP risk factor, TMEM106B is strongly associated with PGRN mutant carriers and has recently been shown to localize to late endosomes and lysosomes (95). Like PGRN, the function of TMEM106B in lysosomes remains unknown, but its localization and genetic association with PGRN further suggests an important role in lysosome function and is the subject of much of this dissertation.

1.3.2 Disruption of RNA homeostasis

Disrupted RNA metabolism has been recognized as a major feature of FTLD-TDP and ALS (as well as FTLD and ALS caused by FUS mutations). In addition to models that propose a gain of function toxicity from TDP-43 aggregation, another likely contributing factor in disease pathogenesis is loss-of function of TDP-43 caused by cleavage and sequestration of the active protein product. Genome-wide studies of TDP-43's RNA targets in mouse and human brains reveal numerous RNAs whose

levels and splicing are critically regulated by TDP-43 (49,52). Many of these RNA targets have important implications for overall neuronal health and survival. A few of the notable mRNAs of the ~1500 whose levels and splicing are affected by loss of TDP-43 include the FTLD disease linked genes encoding Tau, CHMP2B, VCP, p62, and PGRN, along with the PGRN receptor sortilin (49,183). Interestingly, TDP-43 mediated sortilin splicing is necessary for a functional protein and a loss of TDP-43 results in a non-functional sortilin product, potentially impairing PGRN transport to lysosomes (184). TDP-43 also regulates the levels of ATG7, which is essential for autophagy induction. Genes encoding proteins associated with other neurodegenerative diseases are also affected and include amyloid precursor protein (APP), presenilin, huntingtin, α-synuclein, and survival of motor neuron (SMN) protein among many others (49,183).

An additional explanation for the toxicity of cytoplasmic of TDP-43 aggregates is through the binding and sequestration of critical RNAs in the cytoplasm, preventing their proper localization and translation. A yeast suppressor screen showed that loss of the RNA intron lariat debranching enzyme Dbr1 rescues TDP-43 aggregate toxicity (185). It is hypothesized that the accumulation of RNA lariats may act as decoys which can bind TDP-43 aggregates in the cytosol, allowing normal RNA species to escape sequestration and remain functional.

Altered RNA metabolism is also likely one of the mechanisms by which C9ORF72 repeat expansions cause pathogenesis in FTLD-ALS. GGGGCC containing RNA foci have been reported in the nuclei of postmortem CNS tissue and induced pluripotent stem cells differentiated into neurons (iPSN) from C9ORF72 repeat

expansion carriers (113,186). The RNA-binding proteins hnRNPA3 and Pur-α have been shown to bind GGGGCC repeats *in vitro* and are part of some protein inclusions seen in tissue from C9ORF72 patients (187,188). A recent study using iPSNs demonstrated that GGGGCC repeats cause toxicity by sequestering a number of RNA binding proteins such as the RNA editing enzyme ADARB2, which contributes to glutamate excitotoxicity by preventing RNA editing of the glutamate receptor subunit GluR2 (186). This same study also showed that C9ORF72 repeat expansions cause changes in the expression of hundreds of genes, similar to the effects seen by TDP-43 depletion and antisense mediated knockdown of *C9ORF72* RNA caused a reduction in toxicity.

1.3.3 Current models: impaired proteostasis and defects in RNA metabolism drive loss and gain of function toxicity

It is interesting to note that a large number of the genes regulated by TDP-43 are in turn required for optimal proteostasis, including the removal of excess aggregated TDP-43, further strengthening the link between proteostasis and RNA homeostasis. As mentioned earlier, TDP-43 also negatively regulates its own transcript, and loss of TDP-43 function caused by mislocalization and aggregation could feasibly drive a feed-forward loop driving excess TDP-43 translation, and exacerbating the problem of TDP-43 proteostasis. Taken together, it is increasingly apparent that disrupted proteostasis and RNA homeostasis are intimately linked in a give and take relationship, with defects in one system driving defects in the other.

1.4 Contents of this dissertation

This dissertation explores several mechanisms by which FTLD-TDP and ALS pathogenesis may occur and is split up into three main chapters and several appendices.

Chapter 2 explores the mechanisms governing TDP-43 aggregation and clearance in cell culture models. In it, I explore the role of the C-terminal domain in mediating aggregation and how phosphorylation affects aggregation and clearance. In my experiments, I show that phosphomimetic mutations in the aggregation prone C-terminus of TDP-43 actually suppress aggregation *in vitro*. This is in contrast to many models which correlate phosphorylated TDP-43 with increased insolubility and more aggregation. My work supports a model in which phosphorylation of the C-terminal region of TDP-43 sends a "stop" signal to halt further aggregation. Because these phosphomimetic mutants are present from synthesis, the TDP-43 aggregates have little chance to aggregate in the first place. This finding was confirmed by another paper which came out shortly after our's was published (189). Additionally, I report a role of p62 in facilitating the clearance of aggregated TDP-43 fragments *in vitro* and demonstrate that this occurs through both the UPS and autophagy pathways, with the autophagy pathway playing a more prominent role in our experiments. This model of cooperation between the UPS and autophagy pathways in clearing TDP-43 has been reported by other groups at around the same time. Shortly after this was published p62 was identified to bind TDP-43 less effectively in the brains of FTLD-TDP patients compared to healthy controls, strengthening the case for p62 in mediating the clearance of TDP-43 *in vivo* (143,154).

Chapters 3 and 4 explore the basic biochemical and cell biological properties of the recently identified FTLD-TDP risk factor, TMEM106B, in order to ascertain a function for this previously unstudied membrane protein. Chapter 3 characterized the localization of TMEM106B to late endosomes/lysosomes and supports a role for TMEM106B in regulating lysosome morphology and number, with elevated levels leading to lysosome dysfunction in our cell culture model system. These results were mostly supported by several papers released at around the same time (95-97). Interestingly, we also observed a correlation between increased TMEM106B levels and increased full-length PGRN, but not PGRN mRNA, potentially due to defects in lysosomal degradation of PGRN. This remains controversial as elevated TMEM106B levels are thought to be correlated with decreased PGRN in patients carrying the risk allele of *TMEM106B* (88,89). Nonetheless, my results were supported by two of the recently mentioned reports on TMEM106B, and further implicate both PGRN and TMEM106B as playing important roles in regulating lysosome functions (96,97).

Chapter 4 reports TMEM106B as a substrate for regulated intramembrane proteolysis (RIP) by an unidentified lysosomal enzyme(s) and the intramembrane cleaving protease (i-CLIP), SPPL2a. These results are significant because TMEM106B levels are thought to be increased in disease and this identifies a potential cellular mechanism for controlling TMEM106B levels *in vivo*. Additionally, this study contributes to the small, but growing list of transmembrane protein substrates that are known to be cleaved by the SPPL2 family of i-CLIPs. These results have also led the project to new directions which are actively being pursued in the lab in order to further

characterize the trafficking, degradation, and functional roles of TMEM106B. As of the time of this writing, these results are being revised for submission and publication.

REFERENCES

1. Neary, D., Snowden, J., and Mann, D. (2005) Frontotemporal dementia. *Lancet Neurol* 4, 771-780
2. Rowland, L. P., and Shneider, N. A. (2001) Amyotrophic lateral sclerosis. *N Engl J Med* 344, 1688-1700
3. Geser, F., Martinez-Lage, M., Kwong, L. K., Lee, V. M., and Trojanowski, J. Q. (2009) Amyotrophic lateral sclerosis, frontotemporal dementia and beyond: the TDP-43 diseases. *J Neurol* 256, 1205-1214
4. Rossor, M. N., Fox, N. C., Mummery, C. J., Schott, J. M., and Warren, J. D. (2010) The diagnosis of young-onset dementia. *Lancet Neurol* 9, 793-806
5. Ratnavalli, E., Brayne, C., Dawson, K., and Hodges, J. R. (2002) The prevalence of frontotemporal dementia. *Neurology* 58, 1615-1621
6. Gass, J., Prudencio, M., Stetler, C., and Petrucelli, L. (2012) Progranulin: an emerging target for FTLD therapies. *Brain Res* 1462, 118-128
7. Knopman, D. S., Petersen, R. C., Edland, S. D., Cha, R. H., and Rocca, W. A. (2004) The incidence of frontotemporal lobar degeneration in Rochester, Minnesota, 1990 through 1994. *Neurology* 62, 506-508
8. Mercy, L., Hodges, J. R., Dawson, K., Barker, R. A., and Brayne, C. (2008) Incidence of early-onset dementias in Cambridgeshire, United Kingdom. *Neurology* 71, 1496-1499
9. Rosso, S. M., Donker Kaat, L., Baks, T., Joosse, M., de Koning, I., Pijnenburg, Y., de Jong, D., Dooijes, D., Kamphorst, W., Ravid, R., Niermeijer, M. F., Verheij, F., Kremer, H. P., Scheltens, P., van Duijn, C. M., Heutink, P., and van Swieten, J. C. (2003) Frontotemporal dementia in The Netherlands: patient characteristics and prevalence estimates from a population-based study. *Brain* 126, 2016-2022
10. Chow, T. W., Miller, B. L., Hayashi, V. N., and Geschwind, D. H. (1999) Inheritance of frontotemporal dementia. *Arch Neurol* 56, 817-822
11. Hodges, J. R., Davies, R., Xuereb, J., Kril, J., and Halliday, G. (2003) Survival in frontotemporal dementia. *Neurology* 61, 349-354
12. Rascovsky, K., Salmon, D. P., Lipton, A. M., Leverenz, J. B., DeCarli, C., Jagust, W. J., Clark, C. M., Mendez, M. F., Tang-Wai, D. F., Graff-Radford, N. R., and Galasko, D. (2005) Rate of progression differs in frontotemporal dementia and Alzheimer disease. *Neurology* 65, 397-403
13. Vossel, K. A., and Miller, B. L. (2008) New approaches to the treatment of frontotemporal lobar degeneration. *Curr Opin Neurol* 21, 708-716
14. Lillo, P., and Hodges, J. R. (2009) Frontotemporal dementia and motor neurone disease: overlapping clinic-pathological disorders. *J Clin Neurosci* 16, 1131-1135
15. Van Langenhove, T., van der Zee, J., and Van Broeckhoven, C. (2012) The molecular basis of the frontotemporal lobar degeneration-amyotrophic lateral sclerosis spectrum. *Ann Med* 44, 817-828
16. Johnson, J. K., Diehl, J., Mendez, M. F., Neuhaus, J., Shapira, J. S., Forman, M., Chute, D. J., Roberson, E. D., Pace-Savitsky, C., Neumann, M., Chow, T.

W., Rosen, H. J., Forstl, H., Kurz, A., and Miller, B. L. (2005) Frontotemporal lobar degeneration: demographic characteristics of 353 patients. *Arch Neurol* 62, 925-930
17. Torralva, T., Roca, M., Gleichgerrcht, E., Bekinschtein, T., and Manes, F. (2009) A neuropsychological battery to detect specific executive and social cognitive impairments in early frontotemporal dementia. *Brain* 132, 1299-1309
18. Neary, D., Snowden, J. S., Gustafson, L., Passant, U., Stuss, D., Black, S., Freedman, M., Kertesz, A., Robert, P. H., Albert, M., Boone, K., Miller, B. L., Cummings, J., and Benson, D. F. (1998) Frontotemporal lobar degeneration: a consensus on clinical diagnostic criteria. *Neurology* 51, 1546-1554
19. Davies, R. R., Halliday, G. M., Xuereb, J. H., Kril, J. J., and Hodges, J. R. (2009) The neural basis of semantic memory: evidence from semantic dementia. *Neurobiol Aging* 30, 2043-2052
20. Hodges, J. R., and Patterson, K. (2007) Semantic dementia: a unique clinicopathological syndrome. *Lancet Neurol* 6, 1004-1014
21. Gorno-Tempini, M. L., Hillis, A. E., Weintraub, S., Kertesz, A., Mendez, M., Cappa, S. F., Ogar, J. M., Rohrer, J. D., Black, S., Boeve, B. F., Manes, F., Dronkers, N. F., Vandenberghe, R., Rascovsky, K., Patterson, K., Miller, B. L., Knopman, D. S., Hodges, J. R., Mesulam, M. M., and Grossman, M. (2011) Classification of primary progressive aphasia and its variants. *Neurology* 76, 1006-1014
22. Hodges, J. R., Patterson, K., Oxbury, S., and Funnell, E. (1992) Semantic dementia. Progressive fluent aphasia with temporal lobe atrophy. *Brain* 115 (Pt 6), 1783-1806
23. Mackenzie, I. R., Neumann, M., Bigio, E. H., Cairns, N. J., Alafuzoff, I., Kril, J., Kovacs, G. G., Ghetti, B., Halliday, G., Holm, I. E., Ince, P. G., Kamphorst, W., Revesz, T., Rozemuller, A. J., Kumar-Singh, S., Akiyama, H., Baborie, A., Spina, S., Dickson, D. W., Trojanowski, J. Q., and Mann, D. M. (2010) Nomenclature and nosology for neuropathologic subtypes of frontotemporal lobar degeneration: an update. *Acta Neuropathol* 119, 1-4
24. Ling, S. C., Polymenidou, M., and Cleveland, D. W. (2013) Converging mechanisms in ALS and FTD: disrupted RNA and protein homeostasis. *Neuron* 79, 416-438
25. Hutton, M., Lendon, C. L., Rizzu, P., Baker, M., Froelich, S., Houlden, H., Pickering-Brown, S., Chakraverty, S., Isaacs, A., Grover, A., Hackett, J., Adamson, J., Lincoln, S., Dickson, D., Davies, P., Petersen, R. C., Stevens, M., de Graaff, E., Wauters, E., van Baren, J., Hillebrand, M., Joosse, M., Kwon, J. M., Nowotny, P., Che, L. K., Norton, J., Morris, J. C., Reed, L. A., Trojanowski, J., Basun, H., Lannfelt, L., Neystat, M., Fahn, S., Dark, F., Tannenberg, T., Dodd, P. R., Hayward, N., Kwok, J. B., Schofield, P. R., Andreadis, A., Snowden, J., Craufurd, D., Neary, D., Owen, F., Oostra, B. A., Hardy, J., Goate, A., van Swieten, J., Mann, D., Lynch, T., and Heutink, P. (1998) Association of missense and 5'-splice-site mutations in tau with the inherited dementia FTDP-17. *Nature* 393, 702-705

26. Iyer, A., Lapointe, N. E., Zielke, K., Berdynski, M., Guzman, E., Barczak, A., Chodakowska-Zebrowska, M., Barcikowska, M., Feinstein, S., and Zekanowski, C. (2013) A Novel MAPT Mutation, G55R, in a Frontotemporal Dementia Patient Leads to Altered Tau Function. *PLoS One* 8, e76409
27. Schaffer, B. A., Bertram, L., Miller, B. L., Mullin, K., Weintraub, S., Johnson, N., Bigio, E. H., Mesulam, M., Wiedau-Pazos, M., Jackson, G. R., Cummings, J. L., Cantor, R. M., Levey, A. I., Tanzi, R. E., and Geschwind, D. H. (2008) Association of GSK3B with Alzheimer disease and frontotemporal dementia. *Arch Neurol* 65, 1368-1374
28. Arai, T., Hasegawa, M., Akiyama, H., Ikeda, K., Nonaka, T., Mori, H., Mann, D., Tsuchiya, K., Yoshida, M., Hashizume, Y., and Oda, T. (2006) TDP-43 is a component of ubiquitin-positive tau-negative inclusions in frontotemporal lobar degeneration and amyotrophic lateral sclerosis. *Biochem Biophys Res Commun* 351, 602-611
29. Neumann, M., Sampathu, D. M., Kwong, L. K., Truax, A. C., Micsenyi, M. C., Chou, T. T., Bruce, J., Schuck, T., Grossman, M., Clark, C. M., McCluskey, L. F., Miller, B. L., Masliah, E., Mackenzie, I. R., Feldman, H., Feiden, W., Kretzschmar, H. A., Trojanowski, J. Q., and Lee, V. M. (2006) Ubiquitinated TDP-43 in frontotemporal lobar degeneration and amyotrophic lateral sclerosis. *Science* 314, 130-133
30. Zhang, Y. J., Xu, Y. F., Dickey, C. A., Buratti, E., Baralle, F., Bailey, R., Pickering-Brown, S., Dickson, D., and Petrucelli, L. (2007) Progranulin mediates caspase-dependent cleavage of TAR DNA binding protein-43. *J Neurosci* 27, 10530-10534
31. Janssens, J., and Van Broeckhoven, C. (2013) Pathological mechanisms underlying TDP-43 driven neurodegeneration in FTLD-ALS spectrum disorders. *Hum Mol Genet* 22, R77-87
32. Ling, S.-C., Polymenidou, M., and Cleveland, Don W. (2013) Converging Mechanisms in ALS and FTD: Disrupted RNA and Protein Homeostasis. *Neuron* 79, 416-438
33. Freeman, S. H., Spires-Jones, T., Hyman, B. T., Growdon, J. H., and Frosch , M. P. (2008) TAR-DNA binding protein 43 in Pick disease. *J Neuropathol Exp Neurol* 67, 62-67
34. Lin, W. L., and Dickson, D. W. (2008) Ultrastructural localization of TDP-43 in filamentous neuronal inclusions in various neurodegenerative diseases. *Acta Neuropathol* 116, 205-213
35. Schwab, C., Arai, T., Hasegawa, M., Yu, S., and McGeer, P. L. (2008) Colocalization of transactivation-responsive DNA-binding protein 43 and huntingtin in inclusions of Huntington disease. *J Neuropathol Exp Neurol* 67, 1159-1165
36. Covy, J. P., Yuan, W., Waxman, E. A., Hurtig, H. I., Van Deerlin, V. M., and Giasson, B. I. (2009) Clinical and pathological characteristics of patients with leucine-rich repeat kinase-2 mutations. *Mov Disord* 24, 32-39
37. Tan, C. F., Yamada, M., Toyoshima, Y., Yokoseki, A., Miki, Y., Hoshi, Y., Kaneko, H., Ikeuchi, T., Onodera, O., Kakita, A., and Takahashi, H. (2009)

Selective occurrence of TDP-43-immunoreactive inclusions in the lower motor neurons in Machado-Joseph disease. *Acta Neuropathol* 118, 553-560
38. Ash, P. E., Zhang, Y. J., Roberts, C. M., Saldi, T., Hutter, H., Buratti, E., Petrucelli, L., and Link, C. D. (2010) Neurotoxic effects of TDP-43 overexpression in C. elegans. *Hum Mol Genet* 19, 3206-3218
39. Li, Y., Ray, P., Rao, E. J., Shi, C., Guo, W., Chen, X., Woodruff, E. A., 3rd, Fushimi, K., and Wu, J. Y. (2010) A Drosophila model for TDP-43 proteinopathy. *Proc Natl Acad Sci U S A* 107, 3169-3174
40. Xu, Y. F., Gendron, T. F., Zhang, Y. J., Lin, W. L., D'Alton, S., Sheng, H., Casey, M. C., Tong, J., Knight, J., Yu, X., Rademakers, R., Boylan, K., Hutton, M., McGowan, E., Dickson, D. W., Lewis, J., and Petrucelli, L. (2010) Wild-type human TDP-43 expression causes TDP-43 phosphorylation, mitochondrial aggregation, motor deficits, and early mortality in transgenic mice. *J Neurosci* 30, 10851-10859
41. Kraemer, B. C., Schuck, T., Wheeler, J. M., Robinson, L. C., Trojanowski, J. Q., Lee, V. M., and Schellenberg, G. D. (2010) Loss of murine TDP-43 disrupts motor function and plays an essential role in embryogenesis. *Acta Neuropathol* 119, 409-419
42. Sephton, C. F., Good, S. K., Atkin, S., Dewey, C. M., Mayer, P., 3rd, Herz, J., and Yu, G. (2010) TDP-43 is a developmentally regulated protein essential for early embryonic development. *J Biol Chem* 285, 6826-6834
43. Ou, S. H., Wu, F., Harrich, D., Garcia-Martinez, L. F., and Gaynor, R. B. (1995) Cloning and characterization of a novel cellular protein, TDP-43, that binds to human immunodeficiency virus type 1 TAR DNA sequence motifs. *J Virol* 69, 3584-3596
44. Lalmansingh, A. S., Urekar, C. J., and Reddi, P. P. (2011) TDP-43 is a transcriptional repressor: the testis-specific mouse acrv1 gene is a TDP-43 target in vivo. *J Biol Chem* 286, 10970-10982
45. Buratti, E., Dork, T., Zuccato, E., Pagani, F., Romano, M., and Baralle, F. E. (2001) Nuclear factor TDP-43 and SR proteins promote in vitro and in vivo CFTR exon 9 skipping. *EMBO J* 20, 1774-1784
46. Mercado, P. A., Ayala, Y. M., Romano, M., Buratti, E., and Baralle, F. E. (2005) Depletion of TDP 43 overrides the need for exonic and intronic splicing enhancers in the human apoA-II gene. *Nucleic Acids Res* 33, 6000-6010
47. Passoni, M., De Conti, L., Baralle, M., and Buratti, E. (2012) UG repeats/TDP-43 interactions near 5' splice sites exert unpredictable effects on splicing modulation. *J Mol Biol* 415, 46-60
48. Fiesel, F. C., Weber, S. S., Supper, J., Zell, A., and Kahle, P. J. (2012) TDP-43 regulates global translational yield by splicing of exon junction complex component SKAR. *Nucleic Acids Res* 40, 2668-2682
49. Polymenidou, M., Lagier-Tourenne, C., Hutt, K. R., Huelga, S. C., Moran, J., Liang, T. Y., Ling, S. C., Sun, E., Wancewicz, E., Mazur, C., Kordasiewicz, H., Sedaghat, Y., Donohue, J. P., Shiue, L., Bennett, C. F., Yeo, G. W., and Cleveland, D. W. (2011) Long pre-mRNA depletion and RNA missplicing

contribute to neuronal vulnerability from loss of TDP-43. *Nat Neurosci* 14, 459-468
50. Avendano-Vazquez, S. E., Dhir, A., Bembich, S., Buratti, E., Proudfoot, N., and Baralle, F. E. (2012) Autoregulation of TDP-43 mRNA levels involves interplay between transcription, splicing, and alternative polyA site selection. *Genes Dev* 26, 1679-1684
51. Kapranov, P., Cheng, J., Dike, S., Nix, D. A., Duttagupta, R., Willingham, A. T., Stadler, P. F., Hertel, J., Hackermuller, J., Hofacker, I. L., Bell, I., Cheung, E., Drenkow, J., Dumais, E., Patel, S., Helt, G., Ganesh, M., Ghosh, S., Piccolboni, A., Sementchenko, V., Tammana, H., and Gingeras, T. R. (2007) RNA maps reveal new RNA classes and a possible function for pervasive transcription. *Science* 316, 1484-1488
52. Tollervey, J. R., Curk, T., Rogelj, B., Briese, M., Cereda, M., Kayikci, M., Konig, J., Hortobagyi, T., Nishimura, A. L., Zupunski, V., Patani, R., Chandran, S., Rot, G., Zupan, B., Shaw, C. E., and Ule, J. (2011) Characterizing the RNA targets and position-dependent splicing regulation by TDP-43. *Nat Neurosci* 14, 452-458
53. Buratti, E., De Conti, L., Stuani, C., Romano, M., Baralle, M., and Baralle, F. (2010) Nuclear factor TDP-43 can affect selected microRNA levels. *FEBS J* 277, 2268-2281
54. Ling, S. C., Albuquerque, C. P., Han, J. S., Lagier-Tourenne, C., Tokunaga, S., Zhou, H., and Cleveland, D. W. (2010) ALS-associated mutations in TDP-43 increase its stability and promote TDP-43 complexes with FUS/TLS. *Proc Natl Acad Sci U S A* 107, 13318-13323
55. Freibaum, B. D., Chitta, R. K., High, A. A., and Taylor, J. P. (2010) Global analysis of TDP-43 interacting proteins reveals strong association with RNA splicing and translation machinery. *J Proteome Res* 9, 1104-1120
56. Kawahara, Y., and Mieda-Sato, A. (2012) TDP-43 promotes microRNA biogenesis as a component of the Drosha and Dicer complexes. *Proc Natl Acad Sci U S A* 109, 3347-3352
57. Ayala, Y. M., Zago, P., D'Ambrogio, A., Xu, Y. F., Petrucelli, L., Buratti, E., and Baralle, F. E. (2008) Structural determinants of the cellular localization and shuttling of TDP-43. *J Cell Sci* 121, 3778-3785
58. Gilks, N., Kedersha, N., Ayodele, M., Shen, L., Stoecklin, G., Dember, L. M., and Anderson, P. (2004) Stress granule assembly is mediated by prion-like aggregation of TIA-1. *Mol Biol Cell* 15, 5383-5398
59. Buchan, J. R., Kolaitis, R. M., Taylor, J. P., and Parker, R. (2013) Eukaryotic stress granules are cleared by autophagy and Cdc48/VCP function. *Cell* 153, 1461-1474
60. Watts, G. D., Wymer, J., Kovach, M. J., Mehta, S. G., Mumm, S., Darvish, D., Pestronk, A., Whyte, M. P., and Kimonis, V. E. (2004) Inclusion body myopathy associated with Paget disease of bone and frontotemporal dementia is caused by mutant valosin-containing protein. *Nat Genet* 36, 377-381
61. Weihl, C. C., Temiz, P., Miller, S. E., Watts, G., Smith, C., Forman, M., Hanson, P. I., Kimonis, V., and Pestronk, A. (2008) TDP-43 accumulation in

inclusion body myopathy muscle suggests a common pathogenic mechanism with frontotemporal dementia. *J Neurol Neurosurg Psychiatry* 79, 1186-1189
62. Meyer, H., Bug, M., and Bremer, S. (2012) Emerging functions of the VCP/p97 AAA-ATPase in the ubiquitin system. *Nat Cell Biol* 14, 117-123
63. Uchiyama, K., Jokitalo, E., Kano, F., Murata, M., Zhang, X., Canas, B., Newman, R., Rabouille, C., Pappin, D., Freemont, P., and Kondo, H. (2002) VCIP135, a novel essential factor for p97/p47-mediated membrane fusion, is required for Golgi and ER assembly in vivo. *J Cell Biol* 159, 855-866
64. Vaz, B., Halder, S., and Ramadan, K. (2013) Role of p97/VCP (Cdc48) in genome stability. *Front Genet* 4, 60
65. Baker, M., Mackenzie, I. R., Pickering-Brown, S. M., Gass, J., Rademakers, R., Lindholm, C., Snowden, J., Adamson, J., Sadovnick, A. D., Rollinson, S., Cannon, A., Dwosh, E., Neary, D., Melquist, S., Richardson, A., Dickson, D., Berger, Z., Eriksen, J., Robinson, T., Zehr, C., Dickey, C. A., Crook, R., McGowan, E., Mann, D., Boeve, B., Feldman, H., and Hutton, M. (2006) Mutations in progranulin cause tau-negative frontotemporal dementia linked to chromosome 17. *Nature* 442, 916-919
66. Cruts, M., Kumar-Singh, S., and Van Broeckhoven, C. (2006) Progranulin mutations in ubiquitin-positive frontotemporal dementia linked to chromosome 17q21. *Curr Alzheimer Res* 3, 485-491
67. Rademakers, R., Baker, M., Gass, J., Adamson, J., Huey, E. D., Momeni, P., Spina, S., Coppola, G., Karydas, A. M., Stewart, H., Johnson, N., Hsiung, G. Y., Kelley, B., Kuntz, K., Steinbart, E., Wood, E. M., Yu, C. E., Josephs, K., Sorenson, E., Womack, K. B., Weintraub, S., Pickering-Brown, S. M., Schofield, P. R., Brooks, W. S., Van Deerlin, V. M., Snowden, J., Clark, C. M., Kertesz, A., Boylan, K., Ghetti, B., Neary, D., Schellenberg, G. D., Beach, T. G., Mesulam, M., Mann, D., Grafman, J., Mackenzie, I. R., Feldman, H., Bird, T., Petersen, R., Knopman, D., Boeve, B., Geschwind, D. H., Miller, B., Wszolek, Z., Lippa, C., Bigio, E. H., Dickson, D., Graff-Radford, N., and Hutton, M. (2007) Phenotypic variability associated with progranulin haploinsufficiency in patients with the common 1477C-->T (Arg493X) mutation: an international initiative. *Lancet Neurol* 6, 857-868
68. Nicholson, A. M., Finch, N. A., and Rademakers, R. (2011) Human genetics as a tool to identify progranulin regulators. *J Mol Neurosci* 45, 532-537
69. Shankaran, S. S., Capell, A., Hruscha, A. T., Fellerer, K., Neumann, M., Schmid, B., and Haass, C. (2008) Missense mutations in the progranulin gene linked to frontotemporal lobar degeneration with ubiquitin-immunoreactive inclusions reduce progranulin production and secretion. *J Biol Chem* 283, 1744-1753
70. Wang, J., Van Damme, P., Cruchaga, C., Gitcho, M. A., Vidal, J. M., Seijo-Martinez, M., Wang, L., Wu, J. Y., Robberecht, W., and Goate, A. (2010) Pathogenic cysteine mutations affect progranulin function and production of mature granulins. *J Neurochem* 112, 1305-1315
71. Masellis, M., Momeni, P., Meschino, W., Heffner, R., Jr., Elder, J., Sato, C., Liang, Y., St George-Hyslop, P., Hardy, J., Bilbao, J., Black, S., and Rogaeva,

E. (2006) Novel splicing mutation in the progranulin gene causing familial corticobasal syndrome. *Brain* 129, 3115-3123
72. Kleinberger, G., Wils, H., Ponsaerts, P., Joris, G., Timmermans, J. P., Van Broeckhoven, C., and Kumar-Singh, S. (2010) Increased caspase activation and decreased TDP-43 solubility in progranulin knockout cortical cultures. *J Neurochem* 115, 735-747
73. Tolkatchev, D., Malik, S., Vinogradova, A., Wang, P., Chen, Z., Xu, P., Bennett, H. P., Bateman, A., and Ni, F. (2008) Structure dissection of human progranulin identifies well-folded granulin/epithelin modules with unique functional activities. *Protein Sci* 17, 711-724
74. Zhu, J., Nathan, C., Jin, W., Sim, D., Ashcroft, G. S., Wahl, S. M., Lacomis, L., Erdjument-Bromage, H., Tempst, P., Wright, C. D., and Ding, A. (2002) Conversion of proepithelin to epithelins: roles of SLPI and elastase in host defense and wound repair. *Cell* 111, 867-878
75. Kessenbrock, K., Frohlich, L., Sixt, M., Lammermann, T., Pfister, H., Bateman, A., Belaaouaj, A., Ring, J., Ollert, M., Fassler, R., and Jenne, D. E. (2008) Proteinase 3 and neutrophil elastase enhance inflammation in mice by inactivating antiinflammatory progranulin. *J Clin Invest* 118, 2438-2447
76. Butler, G. S., Dean, R. A., Tam, E. M., and Overall, C. M. (2008) Pharmacoproteomics of a metalloproteinase hydroxamate inhibitor in breast cancer cells: dynamics of membrane type 1 matrix metalloproteinase-mediated membrane protein shedding. *Mol Cell Biol* 28, 4896-4914
77. Bai, X. H., Wang, D. W., Kong, L., Zhang, Y., Luan, Y., Kobayashi, T., Kronenberg, H. M., Yu, X. P., and Liu, C. J. (2009) ADAMTS-7, a direct target of PTHrP, adversely regulates endochondral bone growth by associating with and inactivating GEP growth factor. *Mol Cell Biol* 29, 4201-4219
78. Hu, F., Padukkavidana, T., Vaegter, C. B., Brady, O. A., Zheng, Y., Mackenzie, I. R., Feldman, H. H., Nykjaer, A., and Strittmatter, S. M. (2010) Sortilin-mediated endocytosis determines levels of the frontotemporal dementia protein, progranulin. *Neuron* 68, 654-667
79. Zheng, Y., Brady, O. A., Meng, P. S., Mao, Y., and Hu, F. (2011) C-terminus of progranulin interacts with the beta-propeller region of sortilin to regulate progranulin trafficking. *PLoS One* 6, e21023
80. Martens, L. H., Zhang, J., Barmada, S. J., Zhou, P., Kamiya, S., Sun, B., Min, S. W., Gan, L., Finkbeiner, S., Huang, E. J., and Farese, R. V., Jr. (2012) Progranulin deficiency promotes neuroinflammation and neuron loss following toxin-induced injury. *J Clin Invest* 122, 3955-3959
81. Kumar-Singh, S. (2011) Progranulin and TDP-43: mechanistic links and future directions. *J Mol Neurosci* 45, 561-573
82. Tang, W., Lu, Y., Tian, Q. Y., Zhang, Y., Guo, F. J., Liu, G. Y., Syed, N. M., Lai, Y., Lin, E. A., Kong, L., Su, J., Yin, F., Ding, A. H., Zanin-Zhorov, A., Dustin, M. L., Tao, J., Craft, J., Yin, Z., Feng, J. Q., Abramson, S. B., Yu, X. P., and Liu, C. J. (2011) The growth factor progranulin binds to TNF receptors and is therapeutic against inflammatory arthritis in mice. *Science* 332, 478-484

83. Chen, X., Chang, J., Deng, Q., Xu, J., Nguyen, T. A., Martens, L. H., Cenik, B., Taylor, G., Hudson, K. F., Chung, J., Yu, K., Yu, P., Herz, J., Farese, R. V., Jr., Kukar, T., and Tansey, M. G. (2013) Progranulin does not bind tumor necrosis factor (TNF) receptors and is not a direct regulator of TNF-dependent signaling or bioactivity in immune or neuronal cells. *J Neurosci* 33, 9202-9213
84. He, Z., Ong, C. H., Halper, J., and Bateman, A. (2003) Progranulin is a mediator of the wound response. *Nat Med* 9, 225-229
85. Xu, J., Xilouri, M., Bruban, J., Shioi, J., Shao, Z., Papazoglou, I., Vekrellis, K., and Robakis, N. K. (2011) Extracellular progranulin protects cortical neurons from toxic insults by activating survival signaling. *Neurobiol Aging* 32, 2326 e2325-2316
86. Van Deerlin, V. M., Wood, E. M., Moore, P., Yuan, W., Forman, M. S., Clark, C. M., Neumann, M., Kwong, L. K., Trojanowski, J. Q., Lee, V. M., and Grossman, M. (2007) Clinical, genetic, and pathologic characteristics of patients with frontotemporal dementia and progranulin mutations. *Arch Neurol* 64, 1148-1153
87. Van Deerlin, V. M., Sleiman, P. M., Martinez-Lage, M., Chen-Plotkin, A., Wang, L. S., Graff-Radford, N. R., Dickson, D. W., Rademakers, R., Boeve, B. F., Grossman, M., Arnold, S. E., Mann, D. M., Pickering-Brown, S. M., Seelaar, H., Heutink, P., van Swieten, J. C., Murrell, J. R., Ghetti, B., Spina, S., Grafman, J., Hodges, J., Spillantini, M. G., Gilman, S., Lieberman, A. P., Kaye, J. A., Woltjer, R. L., Bigio, E. H., Mesulam, M., Al-Sarraj, S., Troakes, C., Rosenberg, R. N., White, C. L., 3rd, Ferrer, I., Llado, A., Neumann, M., Kretzschmar, H. A., Hulette, C. M., Welsh-Bohmer, K. A., Miller, B. L., Alzualde, A., Lopez de Munain, A., McKee, A. C., Gearing, M., Levey, A. I., Lah, J. J., Hardy, J., Rohrer, J. D., Lashley, T., Mackenzie, I. R., Feldman, H. H., Hamilton, R. L., Dekosky, S. T., van der Zee, J., Kumar-Singh, S., Van Broeckhoven, C., Mayeux, R., Vonsattel, J. P., Troncoso, J. C., Kril, J. J., Kwok, J. B., Halliday, G. M., Bird, T. D., Ince, P. G., Shaw, P. J., Cairns, N. J., Morris, J. C., McLean, C. A., DeCarli, C., Ellis, W. G., Freeman, S. H., Frosch, M. P., Growdon, J. H., Perl, D. P., Sano, M., Bennett, D. A., Schneider, J. A., Beach, T. G., Reiman, E. M., Woodruff, B. K., Cummings, J., Vinters, H. V., Miller, C. A., Chui, H. C., Alafuzoff, I., Hartikainen, P., Seilhean, D., Galasko, D., Masliah, E., Cotman, C. W., Tunon, M. T., Martinez, M. C., Munoz, D. G., Carroll, S. L., Marson, D., Riederer, P. F., Bogdanovic, N., Schellenberg, G. D., Hakonarson, H., Trojanowski, J. Q., and Lee, V. M. (2010) Common variants at 7p21 are associated with frontotemporal lobar degeneration with TDP-43 inclusions. *Nat Genet* 42, 234-239
88. Cruchaga, C., Graff, C., Chiang, H. H., Wang, J., Hinrichs, A. L., Spiegel, N., Bertelsen, S., Mayo, K., Norton, J. B., Morris, J. C., and Goate, A. (2011) Association of TMEM106B gene polymorphism with age at onset in granulin mutation carriers and plasma granulin protein levels. *Arch Neurol* 68, 581-586
89. Finch, N., Carrasquillo, M. M., Baker, M., Rutherford, N. J., Coppola, G., Dejesus-Hernandez, M., Crook, R., Hunter, T., Ghidoni, R., Benussi, L.,

Crook, J., Finger, E., Hantanpaa, K. J., Karydas, A. M., Sengdy, P., Gonzalez, J., Seeley, W. W., Johnson, N., Beach, T. G., Mesulam, M., Forloni, G., Kertesz, A., Knopman, D. S., Uitti, R., White, C. L., 3rd, Caselli, R., Lippa, C., Bigio, E. H., Wszolek, Z. K., Binetti, G., Mackenzie, I. R., Miller, B. L., Boeve, B. F., Younkin, S. G., Dickson, D. W., Petersen, R. C., Graff-Radford, N. R., Geschwind, D. H., and Rademakers, R. (2011) TMEM106B regulates *Neurology* 76, 467-474

90. van der Zee, J., Van Langenhove, T., Kleinberger, G., Sleegers, K., Engelborghs, S., Vandenberghe, R., Santens, P., Van den Broeck, M., Joris, G., Brys, J., Mattheijssens, M., Peeters, K., Cras, P., De Deyn, P. P., Cruts, M., and Van Broeckhoven, C. (2011) TMEM106B is associated with frontotemporal lobar degeneration in a clinically diagnosed patient cohort. *Brain* 134, 808-815
91. Wood, H. B. (2010) TMEM106B is a susceptibility locus for Ftld. *Nat Rev Neurol* 6, 184
92. Rutherford, N. J., Carrasquillo, M. M., Li, M., Bisceglio, G., Menke, J., Josephs, K. A., Parisi, J. E., Petersen, R. C., Graff-Radford, N. R., Younkin, S. G., Dickson, D. W., and Rademakers, R. (2012) TMEM106B risk variant is implicated in the pathologic presentation of Alzheimer disease. *Neurology* 79, 717-718
93. Vass, R., Ashbridge, E., Geser, F., Hu, W. T., Grossman, M., Clay-Falcone, D., Elman, L., McCluskey, L., Lee, V. M., Van Deerlin, V. M., Trojanowski, J. Q., and Chen-Plotkin, A. S. (2011) Risk genotypes at TMEM106B are associated with cognitive impairment in amyotrophic lateral sclerosis. *Acta Neuropathol* 121, 373-380
94. Lu, R. C., Wang, H., Tan, M. S., Yu, J. T., and Tan, L. (2013) TMEM106B and APOE polymorphisms interact to confer risk for late-onset Alzheimer's disease in Han Chinese. *J Neural Transm*
95. Lang, C. M., Fellerer, K., Schwenk, B. M., Kuhn, P. H., Kremmer, E., Edbauer, D., Capell, A., and Haass, C. (2012) Membrane orientation and subcellular localization of transmembrane protein 106B (TMEM106B), a major risk factor for frontotemporal lobar degeneration. *J Biol Chem* 287, 19355-19365
96. Chen-Plotkin, A. S., Unger, T. L., Gallagher, M. D., Bill, E., Kwong, L. K., Volpicelli-Daley, L., Busch, J. I., Akle, S., Grossman, M., Van Deerlin, V., Trojanowski, J. Q., and Lee, V. M. (2012) TMEM106B, the risk gene for frontotemporal dementia, is regulated by the microRNA-132/212 cluster and affects progranulin pathways. *J Neurosci* 32, 11213-11227
97. Nicholson, A. M., Finch, N. A., Wojtas, A., Baker, M. C., Perkerson, R. B., 3rd, Castanedes-Casey, M., Rousseau, L., Benussi, L., Binetti, G., Ghidoni, R., Hsiung, G. Y., Mackenzie, I. R., Finger, E., Boeve, B. F., Ertekin-Taner, N., Graff-Radford, N. R., Dickson, D. W., and Rademakers, R. (2013) TMEM106B p.T185S regulates TMEM106B protein levels: implications for frontotemporal dementia. *J Neurochem*

98. Brady, O. A., Zheng, Y., Murphy, K., Huang, M., and Hu, F. (2013) The frontotemporal lobar degeneration risk factor, TMEM106B, regulates lysosomal morphology and function. *Hum Mol Genet* 22, 685-695
99. Kwiatkowski, T. J., Jr., Bosco, D. A., Leclerc, A. L., Tamrazian, E., Vanderburg, C. R., Russ, C., Davis, A., Gilchrist, J., Kasarskis, E. J., Munsat, T., Valdmanis, P., Rouleau, G. A., Hosler, B. A., Cortelli, P., de Jong, P. J., Yoshinaga, Y., Haines, J. L., Pericak-Vance, M. A., Yan, J., Ticozzi, N., Siddique, T., McKenna-Yasek, D., Sapp, P. C., Horvitz, H. R., Landers, J. E., and Brown, R. H., Jr. (2009) Mutations in the FUS/TLS gene on chromosome 16 cause familial amyotrophic lateral sclerosis. *Science* 323, 1205-1208
100. Vance, C., Rogelj, B., Hortobagyi, T., De Vos, K. J., Nishimura, A. L., Sreedharan, J., Hu, X., Smith, B., Ruddy, D., Wright, P., Ganesalingam, J., Williams, K. L., Tripathi, V., Al-Saraj, S., Al-Chalabi, A., Leigh, P. N., Blair, I. P., Nicholson, G., de Belleroche, J., Gallo, J. M., Miller, C. C., and Shaw, C. E. (2009) Mutations in FUS, an RNA processing protein, cause familial amyotrophic lateral sclerosis type 6. *Science* 323, 1208-1211
101. Gardiner, M., Toth, R., Vandermoere, F., Morrice, N. A., and Rouse, J. (2008) Identification and characterization of FUS/TLS as a new target of ATM. *Biochem J* 415, 297-307
102. Lagier-Tourenne, C., Polymenidou, M., Hutt, K. R., Vu, A. Q., Baughn, M., Huelga, S. C., Clutario, K. M., Ling, S. C., Liang, T. Y., Mazur, C., Wancewicz, E., Kim, A. S., Watt, A., Freier, S., Hicks, G. G., Donohue, J. P., Shiue, L., Bennett, C. F., Ravits, J., Cleveland, D. W., and Yeo, G. W. (2012) Divergent roles of ALS-linked proteins FUS/TLS and TDP-43 intersect in processing long pre-mRNAs. *Nat Neurosci* 15, 1488-1497
103. Isaacs, A. M., Johannsen, P., Holm, I., and Nielsen, J. E. (2011) Frontotemporal dementia caused by CHMP2B mutations. *Curr Alzheimer Res* 8, 246-251
104. Fader, C. M., and Colombo, M. I. (2009) Autophagy and multivesicular bodies: two closely related partners. *Cell Death Differ* 16, 70-78
105. Raiborg, C., and Stenmark, H. (2009) The ESCRT machinery in endosomal sorting of ubiquitylated membrane proteins. *Nature* 458, 445-452
106. Lomen-Hoerth, C., Anderson, T., and Miller, B. (2002) The overlap of amyotrophic lateral sclerosis and frontotemporal dementia. *Neurology* 59, 1077-1079
107. Murphy, J. M., Henry, R. G., Langmore, S., Kramer, J. H., Miller, B. L., and Lomen-Hoerth, C. (2007) Continuum of frontal lobe impairment in amyotrophic lateral sclerosis. *Arch Neurol* 64, 530-534
108. Ringholz, G. M., Appel, S. H., Bradshaw, M., Cooke, N. A., Mosnik, D. M., and Schulz, P. E. (2005) Prevalence and patterns of cognitive impairment in sporadic ALS. *Neurology* 65, 586-590
109. Wheaton, M. W., Salamone, A. R., Mosnik, D. M., McDonald, R. O., Appel, S. H., Schmolck, H. I., Ringholz, G. M., and Schulz, P. E. (2007) Cognitive impairment in familial ALS. *Neurology* 69, 1411-1417

110. Laaksovirta, H., Peuralinna, T., Schymick, J. C., Scholz, S. W., Lai, S. L., Myllykangas, L., Sulkava, R., Jansson, L., Hernandez, D. G., Gibbs, J. R., Nalls, M. A., Heckerman, D., Tienari, P. J., and Traynor, B. J. (2010) Chromosome 9p21 in amyotrophic lateral sclerosis in Finland: a genome-wide association study. *Lancet Neurol* 9, 978-985
111. Shatunov, A., Mok, K., Newhouse, S., Weale, M. E., Smith, B., Vance, C., Johnson, L., Veldink, J. H., van Es, M. A., van den Berg, L. H., Robberecht, W., Van Damme, P., Hardiman, O., Farmer, A. E., Lewis, C. M., Butler, A. W., Abel, O., Andersen, P. M., Fogh, I., Silani, V., Chio, A., Traynor, B. J., Melki, J., Meininger, V., Landers, J. E., McGuffin, P., Glass, J. D., Pall, H., Leigh, P. N., Hardy, J., Brown, R. H., Jr., Powell, J. F., Orrell, R. W., Morrison, K. E., Shaw, P. J., Shaw, C. E., and Al-Chalabi, A. (2010) Chromosome 9p21 in sporadic amyotrophic lateral sclerosis in the UK and seven other countries: a genome-wide association study. *Lancet Neurol* 9, 986-994
112. van Es, M. A., Veldink, J. H., Saris, C. G., Blauw, H. M., van Vught, P. W., Birve, A., Lemmens, R., Schelhaas, H. J., Groen, E. J., Huisman, M. H., van der Kooi, A. J., de Visser, M., Dahlberg, C., Estrada, K., Rivadeneira, F., Hofman, A., Zwarts, M. J., van Doormaal, P. T., Rujescu, D., Strengman, E., Giegling, I., Muglia, P., Tomik, B., Slowik, A., Uitterlinden, A. G., Hendrich, C., Waibel, S., Meyer, T., Ludolph, A. C., Glass, J. D., Purcell, S., Cichon, S., Nothen, M. M., Wichmann, H. E., Schreiber, S., Vermeulen, S. H., Kiemeney, L. A., Wokke, J. H., Cronin, S., McLaughlin, R. L., Hardiman, O., Fumoto, K., Pasterkamp, R. J., Meininger, V., Melki, J., Leigh, P. N., Shaw, C. E., Landers, J. E., Al-Chalabi, A., Brown, R. H., Jr., Robberecht, W., Andersen, P. M., Ophoff, R. A., and van den Berg, L. H. (2009) Genome-wide association study identifies 19p13.3 (UNC13A) and 9p21.2 as susceptibility loci for sporadic amyotrophic lateral sclerosis. *Nat Genet* 41, 1083-1087
113. DeJesus-Hernandez, M., Mackenzie, I. R., Boeve, B. F., Boxer, A. L., Baker, M., Rutherford, N. J., Nicholson, A. M., Finch, N. A., Flynn, H., Adamson, J., Kouri, N., Wojtas, A., Sengdy, P., Hsiung, G. Y., Karydas, A., Seeley, W. W., Josephs, K. A., Coppola, G., Geschwind, D. H., Wszolek, Z. K., Feldman, H., Knopman, D. S., Petersen, R. C., Miller, B. L., Dickson, D. W., Boylan, K. B., Graff-Radford, N. R., and Rademakers, R. (2011) Expanded GGGGCC hexanucleotide repeat in noncoding region of C9ORF72 causes chromosome 9p-linked FTD and ALS. *Neuron* 72, 245-256
114. Renton, A. E., Majounie, E., Waite, A., Simon-Sanchez, J., Rollinson, S., Gibbs, J. R., Schymick, J. C., Laaksovirta, H., van Swieten, J. C., Myllykangas, L., Kalimo, H., Paetau, A., Abramzon, Y., Remes, A. M., Kaganovich, A., Scholz, S. W., Duckworth, J., Ding, J., Harmer, D. W., Hernandez, D. G., Johnson, J. O., Mok, K., Ryten, M., Trabzuni, D., Guerreiro, R. J., Orrell, R. W., Neal, J., Murray, A., Pearson, J., Jansen, I. E., Sondervan, D., Seelaar, H., Blake, D., Young, K., Halliwell, N., Callister, J. B., Toulson, G., Richardson, A., Gerhard, A., Snowden, J., Mann, D., Neary, D., Nalls, M. A., Peuralinna, T., Jansson, L., Isoviita, V. M., Kaivorinne, A. L., Holtta-

Vuori, M., Ikonen, E., Sulkava, R., Benatar, M., Wuu, J., Chio, A., Restagno, G., Borghero, G., Sabatelli, M., Heckerman, D., Rogaeva, E., Zinman, L., Rothstein, J. D., Sendtner, M., Drepper, C., Eichler, E. E., Alkan, C., Abdullaev, Z., Pack, S. D., Dutra, A., Pak, E., Hardy, J., Singleton, A., Williams, N. M., Heutink, P., Pickering-Brown, S., Morris, H. R., Tienari, P. J., and Traynor, B. J. (2011) A hexanucleotide repeat expansion in C9ORF72 is the cause of chromosome 9p21-linked ALS-FTD. *Neuron* 72, 257-268

115. Boeve, B. F., Boylan, K. B., Graff-Radford, N. R., DeJesus-Hernandez, M., Knopman, D. S., Pedraza, O., Vemuri, P., Jones, D., Lowe, V., Murray, M. E., Dickson, D. W., Josephs, K. A., Rush, B. K., Machulda, M. M., Fields, J. A., Ferman, T. J., Baker, M., Rutherford, N. J., Adamson, J., Wszolek, Z. K., Adeli, A., Savica, R., Boot, B., Kuntz, K. M., Gavrilova, R., Reeves, A., Whitwell, J., Kantarci, K., Jack, C. R., Jr., Parisi, J. E., Lucas, J. A., Petersen, R. C., and Rademakers, R. (2012) Characterization of frontotemporal dementia and/or amyotrophic lateral sclerosis associated with the GGGGCC repeat expansion in C9ORF72. *Brain* 135, 765-783
116. Cooper-Knock, J., Hewitt, C., Highley, J. R., Brockington, A., Milano, A., Man, S., Martindale, J., Hartley, J., Walsh, T., Gelsthorpe, C., Baxter, L., Forster, G., Fox, M., Bury, J., Mok, K., McDermott, C. J., Traynor, B. J., Kirby, J., Wharton, S. B., Ince, P. G., Hardy, J., and Shaw, P. J. (2012) Clinico-pathological features in amyotrophic lateral sclerosis with expansions in C9ORF72. *Brain* 135, 751-764
117. Hsiung, G. Y., DeJesus-Hernandez, M., Feldman, H. H., Sengdy, P., Bouchard-Kerr, P., Dwosh, E., Butler, R., Leung, B., Fok, A., Rutherford, N. J., Baker, M., Rademakers, R., and Mackenzie, I. R. (2012) Clinical and pathological features of familial frontotemporal dementia caused by C9ORF72 mutation on chromosome 9p. *Brain* 135, 709-722
118. Mahoney, C. J., Beck, J., Rohrer, J. D., Lashley, T., Mok, K., Shakespeare, T., Yeatman, T., Warrington, E. K., Schott, J. M., Fox, N. C., Rossor, M. N., Hardy, J., Collinge, J., Revesz, T., Mead, S., and Warren, J. D. (2012) Frontotemporal dementia with the C9ORF72 hexanucleotide repeat expansion: clinical, neuroanatomical and neuropathological features. *Brain* 135, 736-750
119. Snowden, J. S., Rollinson, S., Thompson, J. C., Harris, J. M., Stopford, C. L., Richardson, A. M., Jones, M., Gerhard, A., Davidson, Y. S., Robinson, A., Gibbons, L., Hu, Q., DuPlessis, D., Neary, D., Mann, D. M., and Pickering-Brown, S. M. (2012) Distinct clinical and pathological characteristics of frontotemporal dementia associated with C9ORF72 mutations. *Brain* 135, 693-708
120. Simon-Sanchez, J., Dopper, E. G., Cohn-Hokke, P. E., Hukema, R. K., Nicolaou, N., Seelaar, H., de Graaf, J. R., de Koning, I., van Schoor, N. M., Deeg, D. J., Smits, M., Raaphorst, J., van den Berg, L. H., Schelhaas, H. J., De Die-Smulders, C. E., Majoor-Krakauer, D., Rozemuller, A. J., Willemsen, R., Pijnenburg, Y. A., Heutink, P., and van Swieten, J. C. (2012) The clinical and pathological phenotype of C9ORF72 hexanucleotide repeat expansions. *Brain* 135, 723-735

121. Chio, A., Borghero, G., Restagno, G., Mora, G., Drepper, C., Traynor, B. J., Sendtner, M., Brunetti, M., Ossola, I., Calvo, A., Pugliatti, M., Sotgiu, M. A., Murru, M. R., Marrosu, M. G., Marrosu, F., Marinou, K., Mandrioli, J., Sola, P., Caponnetto, C., Mancardi, G., Mandich, P., La Bella, V., Spataro, R., Conte, A., Monsurro, M. R., Tedeschi, G., Pisano, F., Bartolomei, I., Salvi, F., Lauria Pinter, G., Simone, I., Logroscino, G., Gambardella, A., Quattrone, A., Lunetta, C., Volanti, P., Zollino, M., Penco, S., Battistini, S., Renton, A. E., Majounie, E., Abramzon, Y., Conforti, F. L., Giannini, F., Corbo, M., and Sabatelli, M. (2012) Clinical characteristics of patients with familial amyotrophic lateral sclerosis carrying the pathogenic GGGGCC hexanucleotide repeat expansion of C9ORF72. *Brain* 135, 784-793
122. Levine, T. P., Daniels, R. D., Gatta, A. T., Wong, L. H., and Hayes, M. J. (2013) The product of C9orf72, a gene strongly implicated in neurodegeneration, is structurally related to DENN Rab-GEFs. *Bioinformatics* 29, 499-503
123. Kim, H. J., Kim, N. C., Wang, Y. D., Scarborough, E. A., Moore, J., Diaz, Z., MacLea, K. S., Freibaum, B., Li, S., Molliex, A., Kanagaraj, A. P., Carter, R., Boylan, K. B., Wojtas, A. M., Rademakers, R., Pinkus, J. L., Greenberg, S. A., Trojanowski, J. Q., Traynor, B. J., Smith, B. N., Topp, S., Gkazi, A. S., Miller, J., Shaw, C. E., Kottlors, M., Kirschner, J., Pestronk, A., Li, Y. R., Ford, A. F., Gitler, A. D., Benatar, M., King, O. D., Kimonis, V. E., Ross, E. D., Weihl, C. C., Shorter, J., and Taylor, J. P. (2013) Mutations in prion-like domains in hnRNPA2B1 and hnRNPA1 cause multisystem proteinopathy and ALS. *Nature* 495, 467-473
124. Cox, L. E., Ferraiuolo, L., Goodall, E. F., Heath, P. R., Higginbottom, A., Mortiboys, H., Hollinger, H. C., Hartley, J. A., Brockington, A., Burness, C. E., Morrison, K. E., Wharton, S. B., Grierson, A. J., Ince, P. G., Kirby, J., and Shaw, P. J. (2010) Mutations in CHMP2B in lower motor neuron predominant amyotrophic lateral sclerosis (ALS). *PLoS One* 5, e9872
125. Parkinson, N., Ince, P. G., Smith, M. O., Highley, R., Skibinski, G., Andersen, P. M., Morrison, K. E., Pall, H. S., Hardiman, O., Collinge, J., Shaw, P. J., and Fisher, E. M. (2006) ALS phenotypes with mutations in CHMP2B (charged multivesicular body protein 2B). *Neurology* 67, 1074-1077
126. Kovacs, G. G., Murrell, J. R., Horvath, S., Haraszti, L., Majtenyi, K., Molnar, M. J., Budka, H., Ghetti, B., and Spina, S. (2009) TARDBP variation associated with frontotemporal dementia, supranuclear gaze palsy, and chorea. *Mov Disord* 24, 1843-1847
127. Gitcho, M. A., Bigio, E. H., Mishra, M., Johnson, N., Weintraub, S., Mesulam, M., Rademakers, R., Chakraverty, S., Cruchaga, C., Morris, J. C., Goate, A. M., and Cairns, N. J. (2009) TARDBP 3'-UTR variant in autopsy-confirmed frontotemporal lobar degeneration with TDP-43 proteinopathy. *Acta Neuropathol* 118, 633-645
128. Borroni, B., Bonvicini, C., Alberici, A., Buratti, E., Agosti, C., Archetti, S., Papetti, A., Stuani, C., Di Luca, M., Gennarelli, M., and Padovani, A. (2009)

Mutation within TARDBP leads to frontotemporal dementia without motor neuron disease. *Hum Mutat* 30, E974-983
129. Benajiba, L., Le Ber, I., Camuzat, A., Lacoste, M., Thomas-Anterion, C., Couratier, P., Legallic, S., Salachas, F., Hannequin, D., Decousus, M., Lacomblez, L., Guedj, E., Golfier, V., Camu, W., Dubois, B., Campion, D., Meininger, V., and Brice, A. (2009) TARDBP mutations in motoneuron disease with frontotemporal lobar degeneration. *Ann Neurol* 65, 470-473
130. Rubino, E., Rainero, I., Chio, A., Rogaeva, E., Galimberti, D., Fenoglio, P., Grinberg, Y., Isaia, G., Calvo, A., Gentile, S., Bruni, A. C., St George-Hyslop, P. H., Scarpini, E., Gallone, S., and Pinessi, L. (2012) SQSTM1 mutations in frontotemporal lobar degeneration and amyotrophic lateral sclerosis. *Neurology* 79, 1556-1562
131. Fecto, F., Yan, J., Vemula, S. P., Liu, E., Yang, Y., Chen, W., Zheng, J. G., Shi, Y., Siddique, N., Arrat, H., Donkervoort, S., Ajroud-Driss, S., Sufit, R. L., Heller, S. L., Deng, H. X., and Siddique, T. (2011) SQSTM1 mutations in familial and sporadic amyotrophic lateral sclerosis. *Arch Neurol* 68, 1440-1446
132. Deng, H. X., Chen, W., Hong, S. T., Boycott, K. M., Gorrie, G. H., Siddique, N., Yang, Y., Fecto, F., Shi, Y., Zhai, H., Jiang, H., Hirano, M., Rampersaud, E., Jansen, G. H., Donkervoort, S., Bigio, E. H., Brooks, B. R., Ajroud, K., Sufit, R. L., Haines, J. L., Mugnaini, E., Pericak-Vance, M. A., and Siddique, T. (2011) Mutations in UBQLN2 cause dominant X-linked juvenile and adult-onset ALS and ALS/dementia. *Nature* 477, 211-215
133. Synofzik, M., Maetzler, W., Grehl, T., Prudlo, J., Vom Hagen, J. M., Haack, T., Rebassoo, P., Munz, M., Schols, L., and Biskup, S. (2012) Screening in ALS and FTD patients reveals 3 novel UBQLN2 mutations outside the PXX domain and a pure FTD phenotype. *Neurobiol Aging* 33, 2949 e2913-2947
134. Douglas, P. M., and Dillin, A. (2010) Protein homeostasis and aging in neurodegeneration. *J Cell Biol* 190, 719-729
135. Korolchuk, V. I., Menzies, F. M., and Rubinsztein, D. C. (2010) Mechanisms of cross-talk between the ubiquitin-proteasome and autophagy-lysosome systems. *FEBS Lett* 584, 1393-1398
136. Ramaswami, M., Taylor, J. P., and Parker, R. (2013) Altered Ribostasis: RNA-Protein Granules in Degenerative Disorders. *Cell* 154, 727-736
137. Zhang, Y. J., Xu, Y. F., Cook, C., Gendron, T. F., Roettges, P., Link, C. D., Lin, W. L., Tong, J., Castanedes-Casey, M., Ash, P., Gass, J., Rangachari, V., Buratti, E., Baralle, F., Golde, T. E., Dickson, D. W., and Petrucelli, L. (2009) Aberrant cleavage of TDP-43 enhances aggregation and cellular toxicity. *Proc Natl Acad Sci U S A* 106, 7607-7612
138. Igaz, L. M., Kwong, L. K., Chen-Plotkin, A., Winton, M. J., Unger, T. L., Xu, Y., Neumann, M., Trojanowski, J. Q., and Lee, V. M. (2009) Expression of TDP-43 C-terminal Fragments in Vitro Recapitulates Pathological Features of TDP-43 Proteinopathies. *J Biol Chem* 284, 8516-8524
139. Zhang, Y. J., Gendron, T. F., Xu, Y. F., Ko, L. W., Yen, S. H., and Petrucelli, L. (2010) Phosphorylation regulates proteasomal-mediated degradation and

solubility of TAR DNA binding protein-43 C-terminal fragments. *Mol Neurodegener* 5, 33
140. Wils, H., Kleinberger, G., Janssens, J., Pereson, S., Joris, G., Cuijt, I., Smits, V., Ceuterick-de Groote, C., Van Broeckhoven, C., and Kumar-Singh, S. (2010) TDP-43 transgenic mice develop spastic paralysis and neuronal inclusions characteristic of ALS and frontotemporal lobar degeneration. *Proc Natl Acad Sci U S A* 107, 3858-3863
141. Johnson, B. S., McCaffery, J. M., Lindquist, S., and Gitler, A. D. (2008) A yeast TDP-43 proteinopathy model: Exploring the molecular determinants of TDP-43 aggregation and cellular toxicity. *Proc Natl Acad Sci U S A* 105, 6439-6444
142. Wang, X., Fan, H., Ying, Z., Li, B., Wang, H., and Wang, G. (2010) Degradation of TDP-43 and its pathogenic form by autophagy and the ubiquitin-proteasome system. *Neurosci Lett* 469, 112-116
143. Urushitani, M., Sato, T., Bamba, H., Hisa, Y., and Tooyama, I. (2010) Synergistic effect between proteasome and autophagosome in the clearance of polyubiquitinated TDP-43. *J Neurosci Res* 88, 784-797
144. Pesiridis, G. S., Lee, V. M., and Trojanowski, J. Q. (2009) Mutations in TDP-43 link glycine-rich domain functions to amyotrophic lateral sclerosis. *Hum Mol Genet* 18, R156-162
145. Luzio, J. P., Pryor, P. R., and Bright, N. A. (2007) Lysosomes: fusion and function. *Nat Rev Mol Cell Biol* 8, 622-632
146. Nixon, R. A., Yang, D. S., and Lee, J. H. (2008) Neurodegenerative lysosomal disorders: a continuum from development to late age. *Autophagy* 4, 590-599
147. Winchester, B., Vellodi, A., and Young, E. (2000) The molecular basis of lysosomal storage diseases and their treatment. *Biochem Soc Trans* 28, 150-154
148. Nixon, R. A. (2013) The role of autophagy in neurodegenerative disease. *Nat Med* 19, 983-997
149. Hara, T., Nakamura, K., Matsui, M., Yamamoto, A., Nakahara, Y., Suzuki-Migishima, R., Yokoyama, M., Mishima, K., Saito, I., Okano, H., and Mizushima, N. (2006) Suppression of basal autophagy in neural cells causes neurodegenerative disease in mice. *Nature* 441, 885-889
150. Fecto, F., and Siddique, T. (2012) UBQLN2/P62 cellular recycling pathways in amyotrophic lateral sclerosis and frontotemporal dementia. *Muscle Nerve* 45, 157-162
151. Walters, K. J., Kleijnen, M. F., Goh, A. M., Wagner, G., and Howley, P. M. (2002) Structural studies of the interaction between ubiquitin family proteins and proteasome subunit S5a. *Biochemistry* 41, 1767-1777
152. Kuusisto, E., Salminen, A., and Alafuzoff, I. (2001) Ubiquitin-binding protein p62 is present in neuronal and glial inclusions in human tauopathies and synucleinopathies. *Neuroreport* 12, 2085-2090
153. Al-Sarraj, S., King, A., Troakes, C., Smith, B., Maekawa, S., Bodi, I., Rogelj, B., Al-Chalabi, A., Hortobagyi, T., and Shaw, C. E. (2011) p62 positive, TDP-43 negative, neuronal cytoplasmic and intranuclear inclusions in the

cerebellum and hippocampus define the pathology of C9orf72-linked FTLD and MND/ALS. *Acta Neuropathol* 122, 691-702
154. Tanji, K., Zhang, H. X., Mori, F., Kakita, A., Takahashi, H., and Wakabayashi, K. (2012) p62/sequestosome 1 binds to TDP-43 in brains with frontotemporal lobar degeneration with TDP-43 inclusions. *J Neurosci Res* 90, 2034-2042
155. N'Diaye, E. N., Kajihara, K. K., Hsieh, I., Morisaki, H., Debnath, J., and Brown, E. J. (2009) PLIC proteins or ubiquilins regulate autophagy-dependent cell survival during nutrient starvation. *EMBO Rep* 10, 173-179
156. Bjorkoy, G., Lamark, T., Pankiv, S., Overvatn, A., Brech, A., and Johansen, T. (2009) Monitoring autophagic degradation of p62/SQSTM1. *Methods Enzymol* 452, 181-197
157. Bjorkoy, G., Lamark, T., Brech, A., Outzen, H., Perander, M., Overvatn, A., Stenmark, H., and Johansen, T. (2005) p62/SQSTM1 forms protein aggregates degraded by autophagy and has a protective effect on huntingtin-induced cell death. *J Cell Biol* 171, 603-614
158. Schwieger, I., Lautz, K., Krause, E., Rosenthal, W., Wiesner, B., and Hermosilla, R. (2008) Derlin-1 and p97/valosin-containing protein mediate the endoplasmic reticulum-associated degradation of human V2 vasopressin receptors. *Mol Pharmacol* 73, 697-708
159. Halawani, D., and Latterich, M. (2006) p97: The cell's molecular purgatory? *Mol Cell* 22, 713-717
160. Wojcik, C., Yano, M., and DeMartino, G. N. (2004) RNA interference of valosin-containing protein (VCP/p97) reveals multiple cellular roles linked to ubiquitin/proteasome-dependent proteolysis. *J Cell Sci* 117, 281-292
161. Jiang, N., Shen, Y., Fei, X., Sheng, K., Sun, P., Qiu, Y., Larner, J., Cao, L., Kong, X., and Mi, J. (2013) Valosin-containing protein regulates the proteasome-mediated degradation of DNA-PKcs in glioma cells. *Cell Death Dis* 4, e647
162. Tresse, E., Salomons, F. A., Vesa, J., Bott, L. C., Kimonis, V., Yao, T. P., Dantuma, N. P., and Taylor, J. P. (2010) VCP/p97 is essential for maturation of ubiquitin-containing autophagosomes and this function is impaired by mutations that cause IBMPFD. *Autophagy* 6, 217-227
163. Ju, J. S., Fuentealba, R. A., Miller, S. E., Jackson, E., Piwnica-Worms, D., Baloh, R. H., and Weihl, C. C. (2009) Valosin-containing protein (VCP) is required for autophagy and is disrupted in VCP disease. *J Cell Biol* 187, 875-888
164. Rodriguez-Ortiz, C. J., Hoshino, H., Cheng, D., Liu-Yescevitz, L., Blurton-Jones, M., Wolozin, B., LaFerla, F. M., and Kitazawa, M. (2013) Neuronal-specific overexpression of a mutant valosin-containing protein associated with IBMPFD promotes aberrant ubiquitin and TDP-43 accumulation and cognitive dysfunction in transgenic mice. *Am J Pathol* 183, 504-515
165. Ritz, D., Vuk, M., Kirchner, P., Bug, M., Schutz, S., Hayer, A., Bremer, S., Lusk, C., Baloh, R. H., Lee, H., Glatter, T., Gstaiger, M., Aebersold, R., Weihl, C. C., and Meyer, H. (2011) Endolysosomal sorting of ubiquitylated caveolin-

1 is regulated by VCP and UBXD1 and impaired by VCP disease mutations. *Nat Cell Biol* 13, 1116-1123
166. Zu, T., Gibbens, B., Doty, N. S., Gomes-Pereira, M., Huguet, A., Stone, M. D., Margolis, J., Peterson, M., Markowski, T. W., Ingram, M. A., Nan, Z., Forster, C., Low, W. C., Schoser, B., Somia, N. V., Clark, H. B., Schmechel, S., Bitterman, P. B., Gourdon, G., Swanson, M. S., Moseley, M., and Ranum, L. P. (2011) Non-ATG-initiated translation directed by microsatellite expansions. *Proc Natl Acad Sci U S A* 108, 260-265
167. Pearson, C. E. (2011) Repeat associated non-ATG translation initiation: one DNA, two transcripts, seven reading frames, potentially nine toxic entities! *PLoS Genet* 7, e1002018
168. Ash, P. E., Bieniek, K. F., Gendron, T. F., Caulfield, T., Lin, W. L., Dejesus-Hernandez, M., van Blitterswijk, M. M., Jansen-West, K., Paul, J. W., 3rd, Rademakers, R., Boylan, K. B., Dickson, D. W., and Petrucelli, L. (2013) Unconventional translation of C9ORF72 GGGGCC expansion generates insoluble polypeptides specific to c9FTD/ALS. *Neuron* 77, 639-646
169. Mori, K., Weng, S. M., Arzberger, T., May, S., Rentzsch, K., Kremmer, E., Schmid, B., Kretzschmar, H. A., Cruts, M., Van Broeckhoven, C., Haass, C., and Edbauer, D. (2013) The C9orf72 GGGGCC repeat is translated into aggregating dipeptide-repeat proteins in FTLD/ALS. *Science* 339, 1335-1338
170. Gijselinck, I., Van Langenhove, T., van der Zee, J., Sleegers, K., Philtjens, S., Kleinberger, G., Janssens, J., Bettens, K., Van Cauwenberghe, C., Pereson, S., Engelborghs, S., Sieben, A., De Jonghe, P., Vandenberghe, R., Santens, P., De Bleecker, J., Maes, G., Baumer, V., Dillen, L., Joris, G., Cuijt, I., Corsmit, E., Elinck, E., Van Dongen, J., Vermeulen, S., Van den Broeck, M., Vaerenberg, C., Mattheijssens, M., Peeters, K., Robberecht, W., Cras, P., Martin, J. J., De Deyn, P. P., Cruts, M., and Van Broeckhoven, C. (2012) A C9orf72 promoter repeat expansion in a Flanders-Belgian cohort with disorders of the frontotemporal lobar degeneration-amyotrophic lateral sclerosis spectrum: a gene identification study. *Lancet Neurol* 11, 54-65
171. Ciura, S., Lattante, S., Le Ber, I., Latouche, M., Tostivint, H., Brice, A., and Kabashi, E. (2013) Loss of function of C9orf72 causes motor deficits in a zebrafish model of Amyotrophic Lateral Sclerosis. *Ann Neurol*
172. Zhang, D., Iyer, L. M., He, F., and Aravind, L. (2012) Discovery of Novel DENN Proteins: Implications for the Evolution of Eukaryotic Intracellular Membrane Structures and Human Disease. *Front Genet* 3, 283
173. Wollert, T., Wunder, C., Lippincott-Schwartz, J., and Hurley, J. H. (2009) Membrane scission by the ESCRT-III complex. *Nature* 458, 172-177
174. Han, J. H., Ryu, H. H., Jun, M. H., Jang, D. J., and Lee, J. A. (2012) The functional analysis of the CHMP2B missense mutation associated with neurodegenerative diseases in the endo-lysosomal pathway. *Biochem Biophys Res Commun* 421, 544-549
175. Urwin, H., Authier, A., Nielsen, J. E., Metcalf, D., Powell, C., Froud, K., Malcolm, D. S., Holm, I., Johannsen, P., Brown, J., Fisher, E. M., van der Zee, J., Bruyland, M., Van Broeckhoven, C., Collinge, J., Brandner, S., Futter, C.,

and Isaacs, A. M. (2010) Disruption of endocytic trafficking in frontotemporal dementia with CHMP2B mutations. *Hum Mol Genet* 19, 2228-2238
176. van der Zee, J., Urwin, H., Engelborghs, S., Bruyland, M., Vandenberghe, R., Dermaut, B., De Pooter, T., Peeters, K., Santens, P., De Deyn, P. P., Fisher, E. M., Collinge, J., Isaacs, A. M., and Van Broeckhoven, C. (2008) CHMP2B C-truncating mutations in frontotemporal lobar degeneration are associated with an aberrant endosomal phenotype in vitro. *Hum Mol Genet* 17, 313-322
177. Filimonenko, M., Stuffers, S., Raiborg, C., Yamamoto, A., Malerod, L., Fisher, E. M., Isaacs, A., Brech, A., Stenmark, H., and Simonsen, A. (2007) Functional multivesicular bodies are required for autophagic clearance of protein aggregates associated with neurodegenerative disease. *J Cell Biol* 179, 485-500
178. Ghazi-Noori, S., Froud, K. E., Mizielinska, S., Powell, C., Smidak, M., Fernandez de Marco, M., O'Malley, C., Farmer, M., Parkinson, N., Fisher, E. M., Asante, E. A., Brandner, S., Collinge, J., and Isaacs, A. M. (2012) Progressive neuronal inclusion formation and axonal degeneration in CHMP2B mutant transgenic mice. *Brain* 135, 819-832
179. Belcastro, V., Siciliano, V., Gregoretti, F., Mithbaokar, P., Dharmalingam, G., Berlingieri, S., Iorio, F., Oliva, G., Polishchuck, R., Brunetti-Pierri, N., and di Bernardo, D. (2011) Transcriptional gene network inference from a massive dataset elucidates transcriptome organization and gene function. *Nucleic Acids Res* 39, 8677-8688
180. Sardiello, M., Palmieri, M., di Ronza, A., Medina, D. L., Valenza, M., Gennarino, V. A., Di Malta, C., Donaudy, F., Embrione, V., Polishchuk, R. S., Banfi, S., Parenti, G., Cattaneo, E., and Ballabio, A. (2009) A gene network regulating lysosomal biogenesis and function. *Science* 325, 473-477
181. Ahmed, Z., Sheng, H., Xu, Y. F., Lin, W. L., Innes, A. E., Gass, J., Yu, X., Wuertzer, C. A., Hou, H., Chiba, S., Yamanouchi, K., Leissring, M., Petrucelli, L., Nishihara, M., Hutton, M. L., McGowan, E., Dickson, D. W., and Lewis, J. (2010) Accelerated lipofuscinosis and ubiquitination in granulin knockout mice suggest a role for progranulin in successful aging. *Am J Pathol* 177, 311-324
182. Smith, K. R., Damiano, J., Franceschetti, S., Carpenter, S., Canafoglia, L., Morbin, M., Rossi, G., Pareyson, D., Mole, S. E., Staropoli, J. F., Sims, K. B., Lewis, J., Lin, W. L., Dickson, D. W., Dahl, H. H., Bahlo, M., and Berkovic, S. F. (2012) Strikingly different clinicopathological phenotypes determined by progranulin-mutation dosage. *Am J Hum Genet* 90, 1102-1107
183. Sephton, C. F., Cenik, C., Kucukural, A., Dammer, E. B., Cenik, B., Han, Y., Dewey, C. M., Roth, F. P., Herz, J., Peng, J., Moore, M. J., and Yu, G. (2011) Identification of neuronal RNA targets of TDP-43-containing ribonucleoprotein complexes. *J Biol Chem* 286, 1204-1215
184. Prudencio, M., Jansen-West, K. R., Lee, W. C., Gendron, T. F., Zhang, Y. J., Xu, Y. F., Gass, J., Stuani, C., Stetler, C., Rademakers, R., Dickson, D. W., Buratti, E., and Petrucelli, L. (2012) Misregulation of human sortilin splicing

leads to the generation of a nonfunctional progranulin receptor. *Proc Natl Acad Sci U S A* 109, 21510-21515
185. Armakola, M., Higgins, M. J., Figley, M. D., Barmada, S. J., Scarborough, E. A., Diaz, Z., Fang, X., Shorter, J., Krogan, N. J., Finkbeiner, S., Farese, R. V., Jr., and Gitler, A. D. (2012) Inhibition of RNA lariat debranching enzyme suppresses TDP-43 toxicity in ALS disease models. *Nat Genet* 44, 1302-1309
186. Donnelly, C. J., Zhang, P. W., Pham, J. T., Heusler, A. R., Mistry, N. A., Vidensky, S., Daley, E. L., Poth, E. M., Hoover, B., Fines, D. M., Maragakis, N., Tienari, P. J., Petrucelli, L., Traynor, B. J., Wang, J., Rigo, F., Bennett, C. F., Blackshaw, S., Sattler, R., and Rothstein, J. D. (2013) RNA Toxicity from the ALS/FTD C9ORF72 Expansion Is Mitigated by Antisense Intervention. *Neuron* 80, 415-428
187. Xu, Z., Poidevin, M., Li, X., Li, Y., Shu, L., Nelson, D. L., Li, H., Hales, C. M., Gearing, M., Wingo, T. S., and Jin, P. (2013) Expanded GGGGCC repeat RNA associated with amyotrophic lateral sclerosis and frontotemporal dementia causes neurodegeneration. *Proc Natl Acad Sci U S A* 110, 7778-7783
188. Mori, K., Lammich, S., Mackenzie, I. R., Forne, I., Zilow, S., Kretzschmar, H., Edbauer, D., Janssens, J., Kleinberger, G., Cruts, M., Herms, J., Neumann, M., Van Broeckhoven, C., Arzberger, T., and Haass, C. (2013) hnRNP A3 binds to GGGGCC repeats and is a constituent of p62-positive/TDP43-negative inclusions in the hippocampus of patients with C9orf72 mutations. *Acta Neuropathol* 125, 413-423
189. Li, H. Y., Yeh, P. A., Chiu, H. C., Tang, C. Y., and Tu, B. P. (2011) Hyperphosphorylation as a defense mechanism to reduce TDP-43 aggregation. *PLoS One* 6, e23075

CHAPTER 2

REGULATION OF TDP-43 AGGREGATION BY PHOSPHORYLATION AND p62/SQSTM1[1]

2.1 Summary

TAR DNA-binding protein-43 (TDP-43) proteinopathy has been linked to several neurodegenerative diseases, such as frontotemporal lobar degeneration with ubiquitin-positive inclusions and amyotrophic lateral sclerosis. Phosphorylated and ubiquitinated TDP-43 C-terminal fragments have been found in cytoplasmic inclusions in frontotemporal lobar degeneration with ubiquitin-positive inclusions and amyotrophic lateral sclerosis patients. However, the factors and pathways that regulate TDP-43 aggregation are still not clear. We found that the C-terminal 15 kDa fragment of TDP-43 is sufficient to induce aggregation but the aggregation phenotype is modified by additional sequences. Aggregation is accompanied by phosphorylation at serine residues 409/410. Mutation of 409/410 to phosphomimetic aspartic acid residues significantly reduces aggregation. Inhibition of either proteasome or autophagy dramatically increases TDP-43 aggregation. Furthermore, TDP-43 aggregates colocalize with markers of autophagy and the adaptor protein p62/SQSTM1. Over-expression of p62/SQSTM1 reduces TDP-43 aggregation in an autophagy and proteasome-dependent manner. These studies suggest that aggregation of TDP-43 C-terminal fragments is regulated by phosphorylation events and both the autophagy and proteasome-mediated degradation pathways.

[1]The results of this study were published in Brady OA, Meng P, Zheng Y, Mao Y, Hu F. *J. Neurochem*. 2011 Jan;116(2):248-59. P.M., and Y.Z. assisted with data collection and analysis. Y.M. performed secondary structure prediction and bioinformatic analysis F.H. generated the ATG5 knockdown cells and took immunofluorescence pictures containing FUS/TLS. All other experiments were performed by O.A.B. O.A.B. and F.H. wrote the manuscript.

2.2 Introduction

Abnormal protein aggregation has become a hallmark of neurodegeneration (Ross and Poirier 2004). TAR DNA-binding protein-43 (TDP-43), a protein involved in transcriptional repression and exon skipping, has emerged as a signature protein in the inclusions of a range of neurodegeneration related diseases, including frontotemporal lobar degeneration with ubiquitin-positive inclusions (FTLD-U), amyotrophic lateral sclerosis (ALS), and recently Alzheimer's and Huntington diseases (1-10). Mutations in the TDP-43 gene have also been genetically linked to ALS, suggesting that TDP-43 proteinopathy alone can cause neurodegeneration (11-14)

TDP-43 is a 43-kDa protein that contains two RNA recognition motifs (RRMs), and a glycine rich C-terminal region. Both a nuclear localization signal and nuclear export signal have been found in TDP-43, mediating its shuttling between nucleus and cytoplasm (15). Also, two potential caspase cleavage sites have been identified in TDP-43, which could generate the 35 and 25 kDa C-terminal fragments (16), although the TDP-43 fragments identified in disease patients do not exactly match the caspase-cleaved products (17,18). In patients with FTLD-U and ALS, the 25 kDa fragments of TDP-43 form cytoplasmic aggregates that are ubiquitinated and phosphorylated (1,19). Although the underlying mechanisms of TDP-43 proteinopathy are still under debate, toxicity resulting from aggregation of these fragments is thought to play an important

role in neurodegeneration involving TDP-43. Transgenic mice over-expressing wild type TDP-43 in neurons display a dose-dependent neurodegeneration phenotype, with the 25 kDa fragment aggregates present in the nucleus (20,21). Overexpression of the 35 and 25 kDa fragments in mammalian cells results in aggregation and cell death, suggesting that these fragments of TDP-43 are aggregation prone and mediate TDP-43 toxicity (22,23). However, the cellular pathways that mediate TDP-43 degradation and clearance are still not clear and cellular factors that regulate TDP-43 aggregates remain to be explored.

Here, we show that the C-terminal fragment of TDP-43 mediates its aggregation. The 15 kDa fragment at the C-terminus of TDP-43 is sufficient to induce TDP-43 aggregation but the aggregation phenotype is modified by additional sequences. When over-expressed in mammalian cells, the C-terminal TDP-43 fragments are phosphorylated at serine residues 409/410. Phosphorylation plays an imporant role in regulating the aggregation of TDP-43 fragments. Furthermore, we show that these fragments are subject to autophagy and proteasome-mediated degradation pathways regulated by the adaptor protein p62/SQSTM1. These findings could have important implications for TDP-43aggregation seen in many neurodegenerative diseases.

2.3 Materials and Methods

Antibodies

The following antibodies were used in our studies for western blot, immunoprecipitations, and immunofluorescence: rabbit anti-TDP-43 (ProteinTech, Chicago, IL, USA), rabbit anti-phospho TDP-43 pS409/410 (Cosmo Bio Co., Tokyo, Japan), mouse anti-green fluorescent protein (anti-GFP) (Covance, Princeton, NJ,

USA), rabbit anti-GFP antiserum (provided by Dr Anthony Bretscher and Dr Scott Emr), mouse anti-c-Myc clone 9E10 (Sigma, St Louis, MO, USA), mouse anti-HA.11 clone 16B12 (Covance), mouse anti- p62/SQSTM1 (BD Biosciences, San Jose, CA, USA), mouse anti-GAPDH (Novus Biologicals, Littleton, CO, USA), rabbit anti-ATG5 (Epitomics, Burlingame, CA, USA, and Novus Biologicals) and goat anti-LC3 (Santa Cruz Biotechnology, Santa Cruz, CA, USA).

Plasmids

Human TDP-43, mouse p62, and mouse FUS cDNAs in the pCMVSport6 vector were obtained from Open Biosystems (Huntsville, AL, USA). GFP-LC3 construct was obtained from Addgene (Cambridge, MA, USA).

All GFP-tagged TDP-43 constructs were subcloned into pEGFP-C1 (pEGFP-C1 was cut with BglII and SalI and ligated to fragments digested with BamHI and XhoI). Site-directed mutants were created using Quick change mutagenesis kit from Stratagene (La Jolla, CA, USA). Full-length TDP-43 was inserted into pcDNA 3.1/myc-His A with BamHI and XhoI. HA tagged FUS and p62 were generated in the pCMV-HA vector (Clontech, Mountain View, CA, USA) using EcoRI and BglII: FUS was inserted as two fragments with a 5' EcoR1 and 3' StuI site and a 5'StuI and 3' BamHI site; mouse p62 (accession no.: BC006019) was inserted as EcoR1 and BamHI digested fragment. Deletion constructs for p62 [p62 ΔUBA, aa1-357, and p62 ΔLIR (Δ323-344: QPEEQMESGNCSGGDDDWTHLS)] were cloned into pCMV-HA using EcoRI and BglII. mCherry-LC3 was generated by replacing enhanced green fluorescent protein (EGFP) with mCherry in the GFP-LC3 construct by using restriction sites NheI and XhoI. mCherry p62 and mCherry-FUS/TLS was created by

replacing LC3 with p62 or FUS/TLS coding sequence in the mCherry-LC3 plasmid by using restriction enzymes EcoRI and KpnI (FUS) or EcoRI and BamHI (p62).

The shRNA construct for mouse *Atg5* gene was created by annealing the following primers (5'-GATCCCCGGCATTATCCAATTGGTTTATTGGTTTATTC-AAGAGATAAACCAATTGGATAATGCCTTTTTA and 5'- TCGATAAAAAGGC-ATTATCCAATTGGTTTATCTCTTGAATAAACCAATTGGATAATGCCGGG) and ligating to the pSuperRetro vector (Oligoengine, Seattle, WA, USA) digested with BglII and XhoI. The target sequence was designed according to published shRNAs for mouse *Atg5* gene that showed effective knockdown (Amaravadi et al. 2007).

Cell culture and transfection

HEK293T, COS-7, NIH3T3 and N2A cells were grown in Dulbecco's modified Eagle's medium supplemented with 10% fetal bovine serum, 1% penicillin–streptomycin at 37º C in a 5% CO2 atmosphere. All cell lines were obtained from ATCC. Cells were transiently transfected with polyethlyeneimine as described (24). Stable N2A cells with pSuperRetro control or pSuperRetro-shRNA (*Atg5*) were selected with 2 µg/mL puromycin.

Immunofluorescence studies

Cells were fixed in 3.7% formaldehyde, 20% sucrose in phosphate buffered saline (PBS) for 15 min, permeabilized and blocked with 0.1% Triton X-100, 5% bovine serum albumin in PBS for 15 min, and incubated with primary antibody for 4 h at 20º C or overnight at 4º C. Secondary antibodies conjugated to Alexa Fluor-488 or -568 (1 : 500) (Invitrogen, Carlsbad, CA, USA) were then applied. Nuclei were stained with Hoechst or Syto63 (Invitrogen). Images were taken with an ImageXpress Micro

automated fluorescent microscope and analyzed with MetaXpress software (Molecular Devices, Palo Alto, CA, USA). For confocal microscopy, cells were plated on glass coverslips. Coverslips were mounted onto microscope slides with Fluoromount-G (Southern Biotech, Birmingham, AL, USA). Images were acquired either on an Intelligent Imaging Innovations CSU-X spinning disc microscope with 63X 1.4 NA objective and Photometrics Quant EM or HQ2 CCD camera. Images were acquired with a Nikon Eclipse TE-2000U microscope. Images were processed with Slidebook 5.0 (3i).

Cell fractionation

Sequential protein extractions were performed to separate protein extracts by solubility. Cells were washed with PBS, scraped and lysed in ice cold RIPA buffer (50 mM Tris pH 7.3, 150 mM NaCl, 1% Triton, 0.1% sodium dodecyl sulfate, 0.5% Deoxycholic acid, 1 mM EDTA) with protease and phosphatase inhibitors (Roche Complete Mini, EDTA-free Protease Inhibitor, 10 µM MG-132, 5 mM NaF, and 10 mM β-glycerol-phosphate). Cell lysates were centrifuged at 18 000 g for 15 min at 4º C and the supernatant saved as the RIPA soluble fraction. The RIPA-insoluble pellets were extracted with urea buffer (7 M urea, 4% 3-[(3-cholamidopro-pyl)dimethylammonio]-1-propanesulfonate, 30 mM Tris, pH 8.5) and centrifuged at 18 000 g for 15 min at 4º C and the supernatant was saved as the RIPA-insoluble, urea-soluble fraction.

Western Blot Analysis

Protein samples in sodium dodecyl sulfate sample buffer containing β-mercaptoethanol were boiled 10 min and centrifuged 1 min at 10,625 g. Samples were run on 12% polyacrylamide gels and transferred to Immobilon-FL polyvinylidene fluoride membranes (Millipore Corporation, Bedford, MA, USA). Membranes were blocked with 5% non-fat milk in PBS for 1 h followed by incubation with primary antibodies for 2 h at 20º C or overnight at 4º C. Membranes were washed for 5 min three times in Tris-buffered saline with 0.1% Tween-20, incubated with secondary antibody for 2 h at 20º C and washed three more times with Tris-buffered saline with 0.1% Tween-20. Blots were imaged using an Odyssey Infrared Imaging System (LI-COR Biosciences, Lincoln, NE, USA).

2.4 Results

TDP-43 C-terminal fragments are aggregation prone

In FTLD-U and ALS, TDP-43 is often cleaved to generate 25 kDa C-terminal fragments (1,19). These fragments are ubiquitinated, phosphorylated and are present in cytoplasmic inclusions. Secondary structure prediction indicates that the C-terminal glycine rich fragment (aa 267-414, 15 kDa) is non-structured and many mutations of TDP-43 linked to ALS have been mapped to this region (13,14). To establish a cellular TDP-43 aggregation model for further characterization, we made expression constructs of GFP fused to TDP-43 full length or C-terminal 35, 25 and 15 kDa fragments (CTD fragments) (Figure 2.1A). When expressed in HEK293T cells, GFP-TDP-43 full- length protein resides mostly in the nucleus with occasional nuclear

aggregates and cytoplasmic localization (Figure 2.1B). Around 8% of transfected cells expressing the 35 kDa fragment exhibit visible aggregates of ~4 µm in size, often close to the nucleus (Figures 2.1B and C). However, the 25 and 15 kDa fragments of TDP-43 readily form aggregates ranging from small punctuate structures to larger ones several micrometers in size (Figure 2.1B and C). About 28% of cells expressing the 25 kDa fragment exhibit large aggregates of ~7 µm in size, whereas 14% of cells expressing the 15 kDa fragment exhibit aggregates with an average size of ~4 µm. The 15 kDa expressing cells tend to have smaller but more aggregates per cell than the 25 kDa fragment (Figure 2.1C). Although cytoplasmic aggregates were observed most of the time, nuclear aggregates were also often detected when the 25 or 15 kDa TDP-43 fragments were over-expressed, suggesting that the aggregation can propagate into the nucleus under certain conditions. Distinct aggregation phenotypes were also seen when these fragments are over-expressed in COS-7 cells, with a dramatic aggregation phenotype of 25 and 15 kDa but minimal aggregation of the 35 kDa fragment (Figure S2.1A). These distinct aggregation phenotypes suggest that although the presence of the 15 kDa fragment is sufficient to cause aggregation, the presence of additional sequences could modify the characteristics of the aggregates formed. Similar aggregation phenotypes were also seen in the neuroblastoma cell lines M17 and N2A (our unpublished observation), although the percentage of aggregation observed was lower. This could be due to lower levels of protein expression in these cells.

Regulation of TDP-43 aggregation by phosphorylation

The TDP-43 C-terminal glycine rich region is enriched with serine residues and several antibodies specific for phosphorylated forms of TDP-43 have been developed

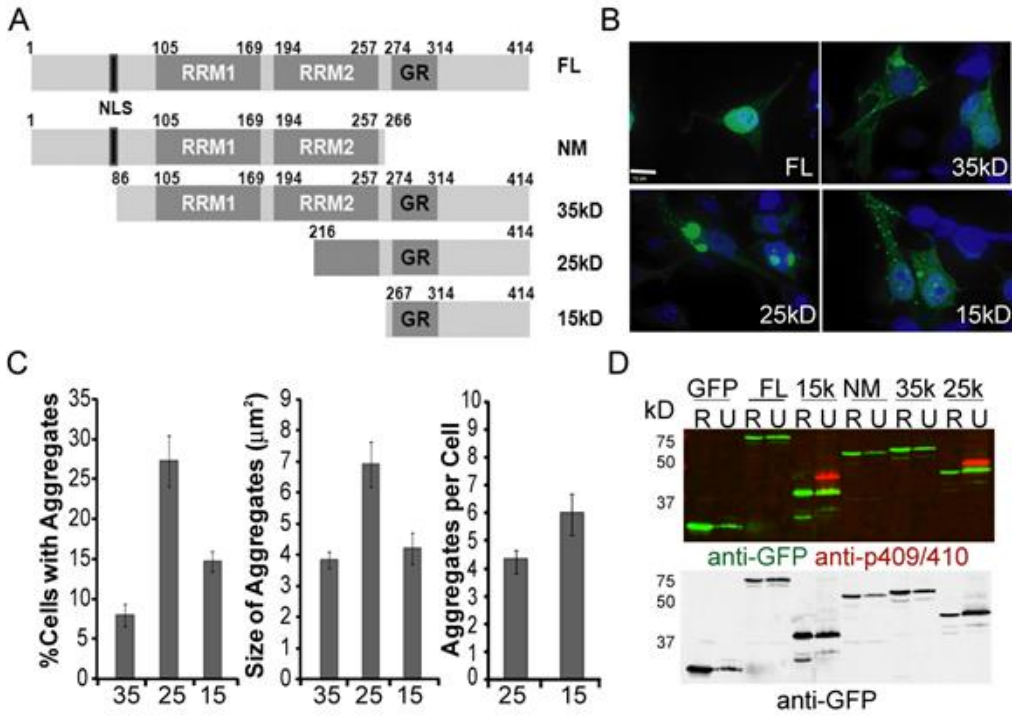

Figure 2.1: The residues 267–414 of TDP-43 (15 kDa fragment) are sufficient for aggregation. (a) Schematic representation of the constructs used in this study. All constructs used have an N-terminal EGFP tag unless otherwise noted. NM fragment appears much like FL (data not shown). (b) Confocal microscopy of HEK293T cells transfected with GFP fused TDP-43 constructs. Images were acquired 2 days after transfection. Scale bar = 10 lm. (c) Quantification of the average size of the aggregates and the number of cells exhibiting aggregates with the expression of the 35, 25, and 15 kDa fragments in HEK293T cells. The average number of aggregates per positively scored cell transfected with 25 and 15 kDa fragments was also quantified. Images were acquired using the ImageXpress system and analyzed using the MetaXpress software. (~1000-3000 cells counted per trial, mean ± SEM, n = 3–6). (d) The 25 and 15 kDa fragments of TDP-43 expressed in N2A cells are phosphorylated at serines 409/410 in the RIPA-insoluble urea soluble fraction. R, RIPA fraction; U, urea fraction. Similar results were seen in HEK293T and COS-7 cells.

(25,26). Casein kinase was shown to phosphorylate several serine residues in the glycine rich region of TDP-43 in vitro (27), although whether it is responsible for TDP-43 phosphorylation in vivo is still unclear. Phosphorylation of serines 409/410 were observed in FTLD-U patients (28,29), suggesting that TDP-43 phosphorylation could play a role in the disease mechanism. To determine whether aggregated TDP-43 fragments are phosphorylated, we fractionated cell lysates into RIPA-soluble (R) and urea-soluble (U) fractions. GFP-tagged TDP-43 full-length protein and 35, 25 and 15 kDa fragments expressed in N2A and COS-7 cells were detected in both RIPA and urea fractions, with the 25 and 15 kDa fragments showing increased insolubility in RIPA (Figure 2.1D and Figure S2.1B). We also found that the 25 and 15 kDa fragments expressed in these cells showed much more phosphorylation of serine 409/410 in the RIPA insoluble fraction than the full-length TDP-43 or the 35 kDa fragment when blotted with antibodies specific for phospho-409/410 (Figure 2.1D). This suggests that the level of phosphorylation is directly correlated with the degree of aggregation. Phospho-409/410 detected a band that migrates more slowly than the unphosphorylated form of TDP-43 (Figure 2.1D), indicating that additional phosphorylation or ubiquitination might be involved in the mobility shift. However, phosphorylated species only represent a small portion of RIPA-insoluble and urea-soluble proteins, even in the case of 25 and 15 kDa fragments (Figure 2.1D).

To determine the effect of phosphorylation on aggregate formation, we mutated serine residues at 409 and 410 (SS) to aspartic acid (DD) to mimic its phosphorylated state or to alanines (AA) to a non-phosphorylatable state. The AA mutant has a slightly reduced (by 15%) aggregation compared with wild-type (Figure 2.2A–C), suggesting

that phosphorylation is not an absolute requirement for aggregation. Surprisingly, we found that the phosphomimetic DD mutation dramatically reduces (by 60%) the aggregation of the 25 and 15 kDa fragments (Figure 2.2A–C). Biochemical fractionation revealed that the DD mutant is much more soluble in RIPA buffer than the wild-type and the AA mutant (Figure 2.2D and E). Similar results were found in N2A cells, although aggregation and insoluble protein levels were lower overall in N2A cells. These results indicate that phosphorylation could play a critical role in regulating aggregation.

TDP-43 aggregates are substrates of autophagy

The ubiquitin proteasome system and autophagy are the two main pathways for protein degradation in the cell. To determine which pathway is involved in clearing TDP-43 aggregates, we treated N2A and HEK293T cells expressing TDP-43 fragments with MG-132, an inhibitor of the 26S proteasome or 3-methyladenine (3-MA), a drug that inhibits the class III PI3-kinase, VPS34, which is required for autophagosome formation (30). Although MG-132 treatment led to an increase of TDP-43 aggregation compared with untreated control, the effect of 3-MA treatment was more pronounced, especially in the case of the 15 kDa fragment (Figure 2.3A). This suggests that autophagy might be the dominant pathway for clearing TDP-43 aggregates, especially for the 15 kDa fragment. Moreover, 3-MA treatment dramatically increased the buildup of the TDP-43 full-length protein and fragments in the RIPA insoluble fractions and the phosphorylation at 409/410 residues (Figure 2.3C and D). As 3-MA might have non-specific effects, we generated N2A cells stably expressing shRNAs against *Atg5*, a gene essential for autophagosome formation (31).

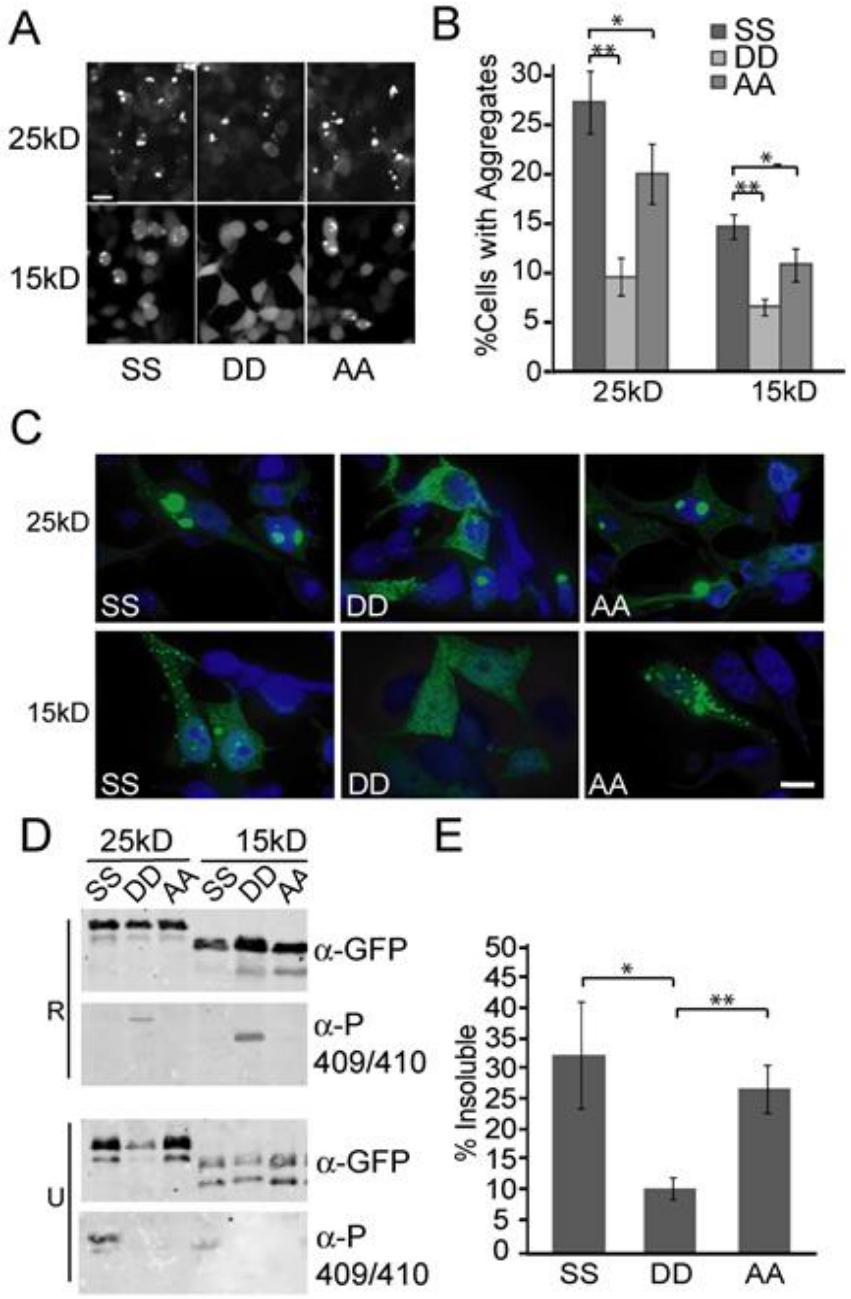
A
25kD
15kD
SS
DD
AA
B
%Cells with Aggregates
SS
DD
AA
25kD
15kD
C
25kD
15kD
SS
DD
AA
D
25kD
15kD
SS
DD
AA
α-GFP
α-P 409/410
R
U
E
% Insoluble
SS
DD
AA

Figure 2.2: Effects of phosphorylation on aggregation of TDP-43 fragments.
(**A**) Representative examples of HEK293T cells transfected with the 25 or 15 kDa fragment fused with GFP. Images were acquired using the ImagXpress system. Scale bar = 20 lm. (**B**) The S409D S410D (DD) and S409A S410A (AA) mutations reduce the aggregation of 15 and 25 kDa fragment in HEK293T cells. Cells were transfected with GFP-tagged TDP-43 fragments and percentages of cells with aggregates were scored 2 days after transfection using the ImageXpress imaging system. (~1000-2000 cells counted per trial, mean ± SEM, n = 6, *p < 0.05, **p < 0.01, paired Student's t-test). (**C**) Representative examples of HEK293T cells transfected with the 25 or15 kDa fragment. Images were acquired using confocal microscopy with nuclei in blue. Scale bar = 10 lm. (**D**) The DD mutant is more RIPA soluble than the SS and AA fragments. HEK293T cells transfected with various constructs as indicated were lysed 2 days after transfection and fractionated into RIPA (R) and urea (U) soluble fractions. The lysates were blotted with antibodies against GFP or phosphorylated 409/410. (**E**) Quantification of panel (**D**) was performed using densitometry with Odyssey Infrared Imaging software (for the 15 kDa fragment). Data were presented as the percentage of urea fraction of total protein (RIPA + urea fractions) (mean ± SEM, n = 3, *p < 0.05, **p < 0.01, paired Student's t-test).

Atg5 shRNA effectively reduced *Atg5* expression in N2A cells compared to control shRNA (Figure 2.3E), which resulted in a significantly increased aggregation of TDP-43 C-terminal fragments (Figure 2.3F). This result confirms a critical role of autophagy in clearing TDP-43 aggregates in all cell types, including neurons.

To further confirm the role of autophagy in TDP-43 regulation, we examined the colocalization of autophagy markers with the TDP-43 aggregates using confocal microscopy. We failed to detect the colocalization of small aggregates with ubiquitin or the autophagy marker LC3 (Figure 2.4A). However, it appears that at later stages of aggregation, the TDP-43 fragments get ubiquitinated and become substrates of autophagy. Colocalization of GFP tagged TDP-43 fragments with HA-ubiquitin and mCherrytagged LC3 was observed in larger aggregates that were irregularly shaped and had poorly defined edges compared with aggregates without ubiquitin and LC3 colocalization (Figure 2.4A and B). This may indicate that a critical size threshold must be reached before aggregates can be ubiquitinated and recognized by autophagy proteins. In most cases, biquitin and LC3 signals appeared like a shell surrounding the TDP-43 aggregates tagged with GFP, with the GFP signal becoming much dimmer in some cases. To avoid the potential problems of protein over-expression, we also examined the localization of endogenous ATG5 protein in the aggregates. Consistent with ubiquitin and LC3 localization, endogenous ATG5 forms a shell-like structure around the irregularly shaped aggregates (Figure 2.4C).

Reduction of TDP-43 aggregation by p62/SQSTM1 overexpression

UBA domain containing adaptor proteins play important roles in protein degradation (32). p62, also known as sequestosome 1 (SQSTM1), contains both a UBA domain

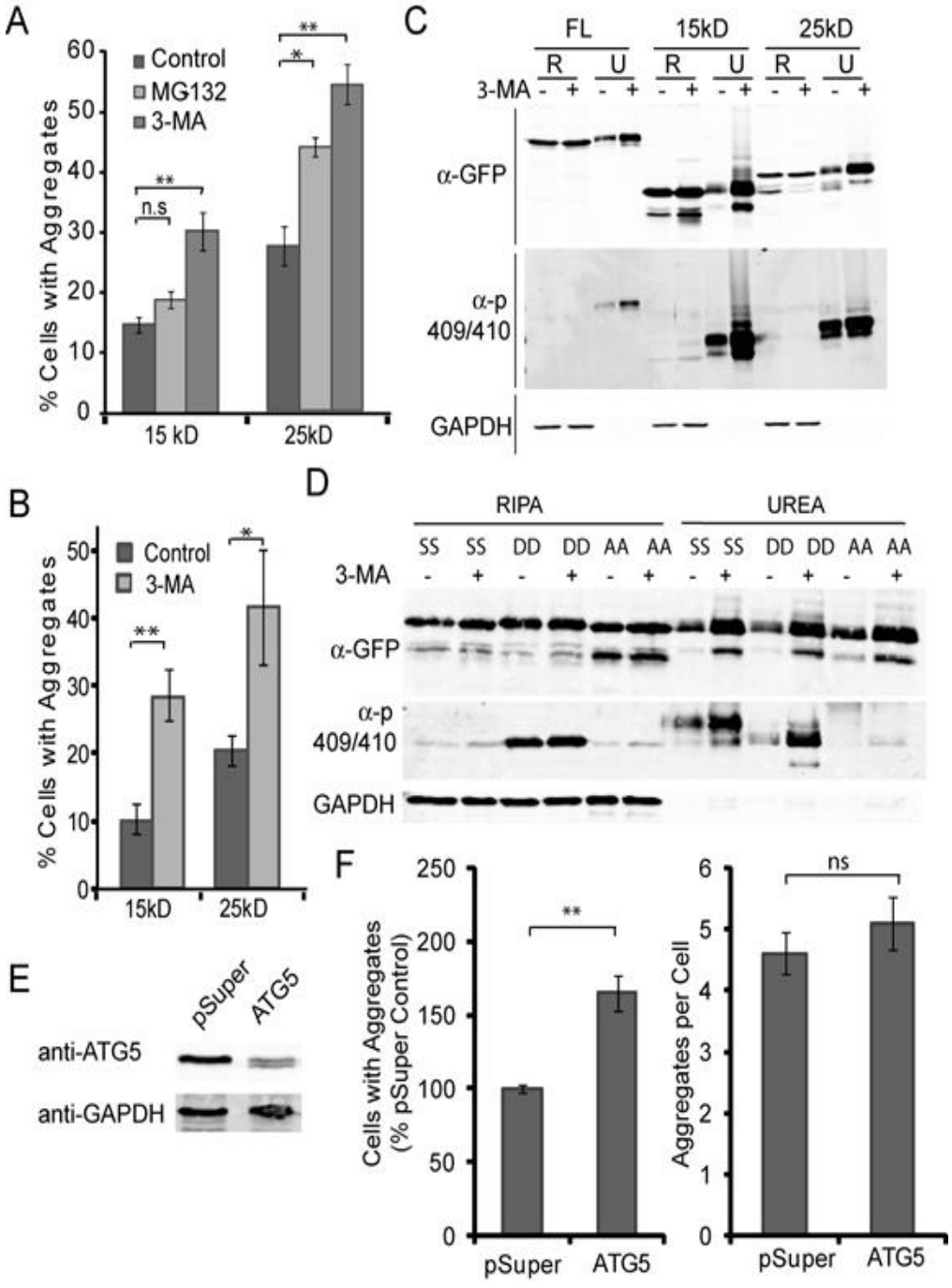
A
% Cells with Aggregates
Control
MG132
3-MA
n.s
**
*
15 kD
25kD
B
% Cells with Aggregates
Control
3-MA
15kD
25kD
C
FL
15kD
25kD
R
U
3-MA
α-GFP
α-p 409/410
GAPDH
D
RIPA
UREA
SS
DD
AA
3-MA
α-GFP
α-p 409/410
GAPDH
E
pSuper
ATG5
anti-ATG5
anti-GAPDH
F
Cells with Aggregates (% pSuper Control)
Aggregates per Cell
ns
pSuper
ATG5

Figure 2.3: Autophagy inhibition increases aggregate formation of TDP-43 C-terminal fragments.
(**A**) HEK293T cells transfected with GFP-tagged 25 and 15 kDa fragments exhibit increased aggregation when treated with a proteasome inhibitor (2 μM MG-132) and an autophagy inhibitor (10 mM 3-MA). Cells were treated 24 h after transfection for an additional 24 h with MG-132 or 3-MA (~1000-3000 cells counted per trial, mean ± SEM, n = 6, *p < 0.05, **p < 0.01, paired Student's t-test). (**B**) Autophagy inhibition in N2A cells also leads to accumulation of TDP-43 aggregates. N2A cells expressing GFP-tagged 25 or 15 kDa fragments were treated with 10 mM 3-MA for 24 h and the percentages of cells with aggregates were scored (> 400 cells scored per trial, mean ± SEM, n = 3, *p < 0.05, **p < 0.01). (**C**) Autophagy inhibition decreases the solubility of GFP-tagged TDP-43 proteins in N2A cells. N2A cells transfected with indicated constructs were treated with 10 mM 3-MA for 24 h and fractionated into RIPA (R) or urea (U) fraction. Phosphorylation at 409/410 is also increased in the presence of autophagy inhibition, as indicated by western blotting using phospho-specific antibodies. (**D**) Levels of the RIPA-insoluble, urea-soluble fraction of the 15 kDa mutants are increased under conditions of autophagy inhibition in N2A cells. N2A cells transfected with indicated constructs were treated with 10 mM 3-MA for 24 h and fractionated into R or U fraction. (**E**) Western blot of ATG5 protein in N2A cells stably expressing shRNAs against *Atg5* compared with pSuper control. (**F**) *Atg5* knockdown in N2A cells leads to increased aggregation of the 15 kDa fragment with no change in the average number of aggregates per cell. Images were acquired using the ImageXrpess system and analyzed using the Metaexpress software (~1000-2000 cells counted per trial, mean ± SEM, n = 3, **p < 0.01).

that can bind to ubiquitinated proteins and an LC3-interacting region (LIR) that can bind to LC3 and thus was proposed to be an adaptor protein for the autophagy pathway (33). To determine whether p62 is associated with TDP-43 aggregates, we performed confocal colocalization studies with antibodies to endogenous p62. Similar to our results with ubiquitin and LC3, we failed to detect a colocalization of the small aggregates with p62. However, the larger and irregularly shaped aggregates were positive for p62 staining (Figure 2.4D). The same results were seen with mCherry-tagged p62 (data not shown), but not with mCherry-tagged FUS/TLS (Figure S2.3), suggesting that the recruitment of p62 to TDP-43 aggregates is specific.

To delineate a function for p62 in TDP-43 aggregation, we determined the effect of p62 over-expression on TDP-43 solubility and aggregation. We found that over-expression of p62 in N2A cells leads to less insoluble TDP-43 or TDP-43 fragments (Figure 2.5A) and significantly less TDP-43 aggregation (Figure 2.5B), thus increased levels of p62 could reduce TDP-43 aggregation. In addition to targeting ubiquitinated substrates to autophagy, p62 has also been reported to shuttle protein cargoes to the proteasome (34,35). To determine whether p62 over-expression affects proteasome activity in our system, we examined the turnover of a reporter construct, global protein stability (GPS) (36). GPS contains EGFP fused with mutant of the ornithine decarboxylase degron (d1GFP) with a half-life of the GFP around 1 h. GPS also contains *Discosoma* red fluorescent protein (DsRed) expressed under the same promoter with d1GFP (DsRed-IRES-d1GFP), with DsRed serving as an internal control. When the GPS construct was expressed in N2A cells, MG-132 but not 3-MA

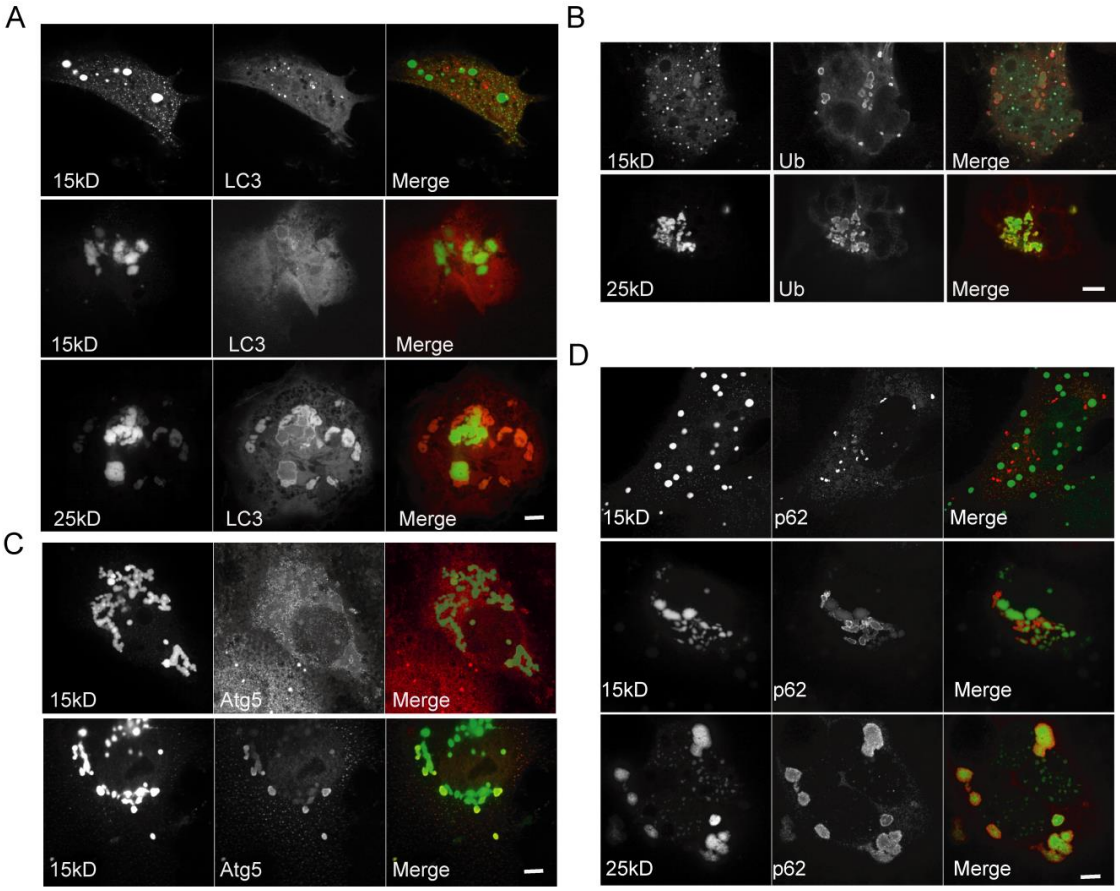

Figure 2.4: Colocalization of the 25 and 15 kDa fragments with autophagic markers and adaptor proteins in COS-7 cells.
(**A**) LC3, an autophagosomal membrane marker, forms a shell around the bigger 25 and 15 kDa TDP-43 aggregates, but is only sparsely associated with the smaller aggregates. COS-7 cells were co-tranfected with mCherry-LC3 and GFP-tagged TDP-43 fragments. Confocal images were acquired 2 days after transfection. (**B**) Ubiquitin forms a shell around the irregularly shaped aggregates of the 25 and 15 kDa fragments. Cells were co-transfected with HA-ubiquitin and GFP-TDP-43 fragments and stained with anti-HA antibodies. (**C**) The autophagy protein ATG5 also showed a shell-like structure around the big and irregular aggregates. Cells were transfected with GFP-TDP-43 fragments and stained for endogenous ATG5. (**D**) The adaptor protein p62 surrounds bigger aggregates of GFP-tagged TDP-43 fragments but is absent from the smaller aggregates. Cells were transfected with GFP-TDP-43 fragments and stained for endogenous p62. Images were taken using confocal microscope. Scale bar = 10 µm.

treatment led to robust accumulation of the GFP protein with DsRed unchanged, confirming that d1GFP protein level could be used as an indicator of proteasomal activity (Figure 2.5C). When p62 is over-expressed, the d1GFP signal was dramatically reduced, indicating that p62 over-expression does stimulate proteasomal activity (Figure 2.5C). We also examined the effect of p62 on autophagy using the modification of LC3-I to LC3-II as an indicator. LC3-II is the lipidated form of LC3 that associates with the autophagosome membrane. The ratio of LC3-II/I has been widely used as an indicator of autophagy activity (37). Over-expression of p62 in N2A cells led to more LC3-II, confirming that p62 over-expression also stimulates autophagy (Figure 2.5C). Thus, stimulation of both proteasomal and autophagy activity is likely to contribute to the effect of p62 over-expression on TDP-43 aggregates. To test this, we treated N2A cells expressing p62 and GFP-15 kDa fragments with MG-132 or 3-MA. Both treatments led to a significant increase of TDP-43 aggregates in the p62 over-expressed cells (Figure 2.5D), confirming that increase in both proteasome and autophagy activities is responsible for decreased TDP-43 aggregation when p62 is over-expressed. A role of autophagy in TDP-43 clearance in p62 over-expressing cells was also confirmed in N2A cells with *Atg5* expression knocked down with shRNAs. The effect of p62 on TDP-43 C-terminal aggregates was much reduced in *Atg5* shRNA expressing cells compared with control cells, although some p62 activity was still detectable, which is likely caused by the stimulation of proteasome activity by p62 (Figure 2.5E).

This result is further confirmed by examination of p62 deletion mutants. Over-expression of p62 mutants with the UBA or the LIR domain deleted (p62ΔUBA or

p62ΔLIR) resulted in a significantly reduced effect on TDP-43 aggregation compared with full-length p62, indicating that both domains are important for its activity (Figure S2.2). This effect of p62ΔUBA on TDP-43 aggregation also indicates that p62 might have ubiquitin-independent regulation of autophagy and possibly the proteasome pathway, as shown by other studies (38). Likewise, the effect of p62ΔLIR on TDP-43 aggregation is likely caused by stimulation of the proteasome pathway, as indicated by the results of the GPS assay (Figure 2.5C).

Aggregation of TDP-43 does not sequester FUS/TLS protein

Recently mutations in another RNA-binding protein FUS/TLS have also been genetically linked to ALS (39,40). Aggregates of FUS protein were also observed in ALS patients (39,40). Whether TDP-43 and FUS could co-aggregate is still under debate. Several studies suggested aggregates of TDP-43 and FUS occur in distinct patients (41,42), whereas other studies demonstrated co-aggregation of these two proteins (43-45). Physical and functional interactions of TDP-43 and FUS have also been reported (46,47). To determine whether FUS and TDP-43 could co-aggregate with each other in our cell-culture model, we co-expressed GFP-tagged TDP-43 25 kDa fragment with mCherry-tagged FUS. FUS remains in the nucleus in the presence of TDP-43 25 kDa fragment (Figure S2.3), indicating that TDP-43 aggregation does not affect the homeostasis of FUS. When FUS/TLS is over-expressed together with TDP-43 full-length protein or TDP-43 fragments, FUS does not affect the solubility of TDP-43 (Figure 2.5A), suggesting FUS and TDP-43 aggregation are independent of each other.

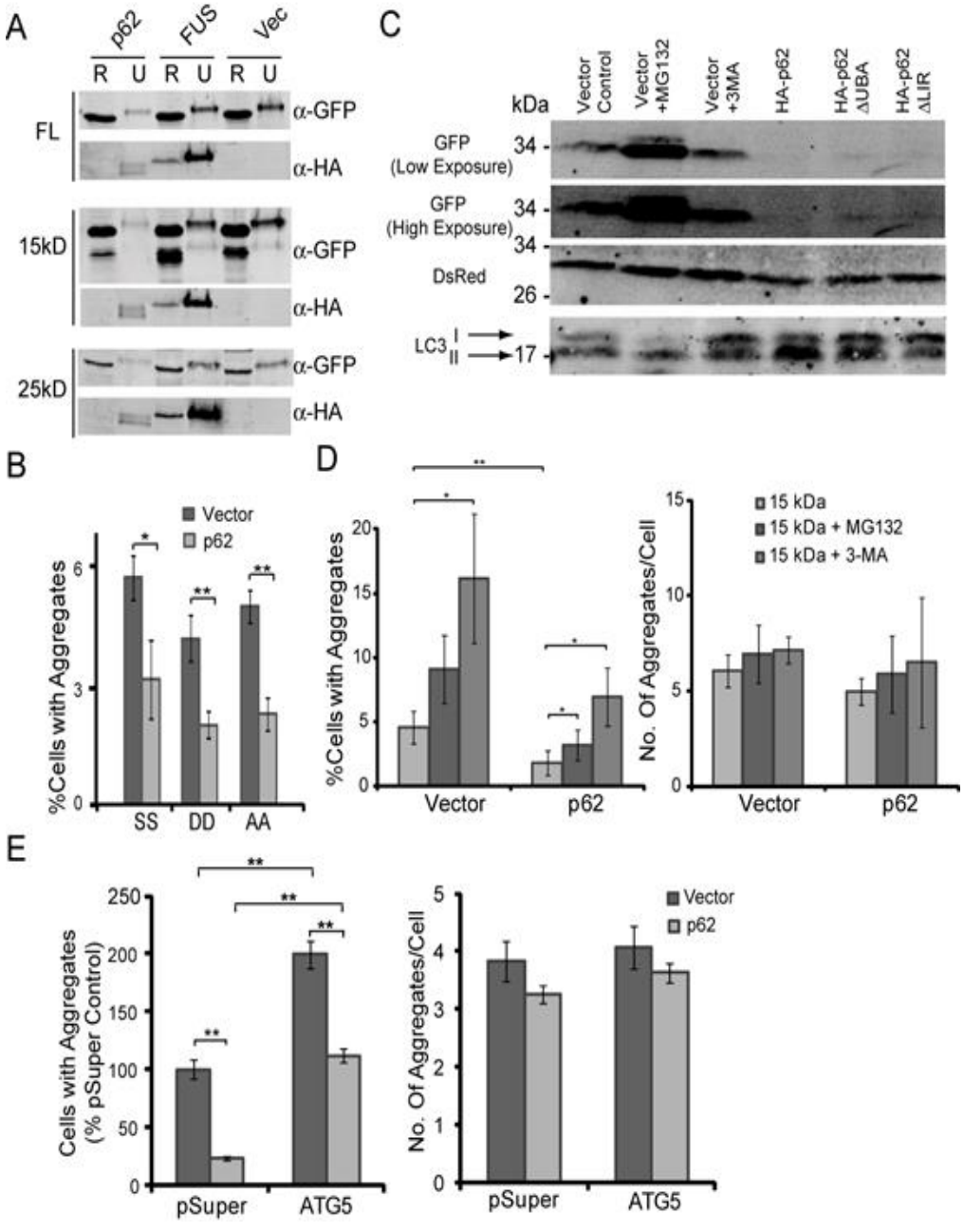
A
p62
FUS
Vec
R U R U R U
FL
α-GFP
α-HA
15kD
α-GFP
α-HA
25kD
α-GFP
α-HA
C
kDa
Vector Control
Vector +MG132
Vector +3MA
HA-p62
HA-p62 ΔUBA
HA-p62 ΔLIR
GFP (Low Exposure)
34
GFP (High Exposure)
34
34
DsRed
26
LC3 I
II
17
B
Vector
p62
%Cells with Aggregates
SS
DD
AA
D
%Cells with Aggregates
Vector
p62
15 kDa
15 kDa + MG132
15 kDa + 3-MA
No. Of Aggregates/Cell
Vector
p62
E
Cells with Aggregates (% pSuper Control)
pSuper
ATG5
Vector
p62
No. Of Aggregates/Cell
pSuper
ATG5

Figure 2.5: Over-expression of p62 decreases TDP-43 aggregation.
(**A**) p62 reduces the insoluble portion of full-length TDP-43, the 25 kDa fragment, and the 15 kDa in N2A cells. N2A cells were cotransfected with vector control (Vect), HA-p62 or HA-FUS together with GFP tagged TDP-43 constructs as indicated. Cell lysates were fractioned 2 days after transfection. (**B**) p62 over-expression decreases aggregate formation of the 15 kDa fragment and its mutants in N2A cells. Cells were co-transfected with GFP-15 kDa fragments or its mutants together with vector control or HA-p62. Aggregates were scored 2 days after transfection (> 400 cells counted per trial, mean ± SEM, n = 5, *p < 0.05, **p < 0.01). (**C**) Effect of p62 and its ΔUBA and ΔLIR mutants on proteasome and autophagy activity. N2A cells were co-transfected with the GPS-d1GFP construct and vector control, HA-p62 or p62 deletion mutants. Duplicates of vector transfected cells were treated with 10 μM MG-132 or 10 mM 3-MA for 24 h the next day after transfection. Cells were lysed in sodium dodecyl sulfate (SDS) sample buffer and blotted for GFP, DsRed or LC3 as indicated. (**D**) Both MG-132 and 3-MA lead to an increase in the percentage of cells with aggregates in N2A cells co-transfected with HA-p62 and the 15 kDa fragment. The average number of aggregates per positively scored cell did not change significantly under any of the conditions tested. Cells were treated for 24 h with 10 μM MG-132 or 10 mM 3-MA. Only live cells were counted (> 200 cells counted per trial, mean ± SEM, n = 3, *p < 0.05, **p < 0.01). (**E**) Knockdown of Atg5 expression reduces the effect of p62 expression on TDP-43 15 kDa fragment. N2A cells stably transfected with pSuper or pSuper-shRNA (*Atg5*) were co-transfected with HA-p62 and GFP-15 kDa. Images were acquired and analyzed two days later with the ImageXpress system. No significant changes were detected in the average number of aggregates per positively scored cell (~1000-2000 cells counted per trial, mean ± SEM, n = 3, *p < 0.05, **p < 0.01).

2.5 Discussion

Sequence determinant of TDP-43 aggregation

Our data suggest that the 15 kDa fragment of TDP-43 containing the glycine-rich region (aa 267–414) is sufficient to form aggregates when over-expressed as a GFP fusion protein in mammalian cells. This fragment of TDP-43 does not possess any recognizable secondary structure and thus is presumably non-structured. According to IUPRED, a software that predicts non-structured regions in proteins (48), amino acids 260–304 and 335–385 are predicted to be intrinsically unstructured regions. These correspond roughly to the glycine-rich domain and the C-terminal tail, both of which are part of the 15 kDa fragment used in these studies, which may correlate with the minimal sequence required for TDP-43 aggregation. This region has also been implicated in mediating interactions between TDP-43 and other RNAbinding proteins (49). It is possible that in full-length TDP-43, the 15 kDa fragment is buried inside of the protein or protein complex, and thus not exposed. Cleavage of TDP-43 into 25 kDa or smaller fragment may expose this aggregation prone fragment resulting in its aggregation. Although the 15 kDa fragment is sufficient to cause aggregation, the presence of additional sequences could change the aggregation rates and morphologies seen in the larger fragments. We have observed bigger and less numerous aggregates per cell formed by the 25 kDa fragment (Figure 2.1C), which has part of the second RRM motif in addition to the 15 kDa fragment. However, the 35 kDa fragment of TDP-43, which contains two intact RRM domains in addition to the 15 kDa region forms very few aggregates when over-expressed, indicative of a moderating effect of the two fully intact RRM domains on the extent of aggregation.

Regulation of TDP-43 aggregation by phosphorylation

TDP-43 aggregates seen in neurodegenerative diseases are often phosphorylated and ubiquitinated. Specifically, phosphorylation at serines 403/404 and 409/410 is observed in disease states (28,29). However, the role of phosphorylation and ubiquitination on TDP-43 aggregation is still not clear. Our data suggest the level of phosphorylation directly correlates with the degree of aggregation. The aggregation prone 25 and 15 kDa fragments have dramatic phosphorylation at 409/410 compared with the 35 kDa fragment and full-length protein, in direct correlation with the degree of aggregation these fragments exhibit (Figure 2.1D). 3-MA treatment increases aggregation of the 15 and 25 kDa fragments, which is accompanied by an increase in their phosphorylation (Figure 2.3C and D).

Our analysis of the DD and AA mutants also indicates an important role of phosphorylation in regulating aggregation. Although DD and AA mimic the charge of the phosphorylated and non-phosphorylatable form of TDP-43 CTD fragment, it is hard to judge whether they fully mimic the conformation of the phosphorylated and non-phosphorylated form. The fact that the DD mutant is recognized by phosphorylation specific antibody suggests that it mimics the phosphorylated state to some extent. The fact that the DD mutant mitigates ~60% of aggregate formation (Figure 2.2A and B) indeed suggests that having phosphorylated 409/410 when the protein is synthesized might reduce aggregation. We propose that phosphorylation happens after aggregation as a cellular attempt to reduce aggregation or prevent the formation of large aggregates, possibly by electrostatic repulsion. Having the negative charges conferred by aspartic acid residues in place of serine when the protein is

synthesized could significantly reduce initial aggregation formation or prevent the fusion of small aggregates into big aggregates, which has been demonstrated for TDP-43 fragments in cell culture (50). If phosphorylation of 409/410 prevents aggregation, it is puzzling that the AA mutant exhibits slightly reduced aggregation instead of having elevated aggregation. Several possible explanations exist. One possibility is that compensatory phosphorylation events, such as serine 403/404 could still take place in the AA mutant to prevent aggregation. The other possible explanation is that phosphorylation plays a dual role in regulating TDP-43 aggregation and clearance: (i) to reduce aggregation at early stage (in the case of the DD mutant); and (ii) to prevent clearance in the later stage. A recent study suggested that the phosphorylated form of TDP-43 CTD fragments are much harder to degrade than the nonphosphorylated form (50), consistent with the second model.

Regulation of TDP-43 clearance by proteasome and autophagy

The ubiquitin proteasome system and autophagy are the two main pathways for protein degradation and clearance. Autophagy is an intracellular degradation process which involves the formation of double-membrane autophagosomes around cytoplasmic components followed by fusion with lysosomes for degradation (30). Autophagy is responsible for the clearance of most long lived proteins, dysfunctional organelles and protein aggregates. Decreased autophagy has been implicated in various neurodegenerative disorders with protein aggregation. Autophagy deficiency in neurons in the neuron specific *Atg5* knockout mice causes a neurodegenerative phenotype (51). Induction of autophagy enhances the clearance of protein aggregates that cause neurodegeneration and confers cytoprotective roles in cell and animal

models (52). Many aggregation prone proteins implicated in neurodegeneration have been shown to be substrates for autophagy, including alpha synuclein and poly-glutamine expanded Huntington (52). Our data strongly suggest that TDP-43 aggregates are substrates of autophagy. We found inhibition of autophagy leads to increases in aggregation and insolubility of TDP-43 C-terminal fragments. Furthermore, inhibition of autophagy leads to relocalization of TDP-43 from the nucleus to cytoplasm (53,54) (Figure S2.4), suggesting that autophagy could regulate the balance of TDP-43 nuclearcytoplasmic shuttling. The proteasome-dependent degradation pathway also plays a role in clearing TDP-43 aggregates, because inhibition of proteasome function by MG-132 leads to increased TDP-43 aggregation as well, although not to the same extent as the autophagy inhibitor 3-MA (Figure 2.3A).

p62/SQSTM1is a multi-functional adaptor protein that could target ubiquitinated substrates to proteasome or autophagy for degradation (55). We found that over-expression of p62 decreases TDP-43 aggregation and p62 colocalizes with TDP-43 aggregates at later stages of aggregation. Furthermore, we showed p62 over-expression enhances both proteasome and autophagy activities (Figure 2.5C). Inhibition of either proteasome activity or autophagy activity reduces the effect of p62 overexpression on TDP-43 aggregation (Figure 2.5D and E). Deleting the UBA or LIR domain in p62 also affects the ability of p62 to reduce TDP-43 aggregation (Figure S2.2). These data implicate an important role of p62 in the clearance of TDP- 43 aggregates and further support the involvement of both proteasome and autophagy in the clearance of TDP-43 aggregates.

A model for TDP-43 aggregation and clearance

Taking our data together, we propose the following model for TDP-43 aggregation (Figure S2.5). Cleavage of TDP-43 generates aggregation prone 25 kDa and smaller fragments. These fragments form aggregates in a concentration-dependent manner. Phosphorylation happens as a result of initial aggregation as a cellular attempt to reduce aggregation. Ubiquitination occurs at a later stage of aggregation as a signal for proteasome or autophagy-mediated degradation. Subsequent binding and recruitment of p62 to the ubiquitinated TDP-43 aggregates allows degradation of the TDP-43 aggregates by either the proteasome or the autophagy pathway. More understanding of phosphorylation, ubiquitination and ubiquitin-binding proteins involved in the aggregation and clearance process will lead to a better view of TDP-43 aggregation and clearance, which is important for many neurodegenerative diseases with TDP-43 proteinopathy.

2.6 Acknowledgements

We thank Bret Judson for assistance with confocal imaging and members of Dr. Scott Emr, Dr. Anthony Bretscher and Dr. Ling Qi's laboratories for their kind help. We thank Dr. Stephen Elledge at Harvard University for the GPS construct. This work is supported by start up fund to F.H. from Weill Institute for Cell and Molecular Biology and by the Rosalinde and Arthur Gilbert Foundation/AFAR New Investigator Award. O.A.B is supported by the Biochemistry, Molecular and Cell Biology training grant.

2.7 Supplementary Information

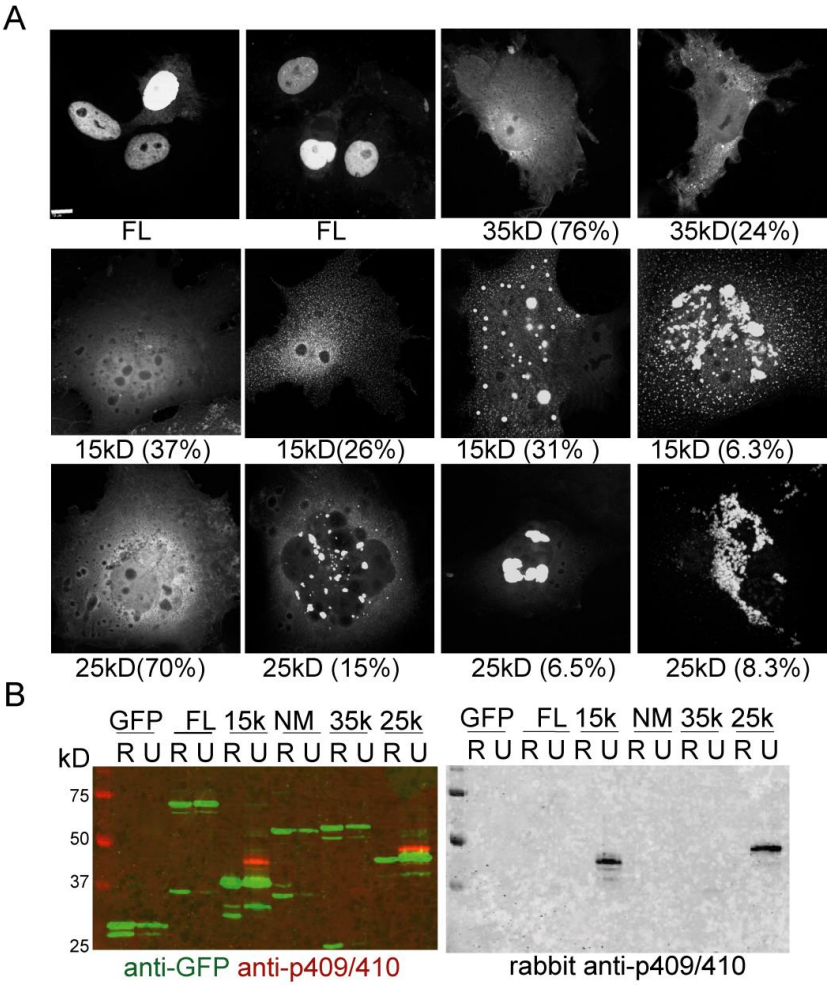

Figure S2.1: Aggregation of TDP-43 fragments in COS-7 cells.
(**A**) Examples of the full length (FL), 35 kDa, 25 kDa, and 15 kDa fragments of TDP-43 expressed as GFP fusion protein in COS-7 cells examined under confocal microscope. The frequency of various aggregation phenotypes is indicated. Scale bar = 10 µm. (**B**) The 25 kDa and 15 kDa fragments of TDP-43 expressed in COS-7 cells are phosphorylated at serines 409/410 in the RIPA insoluble urea soluble fraction. R: RIPA fraction; U: Urea fraction.

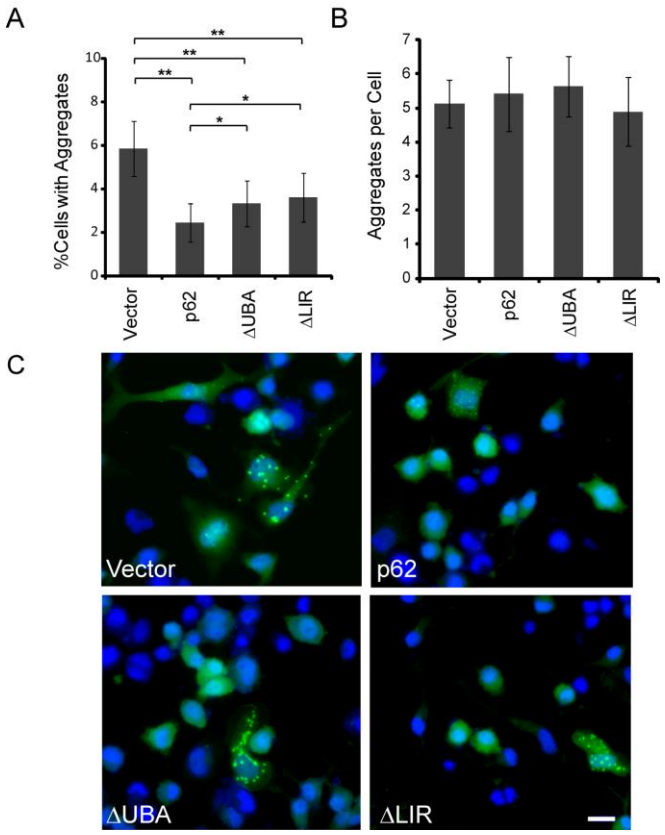

Figure S2.2: Overexpression of full length p62, p62ΔUBA or p62ΔLIR mutants decreases TDP-43 15kDa fragment aggregation. (**A**,**B**) N2A cells were co-transfected with the 15kDa fragment and vector control, HA-tagged p62 or p62 deletion mutants. Full length p62 more potently reduced the percentage of cells exhibiting aggregation than either the ΔUBA or ΔLIR mutant. No change was detected in the average number of aggregates per positively scored cell. (>200 cells counted per trial, mean+/-SEM, n = 3-4, *p<0.05, **p<0.01). (**C**) Representative examples of N2A cells co-transfected with the 15kDa fragment and either vector control, HA-tagged p62 or p62 ΔUBA and ΔLIR mutants. Images were acquired using the ImageXpress system.

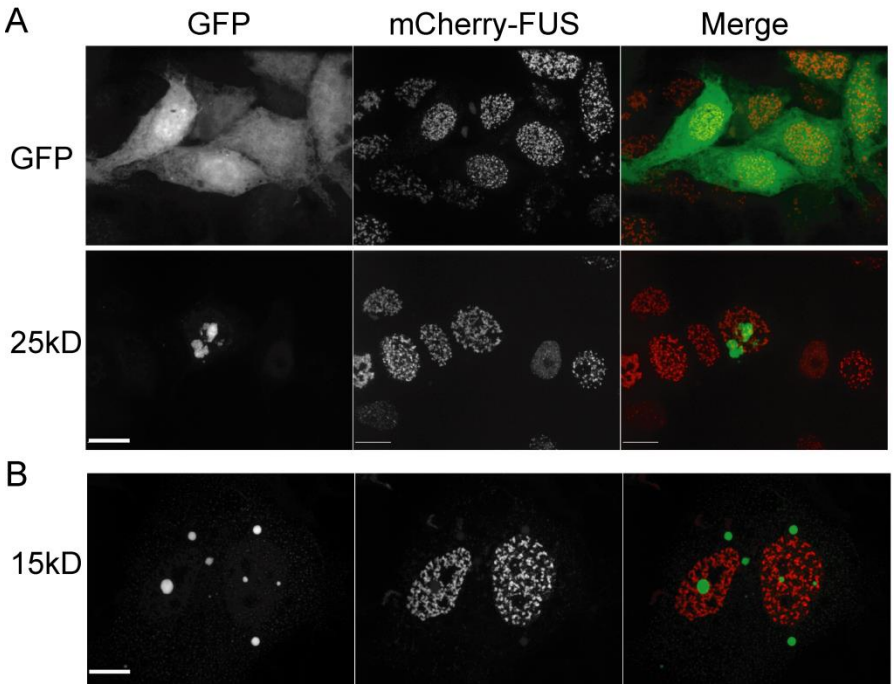

Figure S2.3: TDP-43 C-terminal aggregates do not sequester FUS/TLS. GFP-TDP-43-15kDa or 25 kDa fragment and mCherry tagged FUS/TLS were co-transfected into HEK293T cells (**A**) or COS-7 cells (**B**). Images were taken using confocal microscope. Scale bar=10 μm

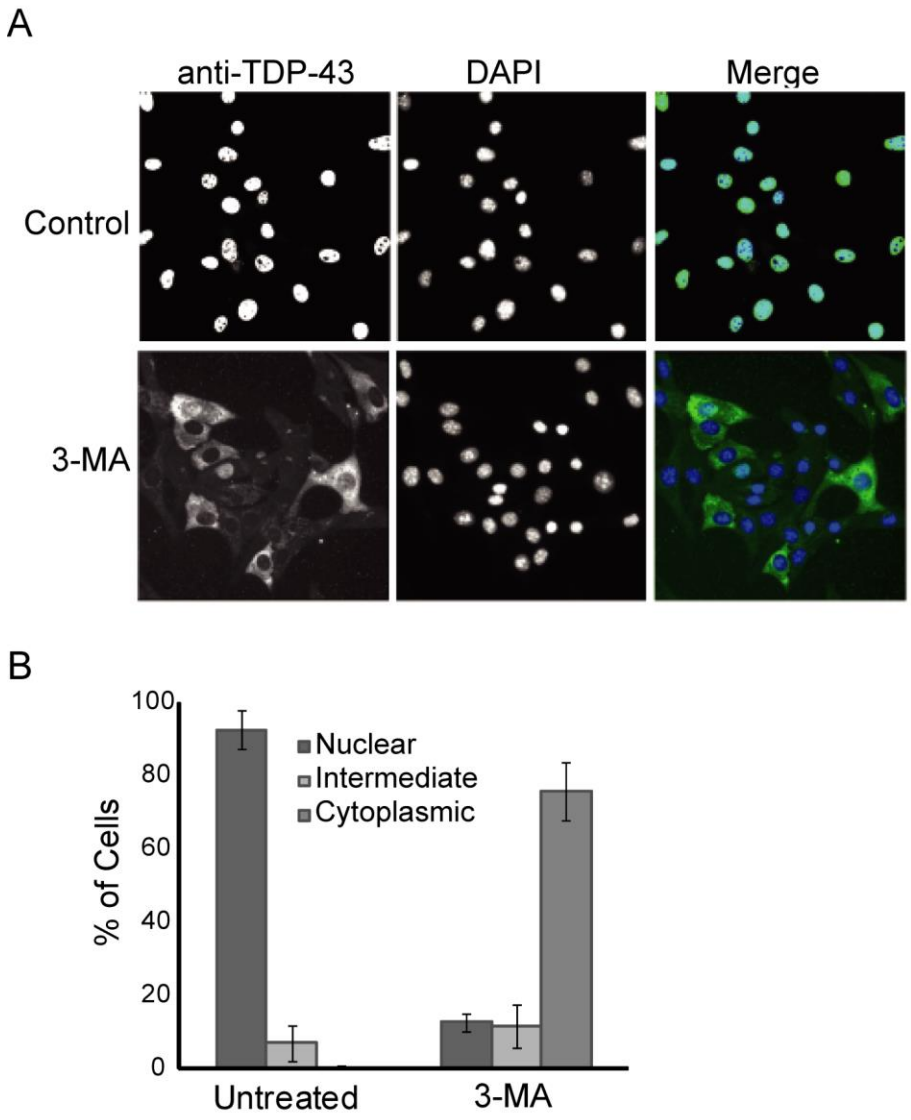

Figure S2.4: Autophagy inhibition results in shuttling of TDP-43 to the cytosol. (**A**) 3T3 cells were treated with 10mM 3-MA for 24 hours and stained with rabbit anti-TDP-43 antibodies. (**B**) Quantification of experiment in (**A**) (>1000 cells per trial, mean+/-SEM, n=3).

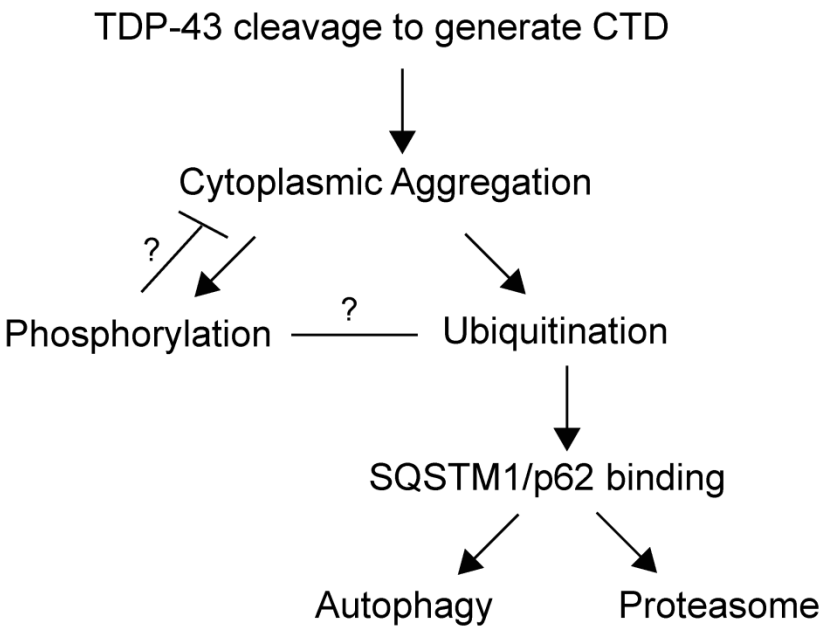

Figure S2.5: A model for the role of phosphorylation, ubiquitin, p62, autophagy and proteasome in regulating TDP-43 aggregation and clearance.

REFERENCES

1. Neumann, M., Sampathu, D. M., Kwong, L. K., Truax, A. C., Micsenyi, M. C., Chou, T. T., Bruce, J., Schuck, T., Grossman, M., Clark, C. M., McCluskey, L. F., Miller, B. L., Masliah, E., Mackenzie, I. R., Feldman, H., Feiden, W., Kretzschmar, H. A., Trojanowski, J. Q., and Lee, V. M. (2006) Ubiquitinated TDP-43 in frontotemporal lobar degeneration and amyotrophic lateral sclerosis. *Science* **314**, 130-133
2. Amador-Ortiz, C., Lin, W. L., Ahmed, Z., Personett, D., Davies, P., Duara, R., Graff-Radford, N. R., Hutton, M. L., and Dickson, D. W. (2007) TDP-43 immunoreactivity in hippocampal sclerosis and Alzheimer's disease. *Ann Neurol* **61**, 435-445
3. Buratti, E., and Baralle, F. E. (2008) Multiple roles of TDP-43 in gene expression, splicing regulation, and human disease. *Front Biosci* **13**, 867-878
4. Foulds, P., McAuley, E., Gibbons, L., Davidson, Y., Pickering-Brown, S. M., Neary, D., Snowden, J. S., Allsop, D., and Mann, D. M. (2008) TDP-43 protein in plasma may index TDP-43 brain pathology in Alzheimer's disease and frontotemporal lobar degeneration. *Acta Neuropathol* **116**, 141-146
5. Higashi, S., Iseki, E., Yamamoto, R., Minegishi, M., Hino, H., Fujisawa, K., Togo, T., Katsuse, O., Uchikado, H., Furukawa, Y., Kosaka, K., and Arai, H. (2007) Concurrence of TDP-43, tau and alpha-synuclein pathology in brains of Alzheimer's disease and dementia with Lewy bodies. *Brain Res* **1184**, 284-294
6. Jellinger, K. A. (2008) Neuropathological aspects of Alzheimer disease, Parkinson disease and frontotemporal dementia. *Neurodegener Dis* **5**, 118-121
7. Nakashima-Yasuda, H., Uryu, K., Robinson, J., Xie, S. X., Hurtig, H., Duda, J. E., Arnold, S. E., Siderowf, A., Grossman, M., Leverenz, J. B., Woltjer, R., Lopez, O. L., Hamilton, R., Tsuang, D. W., Galasko, D., Masliah, E., Kaye, J., Clark, C. M., Montine, T. J., Lee, V. M., and Trojanowski, J. Q. (2007) Co-morbidity of TDP-43 proteinopathy in Lewy body related diseases. *Acta Neuropathol* **114**, 221-229
8. Schwab, C., Arai, T., Hasegawa, M., Yu, S., and McGeer, P. L. (2008) Colocalization of transactivation-responsive DNA-binding protein 43 and huntingtin in inclusions of Huntington disease. *J Neuropathol Exp Neurol* **67**, 1159-1165
9. Uryu, K., Nakashima-Yasuda, H., Forman, M. S., Kwong, L. K., Clark, C. M., Grossman, M., Miller, B. L., Kretzschmar, H. A., Lee, V. M., Trojanowski, J. Q., and Neumann, M. (2008) Concomitant TAR-DNA-binding protein 43 pathology is present in Alzheimer disease and corticobasal degeneration but not in other tauopathies. *J Neuropathol Exp Neurol* **67**, 555-564
10. Wang, I. F., Wu, L. S., and Shen, C. K. (2008) TDP-43: an emerging new player in neurodegenerative diseases. *Trends Mol Med* **14**, 479-485
11. Kabashi, E., Valdmanis, P. N., Dion, P., Spiegelman, D., McConkey, B. J., Vande Velde, C., Bouchard, J. P., Lacomblez, L., Pochigaeva, K., Salachas, F., Pradat, P. F., Camu, W., Meininger, V., Dupre, N., and Rouleau, G. A. (2008)

TARDBP mutations in individuals with sporadic and familial amyotrophic lateral sclerosis. *Nat Genet* **40**, 572-574
12. Rutherford, N. J., Zhang, Y. J., Baker, M., Gass, J. M., Finch, N. A., Xu, Y. F., Stewart, H., Kelley, B. J., Kuntz, K., Crook, R. J., Sreedharan, J., Vance, C., Sorenson, E., Lippa, C., Bigio, E. H., Geschwind, D. H., Knopman, D. S., Mitsumoto, H., Petersen, R. C., Cashman, N. R., Hutton, M., Shaw, C. E., Boylan, K. B., Boeve, B., Graff-Radford, N. R., Wszolek, Z. K., Caselli, R. J., Dickson, D. W., Mackenzie, I. R., Petrucelli, L., and Rademakers, R. (2008) Novel mutations in TARDBP (TDP-43) in patients with familial amyotrophic lateral sclerosis. *PLoS Genet* **4**, e1000193
13. Sreedharan, J., Blair, I. P., Tripathi, V. B., Hu, X., Vance, C., Rogelj, B., Ackerley, S., Durnall, J. C., Williams, K. L., Buratti, E., Baralle, F., de Belleroche, J., Mitchell, J. D., Leigh, P. N., Al-Chalabi, A., Miller, C. C., Nicholson, G., and Shaw, C. E. (2008) TDP-43 mutations in familial and sporadic amyotrophic lateral sclerosis. *Science* **319**, 1668-1672
14. Yokoseki, A., Shiga, A., Tan, C. F., Tagawa, A., Kaneko, H., Koyama, A., Eguchi, H., Tsujino, A., Ikeuchi, T., Kakita, A., Okamoto, K., Nishizawa, M., Takahashi, H., and Onodera, O. (2008) TDP-43 mutation in familial amyotrophic lateral sclerosis. *Ann Neurol* **63**, 538-542
15. Winton, M. J., Igaz, L. M., Wong, M. M., Kwong, L. K., Trojanowski, J. Q., and Lee, V. M. (2008) Disturbance of nuclear and cytoplasmic TAR DNA-binding protein (TDP-43) induces disease-like redistribution, sequestration, and aggregate formation. *J Biol Chem* **283**, 13302-13309
16. Zhang, Y. J., Xu, Y. F., Dickey, C. A., Buratti, E., Baralle, F., Bailey, R., Pickering-Brown, S., Dickson, D., and Petrucelli, L. (2007) Progranulin mediates caspase-dependent cleavage of TAR DNA binding protein-43. *J Neurosci* **27**, 10530-10534
17. Igaz, L. M., Kwong, L. K., Chen-Plotkin, A., Winton, M. J., Unger, T. L., Xu, Y., Neumann, M., Trojanowski, J. Q., and Lee, V. M. (2009) Expression of TDP-43 C-terminal Fragments in Vitro Recapitulates Pathological Features of TDP-43 Proteinopathies. *J Biol Chem* **284**, 8516-8524
18. Nonaka, T., Kametani, F., Arai, T., Akiyama, H., and Hasegawa, M. (2009) Truncation and pathogenic mutations facilitate the formation of intracellular aggregates of TDP-43. *Hum Mol Genet* **18**, 3353-3364
19. Arai, T., Hasegawa, M., Akiyama, H., Ikeda, K., Nonaka, T., Mori, H., Mann, D., Tsuchiya, K., Yoshida, M., Hashizume, Y., and Oda, T. (2006) TDP-43 is a component of ubiquitin-positive tau-negative inclusions in frontotemporal lobar degeneration and amyotrophic lateral sclerosis. *Biochem Biophys Res Commun* **351**, 602-611
20. Wegorzewska, I., Bell, S., Cairns, N. J., Miller, T. M., and Baloh, R. H. (2009) TDP-43 mutant transgenic mice develop features of ALS and frontotemporal lobar degeneration. *Proc Natl Acad Sci U S A* **106**, 18809-18814
21. Wils, H., Kleinberger, G., Janssens, J., Pereson, S., Joris, G., Cuijt, I., Smits, V., Ceuterick-de Groote, C., Van Broeckhoven, C., and Kumar-Singh, S. (2010) TDP-43 transgenic mice develop spastic paralysis and neuronal

inclusions characteristic of ALS and frontotemporal lobar degeneration. *Proc Natl Acad Sci U S A* **107**, 3858-3863
22. Dormann, D., Capell, A., Carlson, A. M., Shankaran, S. S., Rodde, R., Neumann, M., Kremmer, E., Matsuwaki, T., Yamanouchi, K., Nishihara, M., and Haass, C. (2009) Proteolytic processing of TAR DNA binding protein-43 by caspases produces C-terminal fragments with disease defining properties independent of progranulin. *J Neurochem* **110**, 1082-1094
23. Zhang, Y. J., Xu, Y. F., Cook, C., Gendron, T. F., Roettges, P., Link, C. D., Lin, W. L., Tong, J., Castanedes-Casey, M., Ash, P., Gass, J., Rangachari, V., Buratti, E., Baralle, F., Golde, T. E., Dickson, D. W., and Petrucelli, L. (2009) Aberrant cleavage of TDP-43 enhances aggregation and cellular toxicity. *Proc Natl Acad Sci U S A* **106**, 7607-7612
24. Vancha, A. R., Govindaraju, S., Parsa, K. V., Jasti, M., Gonzalez-Garcia, M., and Ballestero, R. P. (2004) Use of polyethyleneimine polymer in cell culture as attachment factor and lipofection enhancer. *BMC Biotechnol* **4**, 23
25. Hasegawa, M., Arai, T., Nonaka, T., Kametani, F., Yoshida, M., Hashizume, Y., Beach, T. G., Buratti, E., Baralle, F., Morita, M., Nakano, I., Oda, T., Tsuchiya, K., and Akiyama, H. (2008) Phosphorylated TDP-43 in frontotemporal lobar degeneration and amyotrophic lateral sclerosis. *Ann Neurol* **64**, 60-70
26. Kadokura, A., Yamazaki, T., Kakuda, S., Makioka, K., Lemere, C. A., Fujita, Y., Takatama, M., and Okamoto, K. (2009) Phosphorylation-dependent TDP-43 antibody detects intraneuronal dot-like structures showing morphological characters of granulovacuolar degeneration. *Neurosci Lett* **463**, 87-92
27. Kametani, F., Nonaka, T., Suzuki, T., Arai, T., Dohmae, N., Akiyama, H., and Hasegawa, M. (2009) Identification of casein kinase-1 phosphorylation sites on TDP-43. *Biochem Biophys Res Commun* **382**, 405-409
28. Inukai, Y., Nonaka, T., Arai, T., Yoshida, M., Hashizume, Y., Beach, T. G., Buratti, E., Baralle, F. E., Akiyama, H., Hisanaga, S., and Hasegawa, M. (2008) Abnormal phosphorylation of Ser409/410 of TDP-43 in FTLD-U and ALS. *FEBS Lett* **582**, 2899-2904
29. Neumann, M., Kwong, L. K., Lee, E. B., Kremmer, E., Flatley, A., Xu, Y., Forman, M. S., Troost, D., Kretzschmar, H. A., Trojanowski, J. Q., and Lee, V. M. (2009) Phosphorylation of S409/410 of TDP-43 is a consistent feature in all sporadic and familial forms of TDP-43 proteinopathies. *Acta Neuropathol* **117**, 137-149
30. Yang, Z., and Klionsky, D. J. (2010) Mammalian autophagy: core molecular machinery and signaling regulation. *Curr Opin Cell Biol* **22**, 124-131
31. Geng, J., and Klionsky, D. J. (2008) The Atg8 and Atg12 ubiquitin-like conjugation systems in macroautophagy. 'Protein modifications: beyond the usual suspects' review series. *EMBO Rep* **9**, 859-864
32. Su, V., and Lau, A. F. (2009) Ubiquitin-like and ubiquitin-associated domain proteins: significance in proteasomal degradation. *Cell Mol Life Sci* **66**, 2819-2833

33. Pankiv, S., Clausen, T. H., Lamark, T., Brech, A., Bruun, J. A., Outzen, H., Overvatn, A., Bjorkoy, G., and Johansen, T. (2007) p62/SQSTM1 binds directly to Atg8/LC3 to facilitate degradation of ubiquitinated protein aggregates by autophagy. *J Biol Chem* **282**, 24131-24145
34. Babu, J. R., Geetha, T., and Wooten, M. W. (2005) Sequestosome 1/p62 shuttles polyubiquitinated tau for proteasomal degradation. *J Neurochem* **94**, 192-203
35. Seibenhener, M. L., Babu, J. R., Geetha, T., Wong, H. C., Krishna, N. R., and Wooten, M. W. (2004) Sequestosome 1/p62 is a polyubiquitin chain binding protein involved in ubiquitin proteasome degradation. *Mol Cell Biol* **24**, 8055-8068
36. Yen, H. C., and Elledge, S. J. (2008) Identification of SCF ubiquitin ligase substrates by global protein stability profiling. *Science* **322**, 923-929
37. Barth, S., Glick, D., and Macleod, K. F. (2010) Autophagy: assays and artifacts. *J Pathol* **221**, 117-124
38. Gal, J., Strom, A. L., Kwinter, D. M., Kilty, R., Zhang, J., Shi, P., Fu, W., Wooten, M. W., and Zhu, H. (2009) Sequestosome 1/p62 links familial ALS mutant SOD1 to LC3 via an ubiquitin-independent mechanism. *J Neurochem* **111**, 1062-1073
39. Kwiatkowski, T. J., Jr., Bosco, D. A., Leclerc, A. L., Tamrazian, E., Vanderburg, C. R., Russ, C., Davis, A., Gilchrist, J., Kasarskis, E. J., Munsat, T., Valdmanis, P., Rouleau, G. A., Hosler, B. A., Cortelli, P., de Jong, P. J., Yoshinaga, Y., Haines, J. L., Pericak-Vance, M. A., Yan, J., Ticozzi, N., Siddique, T., McKenna-Yasek, D., Sapp, P. C., Horvitz, H. R., Landers, J. E., and Brown, R. H., Jr. (2009) Mutations in the FUS/TLS gene on chromosome 16 cause familial amyotrophic lateral sclerosis. *Science* **323**, 1205-1208
40. Vance, C., Rogelj, B., Hortobagyi, T., De Vos, K. J., Nishimura, A. L., Sreedharan, J., Hu, X., Smith, B., Ruddy, D., Wright, P., Ganesalingam, J., Williams, K. L., Tripathi, V., Al-Saraj, S., Al-Chalabi, A., Leigh, P. N., Blair, I. P., Nicholson, G., de Belleroche, J., Gallo, J. M., Miller, C. C., and Shaw, C. E. (2009) Mutations in FUS, an RNA processing protein, cause familial amyotrophic lateral sclerosis type 6. *Science* **323**, 1208-1211
41. Baumer, D., Hilton, D., Paine, S. M., Turner, M. R., Lowe, J., Talbot, K., and Ansorge, O. (2010) Juvenile ALS with basophilic inclusions is a FUS proteinopathy with FUS mutations. *Neurology* **75**, 611-618
42. Fujita, Y., Fujita, S., Takatama, M., Ikeda, M., and Okamoto, K. (2011) Numerous FUS-positive inclusions in an elderly woman with motor neuron disease. *Neuropathology* **31**, 170-176
43. Cohen, N. R., Hammans, S. R., Macpherson, J., and Nicoll, J. A. (2011) New neuropathological findings in Unverricht-Lundborg disease: neuronal intranuclear and cytoplasmic inclusions. *Acta Neuropathol* **121**, 421-427
44. Deng, H. X., Zhai, H., Bigio, E. H., Yan, J., Fecto, F., Ajroud, K., Mishra, M., Ajroud-Driss, S., Heller, S., Sufit, R., Siddique, N., Mugnaini, E., and Siddique, T. (2010) FUS-immunoreactive inclusions are a common feature in

sporadic and non-SOD1 familial amyotrophic lateral sclerosis. *Ann Neurol* **67**, 739-748
45. Shan, X., Chiang, P. M., Price, D. L., and Wong, P. C. (2010) Altered distributions of Gemini of coiled bodies and mitochondria in motor neurons of TDP-43 transgenic mice. *Proc Natl Acad Sci U S A* **107**, 16325-16330
46. Kim, S. H., Shanware, N. P., Bowler, M. J., and Tibbetts, R. S. (2010) Amyotrophic lateral sclerosis-associated proteins TDP-43 and FUS/TLS function in a common biochemical complex to co-regulate HDAC6 mRNA. *J Biol Chem* **285**, 34097-34105
47. Ling, S. C., Albuquerque, C. P., Han, J. S., Lagier-Tourenne, C., Tokunaga, S., Zhou, H., and Cleveland, D. W. (2010) ALS-associated mutations in TDP-43 increase its stability and promote TDP-43 complexes with FUS/TLS. *Proc Natl Acad Sci U S A* **107**, 13318-13323
48. Dosztanyi, Z., Csizmok, V., Tompa, P., and Simon, I. (2005) The pairwise energy content estimated from amino acid composition discriminates between folded and intrinsically unstructured proteins. *J Mol Biol* **347**, 827-839
49. Buratti, E., Brindisi, A., Giombi, M., Tisminetzky, S., Ayala, Y. M., and Baralle, F. E. (2005) TDP-43 binds heterogeneous nuclear ribonucleoprotein A/B through its C-terminal tail: an important region for the inhibition of cystic fibrosis transmembrane conductance regulator exon 9 splicing. *J Biol Chem* **280**, 37572-37584
50. Zhang, Y. J., Gendron, T. F., Xu, Y. F., Ko, L. W., Yen, S. H., and Petrucelli, L. (2010) Phosphorylation regulates proteasomal-mediated degradation and solubility of TAR DNA binding protein-43 C-terminal fragments. *Mol Neurodegener* **5**, 33
51. Hara, T., Nakamura, K., Matsui, M., Yamamoto, A., Nakahara, Y., Suzuki-Migishima, R., Yokoyama, M., Mishima, K., Saito, I., Okano, H., and Mizushima, N. (2006) Suppression of basal autophagy in neural cells causes neurodegenerative disease in mice. *Nature* **441**, 885-889
52. Garcia-Arencibia, M., Hochfeld, W. E., Toh, P. P., and Rubinsztein, D. C. (2010) Autophagy, a guardian against neurodegeneration. *Semin Cell Dev Biol* **21**, 691-698
53. Filimonenko, M., Stuffers, S., Raiborg, C., Yamamoto, A., Malerod, L., Fisher, E. M., Isaacs, A., Brech, A., Stenmark, H., and Simonsen, A. (2007) Functional multivesicular bodies are required for autophagic clearance of protein aggregates associated with neurodegenerative disease. *J Cell Biol* **179**, 485-500
54. Ju, J. S., Fuentealba, R. A., Miller, S. E., Jackson, E., Piwnica-Worms, D., Baloh, R. H., and Weihl, C. C. (2009) Valosin-containing protein (VCP) is required for autophagy and is disrupted in VCP disease. *J Cell Biol* **187**, 875-888
55. Seibenhener, M. L., Geetha, T., and Wooten, M. W. (2007) Sequestosome 1/p62--more than just a scaffold. *FEBS Lett* **581**, 175-179

CHAPTER 3

THE FRONTOTEMPORAL LOBAR DEGENERATION RISK FACTOR, TMEM106B, REGULATES LYSOSOMAL MORPHOLOGY AND FUNCTION[1]

3.1 Summary

Haplo-insufficiency of *Progranulin (PGRN)*, a gene encoding a secreted glycoprotein, is a major cause of frontotemporal lobar degeneration with ubiquitin positive inclusions (FTLD-U). Single nucleotide polymorphisms in the *TMEM106B* gene were recently discovered as a risk factor for FTLD-U, especially in patients with PGRN mutations. TMEM106B is also associated with cognitive impairment in ALS patients. Despite these studies, little is known about TMEM106B at molecular and cellular levels and how TMEM106B contributes to FTLD. Here we show that TMEM106B is localized in the late endosome/lysosome compartments and TMEM106B levels are regulated by lysosomal activities. Ectopic expression of TMEM106B induces morphological changes of lysosome compartments and delays the degradation of endocytic cargoes by the endolysosomal pathway. Furthermore, overexpression of TMEM106B correlates with elevated levels of PGRN, possibly by attenuating lysosomal degradation of PGRN. These results shed light on the cellular functions of TMEM106B and the roles of TMEM106B in the pathogenesis of FTLD-U with PGRN mutations.

[1]The results of this study were published in Brady OA, Zheng Y, Murphy K, Huang M, Hu F. *Hum. Mol.Genet.* 2013 Feb 15;22(4):685-95. Y.Z., K.M., and M.H. assisted with data acquisition and analysis. All experiments were performed by O.A.B. O.A.B. and F.H. wrote the manuscript.

3.2 Introduction

Frontotemporal lobar degeneration (FTLD) is one of the most prevalent forms of early onset dementia, second only to Alzheimer's disease (1,2). Mutations in the *Progranulin (PGRN)* gene were recently shown to be the major cause of FTLD with ubiquitin positive inclusions of TDP-43 (FTLD-U) (3-5). Most PGRN mutations result in a decrease in the amount of PGRN expressed or secreted, rather than a gain of toxicity (3,4). Thus, progranulin haplo-insufficiency is strongly associated with FTLD-U. PGRN encodes an evolutionarily conserved, secreted glycoprotein of 88 kDa involved in would healing, inflammation, tumorigenesis and neuronal survival (6). A member of the VPS10 family, sortilin, was recently identified as a binding partner for PGRN (7). Sortilin regulates PGRN trafficking by mediating PGRN endocytosis and targeting to lysosomes, thus controlling PGRN levels in the brain (7,8).

However, PGRN mutation carriers show a high variability in age of onset and pathological presentation, even with identical mutations, suggesting that environmental influences or additional genetic factors modify the disease manifestation (9). Recent genome-wide association studies by several groups have pinpointed TMEM106B, a gene encoding a transmembrane protein of unknown function, as a bona fide risk factor for FTLD-U, especially in patients with PGRN mutations (10-13). TMEM106B is also associated with cognitive impairment in ALS patients (14). However, studies with samples from FTLD patients have obtained conflicting results on the effect of TMEM106B polymorphisms on TMEM106B function and on the relationship between TMEM106B and PGRN. First, it is not clear

whether TMEM106B mRNA levels are affected by TMEM106B SNPs (11,12). Secondly, it is not known whether the protein function of TMEM106B is altered by SNPs within the coding region of TMEM106B (10,11,13). Studies have identified a T185S coding variant in TMEM106B associated with the protective allele (10,11,13) and suggested T185S to be in perfect linkage disequilibrium with the strongest SNP associated with FTLD-U, rs1990622 (10,13). However, whether and how T185S affects TMEM106B function remains unknown. Finally, it is still under debate whether TMEM106B polymorphisms affect PGRN levels, although the T185S allele was reported to be protective and was correlated with higher plasma PGRN levels (10,11,13). Thus, despite a strong genetic linkage, the role of TMEM106B in FTLD-U and the relationship between TMEM106B and PGRN are not completely understood from these studies (10-17).

TMEM106B encodes a transmembrane protein of unknown function. To address the role of TMEM106B in FTLD-U with PGRN mutations, we investigated cellular functions of TMEM106B. Consistent with recent findings (18,19), we found that TMEM106B is a lysosomal protein and TMEM106B levels are modulated by lysosomal activities. We further showed that increased TMEM106B levels result in the accumulation of enlarged lysosomes and impair the degradation of endocytic cargoes. Exogenous expression of TMEM106B increases PGRN levels, possibly due to its regulation of the endolysosomal pathway.

3.3 Materials and Methods

Cell culture procedures

T98G, N2A, HEK293T (from ATCC), NSC34 (20) and BV-2 (21) cells were grown in DMEM supplemented with 10% FBS, 1% Penicillin-Streptomycin at 37°C in a 5% CO_2 atmosphere. Cells were transiently transfected with polyethlyeneimine (PEI) as described (22). E17 rat cortical neurons were isolated and cultured as described (7).

Plasmids and siRNAs

Human TMEM106B cDNA was obtained from Open Biosystems (the ORFome collection, T185; in the pCMV-Sport6, S185). FLAG-tagged TMEM106B constructs were generated by cloning TMEM106B into p3XFLAG-CMV7.1 vector (Sigma-Aldrich) using the enzymes HindIII and SalI. TMEM106B-myc was generated by cloning TMEM106B into pcDNA3.1myc his A vector (Invitrogen) using the enzymes HindIII and XhoI. GFP-TMEM106B was generated by cloning TMEM106B into pEGFP-C3 vector (Clontech) using the enzymes HindIII and XhoI/SalI. GFP tagged Rab plasmids are generous gifts from Drs. Bill Brown and Volker Vogt. PGRN and sortilin constructs were obtained as described (7). siRNA against Mouse TMEM106B (D-042561-01,-02,-03,-04**)**, mouse SORT1 (D-041713-01,-02,-03,-04), and pooled control siRNAs (D-001206-13-05) were obtained from Dharmacon and transfected into N2A cells using DharmaFECT according to manufacturer's instructions.

Antibodies and chemicals

The following antibodies were used in the study: sheep anti-mouse PGRN antibodies, goat anti-human PGRN antibodies and goat anti-mouse sortilin from R&D systems; mouse anti-myc (9E10) and anti-FLAG (M2) antibodies from Sigma-Aldrich; mouse

anti-LAMP1 and EEA1 antibodies from BD biosciences; rabbit anti-EGFR, rabbit anti-phospho-Erk1/2, and rabbit anti-cleaved caspase 3 antibodies from Cell Signaling; rat anti-mouse LAMP1 (1D4B) antibodies from BioLegend; rabbit anti-TDP 43 antibodies from Proteintech; and mouse anti-GAPDH antibodies from Millipore. Rabbit anti-cathepsin D antibodies are a generous gift from Dr. Bill Brown.

To generate anti-TMEM106B antibodies, the intracellular domain of TMEM106B (residues 1-96) were expressed and purified as GST fusion proteins from *E. coli*. Recombinant proteins were sent to Covance laboratories to generate rabbit polyclonal antibodies. Serum from the final bleed was diluted 1:2000 for western blot analysis and 1:250 for immunostaining. Antibody specificity was confirmed via Western blot and immunofluorescence by observing overlapping signals between FLAG and TMEM106B antibodies for overexpressed FLAG-TMEM106B and by decreased signals from cells treated with siRNAs against TMEM106B. The antibody does not cross react with the TMEM106B family members TMEM106A and TMEM106C (data not shown).

The following reagents are used in the study: 3-methyladenine (3-MA), chloroquine, ammonium chloride, cycloheximide, and staurosporine from Sigma-Aldrich; recombinant human epidermal growth factor (EGF) from Promega; puromycin from Calbiochem; trichloroacetic acid (TCA) from Acros Organics; MG-132 from Cayman chemical; bafilomycin A1 (Baf1) from LC Laboratories.

Immunofluorescence Microscopy

Cells were plated on coverslips the day prior to transfection. Cells were fixed with 3.7% formaldehyde in PBS 24 or 48 hours post-transfection and washed with PBS, followed by permeabilization and blocked with PBS containing 3% BSA, 0.1% Triton X-100 or 0.05% Saponin. Cells were stained with primary antibody in 1% BSA PBS blocking buffer overnight at 4º C. Cells were washed three times with PBS and incubated 2 hours at room temperature with a 1:500 mixture of Hoechst and secondary antibody (donkey-anti-rabbit/mouse IgG Alexa Fluor488 and 594, donkey-anti-rat AlexaFluor568, and donkey anti-sheep AlexaFluor680 Molecular Probes). For dextran loading experiments Texas Red labeled dextran (70,000 MW, Lysine Fixable, Molecular probes) was used. Cells were either preloaded for 16 hours with 0.5 µg/ml dextran, washed, and chased 4 hours in growth medium to label lysosomes, or cells were transfected and then loaded and chased. Cells were washed three times with PBS and mounted with Fluoromount G (Southern Biotech), then analyzed with a CSU-X spinning disc confocal microscope (Intelligent Imaging Innovations) with an HQ2 CCD camera (Photometrics), or a Zeiss LSM700 confocal microscope with a transmission photomultiplier detector. All confocal pictures were obtained through 63x or 100x objectives.

Lysosomal scoring and Vacuolization Assays

For lysosomal scoring, 0.56 µm confocal slices from N2A cells transfected with either vector control, WT or the T185S allele of TMEM106B were acquired. Slices were obtained through cells to yield the maximum number of lysosomes per field of view. Discrete LAMP1, positive vesicles between 0.3-4.0 µm were counted for each cell and

measured through the widest part of the vesicle. Large swollen vacuoles greater than 4.0 µm were not included in these analyses. Histograms were generated using 200 randomly selected lysosomes from each of these data sets. Analysis was performed with Slidebook software (3I).

For the vacuolization assay, N2A cells were transfected with indicated constructs and treated 24 hours later with any chemicals indicated. Cells were photographed with an ImagXpress Micro (Molecular Devices) at 20x and >200 cells counted per trial by an observer blind to the conditions. Cells were scored as positive by the presence of enlarged (>3µm) phase-lucent vacuoles.

EGFR Degradation Assay

T98G cells were transfected with indicated constructs. Cells were washed with PBS and media replaced with serum free DMEM after 24 hours. After 24 hours in serum free media, cells were stimulated with 100 ng/ml recombinant human EGF in the presence of 25 µg/ml cycloheximide to inhibit further protein synthesis and cells lysed at indicated time points for Western blot analysis.

Western-blot analysis

Protein samples in SDS sample buffer containing β-mercaptoethanol were kept on ice or boiled for 2min. Samples were run on 12% polyacrylamide gels and transferred to Immobilon-FL PVDF membranes (Millipore). Membranes were blocked with Odyssey Blocking Buffer (LI-COR Biosciences) for 1 hour followed by incubation with primary antibodies overnight at 4°C. Membranes were washed for 5 min three times in Tris-Buffered Saline with 0.1% Tween-20 (TBS-T), incubated with secondary antibody for 2 hrs at room temperature and washed three more times with TBS-T.

Blots were imaged and quantified using an Odyssey Infrared Imaging System (LI-COR Biosciences). For quantitation, all immunoreactive bands were normalized to a corresponding GAPDH reference band.

Immunoprecipitation

Cells were lysed in 50 mM Tris, pH 7.5, 150 mM NaCl, 1mM EDTA, 1%Triton, 0.1% sodium deoxycholate, and proteinase and phosphatase inhibitors (Roche). Mouse anti-FLAG conjugated beads (Sigma) were allowed to immunoprecipitate FLAG-TMEM106B in the cell lysates. These beads were incubated with cell lysates for 4 hours at 4°C and washed 4 times with the lysis buffer.

TCA precipitation of conditioned medium

One day after transfection, N2A cells were grown in serum free medium. Conditioned media was collected 24 hours later and centrifuged at 10,000 rcf for 10 min to remove cell debris. Cleared media was incubated with 10% TCA at 4°C. Protein pellets were collected by centrifugation, washed with acetone, and dissolved in SDS sample buffer prior to western blot to determine PGRN levels.

ELISA

PGRN levels were measured in N2A cells with TMEM106B overexpressed or knocked down with siRNAs. Cells were washed 48 hours post transfection and incubated 24 hours in serum-free DMEM. Conditioned media was cleared at 10,000 rcf for 10 min and subjected to a Mouse PGRN ELISA (AdipoGen) according to manufacturer's instructions. PGRN concentrations were converted to percentage of control in order to correct for inter-assay variability. Corresponding cell lysates from these samples were collected in RIPA buffer for Western blot analysis.

RT-PCR

RNA was purified from cells 48 hours after transfection using TRIzol Reagent (Invitrogen). 2 µg total RNA was reverse transcribed using a poly(T) primer and SuperScript III Reverse Transcriptase (Invitrogen). qPCR was performed on a LightCycler 480 (Roche Applied Science) and transcript levels were calculated using efficiency adjusted ΔΔ-CT. All transcripts were normalized to the geometric mean of two reference genes, *Tbp*, and *Actb*. The mouse *Grn* primer pair sequences were 5'AGTTCGAATGTCCTGACTCCGCCA3'and 5'AAGCCACTGCCCTGTTGGTCCT-TT3'. Mouse *Tbp* primers were 5'CCCCACAACTCTTCCATTCT3' and 5'GCAGGAGTGATAGGGGTCAT3' and mouse *Actb* primers were 5'ACGAGGCCCAGAGCAAGAG3' and 5'TCTCCAAGTCGTCCCAGTTG3'.

3.4 Results

TMEM106B is localized in late endosome/lysosome compartments

TMEM106B is a predicted type II transmembrane protein of unknown function. To determine the expression of endogenous TMEM106B, we raised antibodies against the intracellular portion of TMEM106B (a.a. 1-96). The polyclonal antibody specifically detects a 43 kDa band on SDS-PAGE corresponding to endogenous TMEM106B detected in multiple cell lines (Figure 3.1A). Since TMEM106B has 274 residues with a predicted molecular weight of 31 kDa, the discrepancy on migration indicates potential posttranslational modification, likely glycosylation of this protein (19). Consistent with studies by others (18), we found that TMEM106B protein exhibits as

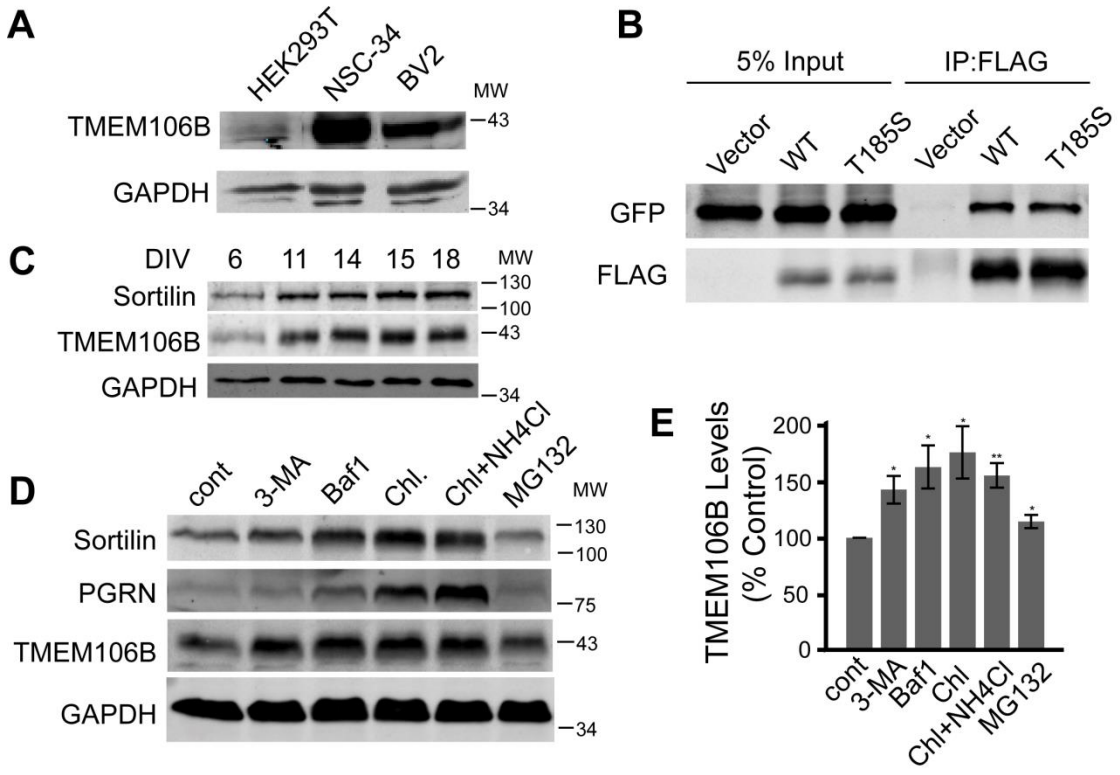

Figure 3.1: Expression of TMEM106B in different cell types. (**A**) Cell lysates from HEK293T, NSC-34 and BV-2 were loaded and blotted with anti-TMEM106B and anti-GAPDH antibodies. (**B**) TMEM106B forms homodimers. FLAG-tagged TMEM106B WT and T185S variants were co-transfected with GFP-TMEM106B WT into HEK293T cells. Anti-FLAG antibodies were used to immunoprecipitate FLAG-TMEM106B. IP products were blotted for GFP and FLAG as indicated. (**C**) TMEM106B expression in rat cortical neurons. E17 rat cortical neurons were isolated and allowed to differentiate for indicated days. Cell lysates were prepared and blotted for sortilin, TMEM106B and GAPDH. Cortical neurons were treated with 2 µM Ara-C after DIV6 in order to inhibit the growth of glial cells. (**D**) N2A cells were treated with 5mM 3-MA, 50 nM Baf1, 15mM NH_4Cl + 100 µM chloroquine or 10 µM MG-132 for 14 hrs as indicated. Cell lysates were prepared and blotted for TMEM106B and GAPDH. (**E**) Quantification of data shown in (**D**), n=4, +/-SEM, * $p<0.05$, ** $p<0.01$ Student's t-test.

an 86kDa band on SDS-PAGE when the samples are not boiled (data not shown), suggesting the presence of a SDS-resistant dimer. This is further confirmed by the co-immunoprecipitation of GFP-tagged TMEM106B with FLAG-tagged TMEM106B (Figure 3.1B). The T185S variant of TMEM106B self-associates to a similar degree as wild type TMEM106B.

With our polyclonal antibodies, we found that TMEM106B is ubiquitously expressed in many different cell types, including neurons and microglia cells, with highest protein levels detected in neuronal cell lines (Figure 3.1A). Analysis of TMEM106B expression levels in cortical neurons showed a positive correlation of TMEM106B protein levels with neuronal maturation in vitro (Figure 3.1C). To investigate cellular localization of endogenous TMEM106B, we stained neuroblastoma N2A cells with our polyclonal antibodies against TMEM106B. We found that a large pool of TMEM106B localized in intracellular vesicles (Figure 3.2A). Knockdown of TMEM106B expression by siRNA abolished this vesicular staining, confirming the specificity of our antibody (Figure 3.2A). To determine the identities of these intracellular vesicles, we examined the colocalization of N-terminal FLAG tagged TMEM106B with GFP-tagged Rab GTPases. TMEM106B shows strong colocalization with late endosome and lysosome markers Rab7 and Rab9, with little colocalization with the early endosome marker Rab5 and the recycling endosome marker Rab11, suggesting that TMEM106B mainly localizes to late endosomes and lysosomes (Figure S3.1A). FLAG-TMEM106B also shows strong colocalization with LAMP1, a transmembrane protein localized mainly on the lysosomes (Figure S3.1B). We further confirmed this with colocalization of endogenous TMEM106B with

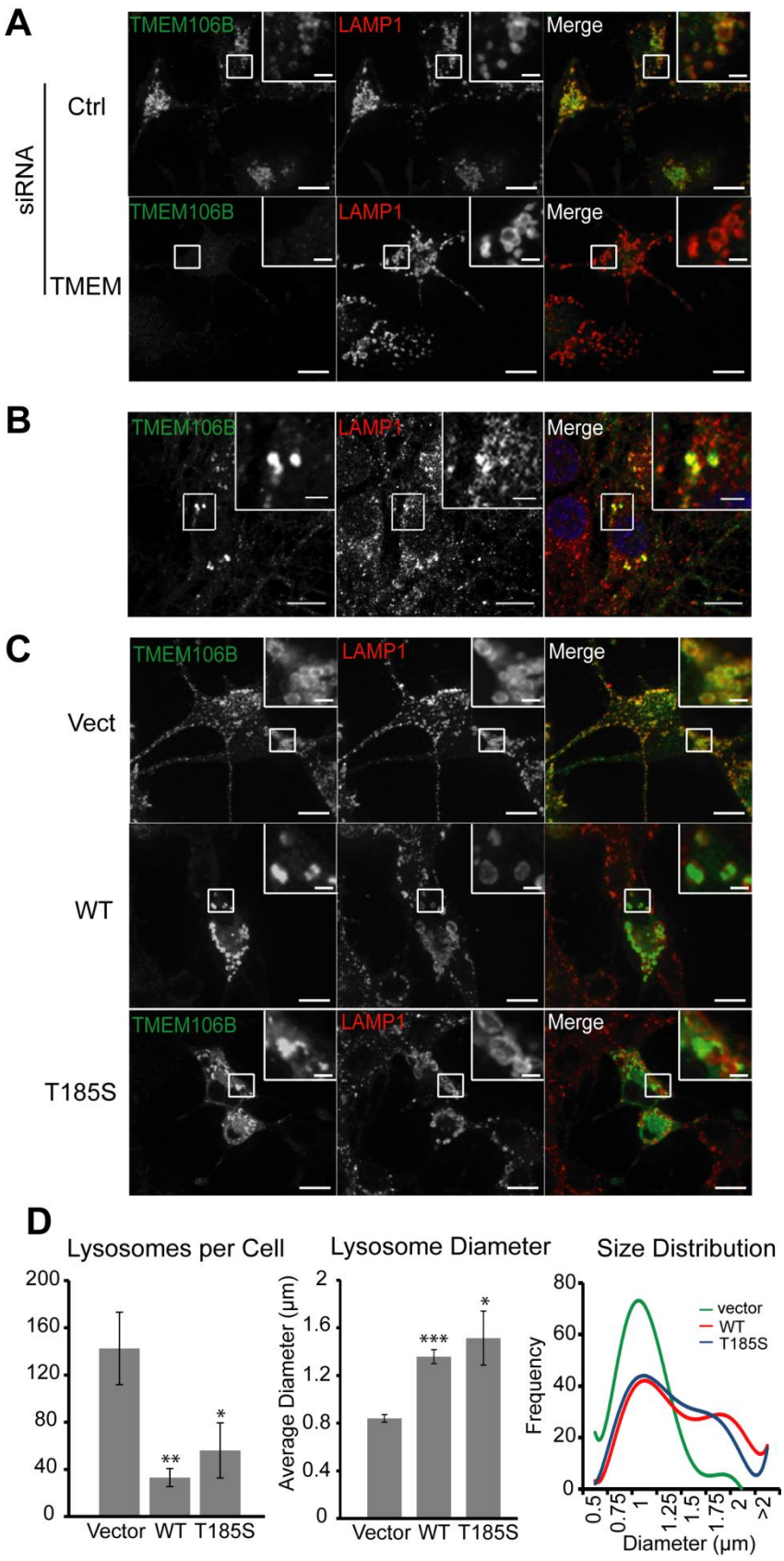
A
TMEM106B
LAMP1
Merge
siRNA
Ctrl
TMEM
B
C
Vect
WT
T185S
D
Lysosomes per Cell
Lysosome Diameter
Size Distribution
Vector WT T185S
Average Diameter (μm)
Frequency
vector
WT
T185S
Diameter (μm)

Figure 3.2: TMEM106B localizes to late endosomes/lysosomes. (**A**) Colocalization of endogenous TMEM106B with LAMP1 positive vesicles. N2A cells were fixed and stained with polyclonal anti-TMEM106B and monoclonal anti-LAMP1 antibodies. siRNA knockdown of TMEM106B confirms the specificity of our anti-TMEM106B antibody. (**B**) Colocalization of endogenous TMEM106B with LAMP1 in DIV15 cortical neurons. (**C**) Overexpression of TMEM106B induces enlarged LAMP1 positive vesicles. Vector control, pCMV-TMEM106B WT and T185S transfected N2A cells were stained with anti-TMEM106B and anti-LAMP1 antibodies. Green fluorescence exposure time was reduced for cells overexpressing TMEM106B to highlight differences in expression levels compared to nearby non-transfected cells. Scale bars: 10 µm (2 µm in the inset). (**D**) Quantification of average number of lysosomes per cell and mean lysosome diameter +/-SEM along with best fit curves of lysosome size histograms from cells imaged in (C). A minimum of 200 lysosomes were measured from six randomly selected cells in each condition. * $p<0.05$, ** $p<0.01$, ***$p<0.001$ Student's t-test.

LAMP1 in N2A cells (Figure 3.2A) and cortical neurons (Figure 3.2B). Endogenous TMEM106B in N2A cells shows much better colocalization with LAMP1 than overexpressed TMEM106B (Figure 3.2 and Figure S3.1), suggesting that TMEM106B overexpression might cause mislocalization of the protein or disturbance of lysosomal compartments. In particular, endogenous TMEM106B usually appeared as a granular, but relatively evenly distributed coat on the lysosomal limiting membrane with the occasional lysosome exhibiting one to several discrete TMEM106B puncta polarized on the lysosome surface. When TMEM106B was overexpressed we saw a preponderance of this polarized/punctate localization pattern compared to vector transfected controls. Overexpressed TMEM106B also frequently appeared within the lumen of the LAMP1 positive vesicles. A small pool of TMEM106B was also detected at the plasma membrane when overexpressed. These data strongly indicate that TMEM106B localization is critically affected by expression level. Live cell staining with external antibodies against the myc epitope tag, which is inserted at C-terminus of TMEM106B, confirms that TMEM106B is a type II transmembrane protein with its C-terminus facing extracellularly or to topologically equivalent luminal spaces (Figure S3.2).

Since TMEM106B is mainly localized on lysosomes, we further investigated whether protein levels of TMEM106B are regulated by lysosomal activities. Treatment with inhibitors of lysosomal acidification, such as bafilomycin (Baf1), ammonium chloride or chloroquine, leads to a significant increase in TMEM106B levels in N2A cells, suggesting that TMEM106B levels are regulated by the lysosomal degradation pathway (Figure 3.1D and E). Treatment with 3-methyladenine (3-MA), an inhibitor

of VPS34, a PI3K involved in autophagy and formation of multivesicular bodies (23), also increases TMEM106B levels (Figure 3.1D and E). This indicates that TMEM106B levels may be regulated by membrane trafficking events. On the other hand, treatment with the proteasome inhibitor MG-132 had minimal effects on TMEM106B levels, suggesting that the ubiquitin-proteosomal pathway is not a major regulator of TMEM106B protein levels

Increased TMEM106B levels induces enlarged lysosomes

Close examination of lysosome morphology in TMEM106B overexpressing N2A cells revealed an enlargement of lysosomes and a reduction of lysosome numbers (Figure 3.2C and D). Examination of lysosomal morphology in other cell lines with TMEM106B overexpression, including HEK293T, COS-7, T98G and motor neuron cell line NSC-34 indicated a much more pronounced lysosomal phenotype in neuronal cell lines upon increases in TMEM106B levels, suggesting an enhanced sensitivity of neuronal cells to elevations in TMEM106B levels (Figure S3.3). Abnormal morphology was also seen in some of the enlarged lysosomes, some of which are reminiscent of intermediates of lysosomal fission or fusion (Figure 3.2C). This phenotype is also seen with GFP-TMEM106B overexpression, which tends to give higher expression levels and results in large vacuoles positive for LAMP1 but negative for the early endosome marker EEA1 (Figure 3.3). These vacuoles are prominent under regular phase microscope in GFP-TMEM106B overexpressing N2A cells and are present in N2A cells overexpressing untagged TMEM106B when treated with 3-MA (Figure S3.4). We fail to detect any significant differences between wild type

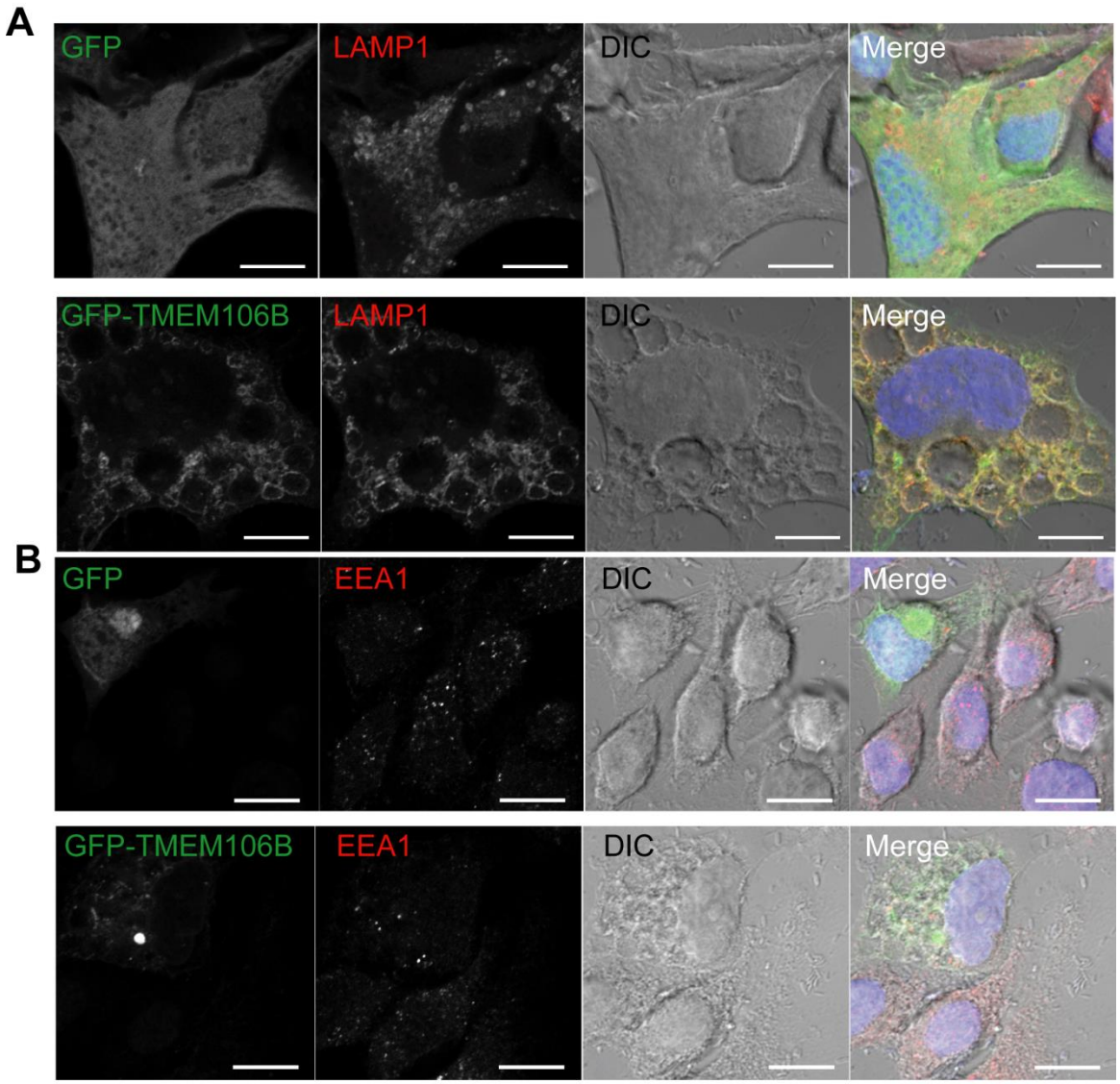
A
GFP
LAMP1
DIC
Merge
GFP-TMEM106B
LAMP1
DIC
Merge
B
GFP
EEA1
DIC
Merge
GFP-TMEM106B
EEA1
DIC
Merge
C
GFP
PGRN
CathD
Merge
GFP
TMEM106B
PGRN
CathD
Merge

Figure 3.3: GFP-TMEM106B overexpression results in LAMP1 positive vacuoles in N2A cells. (**A**) GFP-TMEM106B expression in N2A cells results in enlarged vacuoles that are rimmed by TMEM106B and LAMP1. (**B**) GFP-TMEM106B induced vacuoles are EEA1 negative. (**C**) Co-localization of PGRN with GFP-TMEM106B in some of the vacuoles. Scale bar: 10 µm (2 µm in the inset).

and the T185S variant of TMEM106B in inducing abnormalities in lysosomal morphology (Figure 3.2 and Figure S3.4).

To further confirm the origin of these membranes, we preloaded lysosomes with dextran and then transfected the cells with TMEM106B constructs. It has been shown that preloaded dextran accumulates in lysosomes (24). We found that many of the enlarged vesicles induced by TMEM106B overexpression are positive for dextran (Figure 3.4A), confirming that these are lysosome derived. Although TMEM106B overexpression induces lysosome enlargement, it does not induce apoptosis or TDP-43 mislocalization or cleavage (Figure S3.5).

TMEM106B overexpression impairs endolysosomal degradation

To investigate whether the abnormal morphology of enlarged late endosomes/lysosomes induced by TMEM106B impairs endolysosomal function, the cellular turnover rate of epidermal growth factor receptor (EGFR) was analyzed. T98G cells, which express high levels of endogenous EGFR, were treated with EGF. EGF stimulation leads to the activation of EGFR and phosphorylation of ERK1/2. EGFR signaling continues after EGFR endocytosis until the receptors are inwardly budded into intra-luminal vesicles in MVBs. EGFR is subsequently degraded through lysosomal fusion and degradation (25). We found that GFP-TMEM106B expression appears to attenuate the rate of EGFR degradation in T98G cells. However, EGF downstream signaling, as quantified by the levels of phospho-ERK1/2 is not affected (Figure 3.5). These data suggest that TMEM106B may cause a defect in the later stages of late endosome/lysosome fusion or lysosomal degradation rather than early

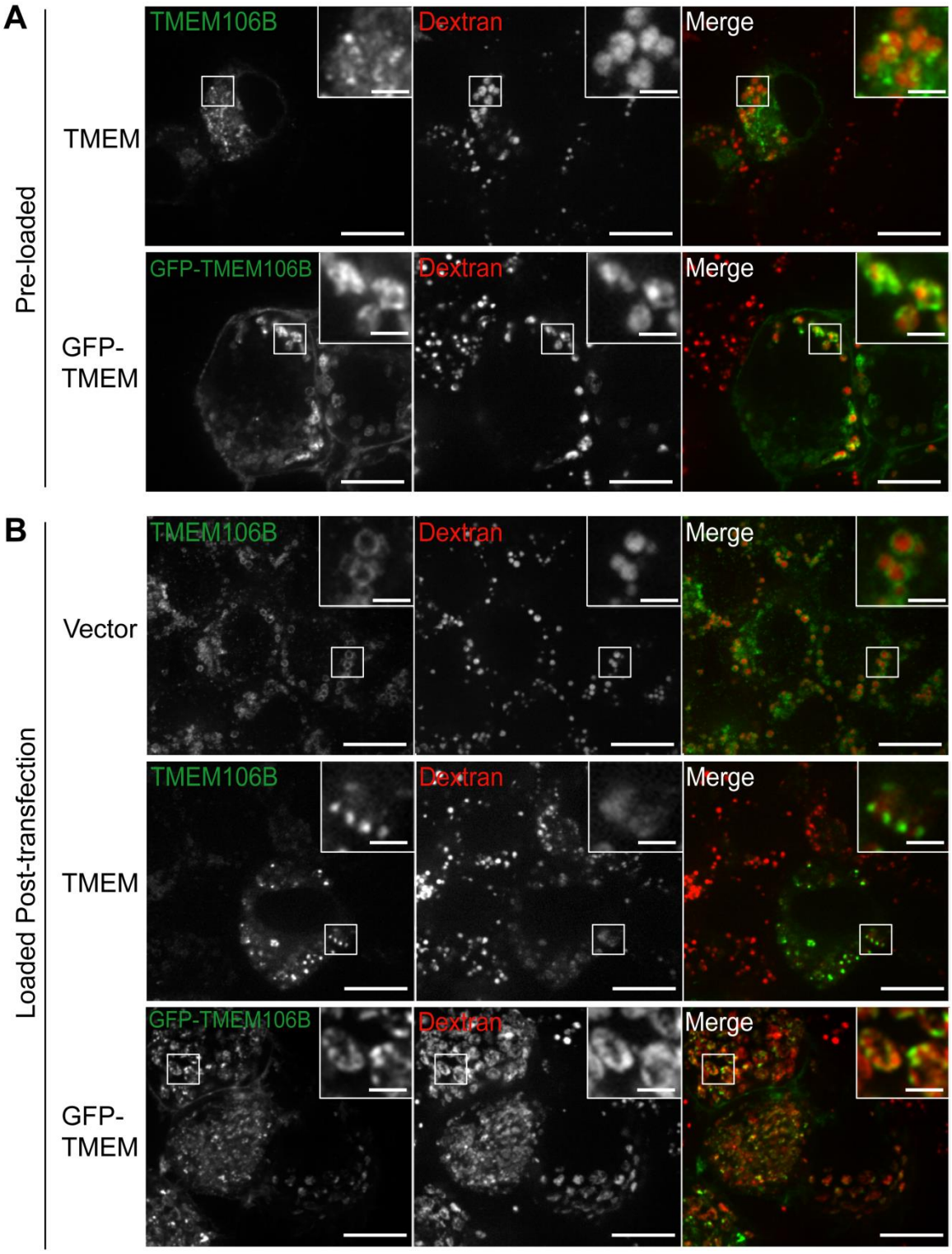
A
Pre-loaded
TMEM
GFP-
TMEM
TMEM106B
Dextran
Merge
GFP-TMEM106B
Dextran
Merge
B
Loaded Post-transfection
Vector
TMEM
GFP-
TMEM
TMEM106B
Dextran
Merge
TMEM106B
Dextran
Merge
GFP-TMEM106B
Dextran
Merge

Figure 3.4: The fluid-phase marker, dextran, accumulates in TMEM106B positive vesicles. (**A**) N2A cells pre-loaded with dextran were transfected with TMEM106B and GFP-TMEM106B. Cells were fixed and stained 24 hrs post-transfection. Untagged and GFP-TMEM106B can be seen on the surface of dextran containing vesicles. (**B**) Dextran labeled endosomes are capable of fusion with TMEM106B enlarged lysosomes. N2A cells were transfected with vector control, TMEM106B, and GFP-TMEM106B. After 28 hrs, cells were loaded with dextran for 16 hrs, washed, and chased 4 hrs in growth medium. Cells were fixed and stained 48 hrs post-transfection. Scale bars: 10 μm (2 μm in the inset).

endocytic trafficking steps or MVB formation. Because the enlarged lysosome phenotype induced by TMEM106B overexpression is much more pronounced in neuronal bcell lines than in T98G cell, a more severe endolysosomal dysfunction is expected in neuronal cell lines. Unfortunately, we were unable to detect eciable amounts of endogenous EGFR in N2A cells, making them unsuitable for this assay.

To determine whether TMEM106B affects endosome/lysosome fusion, we incubated N2A cells overexpressing TMEM106B with the fluid-phase marker, dextran and chased for 4 hours. Dextran signal is present in TMEM106B enlarged lysosomes to a similar extent as in control cells, suggesting that there are no major defects in fusion between TMEM106B induced enlarged lysosomes and incoming endosomes (Figure 3.4B).

TMEM106B modulates PGRN protein levels.

Our previous published results have shown that sortilin mediates PGRN trafficking into lysosomes and plays a critical role in regulating PGRN levels (7). We hypothesized that TMEM106B may play a role in regulating PGRN levels by affecting lysosomal activities. To address this hypothesis, we measured intracellular and secreted PGRN levels in cells overexpressing the wild type or T185S allele of TMEM106B. Both wild type and T185S alleles of TMEM106B increased endogenous PGRN levels in N2A cells (Figure 3.6A-C). These changes in PGRN levels are not due to changes in PGRN mRNA levels as measured by qPCR (Figure 3.6C), suggesting that TMEM106B regulates PGRN levels through post-transcriptional mechanisms. Sortilin expression levels do not appear to be affected by TMEM106B

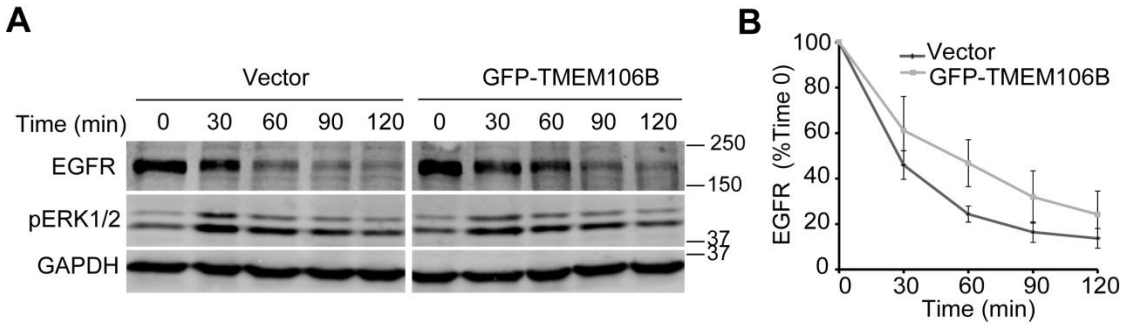

Figure 3.5: GFP-TMEM106B overexpression results in defects in EGFR degradation. (**A**) T98G cells transfected with vector control or GFP-TMEM106B were serum starved and stimulated with EGF in the presence of cycloheximide for indicated times. Levels of EGFR, phosphorylated ERK1/2, and GAPDH were quantified by western blots. A representative image of 3 experiments is shown. (**B**) Quantification of EGFR levels relative to loading control for experiment in (A). n=3 +/-SEM.

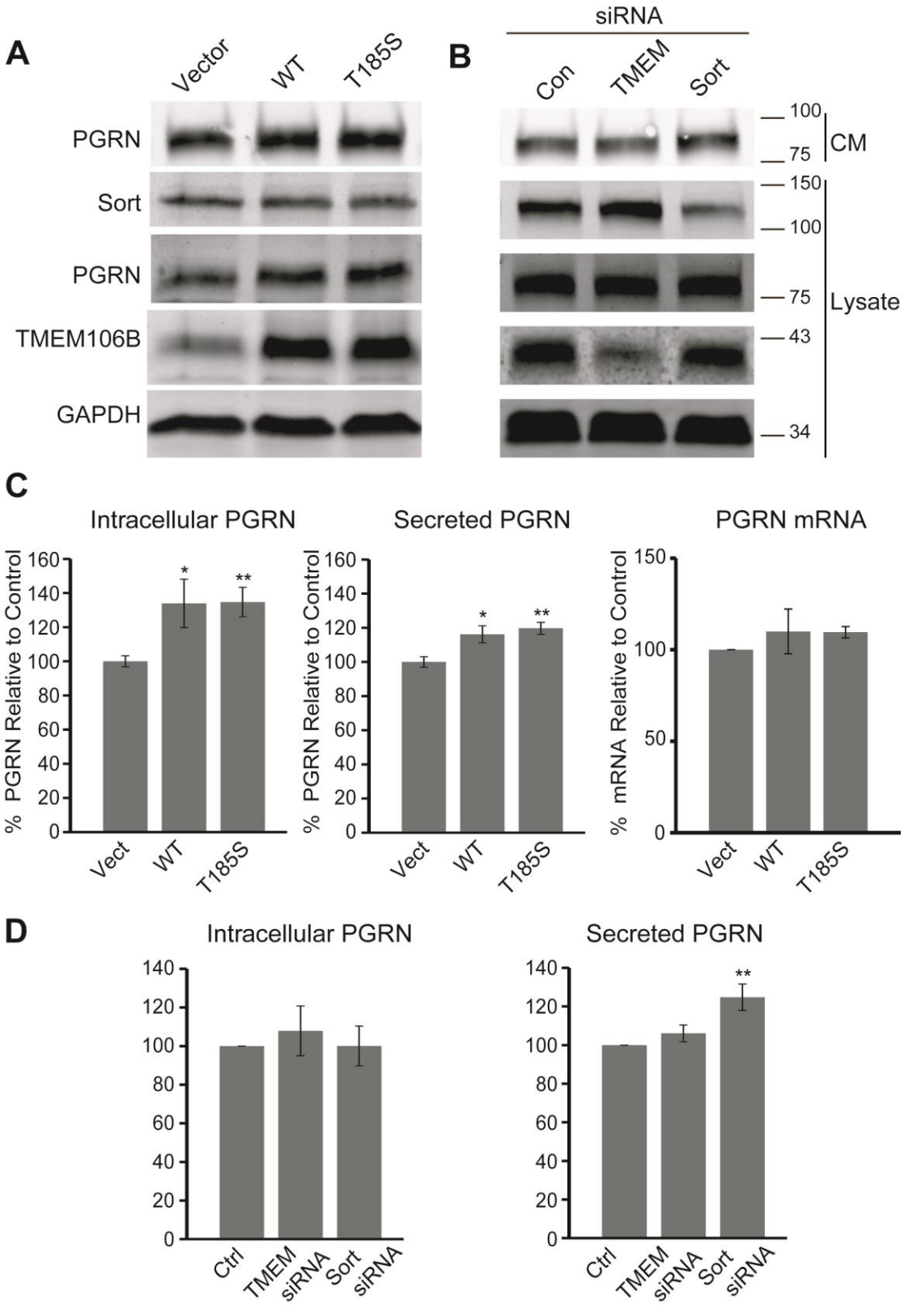
A
Vector
WT
T185S
PGRN
Sort
PGRN
TMEM106B
GAPDH
B
siRNA
Con
TMEM
Sort
100
75
CM
150
100
75
43
34
Lysate
C
Intracellular PGRN
Secreted PGRN
PGRN mRNA
% PGRN Relative to Control
% mRNA Relative to Control
Vect
WT
T185S
D
Intracellular PGRN
Secreted PGRN
Ctrl
TMEM siRNA
Sort siRNA

Figure 3.6: Regulation of PGRN levels by TMEM106B. (**A**) Western blot analysis of N2A cells overexpressing TMEM106B WT and T185S. Transfected cells were changed to serum free medium 24 hrs after transfection. After another 24 hrs, lysates and conditioned media (CM) was collected. CM was further concentrated using TCA precipitation. (**B**) Western blot analysis of N2A cells transfected with control siRNA pool or siRNA pools against TMEM106B and sortilin. Transfected cells were changed to serum free medium 48 hours after siRNA transfection. After another 24 hrs, lysates and conditioned media (CM) was collected. CM was further concentrated using TCA precipitation. (**C**) Overexpression of TMEM106B in N2A cells lead to increased intracellular and secreted PGRN levels as measured by western blot or ELISA, respectively (n=5). PGRN levels were normalized to the mean of two vector transfected controls. No change in PGRN mRNA levels was detected via qPCR (n=3). (**D**) Knockdown of TMEM106B in N2A cells has no effect on intracellular or secreted PGRN levels as measured by western blot or ELISA, respectively (n=6). Sortilin knockdown leads to increased levels of PGRN in the media. * $p<0.05$, ** $p<0.01$, Student's t-test.

(Figure 3.6A), indicating it is unlikely that TMEM106B regulates PGRN levels through sortilin. Furthermore, in cells overexpressing GFP-TMEM106B, accumulation of endogenous PGRN, along with the prototypical lysosomal proteinase cathepsin D, can be detected in some of the GFP-TMEM106B positive vacuoles (Figure 3.3C). Together these results suggest that TMEM106B may regulate PGRN levels through its function in the endolysosomal degradation pathway.

We also examined the effect of TMEM106B loss of function on PGRN levels by knocking down TMEM106B expression in N2A using siRNA. siRNA treatment resulted in ~50-70% reduction of TMEM106B expression (Figure 3.6B and D). In order to test the validity of our assay, we knocked down sortilin expression using siRNA as a positive control and observed an increase in secreted PGRN (Figure 3.6D). However, TMEM106B knockdown did not appear to affect PGRN levels. Further, reduced TMEM106B expression does not appear to affect lysosomal size or morphology (Figure 3.2A). Thus, either residual TMEM106B expression is enough to maintain its function in the lysosomes or TMEM106B loss of function does not directly affect lysosomal morphology or function.

3.5 Discussion

Endolysosomal function is essential for the health of neurons. Several genetic mutations found in FTLD, including those in CHMP2B and VCP/p97, result in the accumulation of enlarged vacuoles and a defect in endo-lysosomal trafficking or autophagosome maturation (26-29). Mutations in the PGRN gene are the main cause for FTLD-U (3-5). PGRN has also been implicated in regulating lysosome functions

and is transcriptionally co-regulated with a number of essential lysosomal genes (30). PGRN knockout mice accumulate lysosomal byproducts, lipofuscin (31) and homozygous PGRN mutant human patients exhibit neuronal ceroid lipofuscinosis (32). In this study, we showed that the FTLD-U risk factor TMEM106B is mainly localized to late endosome/lysosome compartments and regulates lysosomal morphology (Figure 3.2). Overexpression of TMEM106B results in accumulation of enlarged lysosomes (Figure 3.2-3.4) and delays the degradation of endocytic cargoes, such as EGFR (Figure 3.5). TMEM106B does not affect the termination of EGFR signaling (Figure 3.5), suggesting that TMEM106B does not cause defects in membrane invagination into multivesicular bodies. We speculate that TMEM106B may regulate the fusion of late endosomes with lysosomes or the fission of the hybrid organelle after endosome-lysosome fusion. Our examination of endosome-lysosome fusion events using dextran labeling suggested that TMEM106B induced enlarged lysosomes are still capable of fusing with incoming endosomes (Figure 3.4). However, it is still possible that TMEM106B affects the kinetics of endosome-lysosome fusion, which requires detailed analysis of endosome-lysosome fusion using time lapse imaging.

It is still under debate whether TMEM106B polymorphisms result in changes in TMEM106B levels or changes in TMEM106B protein, as one variant, T185S, has been reported to be protective and to be in perfect linkage disequilibrium with the strongest SNP associated with FTLD-U (10-17). We find no differences between the WT and T185S variant of TMEM106B in regards to regulating lysosomal morphology and number, or PGRN levels. Our results are consistent with a model in which

increased expression of TMEM106B perturbs the endolysosomal pathway. This is corroborated by findings of increased TMEM106B mRNA and protein levels in post-mortem brain samples of FTLD-U patients (12,18). Surprisingly, reduced expression of TMEM106B by RNAi treatment does not have any obvious effect on lysosomal morphology. It is possible that residual TMEM106B is sufficient to maintain its function in the lysosomes or that TMEM106B is not essential for lysosomal function. Another possibility is that TMEM106B is functionally redundant and may be compensated by other genes, such as *TMEM106A* and *TMEM106C*. A complete depletion of TMEM106B function using a mouse knockout model might be needed to determine TMEM106B function in vivo.

Progranulin haplo-insufficiency is strongly associated with FTLD-U. However, it is still under debate whether TMEM106B SNPs affects PGRN levels. Previous studies with FTLD patient samples resulted in contradictory conclusions on the regulation of PGRN by TMEM106B (10-13). Here we show that exogenous expression of TMEM106B increases PGRN levels (Figure 3.6) and results in accumulation of PGRN in the lysosomes (Figure 3.4C). Our results indicate that elevated TMEM106B levels could alter plasma PGRN levels in human patients, possibly due to its effect on endolysosomal trafficking. While the majority of the increased PGRN observed appears to be intracellular, likely as a result of abnormal lysosomal degradation, we do detect a modest increase in the levels of extracellular PGRN as measured by ELISA. One potential mechanism to explain this increase in PGRN levels is through an overflow of the increased intracellular PGRN into the

extracellular space via lysosomal exocytosis, a well described process in which lysosomes fuse with the plasma membrane and release their lumenal contents.

In summary, our molecular and cellular characterization of TMEM106B and studies on TMEM106B and PGRN interaction revealed a relationship between PGRN and TMEM106B that converges on regulation of endolysosomal trafficking and function. These results will shed light on how PGRN and TMEM106B affect FTLD-U pathogenesis and how PGRN and TMEM106B are regulated at the molecular and cellular levels. Further studies to monitor the dynamics of endosome-lysosome fusion with live imaging, to examine the detailed morphology of TMEM106B induced vacuoles with electron microscopy, and to identify TMEM106B binding partners will give us insights into mechanisms of endosome-lysosome dynamics regulated by TMEM106B

3.6 Acknowledgements

We thank Drs. Bill Brown, Volker Vogt, Haiyuan Yu for their generous gifts of plasmids and antibodies, Mrs. Xiaochun Wu for technical assistance, Dr. Scott Emr and Tony Bretscher for helpful discussions and Dr. Yuxin Mao for critical reading of the manuscript. This work is supported by funding to F.H. from Weill Institute for Cell and Molecular Biology and from the Association of Frontotemporal Dementia (AFTD), Alzheimer's Association and NIH (R21 NS081357-01). O.A.B is supported by BMCB training grant.

3.7 Supplementary Information

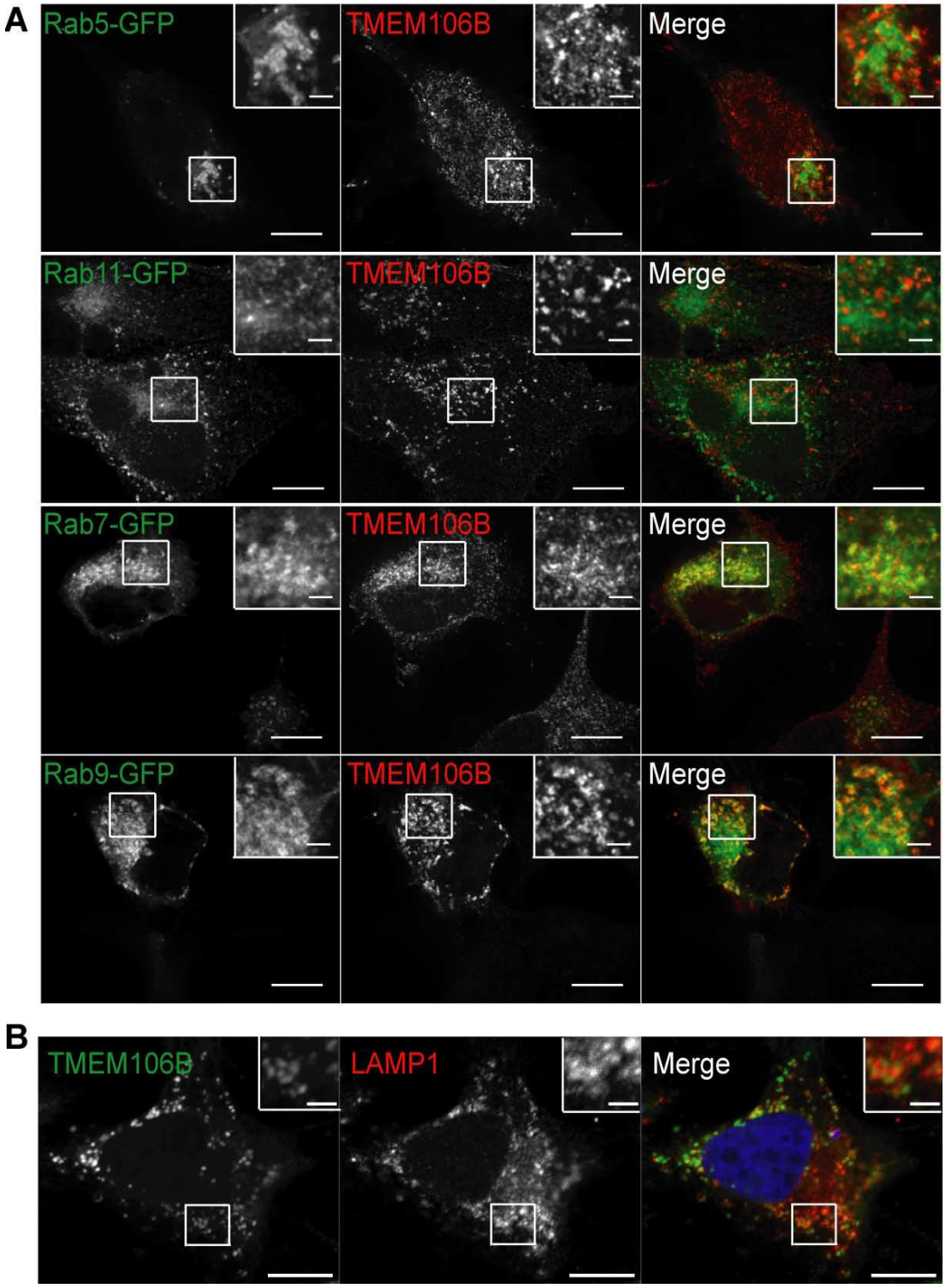

Figure S3.1: TMEM106B localizes to late endosomes/lysosomes. (**A**) Colocalization of TMEM106B with Rab7 and Rab9 in T98G cells. Flag tagged TMEM106B were co-transfected with GFP-tagged Rab GTPases as indicated into T98G cells. Cells were fixed and stained with anti-Flag antibodies. (**B**) Colocalization of TMEM106B with endogenous LAMP1 in T98G cells. Untagged TMEM106B was transfected into T98G cells which were fixed and stained with anti-TMEM106B and LAMP1 antibodies.

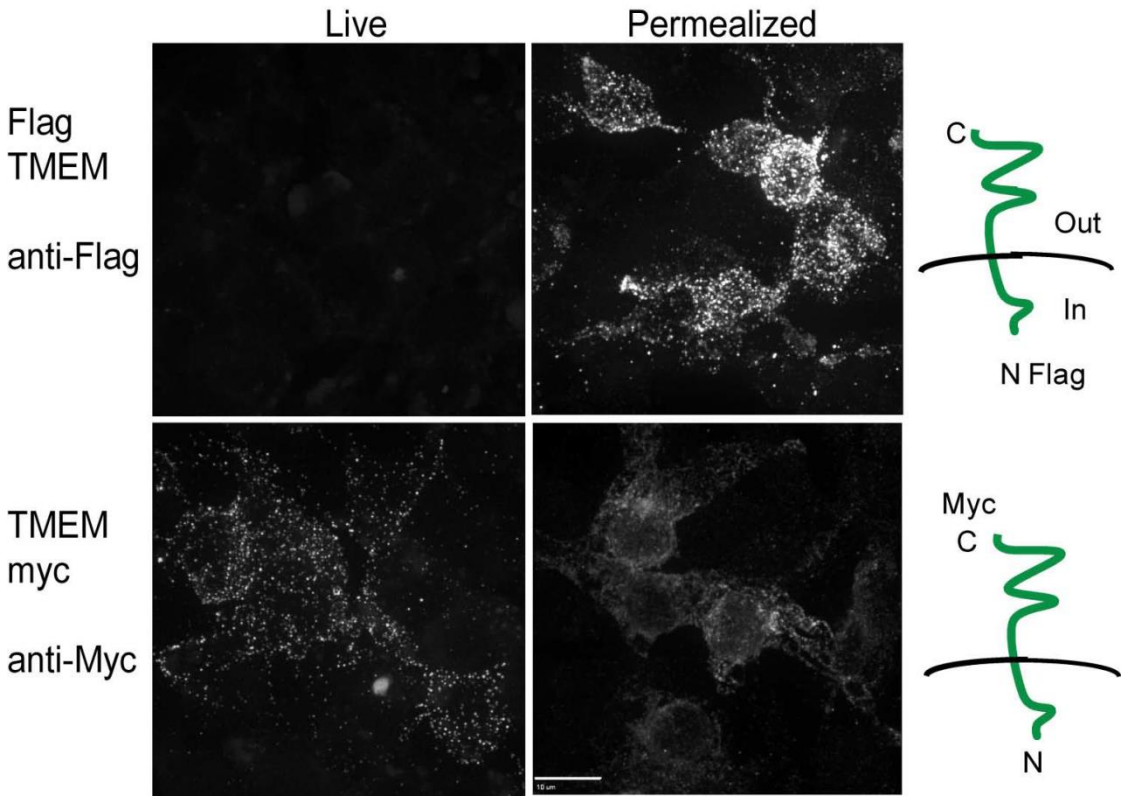

Figure S3.2: TMEM106B is a type II transmembrane protein. HEK293T cells were transfected with N-terminal Flag tagged TMEM106B (Flag-TMEM106B) or C-terminal myc tagged TMEM106B (TMEM106B-myc). Cells were either incubated with anti-Flag or anti-myc antibodies on ice for 2 hours (live) or incubated with these antibodies after fixation and permealization (permeablized). Confocal images were acquired. Scale bar=10μm.

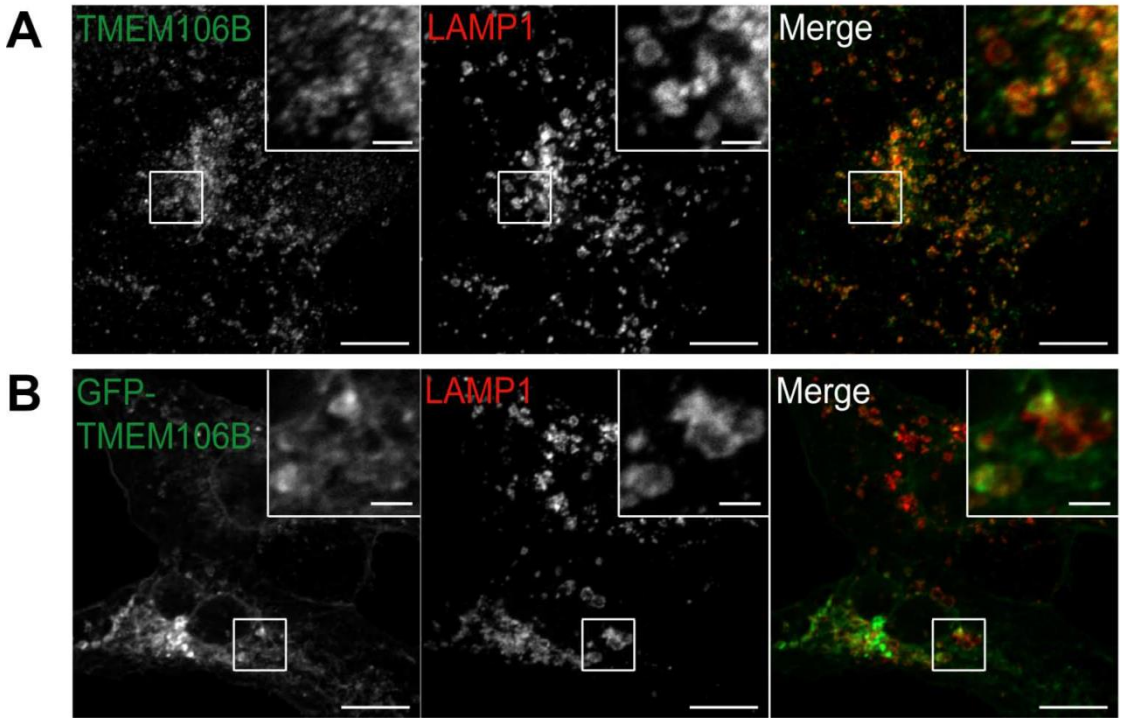

Figure S3.3: GFP-TMEM106B expression in COS7 cells results in enlarged lysosomes. (**A**) Cells were transfected with vector control, fixed and stained with anti-TMEM106B and anti-LAMP1 antibodies. (**B**) Cells were transfected with GFP-TMEM106B, fixed and stained with anti-LAMP1 antibodies.

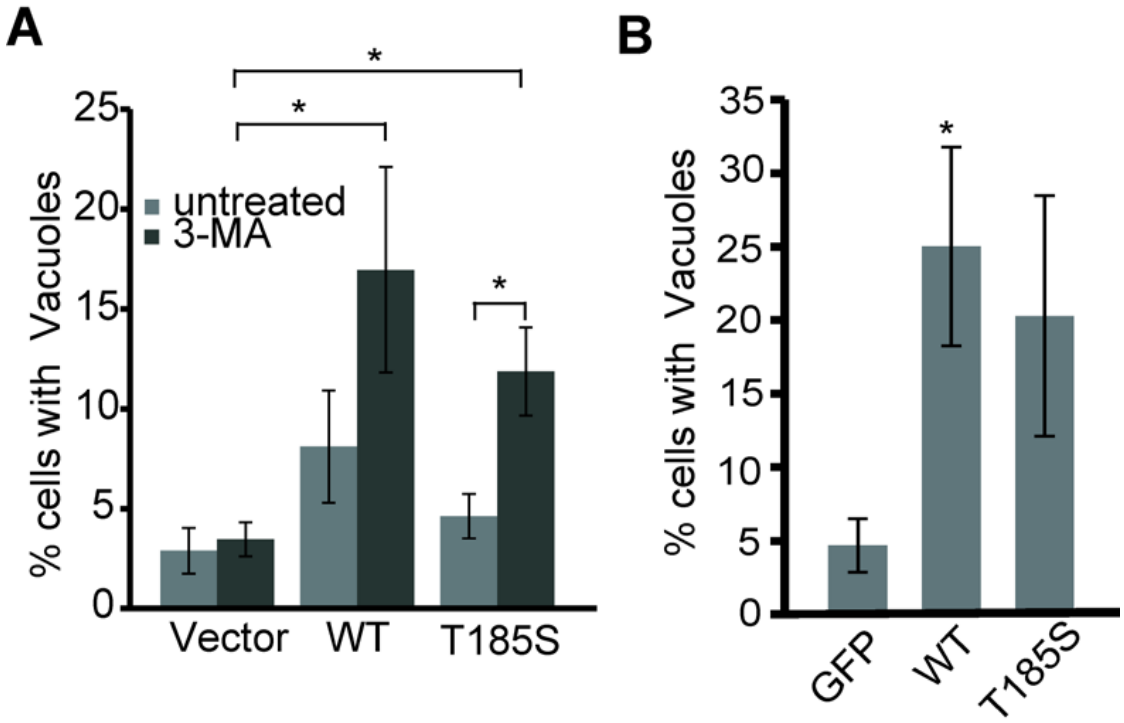

Figure S3.4: TMEM106B overexpression results in enlarged vacuoles in N2A cells. (**A**) 3-MA (5mM for 12 hours) treatment results in enlarged vacuoles with TMEM106B overexpression. Cells with vacuoles • 3 μm in diameter were scored as positive. n=4 * $p<0.05$, Student's t-test. (**B**) GFP-TMEM106B expression in N2A leads the accumulation of vacuoles. Cells with vacuoles • 3 μm in diameter were scored as positive. n=4 * $p<0.05$, Student's t-test.

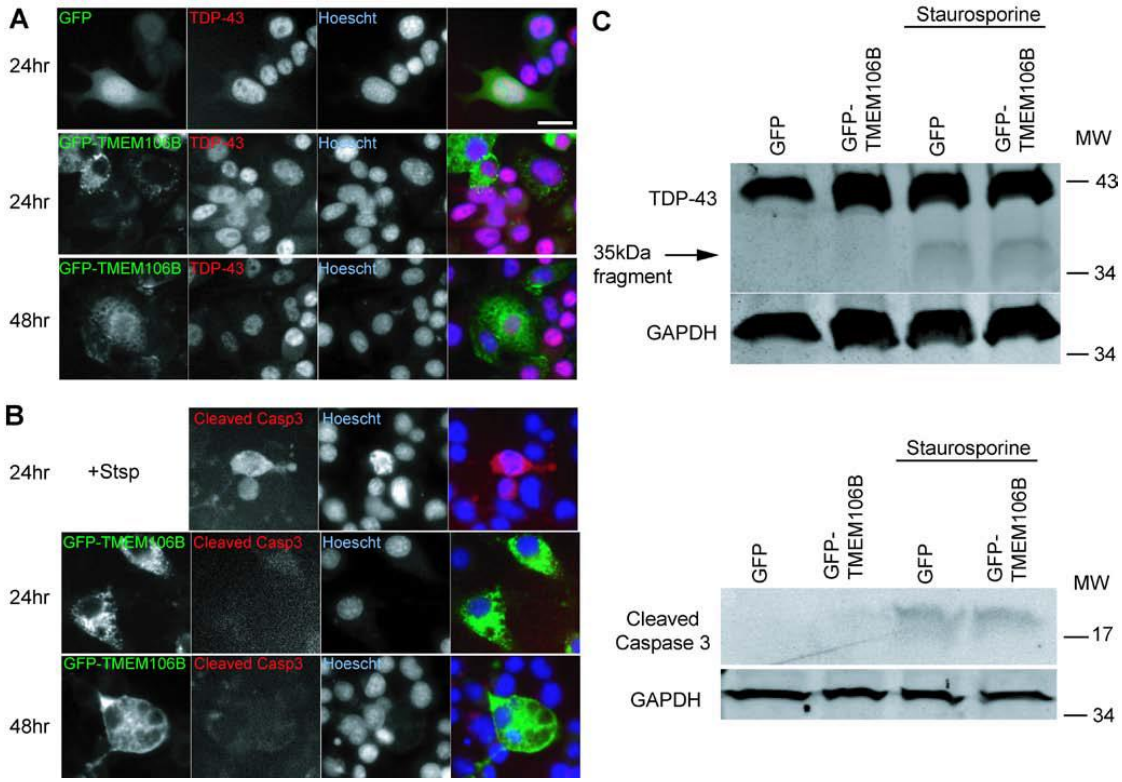

Figure S3.5: GFP-TMEM106B vacuolization does not perturb TDP-43 nuclear localization or cause apoptosis. (**A**) N2A cells were transfected with GFP control or GFP-TMEM106B for 24 hrs and 48 hrs. Cells were fixed and stained with polyclonal rabbit anti-TDP 43 antibodies. (**B**) GFP-TMEM106B expressing cells exhibited minimum caspase-3 staining at 24 hrs and 48 hrs after transfection. As a positive control, N2A cells were treated with 1 μM staurosporine for 3rs to induce apoptosis as indicated by cleaved caspase-3 staining. (**C&D**) Staurosporine, but not GFP-TMEM106B expression alone, induces TDP-43 and caspase 3 cleavage in N2A cells.

REFERENCES

1. Neary, D., Snowden, J., and Mann, D. (2005) Frontotemporal dementia. *Lancet Neurol* **4**, 771-780
2. Ratnavalli, E., Brayne, C., Dawson, K., and Hodges, J. R. (2002) The prevalence of frontotemporal dementia. *Neurology* **58**, 1615-1621
3. Baker, M., Mackenzie, I. R., Pickering-Brown, S. M., Gass, J., Rademakers, R., Lindholm, C., Snowden, J., Adamson, J., Sadovnick, A. D., Rollinson, S., Cannon, A., Dwosh, E., Neary, D., Melquist, S., Richardson, A., Dickson, D., Berger, Z., Eriksen, J., Robinson, T., Zehr, C., Dickey, C. A., Crook, R., McGowan, E., Mann, D., Boeve, B., Feldman, H., and Hutton, M. (2006) Mutations in progranulin cause tau-negative frontotemporal dementia linked to chromosome 17. *Nature* **442**, 916-919
4. Cruts, M., Gijselinck, I., van der Zee, J., Engelborghs, S., Wils, H., Pirici, D., Rademakers, R., Vandenberghe, R., Dermaut, B., Martin, J. J., van Duijn, C., Peeters, K., Sciot, R., Santens, P., De Pooter, T., Mattheijssens, M., Van den Broeck, M., Cuijt, I., Vennekens, K., De Deyn, P. P., Kumar-Singh, S., and Van Broeckhoven, C. (2006) Null mutations in progranulin cause ubiquitin-positive frontotemporal dementia linked to chromosome 17q21. *Nature* **442**, 920-924
5. Gass, J., Cannon, A., Mackenzie, I. R., Boeve, B., Baker, M., Adamson, J., Crook, R., Melquist, S., Kuntz, K., Petersen, R., Josephs, K., Pickering-Brown, S. M., Graff-Radford, N., Uitti, R., Dickson, D., Wszolek, Z., Gonzalez, J., Beach, T. G., Bigio, E., Johnson, N., Weintraub, S., Mesulam, M., White, C. L., 3rd, Woodruff, B., Caselli, R., Hsiung, G. Y., Feldman, H., Knopman, D., Hutton, M., and Rademakers, R. (2006) Mutations in progranulin are a major cause of ubiquitin-positive frontotemporal lobar degeneration. *Hum Mol Genet* **15**, 2988-3001
6. Bateman, A., and Bennett, H. P. (2009) The granulin gene family: from cancer to dementia. *Bioessays* **31**, 1245-1254
7. Hu, F., Padukkavidana, T., Vaegter, C. B., Brady, O. A., Zheng, Y., Mackenzie, I. R., Feldman, H. H., Nykjaer, A., and Strittmatter, S. M. (2010) Sortilin-mediated endocytosis determines levels of the frontotemporal dementia protein, progranulin. *Neuron* **68**, 654-667
8. Carrasquillo, M. M., Nicholson, A. M., Finch, N., Gibbs, J. R., Baker, M., Rutherford, N. J., Hunter, T. A., DeJesus-Hernandez, M., Bisceglio, G. D., Mackenzie, I. R., Singleton, A., Cookson, M. R., Crook, J. E., Dillman, A., Hernandez, D., Petersen, R. C., Graff-Radford, N. R., Younkin, S. G., and Rademakers, R. (2010) Genome-wide screen identifies rs646776 near sortilin as a regulator of progranulin levels in human plasma. *Am J Hum Genet* **87**, 890-897
9. Van Deerlin, V. M., Wood, E. M., Moore, P., Yuan, W., Forman, M. S., Clark, C. M., Neumann, M., Kwong, L. K., Trojanowski, J. Q., Lee, V. M., and Grossman, M. (2007) Clinical, genetic, and pathologic characteristics of

patients with frontotemporal dementia and progranulin mutations. *Arch Neurol* **64**, 1148-1153

10. Cruchaga, C., Graff, C., Chiang, H. H., Wang, J., Hinrichs, A. L., Spiegel, N., Bertelsen, S., Mayo, K., Norton, J. B., Morris, J. C., and Goate, A. (2011) Association of TMEM106B gene polymorphism with age at onset in granulin mutation carriers and plasma granulin protein levels. *Arch Neurol* **68**, 581-586
11. Finch, N., Carrasquillo, M. M., Baker, M., Rutherford, N. J., Coppola, G., Dejesus-Hernandez, M., Crook, R., Hunter, T., Ghidoni, R., Benussi, L., Crook, J., Finger, E., Hantanpaa, K. J., Karydas, A. M., Sengdy, P., Gonzalez, J., Seeley, W. W., Johnson, N., Beach, T. G., Mesulam, M., Forloni, G., Kertesz, A., Knopman, D. S., Uitti, R., White, C. L., 3rd, Caselli, R., Lippa, C., Bigio, E. H., Wszolek, Z. K., Binetti, G., Mackenzie, I. R., Miller, B. L., Boeve, B. F., Younkin, S. G., Dickson, D. W., Petersen, R. C., Graff-Radford, N. R., Geschwind, D. H., and Rademakers, R. (2011) TMEM106B regulates progranulin levels and the penetrance of FTLD in GRN mutation carriers. *Neurology* **76**, 467-474
12. Van Deerlin, V. M., Sleiman, P. M., Martinez-Lage, M., Chen-Plotkin, A., Wang, L. S., Graff-Radford, N. R., Dickson, D. W., Rademakers, R., Boeve, B. F., Grossman, M., Arnold, S. E., Mann, D. M., Pickering-Brown, S. M., Seelaar, H., Heutink, P., van Swieten, J. C., Murrell, J. R., Ghetti, B., Spina, S., Grafman, J., Hodges, J., Spillantini, M. G., Gilman, S., Lieberman, A. P., Kaye, J. A., Woltjer, R. L., Bigio, E. H., Mesulam, M., Al-Sarraj, S., Troakes, C., Rosenberg, R. N., White, C. L., 3rd, Ferrer, I., Llado, A., Neumann, M., Kretzschmar, H. A., Hulette, C. M., Welsh-Bohmer, K. A., Miller, B. L., Alzualde, A., Lopez de Munain, A., McKee, A. C., Gearing, M., Levey, A. I., Lah, J. J., Hardy, J., Rohrer, J. D., Lashley, T., Mackenzie, I. R., Feldman, H. H., Hamilton, R. L., Dekosky, S. T., van der Zee, J., Kumar-Singh, S., Van Broeckhoven, C., Mayeux, R., Vonsattel, J. P., Troncoso, J. C., Kril, J. J., Kwok, J. B., Halliday, G. M., Bird, T. D., Ince, P. G., Shaw, P. J., Cairns, N. J., Morris, J. C., McLean, C. A., DeCarli, C., Ellis, W. G., Freeman, S. H., Frosch, M. P., Growdon, J. H., Perl, D. P., Sano, M., Bennett, D. A., Schneider, J. A., Beach, T. G., Reiman, E. M., Woodruff, B. K., Cummings, J., Vinters, H. V., Miller, C. A., Chui, H. C., Alafuzoff, I., Hartikainen, P., Seilhean, D., Galasko, D., Masliah, E., Cotman, C. W., Tunon, M. T., Martinez, M. C., Munoz, D. G., Carroll, S. L., Marson, D., Riederer, P. F., Bogdanovic, N., Schellenberg, G. D., Hakonarson, H., Trojanowski, J. Q., and Lee, V. M. (2010) Common variants at 7p21 are associated with frontotemporal lobar degeneration with TDP-43 inclusions. *Nat Genet* **42**, 234-239
13. van der Zee, J., Van Langenhove, T., Kleinberger, G., Sleegers, K., Engelborghs, S., Vandenberghe, R., Santens, P., Van den Broeck, M., Joris, G., Brys, J., Mattheijssens, M., Peeters, K., Cras, P., De Deyn, P. P., Cruts, M., and Van Broeckhoven, C. (2011) TMEM106B is associated with frontotemporal lobar degeneration in a clinically diagnosed patient cohort. *Brain* **134**, 808-815

14. Vass, R., Ashbridge, E., Geser, F., Hu, W. T., Grossman, M., Clay-Falcone, D., Elman, L., McCluskey, L., Lee, V. M., Van Deerlin, V. M., Trojanowski, J. Q., and Chen-Plotkin, A. S. (2011) Risk genotypes at TMEM106B are associated with cognitive impairment in amyotrophic lateral sclerosis. *Acta Neuropathol* **121**, 373-380
15. Rollinson, S., Mead, S., Snowden, J., Richardson, A., Rohrer, J., Halliwell, N., Usher, S., Neary, D., Mann, D., Hardy, J., and Pickering-Brown, S. (2011) Frontotemporal lobar degeneration genome wide association study replication confirms a risk locus shared with amyotrophic lateral sclerosis. *Neurobiol Aging* **32**, 758 e751-757
16. van der Zee, J., and Van Broeckhoven, C. (2011) TMEM106B a novel risk factor for frontotemporal lobar degeneration. *J Mol Neurosci* **45**, 516-521
17. Wood, H. B. (2010) TMEM106B is a susceptibility locus for Ftld. *Nat Rev Neurol* **6**, 184
18. Chen-Plotkin, A. S., Unger, T. L., Gallagher, M. D., Bill, E., Kwong, L. K., Volpicelli-Daley, L., Busch, J. I., Akle, S., Grossman, M., Van Deerlin, V., Trojanowski, J. Q., and Lee, V. M. (2012) TMEM106B, the risk gene for frontotemporal dementia, is regulated by the microRNA-132/212 cluster and affects progranulin pathways. *J Neurosci* **32**, 11213-11227
19. Lang, C. M., Fellerer, K., Schwenk, B. M., Kuhn, P. H., Kremmer, E., Edbauer, D., Capell, A., and Haass, C. (2012) Membrane orientation and subcellular localization of transmembrane protein 106B (TMEM106B), a major risk factor for frontotemporal lobar degeneration. *J Biol Chem* **287**, 19355-19365
20. Cashman, N. R., Durham, H. D., Blusztajn, J. K., Oda, K., Tabira, T., Shaw, I. T., Dahrouge, S., and Antel, J. P. (1992) Neuroblastoma x spinal cord (NSC) hybrid cell lines resemble developing motor neurons. *Dev Dyn* **194**, 209-221
21. Blasi, E., Barluzzi, R., Bocchini, V., Mazzolla, R., and Bistoni, F. (1990) Immortalization of murine microglial cells by a v-raf/v-myc carrying retrovirus. *J Neuroimmunol* **27**, 229-237
22. Vancha, A. R., Govindaraju, S., Parsa, K. V., Jasti, M., Gonzalez-Garcia, M., and Ballestero, R. P. (2004) Use of polyethyleneimine polymer in cell culture as attachment factor and lipofection enhancer. *BMC Biotechnol* **4**, 23
23. Backer, J. M. (2008) The regulation and function of Class III PI3Ks: novel roles for Vps34. *Biochem J* **410**, 1-17
24. Ohkuma, S. (1989) Use of fluorescein isothiocyanate-dextran to measure proton pumping in lysosomes and related organelles. *Methods Enzymol* **174**, 131-154
25. Eden, E. R., White, I. J., and Futter, C. E. (2009) Down-regulation of epidermal growth factor receptor signalling within multivesicular bodies. *Biochem Soc Trans* **37**, 173-177
26. Han, J. H., Ryu, H. H., Jun, M. H., Jang, D. J., and Lee, J. A. (2012) The functional analysis of the CHMP2B missense mutation associated with neurodegenerative diseases in the endo-lysosomal pathway. *Biochem Biophys Res Commun* **421**, 544-549

27. Hirabayashi, M., Inoue, K., Tanaka, K., Nakadate, K., Ohsawa, Y., Kamei, Y., Popiel, A. H., Sinohara, A., Iwamatsu, A., Kimura, Y., Uchiyama, Y., Hori, S., and Kakizuka, A. (2001) VCP/p97 in abnormal protein aggregates, cytoplasmic vacuoles, and cell death, phenotypes relevant to neurodegeneration. *Cell Death Differ* **8**, 977-984
28. Lee, J. A., Beigneux, A., Ahmad, S. T., Young, S. G., and Gao, F. B. (2007) ESCRT-III dysfunction causes autophagosome accumulation and neurodegeneration. *Curr Biol* **17**, 1561-1567
29. Urwin, H., Authier, A., Nielsen, J. E., Metcalf, D., Powell, C., Froud, K., Malcolm, D. S., Holm, I., Johannsen, P., Brown, J., Fisher, E. M., van der Zee, J., Bruyland, M., Van Broeckhoven, C., Collinge, J., Brandner, S., Futter, C., and Isaacs, A. M. (2010) Disruption of endocytic trafficking in frontotemporal dementia with CHMP2B mutations. *Hum Mol Genet* **19**, 2228-2238
30. Belcastro, V., Siciliano, V., Gregoretti, F., Mithbaokar, P., Dharmalingam, G., Berlingieri, S., Iorio, F., Oliva, G., Polishchuck, R., Brunetti-Pierri, N., and di Bernardo, D. (2011) Transcriptional gene network inference from a massive dataset elucidates transcriptome organization and gene function. *Nucleic Acids Res* **39**, 8677-8688
31. Ahmed, Z., Sheng, H., Xu, Y. F., Lin, W. L., Innes, A. E., Gass, J., Yu, X., Wuertzer, C. A., Hou, H., Chiba, S., Yamanouchi, K., Leissring, M., Petrucelli, L., Nishihara, M., Hutton, M. L., McGowan, E., Dickson, D. W., and Lewis, J. (2010) Accelerated lipofuscinosis and ubiquitination in granulin knockout mice suggest a role for progranulin in successful aging. *Am J Pathol* **177**, 311-324
32. Smith, K. R., Damiano, J., Franceschetti, S., Carpenter, S., Canafoglia, L., Morbin, M., Rossi, G., Pareyson, D., Mole, S. E., Staropoli, J. F., Sims, K. B., Lewis, J., Lin, W. L., Dickson, D. W., Dahl, H. H., Bahlo, M., and Berkovic, S. F. (2012) Strikingly different clinicopathological phenotypes determined by progranulin-mutation dosage. *Am J Hum Genet* **90**, 1102-1107

CHAPTER 4

REGULATED INTRAMEMBRANE PROTEOLYSIS OF THE FRONTOTEMPORAL LOBAR DEGENERATION (FTLD) RISK FACTOR, TMEM106B, BY SPPL2A AND SPPL2B [1]

4.1 Summary

The sequential processing of single pass transmembrane proteins via ectodomain shedding followed by intramembrane proteolysis is involved in a wide variety of signaling processes as well as maintenance of membrane protein homeostasis. Here we report that the recently identified frontotemporal lobar degeneration (FTLD) risk factor TMEM106B undergoes regulated intramembrane proteolysis. We demonstrate that, when overexpressed, TMEM106B is readily processed to the N-terminal fragment (NTF) containing the transmembrane and intracellular domain. The NTFis further processed into a small, rapidly degraded membrane associated intracellular domain (ICD). The GxGD aspartyl proteases SPPL2a, and to a lesser extent, SPPL2b, are responsible for this second cleavage event. Additionally, the TMEM106B paralog, TMEM106A, is also lysosomally localized and appears to undergo similar proteolytic processing; however, it is not a specific substrate of SPPL2a or SPPL2b. Our data adds to the growing list of proteins that undergo intramembrane proteolysis and may shed light on the regulation of the TMEM106 family of proteins.

[1]The results of this study were submitted for publication in *J Biol. Chem.* The manuscript is currently undergoing revisions to address reviewer comments prior to resubmission. Experiments were designed by O.A.B. and F.H. All experiments were performed by O.A.B. O.A.B. and F.H. wrote the manuscript.

4.2 Introduction

The regulated intramembrane proteolysis (RIP)[2] of transmembrane proteins has emerged as a widespread and evolutionarily conserved mechanism for coordinating both extracellular and intracellular signaling events in cells (1). Generally, an initial proteolytic event results in the shedding of an ectodomain followed by intramembrane processing of the transmembrane stump, liberating an intracellular domain (ICD) and a small peptide corresponding to the transmembrane region between the two cleavage sites. An increasing number functions have been being ascribed to RIP in health and disease, including signaling functions such as transcriptional regulation by ICDs liberated from amyloid precursor protein (APP), and Notch, among many others (2,3). RIP is also implicated in the processing of MHC-I molecules by signal peptide peptidase (SPP) in the ER (4). Finally, RIP may also represent a generalized mechanism for regulating the levels of membrane proteins (5).

Intramembrane cleaving proteases (iCLiPs) are a diverse group of three major protein families: the S2P-metalloproteases, the rhomboid serine proteases, and the GxGD-type aspartyl proteases, all of which are capable of cleaving proteins within the lipid bilayer (6). The signal peptide peptidase-like (SPPL) class of intramembrane proteases is part of the larger family of GxGD aspartyl proteases (7). Within this aspartyl protease family, presenilin, has a strict preference for cleaving type I transmembrane proteins and the SPPL family has a strict requirement for type II

membrane proteins which corresponds to a topological inversion of the catalytic sites within the membrane, relative to presenilin (8,9). Intramembrane cleavage of transmembrane proteins by these proteases requires an initial ectodomain shedding event in order for the substrate to be accessible (10-12). Each member of the SPPL family has a specific subcellular localization and tissue distribution, suggesting that each may have unique substrate preferences (9,13).

TMEM106B was first identified as a genetic risk factor for frontotemporal lobar degeneration (FTLD) caused by mutations in the *progranulin* gene (14,15). TMEM106B is a type II single pass transmembrane protein residing primarily within the limiting membrane of late endosomes and lysosomes (16-18). The SNPs associated with increased risk for FTLD do not result in mutations in the TMEM106B protein, but instead lead to elevated mRNA and protein levels of TMEM106B (14,17). Increased TMEM106B levels have been shown to cause various lysosomal defects including altered morphology, impaired acidification, and reduced degradative capacity (17,18). Furthermore, a coding variant T185S, in linkage disequilibrium with the protective allele of *TMEM106B* has been proposed to be more rapidly degraded, further implicating elevated TMEM106B levels as a potential mechanism underlying FTLD risk (19).

4.3 Materials and Methods

Pharmacological Reagents and Antibodies

The following antibodies were used in this study: mouse anti-FLAG (M2) from Sigma, mouse anti-HA (HA.11) from Covance, mouse anti-GAPDH from Proteintech

Group, Mouse anti-v5 from Invitrogen, and rat anti-mouse LAMP1 (1D4B) from BD Biosciences. Rabbit anti-TMEM106B was generated against the ICD as described (18). 3-methyladenine (3-MA), Phorbol 12-myristate 13-acetate (PMA), leupeptin, and ammonium chloride were purchased from Sigma. TAPI-2, GM6001, BACE IV inhibitor, and $(ZLL)_2$-ketone were from EMD Millipore.

Expression Constructs

Human TMEM106B cDNA was obtained from Open Biosystems in pCMV-Sport6. SPPL2b, SPPL2c, TMEM106A, and TMEM106C were obtained from ORFeome Collection (kind gifts from Dr. Haiyuan Yu). SPPL2a was obtained from the DNASU Plasmid Repository (Arizona State University). All TMEM106 family cDNAs were subloned into the p3XFLAG-CMV7.1 vector (Sigma-Aldrich).All SPPL2 family cDNAs were subcloned into pCDNA3.1(+)-V5/HisA (Invitrogen). The SPPL2a D412A mutant was generated by site directed mutagenesis. HA-TNFα in the pCMV-Tag 4 vector (Stratagene) was kindly provided by Dr. Hening Lin.

Cell Culture, DNA Transfection, and Drug Treatment

Human embryonic kidney HEK293T and mouse N2a cells were maintained in Dulbecco's Modified Eagle's medium (Cellgro) supplemented with 10% fetal bovine serum (Gibco) and 1% Penicillin–Streptomycin (Invitrogen) in a humidified incubator at 37ºC and 5% CO_2. Cells were transiently transfected with polyethyleneamine as described (20). Cells were either treated with 200 nM PMA for 2 hours, or with 50 µM TAPI-2, 50 µM GM6001, 20 µM BACE IV inhibitor, 15 mM ammonium chloride, 250 µM leupeptin, or 50 µM $(ZLL)_2$-ketone for 16 hours. 3-MA was used at 5 or 10 mM for 14 hours.

Western Blot Analysis

Cells were washed with PBS 48 hours post-transfection and whole cell lysates were collected in Laemmli sample buffer with β-mercaptoethanol. Whole cell lysates were sonicated and kept on ice or heated at 95ºC for 2 minutes. Samples were separated on 12% SDS-PAGE gels or 16% tricine gels and transferred to Immobilon-FL polyvinylidene fluoride membranes (Millipore). Membranes were blocked for 1 hour with 5% non-fat milk in PBS and incubated in an equal mix of TBS with 0.1% Tween-20 (TBS-T) and Odyssey blocking buffer (LI-COR Biosciences) containing primary antibodies overnight at 4ºC. Membranes were washed three times with TBS-T, incubated with secondary antibodies conjugated to AlexaFluor 680 (Invitrogen) or IRDye 800 (LI-COR Biosciences) for 1 hour at room temperature. Membranes were washed three more times with TBS-T then imaged and quantified using an Odyssey Infrared Imaging System (LI-COR Biosciences).

Immunofluorescence Microscopy

Cells on coverslips were washed with PBS 48 hours post-transfection and fixed in 4% paraformaldehyde for 15 minutes at room temperature. Cells were washed 3 more times with PBS followed by permeabilization and blocking in blocking buffer (0.05% Saponin, 3% BSA in PBS) for 1 hour. Primary antibodies were incubated in blocking buffer overnight at 4ºC. Cells were washed and incubated in secondary antibodies conjugated to CF488A, CF568, or CF660C (Biotum). Cells were washed three more times and coverslips mounted on to slides with Fluoromount G (SouthernBiotech). Images were acquired on a CSU-X spinning disc confocal microscope (Intelligent

Imaging Innovations) with an HQ2 CCD camera (Photometrics) using a 100x objective.

4.4 Results

TMEM106B is proteolytically processed

When N-terminally FLAG tagged TMEM106B is overexpressed in HEK293T cells, we observed a faint band at 20 kDa in addition to the 50 kDa full length TMEM106B in Western blot using an anti- FLAG antibody. We hypothesized that the 20 kDa band was the N-terminal transmembrane stump remaining after cleavage of the TMEM106B lumenal domain. We refer to this product as the N-terminal fragment (NTF) (Figure 4.1A). Because ectodomain shedding is a prerequisite for most know instances of RIP, we decided to test if this NTF could be further processed by an iCLiP to produce an ICD. Note that ectodomain shedding generally refers to the extracellular release of a soluble protein domain; however, TMEM106B is almost exclusively localized to late endosomes/lysosomes. We will henceforth refer to this analogous shedding event as lumenal domain shedding.

In order to increase the amount of substrate available to increase our chances of detecting an ICD, we treated cells with 3-MA, an inhibitor of the class III PI3 kinase VPS34. Inhibition of this enzyme prevents the induction of autophagy and increases the levels of TMEM106B (18,21). When cells overexpressing FLAG-TMEM106B were treated with 3-MA, we observed a ~18kDa band in addition to the 20 kDa NTF and full length TMEM106B, which we predicted to be the TMEM106B ICD. The SPP family of iCLiPs has been shown to cleave a number of type II

transmembrane proteins at various subcellular locations (13,22-25). Treatment of TMEM106B overexpressing cells with the specific SPP class protease inhibitor $(ZLL)_2$-ketone led to an increase in the relative amount of TMEM106B NTF generated and a concomitant decrease in the ICD, suggesting that an endogenous SPP class protease plays a role in cleaving the TMEM106B NTF in HEK293T cells (Figure 4.1A).

We attempted to reproduce this effect in cells transfected with untagged TMEM106B. To our surprise, untagged TMEM106B produced relatively more TMEM106B NTF and ICD than the FLAG-tagged construct, indicating that the FLAG-tag may be sterically hindering the active protease's access of the NTF substrate. Treatment with $(ZLL)_2$-ketone led to a significant decrease in the amount of ICD generated relative to the NTF and full-length TMEM106B. Treatment with 3-MA elevated the levels of full-length TMEM106B, the NTF, and the ICD; however, the ratios between these fragments when treated with $(ZLL)_2$-ketone were no different from those of cells not treated with 3-MA (Figure 4.1C.).

In order to narrow down the possible enzymes required for the initial lumenal domain shedding event, we screened a number of compounds which are capable of inducing or inhibiting various classes of sheddase. Members of the A disintegrin and metalloproteinase (ADAM) family are often implicated in the primary ectodomain shedding event for transmembrane proteins prior to RIP (26). Cells treated with phorbol myristate acetate (PMA), a protein kinase C inducer which stimulates ADAM sheddase activity, failed to induce TMEM106B lumenal domain shedding as assessed by the levels of NTF produced relative to full-length protein (Figure 4.1B and 4.2A).

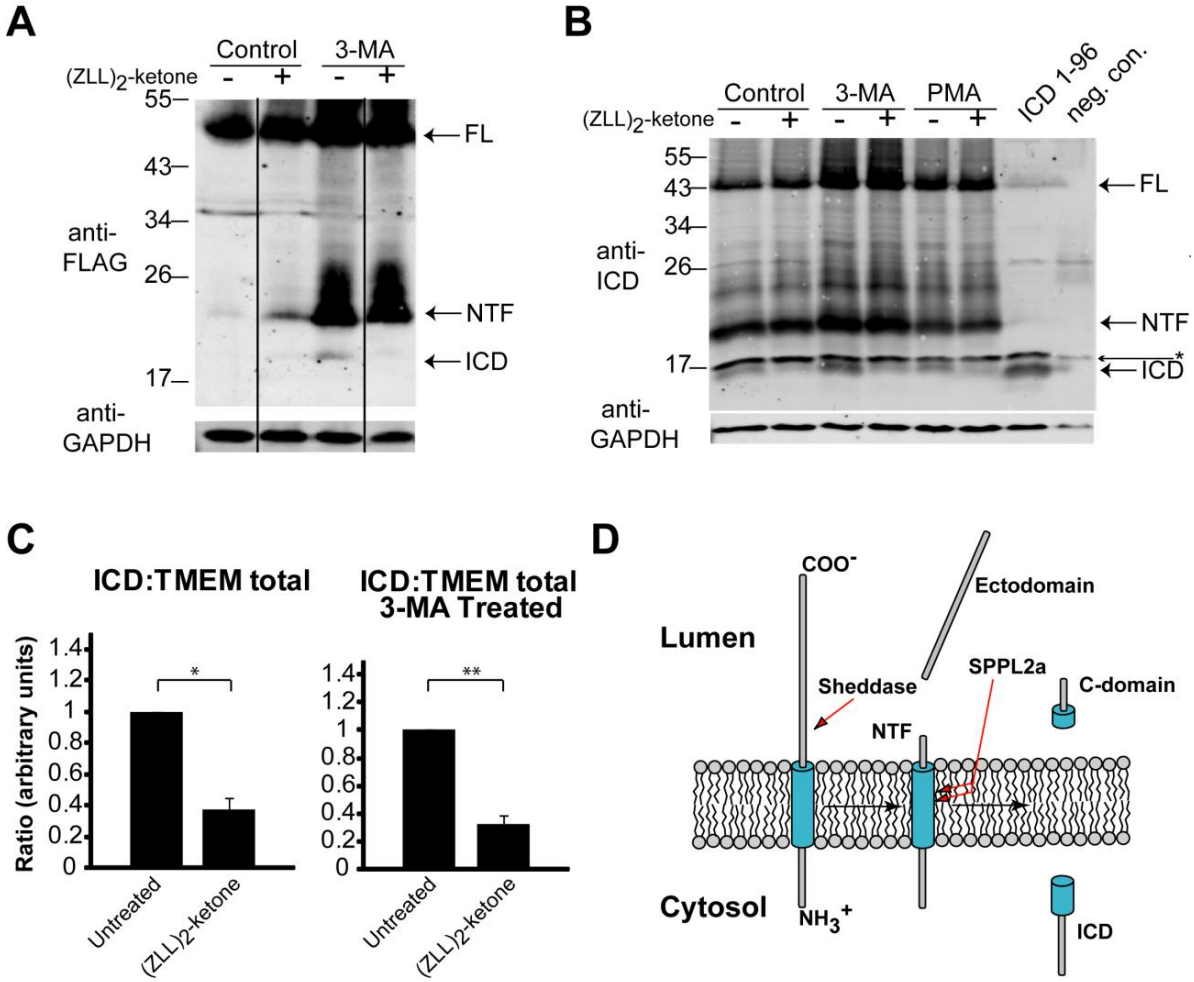
A
Control
3-MA
(ZLL)2-ketone
- + - +
55
43
34
26
17
anti-
FLAG
anti-
GAPDH
FL
NTF
ICD
B
Control
3-MA
PMA
ICD 1-96
neg. con.
(ZLL)2-ketone
- + - + - +
55
43
34
26
17
anti-
ICD
anti-
GAPDH
FL
NTF
ICD*
C
ICD:TMEM total
ICD:TMEM total
3-MA Treated
Ratio (arbitrary units)
1.4
1.2
1
0.8
0.6
0.4
0.2
0
*
**
Untreated
(ZLL)2-ketone
D
COO-
Ectodomain
Lumen
Sheddase
SPPL2a
C-domain
NTF
Cytosol
NH3+
ICD

Figure 4.1: TMEM106B undergoes sequential proteolysis. (**A**) HEK293T cells transfected with FLAG-TMEM106B were treated with 3-MA and/or $(ZLL)_2$-ketone for 14 hours as indicated. Whole cell lysates were subject to anti-FLAG western blot, which revealed a 50 kDa monomeric TMEM106B, a 20 kDa membrane-retained NTF stub, and an 18 kDa ICD. $(ZLL)_2$-ketone inhibits the formation of the ICD, resulting in an increase in the NTF levels. Vertical black lines indicate where the image was cropped from the same blot. (**B**) Untagged TMEM106B is more susceptible to cleavage than FLAG-TMEM106B. Western blots of 293T whole cell lysates transfected with TMEM106B and probed with a rabbit anti-TMEM106B ICD antibody reveal a 43 kDa full length protein, 19 kDa NTF, and 17 kDa ICD. The levels of all of these products are enhanced by treatment with 10 mM 3-MA. Treatment with 200nM PMA for 2 hours does not enhance lumenal domain shedding and NTF formation. Note that the TMEM106B fragment comprising amino acids 1-96 migrates slightly faster than the actual ICD. The asterisk indicates a non-specific band. (**C**) Quantitation of the results from (**B**). The ICD generated was quantitated by densitometry and calculated as a ratio relative to full length and NTF TMEM106B. Values were normalized to GAPDH intensity (n=3 +/- SEM, *p-value <0.05, *p-value <0.01, Student's t-test). (**D**) Schematic illustration of regulated intramembrane proteolysis of TMEM106B, yielding a released lumenal and a membrane-retained NTF which is further processed into an ICD and a small predicted peptide.

Treatment with the hydroxamic acid-based inhibitor TAPI-2, a broad spectrum inhibitor of sheddases in the matrix metalloproteinase (MMP) and ADAM families, failed to inhibit shedding, as assessed by the levels of NTF produced relative to full-length protein (Figure 4.2A). The related MMP inhibitor GM6001 also failed to affect shedding (data not shown). As a positive control for PMA and TAPI-2 activity, we treated TNFα expressing HEK293T cells with PMA pretreated with TAPI-2 or vehicle control. As expected, PMA induced a large decrease in the levels of full length TNFα while TAPI-2 pretreatment prevented this effect (Figure 4.2B). Most ADAM and MMP sheddases are primarily active at the cell surface and cleave extracellularly facing substrates (27,28). Our data confirms that these are unlikely candidates for TMEM106B lumenal shedding. BACE1, the sheddase for amyloid precursor protein required for β-amyloid generation, is active in endosomal and lysosomal compartments (29). However, treatment with BACE Inhibitor IV also failed to inhibit NTF generation (Figure 4.2A). The majority of known sheddases belong to either the metalloprotease family (MMP and ADAM) or the aspartic protease BACE family, none of which appear to be responsible for TMEM106B processing, suggesting a potentially novel mechanism for TMEM106B lumenal domain shedding. Lysosomes harbor a wide range of proteases, which can be inhibited by raising the pH of the lysosome or by direct inhibition with leupeptin, a protease inhibitor (30). Treatment with these lysosomal inhibitors result in a modest decrease in the levels of NTF relative to full TMEM106B compared to the other treatments. This suggests that the TMEM106B lumenal domain shedding event may occur within the lumen of the lysosome by a resident protease

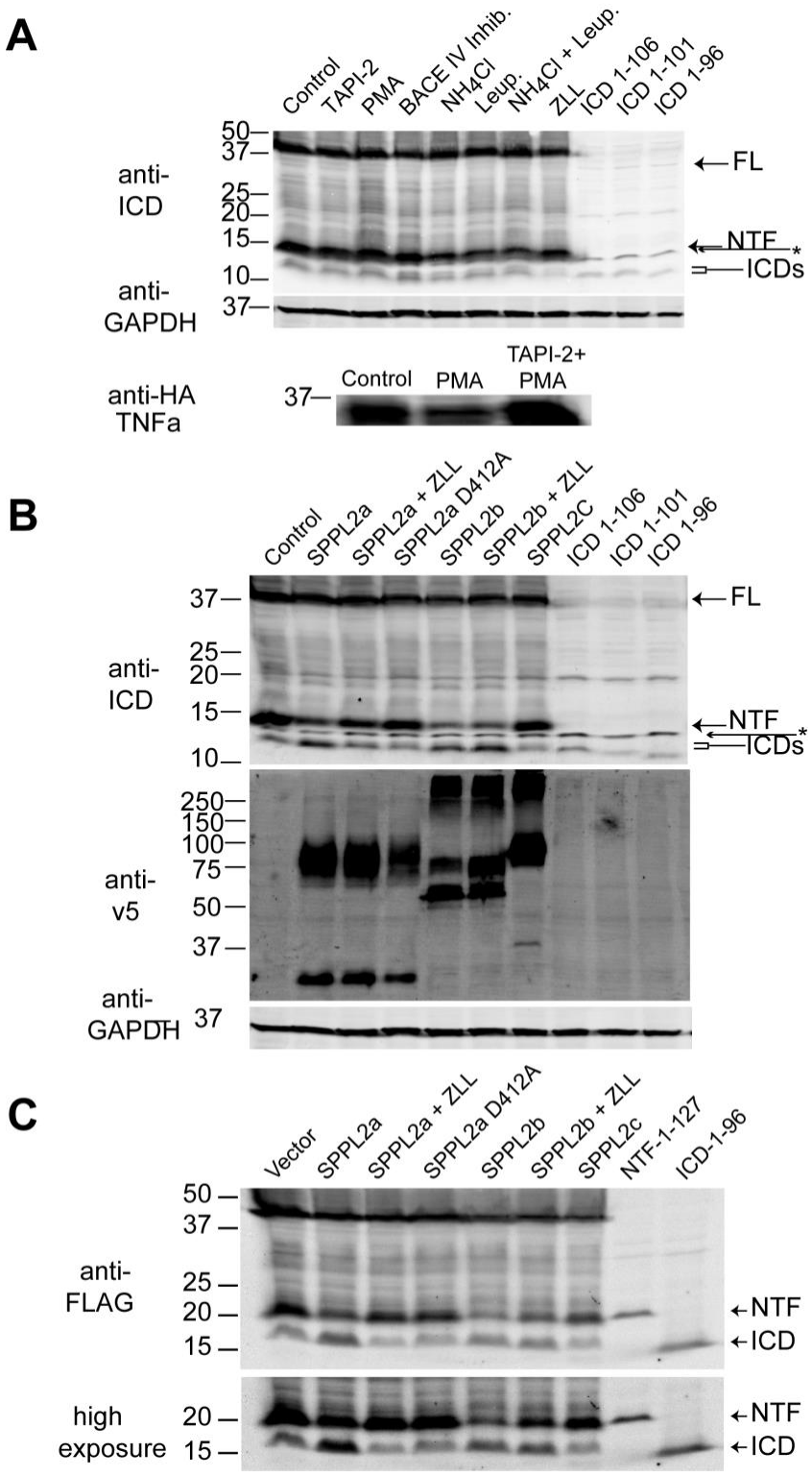
A
Control
TAPI-2
PMA
BACE IV Inhib.
NH4Cl
Leup.
NH4Cl + Leup.
ZLL
ICD 1-106
ICD 1-101
ICD 1-96
anti-ICD
anti-GAPDH
FL
NTF
ICDs
anti-HA TNFa
Control
PMA
TAPI-2+ PMA
B
Control
SPPL2a
SPPL2a + ZLL
SPPL2a D412A
SPPL2b
SPPL2b + ZLL
SPPL2C
ICD 1-106
ICD 1-101
ICD 1-96
anti-ICD
anti-v5
anti-GAPDH
FL
NTF
ICDs
C
Vector
SPPL2a
SPPL2a + ZLL
SPPL2a D412A
SPPL2b
SPPL2b + ZLL
SPPL2c
NTF-1-127
ICD-1-96
anti-FLAG
high exposure
NTF
ICD

Figure 4.2: TMEM106B lumenal domain shedding occurs at the lysosome and its NTF is cleaved by SPPL2a and SPPL2b. (**A**) TMEM106B lumenal domain shedding is not mediated by most known classes of sheddases including ADAMs and MMPs, but is slightly reduced by inhibition of lysosomal proteases. HA-TNFα blot is provided as a positive control for the effects of PMA and TAPI-2. PMA induces ectodomain shedding of full-length TNFα, which is prevented by pre-treatment with TAPI-2. HEK293T cells overexpressing TMEM106B were treated with indicated chemicals for 16 hours, except PMA which was treated for 2 hours. Concentrations used were 50 µM TAPI-2, 200 nM PMA, 20 µM BACE IV inhibitor, 15 mM ammonium chloride, 250 µM leupeptin, and 50 µM $(ZLL)_2$-ketone. ICD standards of different sizes show that the 106 amino acid fragment is closest in size to the ICD generated by TMEM106B. Note that the actual ICD appears as a doublet of two very closely spaced bands. (**B**) SPPL2a promotes the conversion of TMEM106B NTF to the ICD. This is inhibited by $(ZLL)_2$-ketone treatment (50 µM for 16 hours). The catalytically inactive mutant of SPPL2a (D412A) also fails to induce NTF conversion to ICD. SPPL2b promotes conversion of NTF to ICD and is somewhat resistant to $(ZLL)_2$-ketone inhibition under the conditions tested. SPPL2c fails to promote NTF to ICD conversion. The asterisk indicates a non-specific band. (**C**) FLAG-tagged TMEM106B cleavage by SPPL2 family members is similar to untagged TMEM106B. HEK293T cells transfected as indicated were treated with 5 mM 3-MA for 14 hours. FLAG-tagged TMEM106B NTF and ICD standards of 127 and 96 amino acids are run next to these TMEM106B fragments for reference.

The TMEM106B NTF is a substrate for intramembrane proteolysis by SPPL2a and SPPL2b

SPPL2a and SPPL2b have recently been implicated in the intramembrane proteolysis of several type II membrane proteins. To date, five known substrates have been identified: TNFα, Fas Ligand, British dementia protein-2/ITMB2 (Bri2), Transferrin Receptor 1, and CD74 (22-25,31-34). In some cases, SPPL2a and SPPL2b appear to share a common substrate such as TNFα, and Bri2. To test if TMEM106B could be a substrate of either of these enzymes, we co-transfected untagged TMEM106B into HEK293T cells with vector control, or expression constructs for SPPL2a, SPPL2b, and their paralog, SPPL2c. We found that both SPPL2a and SPPL2b, but not SPPL2c were capable of cleaving the TMEM106B NTF to generate smaller ICD fragments and this activity was inhibited by treatment with $(ZLL)_2$-ketone (Figure 4.2B and 4.2C). Additionally, D412A, a catalytically inactive mutant of SPPL2a failed to induce this cleavage, indicating that SPPL2a is indeed an active protease against the TMEM106B NTF.

SPPL2a has been reported to be primarily localized to late endosomes and lysosomes, whereas SPPL2b is primarily expressed at the cell surface (22,35). In order to demonstrate the localization of these proteases in TMEM106B expressing cells, we analyzed the localization of the v5 tagged SPPL2 proteins in N2a cells along with TMEM106B. TMEM106B appears primarily as discrete puncta on LAMP1 positive vesicles. SPPL2a as well as the D412A mutant could be detected on a subset of vesicles containing both LAMP1 and TMEM106B, indicating that SPPL2a could access lysosomal TMEM106B as a substrate (Figure 4.3A and B). SPPL2b localized

very poorly to these TMEM106B positive vesicles (Figure 4.3C). Instead, SPPL2b accumulated in large perinuclear stacks, suggesting that this construct accumulates in the Golgi (Figure 4.3C). SPPL2b might process TMEM106B in the Golgi since a small population of TMEM106B is also observed in the Golgi at steady state. SPPL2c did not co-localize at all with TMEM106B and stained in a reticulated pattern, indicative of its localization to the ER, in agreement with a previous report (Figure 4.3D)(22). In agreement with this, SPPL2C has no activity towards TMEM106B (Figure 4.2B and C).

Determination of the NTF and ICD cleavage sites

In order to determine the approximate location of the cleavage sites for both lumenal domain shedding and intramembrane proteolysis, we generated various C-terminal truncations of TMEM106B to determine which species migrated at the same apparent molecular weight as the NTF and the ICD by SPPL2a during RIP. The first two constructs generated were N-terminally flag tagged and corresponded to amino acids 1-127 and 1-96. Amino acid 127 is 10 residues C-terminal to the predicted end of the transmembrane region while amino acid 96 is the last intracellular residue prior to the start of the transmembrane region. FLAG-1-127 migrated at the exact apparent molecular weight as the FLAG-TMEM106B induced NTF (Figure 4.2C) while FLAG-1-96 migrated slightly faster than the FLAG-TMEM106B induced ICD, suggesting that cleavage is indeed occurring within the transmembrane helix as is predicted for iCLiP activity. To more accurately estimate the intramembrane cleavage site, we generated untagged ICD constructs +5 and +10 amino acids into the transmembrane region relative to the 1-96 ICD. These constructs were run as

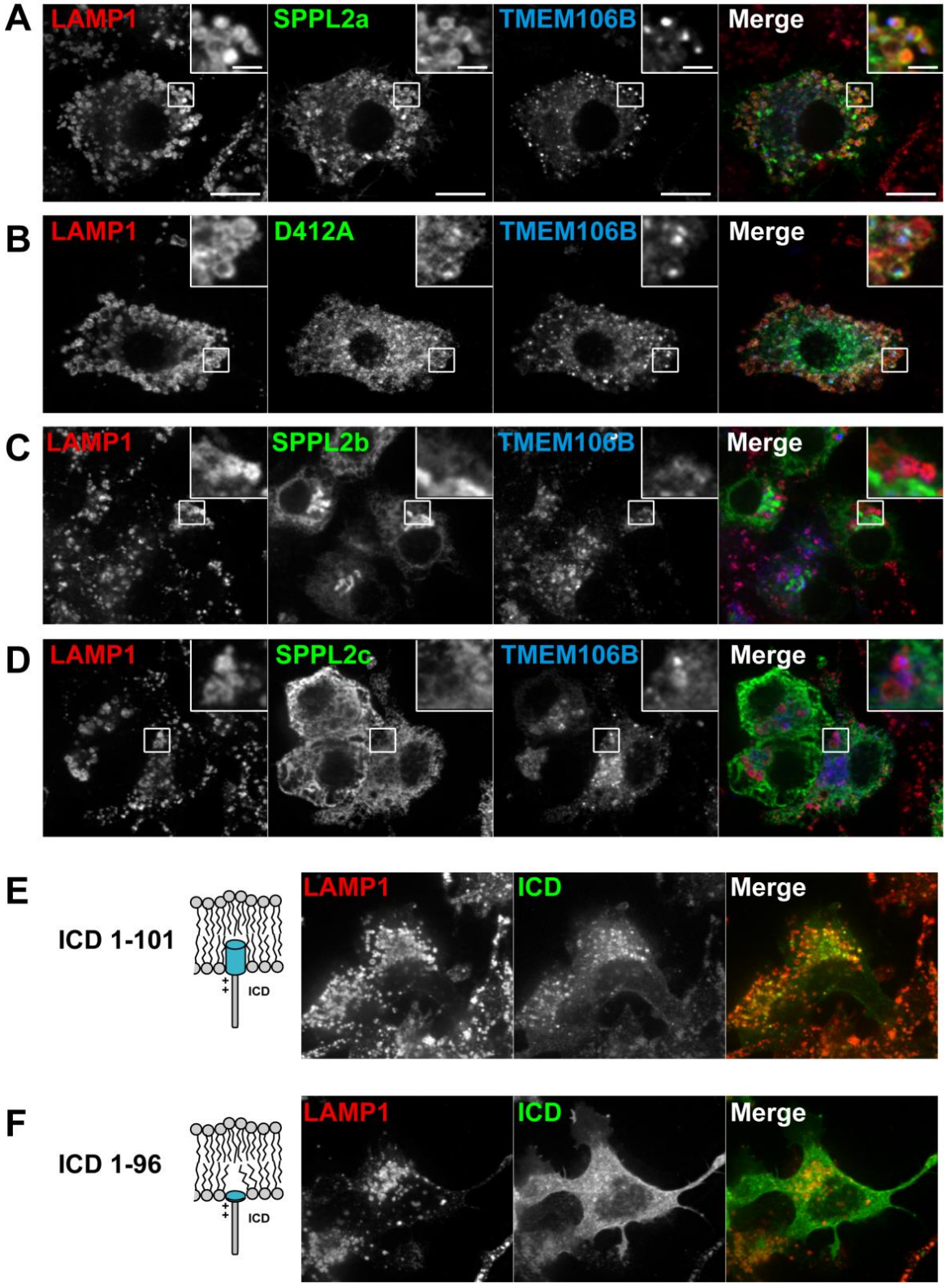
A
LAMP1
SPPL2a
TMEM106B
Merge
B
LAMP1
D412A
TMEM106B
Merge
C
LAMP1
SPPL2b
TMEM106B
Merge
D
LAMP1
SPPL2c
TMEM106B
Merge
E
ICD 1-101
ICD
LAMP1
ICD
Merge
F
ICD 1-96
ICD
LAMP1
ICD
Merge

Figure 4.3: SPPL2a localizes to lysosomes along with TMEM106B and its ICD. (**A**) SPPL2a-V5 co-expressed with TMEM106B co-localizes on LAMP1 positive vesicles in N2a cells. (**B**) A catalytically inactive D412A mutant of SPPL2a also localizes with TMEM106B on LAMP1 positive vesicles. (**C**) SPPL2b-V5 localizes poorly with co-expressed TMEM106B on LAMP1 positive vesicles. Most SPPL2b appears accumulated within ER and Golgi compartments. (**D**) SPPL2c-V5 does not localize with co-expressed TMEM106B. The majority of SPPL2c localizes in the ER. (**E**) A TMEM106B ICD composed of the first 101 amino acids retains its localization with lysosome membranes. (**F**) A truncated TMEM106B ICD composed of the first 96 cytosolic residues is liberated from lysosomes and is diffusely localized throughout the cytosol and associated with the plasma membrane.

standards for experiments in which we expected to see ICD generation. As with the FLAG-ICD the 1-96 fragment ran slightly faster than the actual ICD, while 1-101 and 1-106 appeared to run at nearly the same size, with 1-106 being the closest to the actual ICD in size (Figure 4.2A and B). All of these Western blots were run on 16% tricine gels in order to separate very small protein fragments with similar molecular weights. Interestingly, while the 1-106 fragment appeared the closest overall to the actual ICD in size, at least two extremely closely spaced bands were formed during the generation of the actual ICD, suggesting that there are multiple cut sites within close proximity to each other and centered around residue 106 (Figure 4.2A, 4.5A). This may suggest some degree of degeneracy in the cleavage site by SPPL2a. TMEM106B is a highly conserved protein, detected throughout the vertebrate lineage. Sequence alignment shows that the transmembrane region is absolutely conserved in most mammals and is largely identical even in *Danio rerio* and *Xenopus laevisi* (Figure 4.5B)(36). Similarly, intramembrane proteolysis is a ubiquitous mechanism across all domains of life. This points to the prospect that RIP of TMEM106B may also be an evolutionarily conserved event.

Based on our data, we would expect to see the NTF on the lysosomal limiting membrane; however when overexpressed, FLAG-1-127 localizes exclusively to the cell surface, indicating that there are lumenal determinants, such as glycosylation, required for proper TMEM106B trafficking to lysosomes (16). While we could detect the 1-106 fragment via Western blot in HEK293T cells, it was difficult to distinguish from endogenous TMEM106B via immunofluorescence in N2a cells. Therefore, we looked at the very closely migrating 1-101 fragment, which appeared to localize

primarily to lysosomes, suggesting that the liberated ICD can remain associated with the lysosome membrane after RIP (Figure 4.3E). The 1-96 fragment which contains no transmembrane residues was nearly completely absent from lysosomes but still appeared membrane associated, potentially due to electrostatic interactions between the membrane and the string of basic residues at its C-terminus (Figure 4.3F).

TMEM106A is processed in a similar manner on lysosome membranes

To test the specificity of TMEM106B as a substrate for SPPL2a mediated intramembrane proteolysis, we decided to explore the localization and cleavage pattern of two paralogs of TMEM106B: TMEM106A and TMEM106C. N-terminally FLAG-tagged TMEM106A and TMEM106C constructs were used for staining and for assessing cleavage by SPPL2a and SPPL2b. Like TMEM106B, TMEM106A is primarily localized to lysosomes. TMEM106C does not localize to lysosomes but rather shows a reticulated pattern in staining, indicative of an ER localization. We treated HEK293T cells expressing TMEM106Aor TMEM106C with 3-MA in order to detect any potential N-terminal degradation products. Much like TMEM106B, both TMEM106A and TMEM106C had a characteristic pair of N-terminal cleavage products at approximately ~20-22 and 16-18 kDa as would be expected for homologous NTFs and ICDs. This processing pattern is intriguing as it suggests that the TMEM106 family may be sequentially degraded within their resident membranes in a similar manner. Since TMEM106A is also localized to lysosome membranes, we tested if SPPL2a could also enhance the cleavage of the TMEM106A NTF. We found no evidence for selective reduction in the NTF or enhancement of ICD formation when TMEM106A is co-expressed with SPPL2a (Figure 4.4C), indicating that

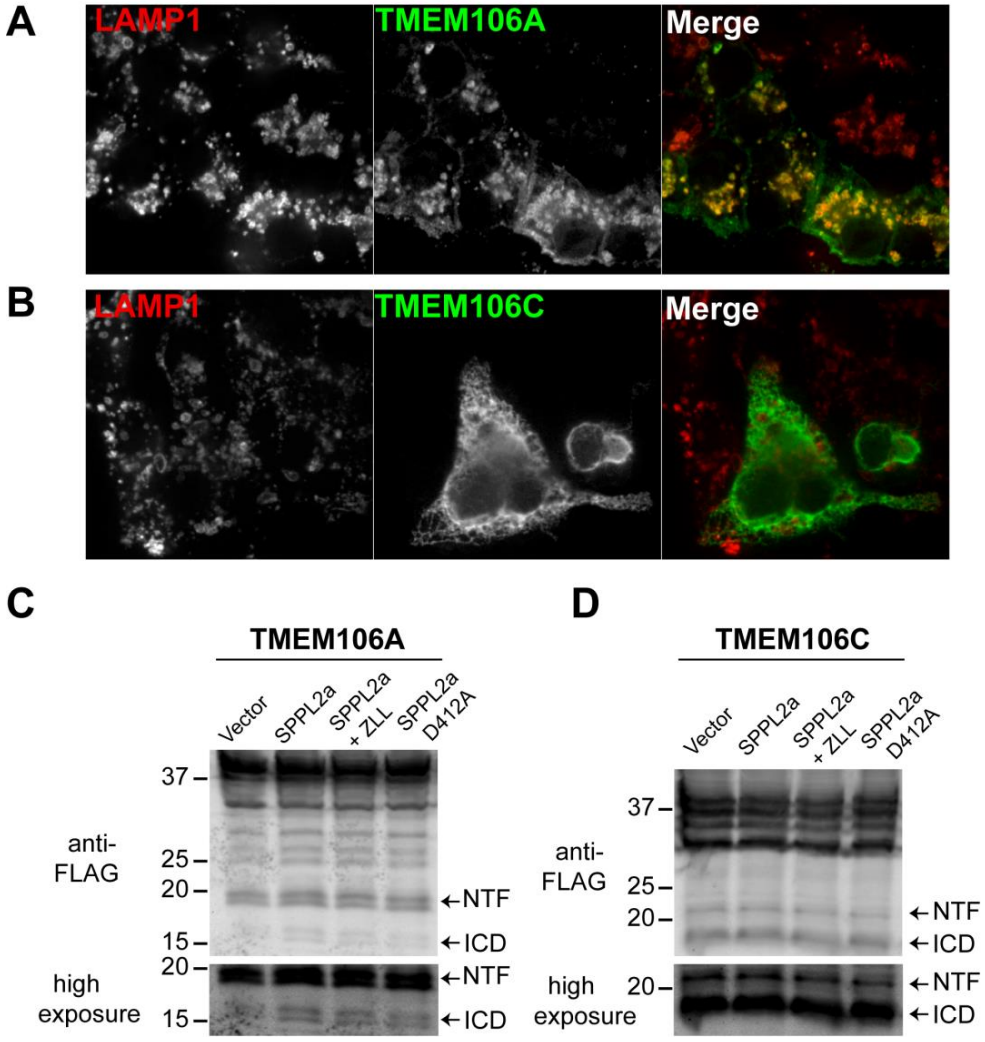

Figure 4.4: The TMEM106B homologue TMEM106A localizes to lysosomes, but is not a substrate for SPPL2a. (**A**) FLAG-TMEM106A expressed in N2a cells is localized primarily to lysosomes, similar to TMEM106B. (**B**) FLAG-TMEM106C expressed in N2a cells does not localize to lysosomes and resides in the ER. (**C**-**D**) HEK293T cells transfected with FLAG-tagged TMEM106A (**C**) or TMEM106C (**D**) were treated with 5 mM 3-MA for 14 hours. Each TMEM106 family member has a similar molecular weight of full length protein and generates a characteristic predicted NTF(s) at ~20-22 and ICD(s) at ~16-18 kDa. Neither TMEM106A or TMEM106C is specifically cleaved by co-expression of SPPL2a-v5.

SPPL2a displays some degree of selectivity in cleavage of type II transmembrane stumps in the lysosomal compartment. Unsurprisingly, SPPL2a had no effect on TMEM106C NTF degradation (Figure 4.4D). Similarly, SPPL2b and SPPL2c had no effect on TMEM106A or TMEM106C NTF processing (data not shown**).**

4.5 Discussion

In this study we demonstrate the selective processing of the lysosome membrane protein TMEM106B via the sequential actions of lumenal domain shedding and RIP.

We showed that inhibition of lysosomal hydrolases with either ammonium chloride and/or leupeptin reduces lumenal domain shedding. It is conceivable that this shedding event may be mediated by one of the multitude of soluble lysosomal proteases present within the lumen. Alternatively, this event may be mediated by an as of yet unidentified sheddase present within the lysosome membrane. Further experiments are needed to accurately identify the responsible enzyme. It will be interesting to understand if this shedding happens constitutively in response to elevated levels of TMEM106B, or if other factors regulate this process.

We show that the GxGD proteases SPPL2a and SPPL2b are capable of cleaving TMEM106B when overexpressed; however SPPL2a appears to be more specifically inhibited by the SPP family inhibitor $(ZLL)_2$-ketone, and it localizes much better to TMEM106B on the lysosomes, in agreement with previous reports showing that SPPL2a is predominantly trafficked to endosomes and lysosomes (22,35). SPPL2b localizes to the cell surface and was also observed to accumulate intracellularly in our immunofluorescence experiments. We speculate that this

overexpression may have saturated the machinery normally required for its trafficking to the cell surface, causing it to accumulate in the secretory pathway where it may be mediating the constitutive degradation of newly synthesized TMEM106B. Microarray studies performed by Friedmann and colleagues show that SPPL2b is expressed at low levels in most tissues except the adrenal cortex and mammary glands. SPPL2a, on the other hand, is expressed at high levels in a large number of tissues, with the highest levels detected in the brain (9). EST profiles of TMEM106B also show it to be expressed in a large number of tissues, including the brain (http://www.ncbi.nlm.nih.gov/UniGene/ESTProfileViewer.cgi?uglist=Hs.396358) (37). Due to these considerations, we predict SPPL2a, and not SPPL2b, to be the major physiologically relevant iCLiP responsible for processing the TMEM106B NTF *in vivo*.

Our data indicates that SPPL2a cleavage is at least somewhat specific, as the highly conserved paralog TMEM106A does not appear to be robustly degraded by SPPL2a, despite having a similar localization and a similar degradation pattern in vitro. While iCLiPs can have a large array of potential substrates, they do appear to display some selectivity even for potentially very similar substrates. This modality is supported by experiments by Martin and colleagues in which they demonstrate that SPPL2b efficiently cleaves the Bri2 protein, but not the highly homologous Bri3, even after it is artificially truncated to mimic the NTF of Bri2 (11). Work by Lemberg and Martoglio supports the idea that helix breaking residues in the transmembrane region of SPP substrates are required for efficient catalysis and this model has been extended to include the SPPL2 family as well with regards to Bri2 degradation by SPPL2b

(38,39). Glycine is the second most helix destabilizing amino acid after proline and TMEM106B has a glycine residue at position 110 in its transmembrane domain (40). We mutated this glycine to alanine, which should yield a much more stable helical transmembrane region; however, we did not observe any differences in ICD generation[3]. This adds complexity to the picture and suggests that while helix breaking residues may be required in many circumstances, they are not an absolute requirement for all substrates.

Our data supports the idea that SPPL2a cleaves the TMEM106B transmembrane region in the vicinity of amino acid 106. However, it also appears that more than one very closely spaced ICD bands are generated leading us to conclude that TMEM106B is cleaved at more than one location within its transmembrane helix. It has been shown by mass spectrometry that a similar pattern of multiple cleavage sites separated by several amino acids has been detected in the case of SPPL2b cleavage of TNFα (31). It has been argued that these multiple cleavage sites are required for the liberation of the TNFα ICD into the cytosol (7). This requirement of multiple intramembrane cleavage sites may explain why even our 1-101 amino acid TMEM106B ICD maintained its association with lysosome membranes. Additionally, this lack of absolute specificity of the intramembrane cleavage site may be a more general feature of the GxGD family of iCLiPs with ceratin substrates, as similar patterns of intramembrane cleavage are seen by proteases such as presenilin. The best characterized example of this is APP processing, which can result in multiple forms of β-amyloid which vary in length (41). Conversely, some presenilin substrates, such as Notch, have a single strictly defined cleavage site, suggesting that these patterns are to

A

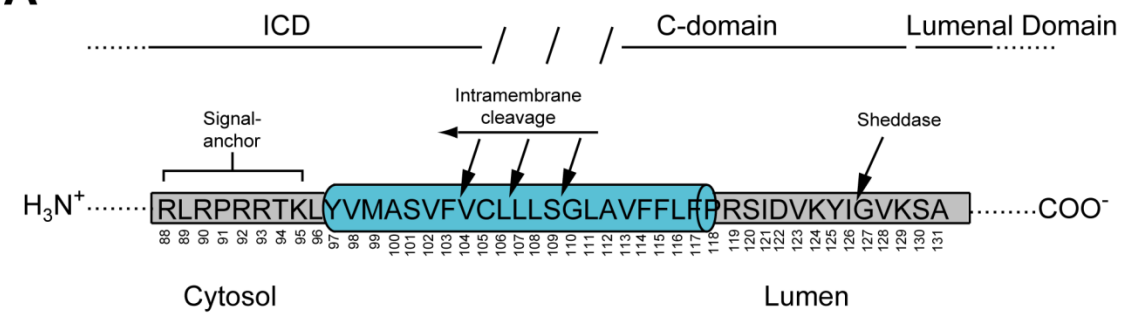

B

Species	Common Name	Sequence
Homo sapiens	Human	YVMASVFVCLLLSGLAVFFLF
Pan troglodytes	Chimpanzee	YVMASVFVCLLLSGLAVFFLF
Bos Taurus	Cow	YVMASVFVCLLLSGLAVFFLF
Rattus norvegicus	Rat	YVMASVFVCLLLSGLAVFFLF
Mus musculus	Mouse	YVMASVFVCLLLSGLAVFFLF
Gallus gallus	Chicken	YVTASVIVCLLLSGLAVFFLF
Xenopus laevis	Frog	YVTVSVIVCLLLSCLAVFFLF
Danio rerio	Zebrafish	YVMASVILCLLLCTLAVFFLF
		** .**::****. *******

Figure 4.5: The TMEM106B intramembrane cleavage site is highly conserved. (**A**) Schematic illustration of the predicted cleavage sites of TMEM106B by an as of yet unidentified sheddase at a lumenal juxtamembrane region near amino acid 127 and within the transmembrane region centered around amino acid 106. The transmembrane region is shown as a blue cylinder. (**B**) Sequence alignment of the TMEM106B transmembrane region from various species shows a high degree of conservation. The predicted region where SPPL2a mediated intramembrane cleavage may occur is indicated by a line above the absolutely conserved residues, "CLLL." Sequence alignment was performed using Clustal Omega.

some degree substrate dependent (42,43). We propose a model in which TMEM106B sheds its lumenal domain at amino acid ~127, generating an NTF. This membrane-retained stub then becomes accessible to cleavage by SPPL2a which can cleave in multiple closely spaced sites centered at approximately amino acid 106 (Figure 4.5A). Interestingly, this region is conserved in all species examined, highlighting the possibility that this TMEM106B membrane processing step is conserved through evolution (Figure 4.5B).

RIP generation of soluble ICDs has been proposed to mediate a large variety of signaling events both in the cytosol and in the nucleus to regulate transcription. Some ICDs generated in this manner, such as the ER to nucleus signaling of the SREBP proteins and ATF6 as well as the cell surface to nuclear signaling of Notch1, have been convincingly shown by a number of approaches (44-46). However, due to the extremely short lived nature of the vast majority of ICDs generated by RIP, many have yet to be detected *in vivo*. Hence, many experimentally reported effects of signaling by ICDs are only seen under artificial conditions such as reporter assays with supraphysiological levels of ICD expressed. Therefore claims of nuclear signaling by ICDs remain controversial for a number of RIP substrates. We see no evidence of the 106 or 101 amino acid ICD fragments in the nucleus when overexpressed. Occasionally, we observed small amounts of our FLAG-1-96 construct in the nucleus; however, whether a fragment of this size is actually generated *in vivo* and if it can affect transcription are unknown. We cannot rule out that the TMEM106B ICD has a signaling function in the nucleus, but given the available evidence this seems unlikely. Whether TMEM106B lumenal domain shedding and/or RIP have functional

consequences with regards to lysosome function or intracellular/nuclear signaling remains to be determined. Perhaps an underappreciated role for some iCLiPs, including presenilin and the SPPL family of proteases, is as a membrane protein quality control mechanism, allowing the efficient removal of unneeded or damaged membrane proteins or for controlling their levels in order to down regulate their expression in response to other signals. This has led some to refer to these proteases as the proteasome of the membrane. Given the accumulating evidence linking elevated TMEM106B levels to FTLD risk, identifying pathways that regulate TMEM106B levels may represent an important avenue in developing strategies for therapeutic intervention.

4.6 Acknowledgements

We thank Dr. Haiyuan Yu and Dr. Hening Lin for their kind gifts of cDNAs and plasmids and Mrs. Xiaochun Wu for technical assistance. This work is supported by funding to F.H. from Weill Institute for Cell and Molecular Biology and from the Association of Frontotemporal Dementia (AFTD), Alzheimer's Association and NINDS (R21 NS081357-01).

References

1. Lemberg, M. K. (2011) Intramembrane proteolysis in regulated protein trafficking. *Traffic* **12**, 1109-1118
2. Cao, X., and Sudhof, T. C. (2001) A transcriptionally [correction of transcriptively] active complex of APP with Fe65 and histone acetyltransferase Tip60. *Science* **293**, 115-120
3. Mumm, J. S., Schroeter, E. H., Saxena, M. T., Griesemer, A., Tian, X., Pan, D. J., Ray, W. J., and Kopan, R. (2000) A ligand-induced extracellular cleavage regulates gamma-secretase-like proteolytic activation of Notch1. *Mol Cell* **5**, 197-206
4. Lemberg, M. K., Bland, F. A., Weihofen, A., Braud, V. M., and Martoglio, B. (2001) Intramembrane proteolysis of signal peptides: an essential step in the generation of HLA-E epitopes. *J Immunol* **167**, 6441-6446
5. Kopan, R., and Ilagan, M. X. (2004) Gamma-secretase: proteasome of the membrane? *Nat Rev Mol Cell Biol* **5**, 499-504
6. Lichtenthaler, S. F., Haass, C., and Steiner, H. (2011) Regulated intramembrane proteolysis--lessons from amyloid precursor protein processing. *J Neurochem* **117**, 779-796
7. Fluhrer, R., Steiner, H., and Haass, C. (2009) Intramembrane proteolysis by signal peptide peptidases: a comparative discussion of GXGD-type aspartyl proteases. *J Biol Chem* **284**, 13975-13979
8. Weihofen, A., Binns, K., Lemberg, M. K., Ashman, K., and Martoglio, B. (2002) Identification of signal peptide peptidase, a presenilin-type aspartic protease. *Science* **296**, 2215-2218
9. Friedmann, E., Lemberg, M. K., Weihofen, A., Dev, K. K., Dengler, U., Rovelli, G., and Martoglio, B. (2004) Consensus analysis of signal peptide peptidase and homologous human aspartic proteases reveals opposite topology of catalytic domains compared with presenilins. *J Biol Chem* **279**, 50790-50798
10. Struhl, G., and Adachi, A. (2000) Requirements for presenilin-dependent cleavage of notch and other transmembrane proteins. *Mol Cell* **6**, 625-636
11. Martin, L., Fluhrer, R., and Haass, C. (2009) Substrate requirements for SPPL2b-dependent regulated intramembrane proteolysis. *J Biol Chem* **284**, 5662-5670
12. Shah, S., Lee, S. F., Tabuchi, K., Hao, Y. H., Yu, C., LaPlant, Q., Ball, H., Dann, C. E., 3rd, Sudhof, T., and Yu, G. (2005) Nicastrin functions as a gamma-secretase-substrate receptor. *Cell* **122**, 435-447
13. Krawitz, P., Haffner, C., Fluhrer, R., Steiner, H., Schmid, B., and Haass, C. (2005) Differential localization and identification of a critical aspartate suggest non-redundant proteolytic functions of the presenilin homologues SPPL2b and SPPL3. *J Biol Chem* **280**, 39515-39523
14. Van Deerlin, V. M., Sleiman, P. M., Martinez-Lage, M., Chen-Plotkin, A., Wang, L. S., Graff-Radford, N. R., Dickson, D. W., Rademakers, R., Boeve, B. F., Grossman, M., Arnold, S. E., Mann, D. M., Pickering-Brown, S. M.,

Seelaar, H., Heutink, P., van Swieten, J. C., Murrell, J. R., Ghetti, B., Spina, S., Grafman, J., Hodges, J., Spillantini, M. G., Gilman, S., Lieberman, A. P., Kaye, J. A., Woltjer, R. L., Bigio, E. H., Mesulam, M., Al-Sarraj, S., Troakes, C., Rosenberg, R. N., White, C. L., 3rd, Ferrer, I., Llado, A., Neumann, M., Kretzschmar, H. A., Hulette, C. M., Welsh-Bohmer, K. A., Miller, B. L., Alzualde, A., Lopez de Munain, A., McKee, A. C., Gearing, M., Levey, A. I., Lah, J. J., Hardy, J., Rohrer, J. D., Lashley, T., Mackenzie, I. R., Feldman, H. H., Hamilton, R. L., Dekosky, S. T., van der Zee, J., Kumar-Singh, S., Van Broeckhoven, C., Mayeux, R., Vonsattel, J. P., Troncoso, J. C., Kril, J. J., Kwok, J. B., Halliday, G. M., Bird, T. D., Ince, P. G., Shaw, P. J., Cairns, N. J., Morris, J. C., McLean, C. A., DeCarli, C., Ellis, W. G., Freeman, S. H., Frosch, M. P., Growdon, J. H., Perl, D. P., Sano, M., Bennett, D. A., Schneider, J. A., Beach, T. G., Reiman, E. M., Woodruff, B. K., Cummings, J., Vinters, H. V., Miller, C. A., Chui, H. C., Alafuzoff, I., Hartikainen, P., Seilhean, D., Galasko, D., Masliah, E., Cotman, C. W., Tunon, M. T., Martinez, M. C., Munoz, D. G., Carroll, S. L., Marson, D., Riederer, P. F., Bogdanovic, N., Schellenberg, G. D., Hakonarson, H., Trojanowski, J. Q., and Lee, V. M. (2010) Common variants at 7p21 are associated with frontotemporal lobar degeneration with TDP-43 inclusions. *Nat Genet* **42**, 234-239

15. van der Zee, J., Van Langenhove, T., Kleinberger, G., Sleegers, K., Engelborghs, S., Vandenberghe, R., Santens, P., Van den Broeck, M., Joris, G., Brys, J., Mattheijssens, M., Peeters, K., Cras, P., De Deyn, P. P., Cruts, M., and Van Broeckhoven, C. (2011) TMEM106B is associated with frontotemporal lobar degeneration in a clinically diagnosed patient cohort. *Brain* **134**, 808-815
16. Lang, C. M., Fellerer, K., Schwenk, B. M., Kuhn, P. H., Kremmer, E., Edbauer, D., Capell, A., and Haass, C. (2012) Membrane orientation and subcellular localization of transmembrane protein 106B (TMEM106B), a major risk factor for frontotemporal lobar degeneration. *J Biol Chem* **287**, 19355-19365
17. Chen-Plotkin, A. S., Unger, T. L., Gallagher, M. D., Bill, E., Kwong, L. K., Volpicelli-Daley, L., Busch, J. I., Akle, S., Grossman, M., Van Deerlin, V., Trojanowski, J. Q., and Lee, V. M. (2012) TMEM106B, the risk gene for frontotemporal dementia, is regulated by the microRNA-132/212 cluster and affects progranulin pathways. *J Neurosci* **32**, 11213-11227
18. Brady, O. A., Zheng, Y., Murphy, K., Huang, M., and Hu, F. (2013) The frontotemporal lobar degeneration risk factor, TMEM106B, regulates lysosomal morphology and function. *Hum Mol Genet* **22**, 685-695
19. Nicholson, A. M., Finch, N. A., Wojtas, A., Baker, M. C., Perkerson, R. B., 3rd, Castanedes-Casey, M., Rousseau, L., Benussi, L., Binetti, G., Ghidoni, R., Hsiung, G. Y., Mackenzie, I. R., Finger, E., Boeve, B. F., Ertekin-Taner, N., Graff-Radford, N. R., Dickson, D. W., and Rademakers, R. (2013) TMEM106B p.T185S regulates TMEM106B protein levels: implications for frontotemporal dementia. *J Neurochem*

20. Vancha, A. R., Govindaraju, S., Parsa, K. V., Jasti, M., Gonzalez-Garcia, M., and Ballestero, R. P. (2004) Use of polyethyleneimine polymer in cell culture as attachment factor and lipofection enhancer. *BMC Biotechnol* **4**, 23
21. Petiot, A., Ogier-Denis, E., Blommaart, E. F., Meijer, A. J., and Codogno, P. (2000) Distinct classes of phosphatidylinositol 3'-kinases are involved in signaling pathways that control macroautophagy in HT-29 cells. *J Biol Chem* **275**, 992-998
22. Friedmann, E., Hauben, E., Maylandt, K., Schleeger, S., Vreugde, S., Lichtenthaler, S. F., Kuhn, P. H., Stauffer, D., Rovelli, G., and Martoglio, B. (2006) SPPL2a and SPPL2b promote intramembrane proteolysis of TNFalpha in activated dendritic cells to trigger IL-12 production. *Nat Cell Biol* **8**, 843-848
23. Kirkin, V., Cahuzac, N., Guardiola-Serrano, F., Huault, S., Luckerath, K., Friedmann, E., Novac, N., Wels, W. S., Martoglio, B., Hueber, A. O., and Zornig, M. (2007) The Fas ligand intracellular domain is released by ADAM10 and SPPL2a cleavage in T-cells. *Cell Death Differ* **14**, 1678-1687
24. Schneppenheim, J., Dressel, R., Huttl, S., Lullmann-Rauch, R., Engelke, M., Dittmann, K., Wienands, J., Eskelinen, E. L., Hermans-Borgmeyer, I., Fluhrer, R., Saftig, P., and Schroder, B. (2013) The intramembrane protease SPPL2a promotes B cell development and controls endosomal traffic by cleavage of the invariant chain. *J Exp Med* **210**, 41-58
25. Zahn, C., Kaup, M., Fluhrer, R., and Fuchs, H. (2013) The transferrin receptor-1 membrane stub undergoes intramembrane proteolysis by signal peptide peptidase-like 2b. *FEBS J* **280**, 1653-1663
26. Edwards, D. R., Handsley, M. M., and Pennington, C. J. (2008) The ADAM metalloproteinases. *Mol Aspects Med* **29**, 258-289
27. Yu, Q., and Stamenkovic, I. (2000) Cell surface-localized matrix metalloproteinase-9 proteolytically activates TGF-beta and promotes tumor invasion and angiogenesis. *Genes Dev* **14**, 163-176
28. Seals, D. F., and Courtneidge, S. A. (2003) The ADAMs family of metalloproteases: multidomain proteins with multiple functions. *Genes Dev* **17**, 7-30
29. Vassar, R., Bennett, B. D., Babu-Khan, S., Kahn, S., Mendiaz, E. A., Denis, P., Teplow, D. B., Ross, S., Amarante, P., Loeloff, R., Luo, Y., Fisher, S., Fuller, J., Edenson, S., Lile, J., Jarosinski, M. A., Biere, A. L., Curran, E., Burgess, T., Louis, J. C., Collins, F., Treanor, J., Rogers, G., and Citron, M. (1999) Beta-secretase cleavage of Alzheimer's amyloid precursor protein by the transmembrane aspartic protease BACE. *Science* **286**, 735-741
30. Tanaka, R. D., Li, A. C., Fogelman, A. M., and Edwards, P. A. (1986) Inhibition of lysosomal protein degradation inhibits the basal degradation of 3-hydroxy-3-methylglutaryl coenzyme A reductase. *J Lipid Res* **27**, 261-273
31. Fluhrer, R., Grammer, G., Israel, L., Condron, M. M., Haffner, C., Friedmann, E., Bohland, C., Imhof, A., Martoglio, B., Teplow, D. B., and Haass, C. (2006) A gamma-secretase-like intramembrane cleavage of TNFalpha by the GxGD aspartyl protease SPPL2b. *Nat Cell Biol* **8**, 894-896

32. Martin, L., Fluhrer, R., Reiss, K., Kremmer, E., Saftig, P., and Haass, C. (2008) Regulated intramembrane proteolysis of Bri2 (Itm2b) by ADAM10 and SPPL2a/SPPL2b. *J Biol Chem* **283**, 1644-1652
33. Beisner, D. R., Langerak, P., Parker, A. E., Dahlberg, C., Otero, F. J., Sutton, S. E., Poirot, L., Barnes, W., Young, M. A., Niessen, S., Wiltshire, T., Bodendorf, U., Martoglio, B., Cravatt, B., and Cooke, M. P. (2013) The intramembrane protease Sppl2a is required for B cell and DC development and survival via cleavage of the invariant chain. *J Exp Med* **210**, 23-30
34. Bergmann, H., Yabas, M., Short, A., Miosge, L., Barthel, N., Teh, C. E., Roots, C. M., Bull, K. R., Jeelall, Y., Horikawa, K., Whittle, B., Balakishnan, B., Sjollema, G., Bertram, E. M., Mackay, F., Rimmer, A. J., Cornall, R. J., Field, M. A., Andrews, T. D., Goodnow, C. C., and Enders, A. (2013) B cell survival, surface BCR and BAFFR expression, CD74 metabolism, and CD8- dendritic cells require the intramembrane endopeptidase SPPL2A. *J Exp Med* **210**, 31-40
35. Behnke, J., Schneppenheim, J., Koch-Nolte, F., Haag, F., Saftig, P., and Schroder, B. (2011) Signal-peptide-peptidase-like 2a (SPPL2a) is targeted to lysosomes/late endosomes by a tyrosine motif in its C-terminal tail. *FEBS Lett* **585**, 2951-2957
36. Sievers, F., Wilm, A., Dineen, D., Gibson, T. J., Karplus, K., Li, W., Lopez, R., McWilliam, H., Remmert, M., Soding, J., Thompson, J. D., and Higgins, D. G. (2011) Fast, scalable generation of high-quality protein multiple sequence alignments using Clustal Omega. *Mol Syst Biol* **7**, 539
37. (2013) Database resources of the National Center for Biotechnology Information. *Nucleic Acids Res* **41**, D8-D20
38. Lemberg, M. K., and Martoglio, B. (2002) Requirements for signal peptide peptidase-catalyzed intramembrane proteolysis. *Mol Cell* **10**, 735-744
39. Fluhrer, R., Martin, L., Klier, B., Haug-Kroper, M., Grammer, G., Nuscher, B., and Haass, C. (2012) The alpha-helical content of the transmembrane domain of the British dementia protein-2 (Bri2) determines its processing by signal peptide peptidase-like 2b (SPPL2b). *J Biol Chem* **287**, 5156-5163
40. Pace, C. N., and Scholtz, J. M. (1998) A helix propensity scale based on experimental studies of peptides and proteins. *Biophys J* **75**, 422-427
41. Steiner, H., Fluhrer, R., and Haass, C. (2008) Intramembrane proteolysis by gamma-secretase. *J Biol Chem* **283**, 29627-29631
42. Chen, F., Yu, G., Arawaka, S., Nishimura, M., Kawarai, T., Yu, H., Tandon, A., Supala, A., Song, Y. Q., Rogaeva, E., Milman, P., Sato, C., Yu, C., Janus, C., Lee, J., Song, L., Zhang, L., Fraser, P. E., and St George-Hyslop, P. H. (2001) Nicastrin binds to membrane-tethered Notch. *Nat Cell Biol* **3**, 751-754
43. Sisodia, S. S., and St George-Hyslop, P. H. (2002) gamma-Secretase, Notch, Abeta and Alzheimer's disease: where do the presenilins fit in? *Nat Rev Neurosci* **3**, 281-290
44. Wang, X., Sato, R., Brown, M. S., Hua, X., and Goldstein, J. L. (1994) SREBP-1, a membrane-bound transcription factor released by sterol-regulated proteolysis. *Cell* **77**, 53-62

45. Ye, J., Rawson, R. B., Komuro, R., Chen, X., Dave, U. P., Prywes, R., Brown, M. S., and Goldstein, J. L. (2000) ER stress induces cleavage of membrane-bound ATF6 by the same proteases that process SREBPs. *Mol Cell* **6**, 1355-1364
46. Selkoe, D., and Kopan, R. (2003) Notch and Presenilin: regulated intramembrane proteolysis links development and degeneration. *Annu Rev Neurosci* **26**, 565-597

CHAPTER 5

CONCLUSIONS AND PERSPECTIVES

The work described here deals with the cellular and molecular basis of FTLD-TDP pathogenesis as on overarching theme. In particular, I explored how the proteins that encode different genetic causes and disease risk modifiers affect various aspects of cellular proteostasis, with a focus on lysosomal function.

In Chapter 2, I described a role of the ubiquitin binding adaptor protein, p62, in mediating cellular clearance of aggregated TDP-43 via the UPS and autophagy-lysosome pathways. Inclusions containing p62 have been reported in a number of neurodegenerative diseases including FTLD; however, their specific role in disease pathogenesis are unknown. Moreover, it is unclear if the presence of p62 in inclusions is a cause of or consequence of inclusion formation (1). To my knowledge, the data presented in chapter 2 is the first published demonstration that p62 can directly lead to reduced TDP-43 aggregation *in vitro*. These data were supported by a recent report that p62 directly binds TDP-43 in the brain and that this interaction is impaired in cases of FTLD-TDP, lending further weight that my study may be applicable *in vivo* as well. In addition, using phosphomimetic TDP-43 mutants in cell culture models of TDP-43 aggregation, I show that phosphorylation of TDP-43 may actually play a role in inhibiting further aggregation events, rather than promoting it, as had been proposed due to the observation that phosphorylation level is often proportional to the level of aggregation (2). Support for my observations came shortly after when another group

reported nearly identical results (3). Nonetheless, the data on this subject are still incompletely understood and seemingly contradictory dependent upon the system and different experimental setups and continues to be a vibrant area of research. This work has laid out an important foundation for further studies exploring the roles of other ubiquitin binding adaptor proteins such as UBQLN1 and UBQLN2 and the effects of other post-translational modifications including alternative phosphorylation sites and ubiquitination on TDP-43 aggregation, toxicity, and degradation. Building upon this data, this work is actively being pursued in our lab.

Chapters 3 and 4, along with the appendices represent the majority of my work here at Cornell. This work begins to illustrate a picture of the recently identified FTLD risk factor, TMEM106B, as a lysosomal membrane protein whose levels must be critically regulated for maintenance of lysosomal homeostasis. Chapter 3 and data in the appendices shows that TMEM106B overexpression in neuronal cell culture models leads to enlarged, dysmorphic lysosomes, which have defects in degradative capacity, lending support to the initial genetic data indicating that increased TMEM106B poses risk for FLTD-TDP patients with *GRN* mutations (4-7). Chapter 3 also demonstrates that elevated TMEM106B levels in and of itself is the likely cause of lysosome dysfunction and not a direct functional difference due to a coding variant in linkage disequilibrium with the risk allele. Interestingly, a recent article claims that the SNPs in the human *TMEM106B* risk allele confer partial resistance to regulation by another miRNA species and hence, higher mRNA levels lead to higher protein expression (8). Another recent report claims that the T185S coding variant, which is associated with the protective allele has a shorter protein half-life, potentially due to changes in a

consensus glycosylation site (9). Regardless if one or both of these mechanisms are in play in mediating the risk conferred by TMEM106B, mine and others' data strongly supports a model in which increased TMEM106B protein levels confer risk for FTLD-TDP through its effects on lysosomes.

Finally, data in chapter 3 suggests that elevated TMEM106B increases intracellular PGRN levels in a post-transcriptional manner, likely due to impaired lysosomal degradation. This data was supported to some degree by two contemporaneous papers exploring the cellular and molecular functions of TMEM106B, but have not been observed by all (8-10). In addition, there is some discrepancy as to the effects of elevated TMEM106B on PGRN levels seen in FTLD-TDP patients and those seen *in vitro* (4,5,8-10). Hence, it will be important to follow up these experiments with more detailed assays to further distinguish the effects of TMEM106B on the levels of extracellular and intracellular as well as full-length and cleaved granulin species. It appears evident to me that intracellular full-length PGRN is elevated by TMEM106B overexpression; however, one limitation of the secreted PGRN data presented in this chapter is that it was measured using an ELISA with polyclonal antibodies and could theoretically be measuring a combination of full-length and cleaved granulin species since PGRN is known to be processed extracellularly by a variety of proteases (11). Once possibility is that increased TMEM106B causes defects in PGRN processing to mature granulins within the lysosomes. Preliminary evidence in our lab indicates that co-expressing sortilin with PGRN leads to an increase in the levels of processed granulins detected intracellularly. Further, determining, PGRN and its granulin products functions in the lysosomes

remains a major goal of this lab, with work being done on this front using a combination of proteomics and traditional cell biology and biochemistry techniques. A more thorough understanding of PGRN processing and its roles in the cell may also shed light on why elevated TMEM106B is so deleterious.

Chapter 4 presents evidence that TMEM106B levels can be regulated *in vitro*, through successive proteolytic processing of TMEM106B within the lumen of lysosomes by an as of yet unidentified protease followed by cleavage within lysosome membranes by the iCLiP, SPPL2a. Whether or not, TMEM106B RIP demonstrated here results in a functional signaling event remains to be determined. Nonetheless, this data is significant as it demonstrates the existence of a pathway which can modulate TMEM106B protein levels. Activation of this pathway may be an attractive therapeutic target if it can be shown to decrease TMEM106B levels *in vivo*. The data presented in this chapter is currently undergoing revisions to address reviewer comments. A number of issues are being addressed as I write this dissertation and include more accurate mapping of the NTF and ICD generating cleavage sites using more TMEM106B fragment constructs as reference standards. I am also repeating all western blot experiments on tricine gels for more consistency in terms of sizes of fragments referred to. Figure 4.2 is being repeated for quantitation and statistical analysis. I will update the pictures in Figure 4.3 showing that SPPL2a-v5 localizes even better with endogenous TMEM106B than overexpressed TMEM106B, which tends to aggregate on lysosome membranes and will update information on the localization of the NTF and ICD fragments used. I have also repeated Figure 4.4 using an untagged TMEM106A construct and a homemade antibody against the

TMEM106A ICD showing that SPPL2a does not promote cleavage of TMEM106A. Finally, I will metabolically label proteins with ^{35}S methionine and immunoprecipitate TMEM106B from various cells in an attempt to detect endogenously produced NTF and ICD products. This last experiment may prove difficult, as the cleavage is not detected at endogenous levels by western blot, but is seen in TMEM106B stable NSC-34 cell lines and transiently overexpressed in HEK293T cells. It has been well established that ICDs generated by RIP from a large number of transmembrane protein precursors are usually turned over extremely rapidly, which makes endogenous detection difficult (12). I have also used a bioinformatic approach, using the SitePrediction software to identify several potential cathepsin cleavage sites in the lumenal domain of TMEM106B and generated mutants which may disrupt sites near the predicted NTF cleavage site (13). Cathepsins are a broad class of lysosomal peptidases with relatively degenerate protease consensus sites, however one feature in common with several of the cathepsins is the preference for cutting between paired hydrophobic residues on substrates, which was taken in to account when choosing sites for mutagenesis (14,15). In all, I have generated both FLAG-tagged and untagged Y125D, S130D, Y132D, and Y125D/Y132D TMEM106B mutants which are predicted to interrupt at least five potential cathepsin cleavage sites. Preliminary data indicates that expression of these mutants results in higher levels of full-length TMEM106B and lower levels of NTF, suggesting that at least some of these mutants disrupt lumenal domain shedding. SPP and SPPL iCLiPs have been shown to prefer substrates with helix-breaking residues in their transmembrane regions, although this may not be a universal requirement (16,17). Using a similar strategy, I have also

generated TMEM106B C105A and P118A mutants which are predicted to increase the helical propensity of the transmembrane region and are currently being tested for their ability to be processed to TMEM106B ICDs by SPPL2a (18).

It is intriguing that in our experiments, overexpression of TMEM106B to a large enough degree appears to trigger its degradation via RIP. TMEM106B protein levels may be under very tight regulatory control and identifying these mechanisms remains an important avenue of research. In Appendix E, I show that ubiquitination at residue K3 in TMEM106B may play a role in regulating TMEM106B levels. These experiments should be followed up in more detail, in particular to test whether ubiquitination at this site affects TMEM106B internalization and degradation within lysosomes and if this is mediated through interaction with the ESCRT pathway, which has been shown to be disrupted in FTLD-UPS caused by mutations in CHMP2B. The levels of TMEM106B and its K3R mutant in the presence of dominant negative ESCRT subunit constructs such as disease causing CHMP2B mutants or an ATPase dead mutant of VPS4 could be examined. Additionally, ultrastructural examination of TMEM106B and the K3R mutant on the limiting membrane and within the lumen of lysosomes should be pursued using immuno-gold electron microscopy.

In our lab we have generated transgenic mice overexpressing human TMEM106B. These mice have been genotyped and confirmed to be expressing elevated levels of the human TMEM106B transcript by qPCR as well as confirmed to be expressing human TMEM106B protein via mass spectrometry. Despite all this, overall levels of TMEM106B detected in the brains and other tissues via western blot appear no different from controls, potentially indicating some sort of autoregulatory

mechanism at the protein level. While surprising to us, this mode of regulation is not unheard of. For example, human TDP-43 transgenic mice show dramatic suppression of expression from the endogenous locus (19). It will be interesting to see if TMEM106B expression levels change when these mice are crossed with a PGRN knockout mouse line to generate a TMEM106B overexpression/PGRN deficient line. Furthermore, PGRN knockout mice have been shown to recapitulate many of the features of FTLD-TDP, including reductions in social engagement and age-related deficits in learning and memory (20-22). Since TMEM106B risk alleles are most prominent in *GRN* mutant carriers, it will be important to test TMEM106B overexpressing mice crossed with $Grn^{+/-}$ and $Grn^{-/-}$ mice. The same behavioral tests used to assay these mice for FTLD-like phenotypes could be repeated in the context of a TMEM106B overexpressing background, which may more accurately recapitulate FTLD symptoms and serve as a better disease model for further studies, including the testing of therapeutics.

REFERENCES

1. Pikkarainen, M., Hartikainen, P., and Alafuzoff, I. (2008) Neuropathologic features of frontotemporal lobar degeneration with ubiquitin-positive inclusions visualized with ubiquitin-binding protein p62 immunohistochemistry. *J Neuropathol Exp Neurol* **67**, 280-298
2. Zhang, Y. J., Gendron, T. F., Xu, Y. F., Ko, L. W., Yen, S. H., and Petrucelli, L. (2010) Phosphorylation regulates proteasomal-mediated degradation and solubility of TAR DNA binding protein-43 C-terminal fragments. *Mol Neurodegener* **5**, 33
3. Li, H. Y., Yeh, P. A., Chiu, H. C., Tang, C. Y., and Tu, B. P. (2011) Hyperphosphorylation as a defense mechanism to reduce TDP-43 aggregation. *PLoS One* **6**, e23075
4. Cruchaga, C., Graff, C., Chiang, H. H., Wang, J., Hinrichs, A. L., Spiegel, N., Bertelsen, S., Mayo, K., Norton, J. B., Morris, J. C., and Goate, A. (2011) Association of TMEM106B gene polymorphism with age at onset in granulin mutation carriers and plasma granulin protein levels. *Arch Neurol* **68**, 581-586
5. Finch, N., Carrasquillo, M. M., Baker, M., Rutherford, N. J., Coppola, G., Dejesus-Hernandez, M., Crook, R., Hunter, T., Ghidoni, R., Benussi, L., Crook, J., Finger, E., Hantanpaa, K. J., Karydas, A. M., Sengdy, P., Gonzalez, J., Seeley, W. W., Johnson, N., Beach, T. G., Mesulam, M., Forloni, G., Kertesz, A., Knopman, D. S., Uitti, R., White, C. L., 3rd, Caselli, R., Lippa, C., Bigio, E. H., Wszolek, Z. K., Binetti, G., Mackenzie, I. R., Miller, B. L., Boeve, B. F., Younkin, S. G., Dickson, D. W., Petersen, R. C., Graff-Radford, N. R., Geschwind, D. H., and Rademakers, R. (2011) TMEM106B regulates progranulin levels and the penetrance of FTLD in GRN mutation carriers. *Neurology* **76**, 467-474
6. Van Deerlin, V. M., Sleiman, P. M., Martinez-Lage, M., Chen-Plotkin, A., Wang, L. S., Graff-Radford, N. R., Dickson, D. W., Rademakers, R., Boeve, B. F., Grossman, M., Arnold, S. E., Mann, D. M., Pickering-Brown, S. M., Seelaar, H., Heutink, P., van Swieten, J. C., Murrell, J. R., Ghetti, B., Spina, S., Grafman, J., Hodges, J., Spillantini, M. G., Gilman, S., Lieberman, A. P., Kaye, J. A., Woltjer, R. L., Bigio, E. H., Mesulam, M., Al-Sarraj, S., Troakes, C., Rosenberg, R. N., White, C. L., 3rd, Ferrer, I., Llado, A., Neumann, M., Kretzschmar, H. A., Hulette, C. M., Welsh-Bohmer, K. A., Miller, B. L., Alzualde, A., Lopez de Munain, A., McKee, A. C., Gearing, M., Levey, A. I., Lah, J. J., Hardy, J., Rohrer, J. D., Lashley, T., Mackenzie, I. R., Feldman, H. H., Hamilton, R. L., Dekosky, S. T., van der Zee, J., Kumar-Singh, S., Van Broeckhoven, C., Mayeux, R., Vonsattel, J. P., Troncoso, J. C., Kril, J. J., Kwok, J. B., Halliday, G. M., Bird, T. D., Ince, P. G., Shaw, P. J., Cairns, N. J., Morris, J. C., McLean, C. A., DeCarli, C., Ellis, W. G., Freeman, S. H., Frosch, M. P., Growdon, J. H., Perl, D. P., Sano, M., Bennett, D. A., Schneider, J. A., Beach, T. G., Reiman, E. M., Woodruff, B. K., Cummings, J., Vinters, H. V., Miller, C. A., Chui, H. C., Alafuzoff, I., Hartikainen, P., Seilhean, D., Galasko, D., Masliah, E., Cotman, C. W., Tunon, M. T.,

Martinez, M. C., Munoz, D. G., Carroll, S. L., Marson, D., Riederer, P. F., Bogdanovic, N., Schellenberg, G. D., Hakonarson, H., Trojanowski, J. Q., and Lee, V. M. (2010) Common variants at 7p21 are associated with frontotemporal lobar degeneration with TDP-43 inclusions. *Nat Genet* **42**, 234-239

7. van der Zee, J., Van Langenhove, T., Kleinberger, G., Sleegers, K., Engelborghs, S., Vandenberghe, R., Santens, P., Van den Broeck, M., Joris, G., Brys, J., Mattheijssens, M., Peeters, K., Cras, P., De Deyn, P. P., Cruts, M., and Van Broeckhoven, C. (2011) TMEM106B is associated with frontotemporal lobar degeneration in a clinically diagnosed patient cohort. *Brain* **134**, 808-815
8. Chen-Plotkin, A. S., Unger, T. L., Gallagher, M. D., Bill, E., Kwong, L. K., Volpicelli-Daley, L., Busch, J. I., Akle, S., Grossman, M., Van Deerlin, V., Trojanowski, J. Q., and Lee, V. M. (2012) TMEM106B, the risk gene for frontotemporal dementia, is regulated by the microRNA-132/212 cluster and affects progranulin pathways. *J Neurosci* **32**, 11213-11227
9. Nicholson, A. M., Finch, N. A., Wojtas, A., Baker, M. C., Perkerson, R. B., 3rd, Castanedes-Casey, M., Rousseau, L., Benussi, L., Binetti, G., Ghidoni, R., Hsiung, G. Y., Mackenzie, I. R., Finger, E., Boeve, B. F., Ertekin-Taner, N., Graff-Radford, N. R., Dickson, D. W., and Rademakers, R. (2013) TMEM106B p.T185S regulates TMEM106B protein levels: implications for frontotemporal dementia. *J Neurochem*
10. Lang, C. M., Fellerer, K., Schwenk, B. M., Kuhn, P. H., Kremmer, E., Edbauer, D., Capell, A., and Haass, C. (2012) Membrane orientation and subcellular localization of transmembrane protein 106B (TMEM106B), a major risk factor for frontotemporal lobar degeneration. *J Biol Chem* **287**, 19355-19365
11. Gass, J., Prudencio, M., Stetler, C., and Petrucelli, L. (2012) Progranulin: an emerging target for FTLD therapies. *Brain Res* **1462**, 118-128
12. Kopan, R., and Ilagan, M. X. (2004) Gamma-secretase: proteasome of the membrane? *Nat Rev Mol Cell Biol* **5**, 499-504
13. Verspurten, J., Gevaert, K., Declercq, W., and Vandenabeele, P. (2009) SitePredicting the cleavage of proteinase substrates. *Trends Biochem Sci* **34**, 319-323
14. Alves, M. F., Puzer, L., Cotrin, S. S., Juliano, M. A., Juliano, L., Bromme, D., and Carmona, A. K. (2003) S3 to S3' subsite specificity of recombinant human cathepsin K and development of selective internally quenched fluorescent substrates. *Biochem J* **373**, 981-986
15. Higaki, J., Catalano, R., Guzzetta, A. W., Quon, D., Nave, J. F., Tarnus, C., D'Orchymont, H., and Cordell, B. (1996) Processing of beta-amyloid precursor protein by cathepsin D. *J Biol Chem* **271**, 31885-31893
16. Fluhrer, R., Martin, L., Klier, B., Haug-Kroper, M., Grammer, G., Nuscher, B., and Haass, C. (2012) The alpha-helical content of the transmembrane domain of the British dementia protein-2 (Bri2) determines its processing by signal peptide peptidase-like 2b (SPPL2b). *J Biol Chem* **287**, 5156-5163

17. Schroder, B., and Saftig, P. (2010) Molecular insights into mechanisms of intramembrane proteolysis through signal peptide peptidase (SPP). *Biochem J* **427**, e1-3
18. Pace, C. N., and Scholtz, J. M. (1998) A helix propensity scale based on experimental studies of peptides and proteins. *Biophys J* **75**, 422-427
19. Igaz, L. M., Kwong, L. K., Lee, E. B., Chen-Plotkin, A., Swanson, E., Unger, T., Malunda, J., Xu, Y., Winton, M. J., Trojanowski, J. Q., and Lee, V. M. (2011) Dysregulation of the ALS-associated gene TDP-43 leads to neuronal death and degeneration in mice. *J Clin Invest* **121**, 726-738
20. Petkau, T. L., Neal, S. J., Milnerwood, A., Mew, A., Hill, A. M., Orban, P., Gregg, J., Lu, G., Feldman, H. H., Mackenzie, I. R., Raymond, L. A., and Leavitt, B. R. (2012) Synaptic dysfunction in progranulin-deficient mice. *Neurobiol Dis* **45**, 711-722
21. Ghoshal, N., Dearborn, J. T., Wozniak, D. F., and Cairns, N. J. (2012) Core features of frontotemporal dementia recapitulated in progranulin knockout mice. *Neurobiol Dis* **45**, 395-408
22. Yin, F., Dumont, M., Banerjee, R., Ma, Y., Li, H., Lin, M. T., Beal, M. F., Nathan, C., Thomas, B., and Ding, A. (2010) Behavioral deficits and progressive neuropathology in progranulin-deficient mice: a mouse model of frontotemporal dementia. *FASEB J* **24**, 4639-4647

APPENDIX A

LIVE CELL IMAGING OF TMEM106B REVEALS ITS DYANMIC NATURE AND POTENTIAL INVOLVEMENT IN MEMBRANE FUSION AND TUBULATION EVENTS

A.1 Summary

Preliminary evidence indicates that TMEM106B regulates lysosome size, number, and morphology. I performed a series of live-imaging experiments in order to more accurately describe lysosome dynamics which may govern this behavior in a TMEM106B overexpression model.

A.2 Introduction

We and others have recently shown that elevated TMEM106B causes defects in lysosome morphology and function. Specifically, overexpression of TMEM106B in cell culture models leads to an increase in the overall size of lysosomes and a concomitant decrease in the total number of lysosomes per cell. These changes were accompanied by increased aggregation of TMEM106B on the lysosome limiting membrane, and accumulation of TMEM106B within the lumen of the lysosomes. (1,2). Lysosomes are dynamic organelles which exhibit a variety of behaviors including fusion events, both with other lysosomes (homotypic fusion) and with related organelles such as MVBs and autophagosomes (heterotypic fusion). Both long-term fusion events, and transient “kiss-and-run” events are known to occur (reviewed in ((3)). On the other side of the coin are fission and reformation events in which

lysosomes can split into two separate organelles or in which lysosomal membranes can reform from hybrid organelles such as autolysosomes, and MVB-Lysosome hybrids. This process typically involves a membrane tubule enriched in lysosome membrane proteins which buds off the hybrid organelle, and can be re-populated by lysosomal hydrolases by the typical mannose-6-phosphate receptor and related transport pathways (4,5). Conceptually, the lysosomal phenotype seen with TMEM106B overexpression could be due to several factors including: increased kinetics of fusion, decreased kinetics of fission or reformation events, or impaired degradation of lumenal contents resulting in swollen vacuoles, or some combination of these events. In these experiments, I attempted to characterize some of these events which may be occurring during TMEM106B overexpression conditions.

A.3 Materials and Methods

Cell culture and transfections

N2a cells were seeded to approximately 40% confluence in a 30 mm glass bottom cell culture dish (MatTek Corporation). 48 hours prior to image acquisition, cells were co-transfected using PEI with GFP control, or GFP-TMEM106B and LAMP1-dsRed Monomer, sub-cloned from to LAMP1-YFP (Addgene# 1816) into pDsRed-Monomer N1 (Clontech). One hour prior to image acquisition, cells were washed with PBS and media replaced with DMEM with no phenol red (Invitrogen), 10% FBS (Sigma), and 50 mM HEPES pH 7.4.

Live Cell Imaging

Plates were kept in a 37ºC heated environmental chamber with 5% CO_2 atmosphere and images acquired at 2-6 second intervals for 10-20 minutes per capture, with multiple locations detected per acquisition using an automated stage. Images were collected with both a Zeiss LSM700 confocal microscope and a CSU-X spinning disc confocal microscope (Intelligent Imaging Innovations) with an HQ2 CCD camera (Photometrics) using a 100x objective. Image series were acquired at 24 hours and 48 hours post-transfection.

A.4 Results and Discussion

GFP-TMEM106B overexpression causes increased lysosomal size and decreased mobility. Consistent with our earlier immunofluorescence experiments reported in (1), I observed a clear qualitative difference in the overall size distribution of GFP-TMEM106B positive lysosomes compared to those from GFP control transfected cells (data not shown). Further, these differences were even more apparent at 48 hours post-transfection than 24 hours, with apparently fewer, but larger GFP-TMEM106B positive lysosomes observed per cell. In addition, these engorged lysosomes appeared much less dynamic than the smaller ones observed earlier in the experiment and in control cells. While this may be due to continued synthesis of GFP-TMEM106B over the course of the experiment, it may also indicate a defect in lysosome fission dynamics. While these observations are preliminary, they provide an important proof of concept that we can image GFP-TMEM106B in combination with LAMP1-dsRed *in vivo* and may pave the way for a more systematic analysis of fusion vs. fission

dynamics, particularly in a stable N2a GFP-TMEM106B line that we have recently generated.

GFP-TMEM106B is a component of lysosomal membrane tubules. In some cases, particularly at 24 hours post-transfection, GFP-TMEM106B was seen on LAMP1 positive lysosomal tubules which emerged from some individual lysosomes. Figure A.1 shows multiple lysosomal tubules which were observed in our experiments. Interestingly, in some cases these tubules appeared to link multiple individual lysosomes together, possibly suggesting a tethering role or perhaps a way of transporting lumenal substrates to nearby lysosomes, analogous to the kiss-and-run dynamics seen in certain instances of lysosomal fusion. Perhaps more likely, is that these tubules are mediating fission events and the presence of TMEM106B on them may suggest a role in this dynamic process. On the other hand, TMEM106B may simply be a passenger on these tubules as a normal component of lysosomal membranes. Support for the previous notion occurs in a recent study by Rong, et al. in which purified autophagic lysosome reformation (ALR) tubules emerging from autolysosomes were purified and subjected to mass spectrometry to determine components enriched on these membranes. In every instance, TMEM106B was identified in their experiments, indicating that TMEM106B can indeed be a component of hybrid organelles and may play a role the process of lysosomal tubulation events (5).

GFP-TMEM106B puncta can be internalized into the lumen of lysosomes and may be transferred from the limiting membranes of adjacent lysosomes. At

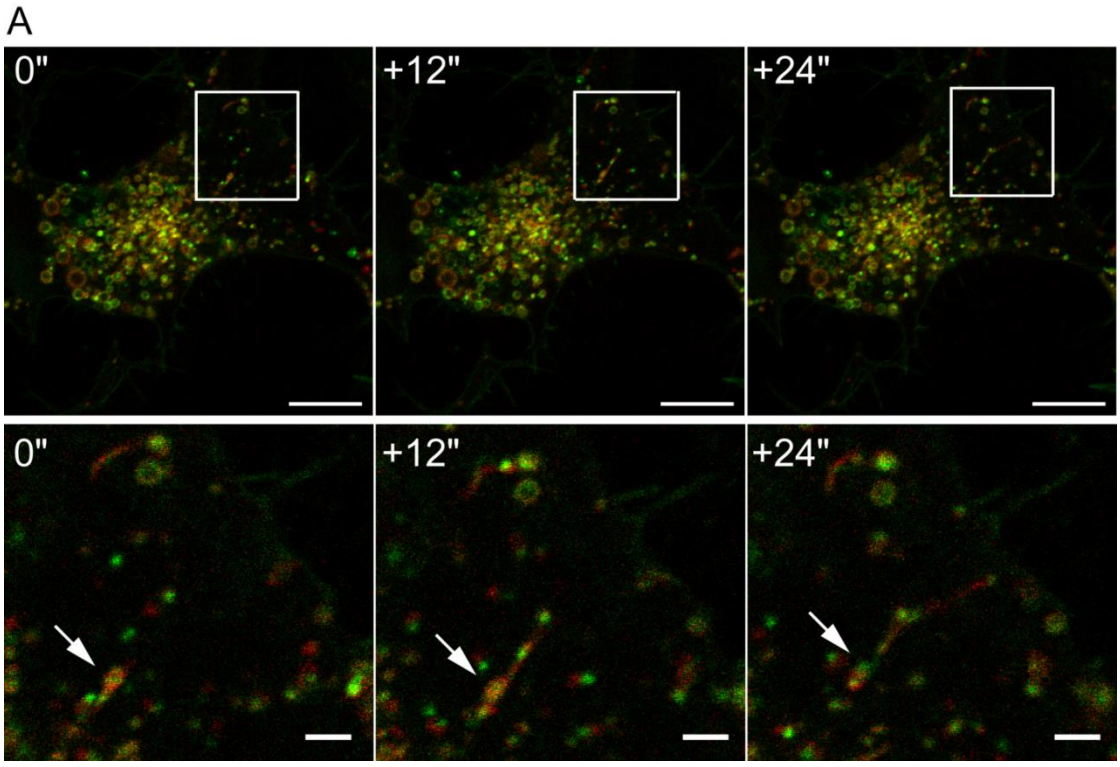

Figure A.1: GFP-TMEM106B is present on lysosomal tubules. N2a cells were co-transfected with GFP-TMEM106B and LAMP1-dsRed and imaged 24 hours post-transfection. Scale bar = 10 µm, 2 µm in lower panel magnification. Images were acquired 12 seconds apart. An arrow indicates a roughly spherical lysosome which projects a TMEM106B positive tubule outwards towards neighboring lysosomes. A second tubulating lysosome can also be seen at the top of the inset.

endogenous levels at steady state, TMEM106B appears to evenly dot the limiting membrane in the form of small puncta. When overexpressed, we frequently observe an increase in the size of these puncta and a more polarized or even internalized distribution on the lysosome limiting membrane and lumen, respectively. Live-imaging with high spatio-temporal resolution (time intervals ~2 seconds) reveals that these puncta are very dynamic on the limiting membranes of lysosomes. They continually track around the membranes and can be seen internalizing into the lumen and returning to the limiting membrane on individual lysosomes, compared to the much more static distribution of LAMP1-dsRed used in these experiments. An example of the former process is illustrated in Figure A.2, in which a GFP-TMEM106B puncta translocates from the membrane to the lumen and back again, potentially highlighting a role for TMEM106B in the transport of membrane components to the lysosome for degradation. This is an intriguing possibility as CHMP2B, which is mutated in cases of FTLD-UPS is implicated in the budding of intralumenal vesicles into the lumen of MVBs.

Another feature of the GFP-TMEM106B puncta observed in these studies is that they tend to accumulate at the interface of adjacent lysosomes. With two puncta from different lysosomes frequently associating together. This is fascinating, as TMEM106B appears to homodimerize through its cytosolic intracellular domain (discussed in Appendix D), potentially indicating a role in mediating lysosome-lysosome contacts and possibly homotypic fusion events. In some cases, it appears that individual puncta can “jump” between two adjacent lysosomes as shown in Figure A.3, further highlighting the extremely dynamic nature of this transmembrane protein.

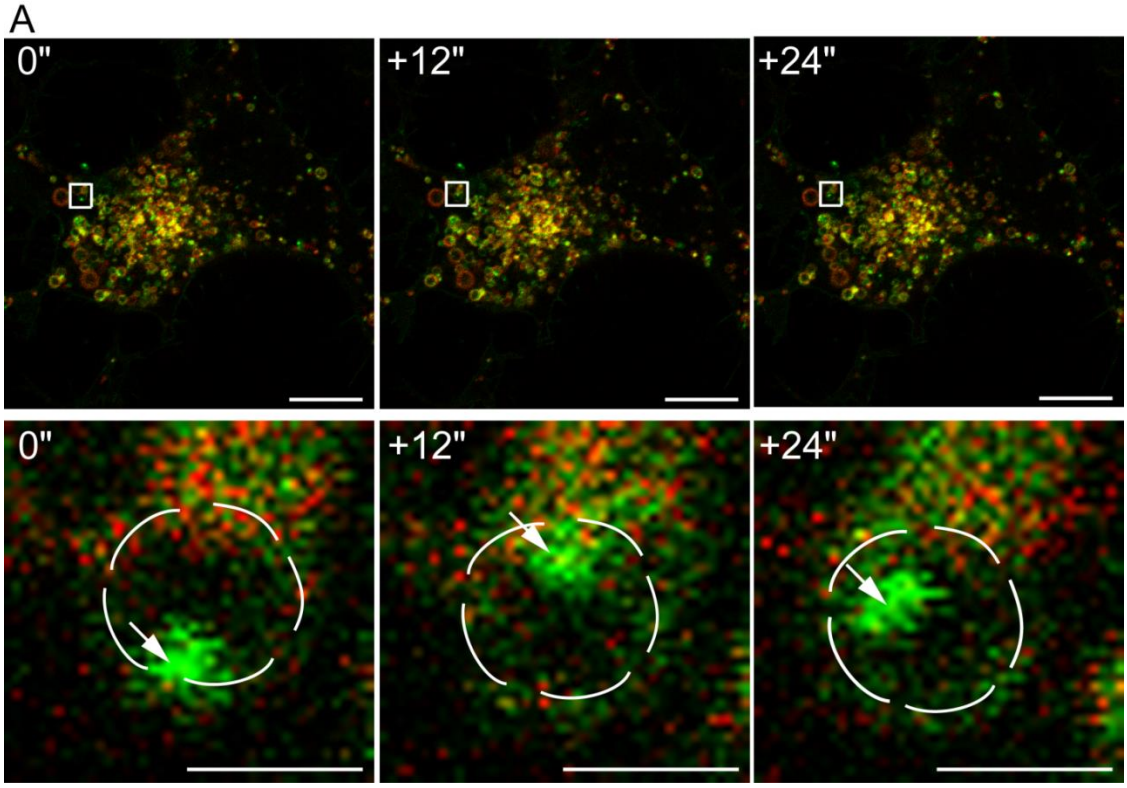

Figure A.2: GFP-TMEM106B traverses the limiting membrane of lysosomes and undergoes internalization. The same cell shown in Figure A.1 is shown at a different time interval. Scale bar = 10 µm, 2 µm in lower panel magnification. The limiting membrane of the lysosome in the inset is highlighted with a dotted line. A single GFP-TMEM106B puncta can be seen moving along the limiting membrane from 0 seconds to 12 seconds followed by internalization into the lysosome lumen from 12 seconds to 24 seconds.

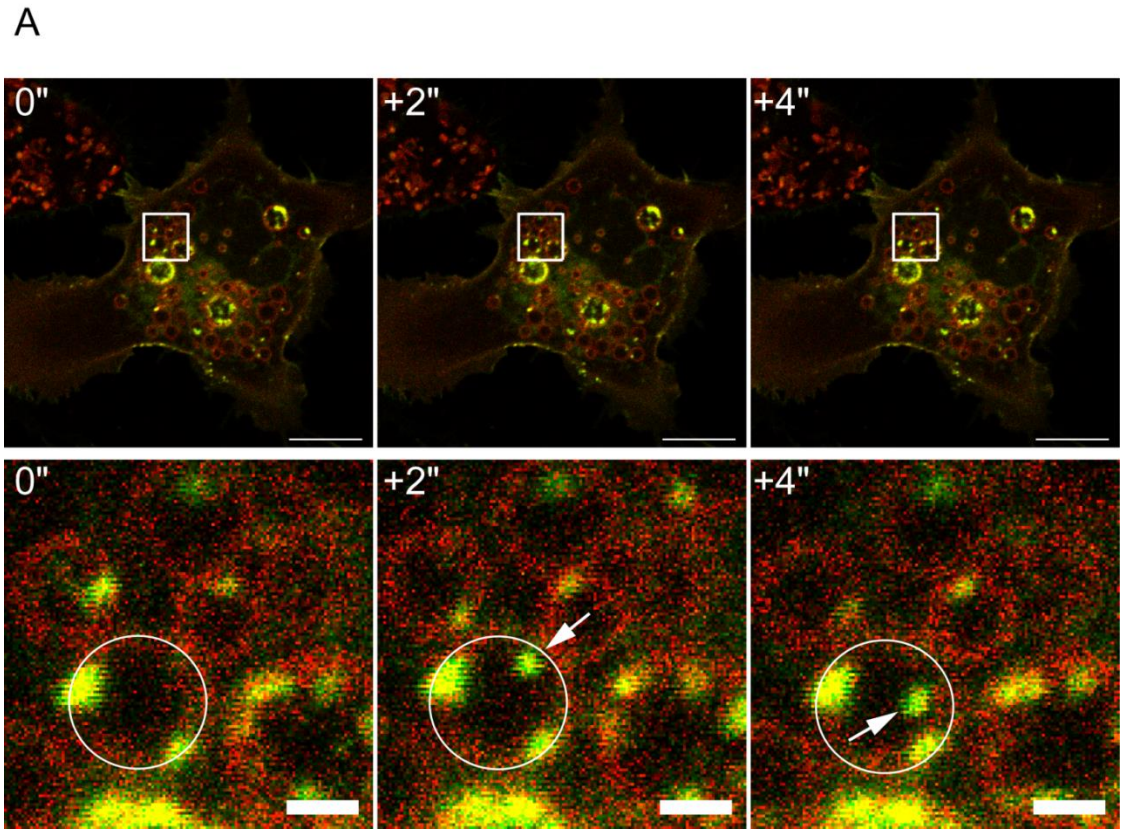

Figure A.3: GFP-TMEM106B is highly dynamic and accumulates at the interface between adjacent lysosomes. N2a cells were co-transfected with GFP-TMEM106B and LAMP1-dsRed and imaged 48 hours post-transfection. Scale bar = 10 µm, 2 µm in lower panel magnification. Images are separated by 2 seconds each. An individual lysosome's limiting membrane is highlighted with a white line. Individual GFP-TMEM106B puncta are capable of moving rapidly. The arrow highlights a single puncta which appears to originate from a neighboring lysosome to the upper right of the highlighted one. This GFP-TMEM106B appears at the interface of the two lysosomes and rapidly internalizes into the neighbor, in an apparent kiss-and-run event.

Nonetheless, caution should be exhibited when interpreting these latter conclusions, as the resolution of the confocal microscope is insufficient to differentiate individual intralumenal vesicles and it is possible that these internalized puncta may still be on the limiting membrane or may be coming into focus from elsewhere on the same vesicle, and hence, these may be artifacts of our imaging capabilities. These conclusions should be confirmed, preferably with super-resolution microscopy or with immuno-electron microscopy to unequivocally demonstrate the presence of TMEM106B within the lysosome lumen and at lysosome contact sites.

APPENDIX B

TMEM106B OVEREXPRESSION CAUSES DEFECTS IN LYSOSOMAL PROTEOLYSIS

B.1 Summary

In this experiment, I use a DQ-BSA proteolysis assay to clarify the lysosomal defects caused by TMEM106B overexpression. I demonstrate that terminal lysosomal proteolysis is impaired.

B.2 Introduction

We have previously shown that TMEM106B overexpression causes a kinetic delay in the degradation of endocytosed EGFR (1). Our results suggested that early and late endocytic trafficking is normal in this system, as measured by the kinetics of the downstream signaling through phospho-ERK. Another report by Chen-Plotkin and colleagues demonstrates impaired acidification in the lysosomes from cells overexpression TMEM106B (2). In this assay, we used the fluorogenic substrate DQ-BSA, which contains a BODIPY dye conjugated to BSA. During proteolysis, the BODIPY becomes dequenched, resulting in a red fluorescence readout proportional to the amount of proteolytic activity occurring.

B.3 Materials and Methods

Cell culture and transfections

N2a cells were seeded at 40% confluence on coverslips in a 24-well plate. Cells were transiently transfected using PEI with pCMV-TMEM106B or Vector control. 24 hours after transfection, lysosomes were loaded with Red DQ-BSA (Invitrogen) by treating cells with 10 µg/ml DQ-BSA for 16 hours. A vector transfected well was treated with 15mM ammonium chloride and 250 µM leupeptin for 16 hours to inhibit lysosomal proteases and served as a positive control. After treatment, cells were washed with PBS to remove excess DQ-BSA and fixed for 20 minutes with 4% paraformaldehyde. Cells on coverslips were permeabilized with PBS containing 0.05% saponin and 3% BSA blocking buffer. Primary rat anti-mouse LAMP1 (BD Biosciences) and rabbit anti-TMEM106B antibodies were incubated overnight in blocking buffer at 4º C. Coverslips were washed 3x with blocking buffer and incubated with anti-Rat fluorescein and anti-rabbit CF660 (Biotum) secondary antibodies at room temperature for 90 minutes. Cells were washed 3x with blocking buffer and again with PBS. Coverslips were mounted with Fluoromount G (Southern Biotech) and imaged on a CSU-X spinning disc confocal microscope (Intelligent Imaging Innovations) with an HQ2 CCD camera (Photometrics) with a 100x objective.

Data analysis

Maximum projection images through the center of the cells of interest were generated across two 0.28 µm slices from confocal Z-stacks using Slidebook software (Intelligent Imaging Innovations). All channels were background corrected and regions of interest drawn around individual cells. Regions were converted to masks

and the mean intensity of DQ-BSA fluorescence contained within each mask was calculated. The mean fluorescence from a minimum of 8 cells from multiple fields of view per condition was analyzed for each of three independent transfections. Significance was determined with Student's t-test.

B.4 Results and Discussion

Our DQ-BSA assay reveals that TMEM106B overexpression causes a statistically significant decrease in the level of DQ-BSA fluorescence observed, with levels at 73.6% of vector controls as shown in Figure B.1 (n=3). Potent inhibition of lysosomal protease activity by treating cells with the alkalizing agent ammonium chloride and the broad-spectrum lysosomal protease inhibitor leupeptin caused a strong reduction in DQ-BSA fluorescence with levels at 47.6% of control cells (n=2), demonstrating the validity of our assay. This result confirms ours and others previous observation that increased TMEM106B levels are correlated with impaired lysosome function. Further, these experiments suggest that elevated TMEM106B causes a primary defect in lysosomal protein degradative function, rather than an indirect defect due to impairments in endocytic or autophagic trafficking to lysosomes. Interestingly, we also looked at the level of Filipin staining, a marker for cholesterol accumulation, which is a characteristic of some neurodegenerative lysosomal diseases such as Niemann-Pick disease (6). In these experiments, we saw no differences in Filipin staining in TMEM106B overexpressing cells versus control cells (data not shown), potentially indicating that certain degradative functions of the lysosome are differentially affected by elevated levels of TMEM106B. These experiments should be

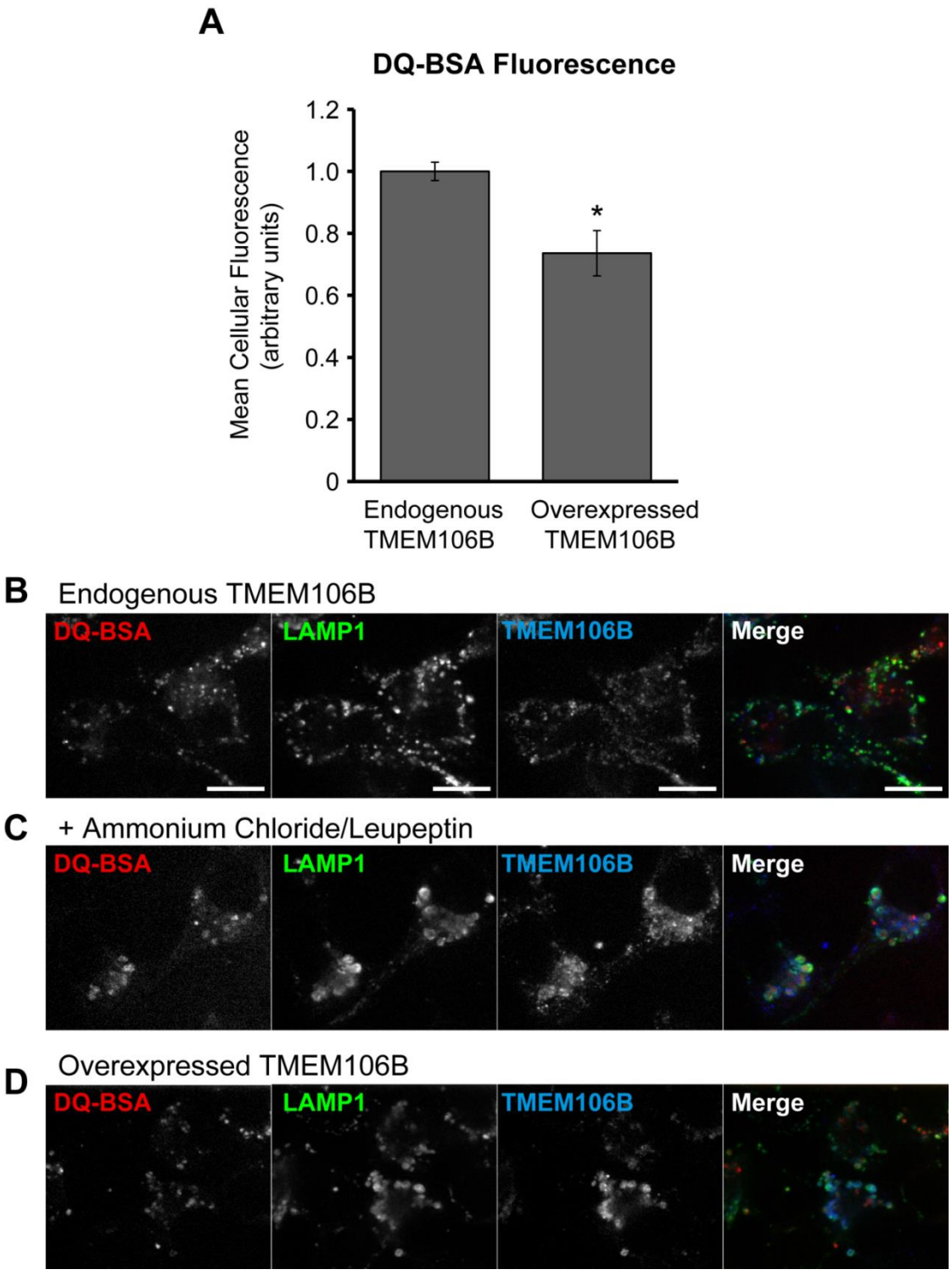
A
DQ-BSA Fluorescence
Mean Cellular Fluorescence (arbitrary units)
1.2
1.0
0.8
0.6
0.4
0.2
0
*
Endogenous TMEM106B
Overexpressed TMEM106B
B
Endogenous TMEM106B
DQ-BSA
LAMP1
TMEM106B
Merge
C
+ Ammonium Chloride/Leupeptin
DQ-BSA
LAMP1
TMEM106B
Merge
D
Overexpressed TMEM106B
DQ-BSA
LAMP1
TMEM106B
Merge

Figure B.1: TMEM106B overexpression leads to impaired lysosomal proteolysis. (**A**) TMEM106B overexpression leads to a significant decrease in the proteolytic capacity of lysosomes as measured by the mean fluorescence intensity of cells pre-loaded with DQ-BSA. Values represent mean +/-SEM, n=3, *$p < 0.05$, paired Student's t-test. (**B**) Representative image of vector transfected control N2a cells loaded for 16 hours with 10 µg/ml DQ-BSA. Scale bar = 10 µm (**C**) Vector transfected N2a cells loaded with DQ-BSA and treated with 15 mM ammonium chloride and 250 µM Leupeptin to inhibit lysosomal proteases served as positive controls. Cells under these conditions exhibited strongly reduced DQ-BSA fluorescence. (**D**) Representative image of N2a cells overexpressing TMEM106B. Cells were loaded with DQ-BSA as in (**B**) and (**C**) and exhibited reduced fluorescence compared to controls.

followed up with more specific fluorogenic substrates in order to determine if certain proteases are specifically affected by TMEM106B overexpression. Examples of these more specific reagents include the specific cathepsin D substrate, Bodipy-FL-pepstatin A, and the Cathepsin B substrate, MR-CatB.

APPENDIX C

TMEM106B TRAFFICKING TO LYSOSOMES DEPENDS ON BOTH INTRACELLULAR DOMAIN AND LUMENAL DOMAIN DETERMINANTS

C.1 Summary

In these experiments, I created a series of TMEM106B point mutants, truncations, and chimeric transmembrane proteins in order to dissect the molecular determinants of TMEM106B trafficking to lysosomes. These experiments reveal that both lumenal and intracellular domains of TMEM106B are essential for proper localization, and that TMEM106B traffics independently of classical lysosomal targeting motifs.

C.2 Introduction

Transmembrane proteins can be trafficked to the lysosome through a variety of different routes including direct Golgi to lysosome trafficking and indirect trafficking via the cell surface. Lumenal domain determinants of transmembrane protein trafficking include N-linked glycosylation signals which may be essential for proper folding and binding to lectin chaperones (7). Resident lysosome membrane proteins in particular, tend have heavily glycosylated lumenal domains to resist degradation by the acidic environment and hydrolytic enzymes present within lysosomes. TMEM106B contains 5 N-linked glycosylation sites which were previously shown to be essential for proper lysosomal targeting (8). The other major determinants of transmembrane protein targeting to lysosomes include the cytosolic trafficking motifs, most notably the YXXΦ, where Φ represents a bulky hydrophobic residue, and di-

leucine type motifs, which are frequently preceded by one or two acidic residues at positions -3 or -4 and -5, respectively (Reviewed in detail in (9)). These sequences typically bind clathrin binding adaptor proteins such as the μ subunits of the AP-2 and AP-3 adaptor complexes in the case of YXXΦ motifs or to the μ or β subunits of the AP complexes or the VHS domains of the Golgi-localized, -ear-containing, ARF-binding (GGA) proteins, in the cases of di-leucine based sorting motifs. Many variations of these motifs have been described with the relative position of the motif in the cytosolic domain and different amino acids in nearby positions affecting the subunit preferences and targeting dynamics in subtle ways.

C.3 Materials and Methods

Plasmids and constructs

TMEM106B sub-cloned into the pCMV3xFLAG7.1 vector (Sigma) provided the basis for most of these experiments. Mutagenesis was performed for indicated constructs using site-directed overlap-extension PCR. Chimeric constructs were generated by PCR of the appropriate fragments from indicated cDNAs and sub-cloned into pCMV3xFLAG7.1 with the conjugate TMEM106B fragment with overlapping restriction sites. TMEM106A, TMEM106C, TfR1, TMEM192 cDNAs were obtained from the ORFeome Collection (courtesy of Dr. Haiyuan Yu). TNF-α cDNA was a kind gift from Dr. Hening Lin.

Cell culture and transfections

N2a cells were seeded at 40% confluence on coverslips in a 24-well plate. Cells were transiently transfected using PEI with the indicated constructs. 48 hours post-

transfection, cells were fixed, stained, and imaged as described above. Primary antibodies used were rat anti-mouse LAMP1 1D4B (BD Biosciences) and mouse anti-FLAG (Sigma). Secondary antibodies were donkey anti-rat CF568 and donkey anti-mouse CF488 (Biotum).

Data analysis

All primary data analysis was performed with Slidebook software (Intelligent Imaging Innovations). All images were background corrected to minimize secondary antibody cross-reactivity. Individual cells were analyzed by creating a mask around the region of interest corresponding to the entire Z-stack of each cell. Pearson correlation coefficients of LAMP1 and TMEM106B immunoreactivity were calculated for the voxels of individual cells in each condition. A minimum of 23 transfected cells from several fields of view were calculated for each condition. Cells were analyzed from a minimum of three independent transfections per condition and statistical significance determined with ANOVA and post-hoc analysis with Tukey's Multiple Comparison Test.

C.4 Results and Discussion

A C-terminal truncation (1-241, Full length = 1-274) from the TMEM106B lumenal domain that removed the N5 glycosylation sites resulted in significantly impaired localization of TMEM106B to lysosomes, with the majority being retained in the ER. This is in agreement with results from Lang, et al. in which they show that point mutations of glycosylation site Asn residues impaired proper localization in their cell culture models (8). Further truncations that remove additional glycosylation sites

yielded consistent results, with mislocalized TMEM106B fragments primarily at the cell surface (data not shown). These results strongly indicate intact N-linked glycosylation is required for proper TMEM106B trafficking.

The intracellular domain of TMEM106B is predicted to comprise amino acids 1-96. An N-terminal truncation construct containing amino acids 70-274 exhibited a significant impairment in lysosomal localization, although this defect was not as severe as the C-terminal truncations. Interestingly, a small subset of cells expressing this construct appeared to have a lysosomal localization, suggesting alternative, but potentially less efficient routes to the lysosome. It should be noted that the levels of this protein product were significantly lower than full length TMEM106B and its C-terminal truncations as determined by Western blotting (see Figure D.1B), suggesting that the ICD of TMEM106B may be important for its long-term stability within the cell. A further N-terminal truncation corresponding to amino acids 80-274 failed to be detected completely, further suggesting that an intact ICD is essential for protein stability.

The intracellular domain of TMEM106B has three potential consensus lysosomal trafficking motifs, including two YXXΦ motifs, and single degenerate di-leucine like motif (18-YDGV-21, 50-YVEF-53, and 81-LI-82). In order to determine if any of these potential trafficking motifs mediate TMEM106B localization to lysosomes, they were mutated individually and combined, with the tyrosine and Φ residues from YXXΦ mutated to alanine and the leucine from the di-leucine like motif mutated to glycine. Surprisingly, none of these mutants resulted in a lysosomal trafficking defect, including when all three motifs were mutated in the same construct

(triple mutant), suggesting that the TMEM106B ICD may contain novel trafficking determinants independent of traditional targeting sequences. These results should be interpreted with caution, however, as TMEM160B is known to dimerize via its ICD (Appendix D), and it is conceivable that these mutant constructs were able to dimerize with endogenous TMEM106B and be trafficked to lysosomes indirectly through interaction with the trafficking motifs of endogenous TMEM106B. Hence, these results should be confirmed in cells with endogenous TMEM106B knocked out.

TMEM106B has two highly conserved paralogs, TMEM106A and TMEM106C, which were also analyzed for localization to lysosomes. TMEM106A had a localization pattern nearly identical to that of TMEM106B, potentially indicating a similar role in lysosome membranes. TMEM106C, on the other hand remained almost entirely within the ER. The results of these trafficking analyses are compiled in Figure C.1.

In order to more accurately determine if either the ICD or lumenal domain of TMEM106B is sufficient for lysosomal targeting, we generated a series of chimeric transmembrane proteins. All chimeras were constructed so as to maintain the type II transmembrane orientation of the relevant TMEM106B domain. A TMEM106B-TNF-α chimera consisting of the lumenal domain of TMEM106B (127-274) and the intracellular and transmembrane region of the plasma membrane bound form of TNF-α (1-55) reveals poor localization to lysosomes compared to TMEM106B alone. A cartoon schematic of this chimera is illustrated in Figure C.2B. Nonetheless, a small subpopulation of this chimeric transmembrane protein managed to localize to lysosomes, in addition to the cell surface as shown in Figure C.2B lower panel. This

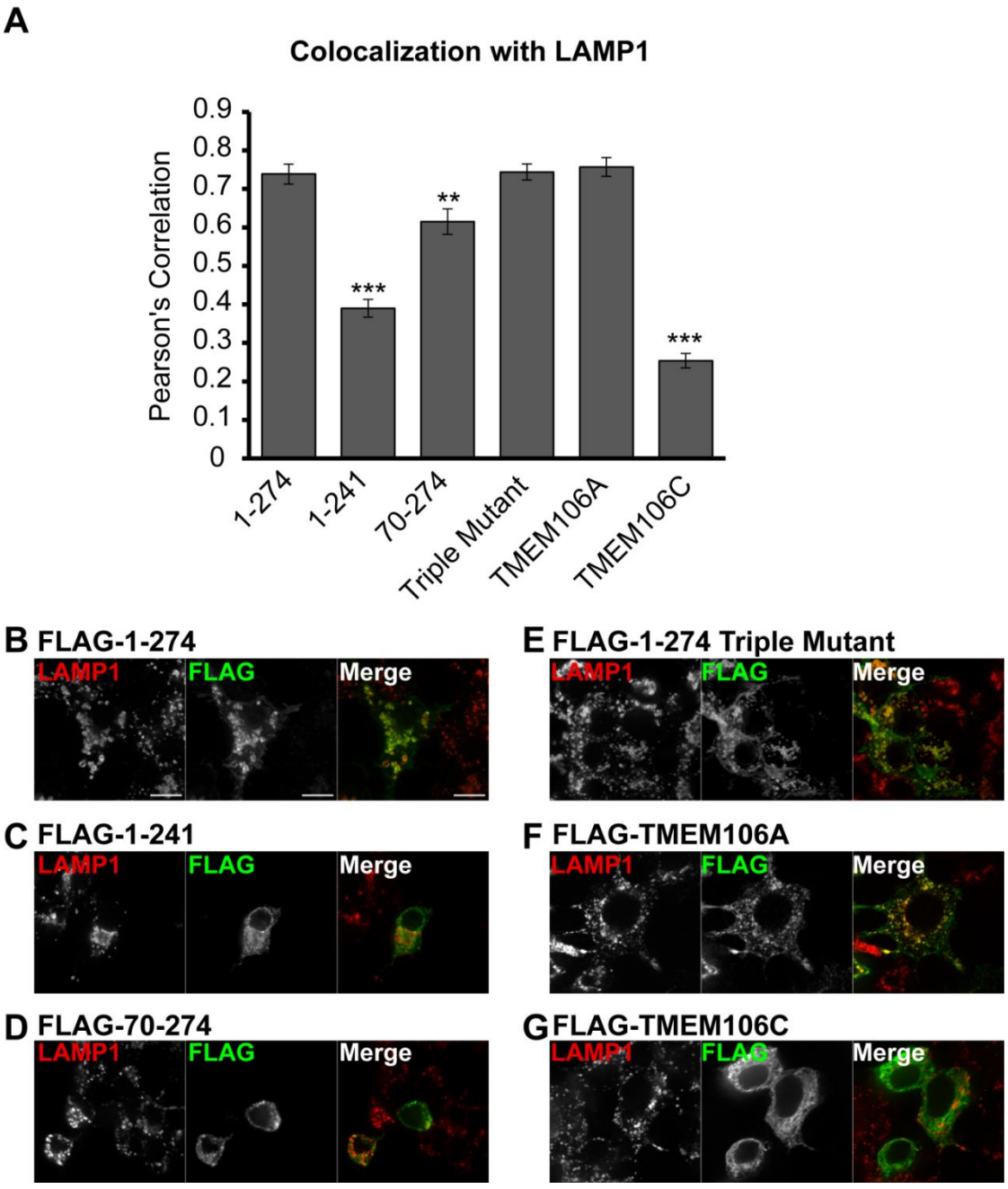
A
Colocalization with LAMP1
Pearson's Correlation
0.9
0.8
0.7
0.6
0.5
0.4
0.3
0.2
0.1
0
***
**
***
1-274
1-241
70-274
Triple Mutant
TMEM106A
TMEM106C
B FLAG-1-274
E FLAG-1-274 Triple Mutant
C FLAG-1-241
F FLAG-TMEM106A
D FLAG-70-274
G FLAG-TMEM106C
LAMP1
FLAG
Merge

Figure C.1: The lumenal domain and ICD of TMEM106B are both necessary for proper lysosomal localization. (**A**) Pearson correlation coefficients between FLAG and LAMP1 immunoreactivity in N2a cells. Values represent mean +/-SEM from a minimum of 23 cells split between at least 3 independent transfections. (**p<0.01, ***p<0.001, one-way ANOVA with Tukey's multiple comparison's test) (**B**) N2a cells transfected with full length FLAG-TMEM106B shows high levels of lysosomal localization. (**C**) A C-terminal truncation of FLAG-TMEM106B (1-241) causes significant reduction in lysosomal localization, with most being retained in the ER. (**D**) An N-terminal truncation of FLAG-TMEM106B (70-274) also exhibits a significant reduction in lysosomal localization, with most located at the cell surface, although a small amount still localizes to lysosomes. (**E**) FLAG-TMEM106B with mutations in three predicted lysosomal targeting motifs localized to lysosomes at levels similar to WT controls. (**F**) The homologue, FLAG-TMEM016A is highly localized to lysosomes similar to FLAG-TMEM106B while the other homologue, (**G**) FLAG-TMEM106C is almost exclusively seen in the ER. Scale bars in B-G = 10μm.

suggests that the lumenal domain alone is not sufficient to mediate localization to lysosomes. Additionally, since the vast majority of this chimera appears at the cell surface, it is possible that the species that are seen localizing to lysosomes have trafficked there for degradation through the endocytic pathway. A separate chimera consisting of the TMEM106B ICD (1-96) and the transmembrane and lumenal domains of TfR1 (68-760), which normally localizes to the cell surface or early and recycling endosomes, was tested (Figure C.2C). Much like the previous chimera, this one also poorly localized to lysosomes, with some localizing to the cell surface and the majority being retained in the ER, which may suggest that this chimera is improperly folded. Similar to the TMEM106B-TNF-α chimera, a small population also localized to the lysosomes, potentially suggesting that the TMEM106B ICD may have some activity in lysosomal trafficking, although to a significantly impaired degree compared to full length TMEM106B. Another possibility is that a portion of these chimeras are being trafficked to the lysosomes for degradation, like many other membrane proteins along the endocytic pathway that are degraded in a regulated manner. Collectively, these two chimeras reveal that both an intact ICD and lumenal domain of TMEM106B are necessary for efficient trafficking to lysosomes, with neither domain alone sufficient to restore proper localization.

As a positive control for lysosomal targeting, I constructed a chimera containing a type II oriented intracellular domain composed of amino acids 1-42 of TMEM192, which contains two di-leucine motifs capable of potently and specifically trafficking to the lysosome (10). The rest of this chimera consisted of the transmembrane region and lumenal domain of TMEM106B (97-274). This chimera

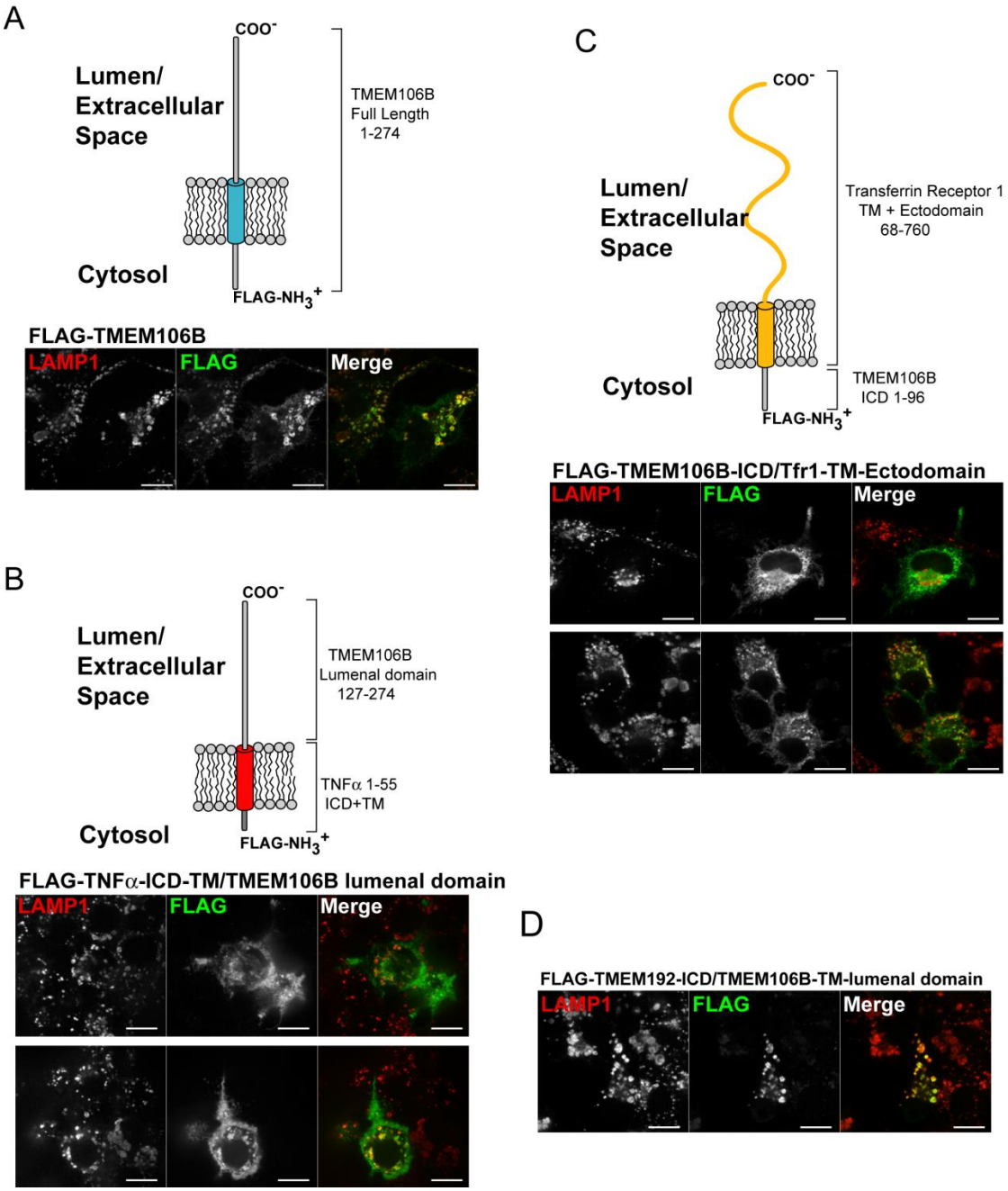
A
COO-
Lumen/
Extracellular
Space
TMEM106B
Full Length
1-274
Cytosol
FLAG-NH3+
FLAG-TMEM106B
LAMP1
FLAG
Merge
B
COO-
Lumen/
Extracellular
Space
TMEM106B
Lumenal domain
127-274
TNFα 1-55
ICD+TM
Cytosol
FLAG-NH3+
FLAG-TNFα-ICD-TM/TMEM106B lumenal domain
LAMP1
FLAG
Merge
C
COO-
Lumen/
Extracellular
Space
Transferrin Receptor 1
TM + Ectodomain
68-760
TMEM106B
ICD 1-96
Cytosol
FLAG-NH3+
FLAG-TMEM106B-ICD/Tfr1-TM-Ectodomain
LAMP1
FLAG
Merge
D
FLAG-TMEM192-ICD/TMEM106B-TM-lumenal domain
LAMP1
FLAG
Merge

Figure C.2: TMEM106B lumenal domain and ICD chimeras highlight the importance of both domains for correct lysosomal targeting. (**A**) Cartoon schematic of the domain structure and orientation of WT FLAG-TMEM106B. It localizes primarily on lysosomes in N2a cells as shown by overlap with LAMP1 staining (scale bar = 10 µm.) (**B**) Domain structure and orientation of the FLAG-TNFα-ICD-TM/TMEM106B lumenal domain chimera. This construct localized poorly with lysosomes (top panel), but a sub-population did localize to lysosomes (bottom panel). (**C**) Domain structure and orientation of the FLAG-TMEM106B-ICD/Tfr1-TM-Ectodomain chimera. Overall, localization to lysosomes was very poor with a large amount retained in the ER as exemplified by the upper panel. A small population of this chimera did appear to partially co-localize with LAMP1 as shown in the lower panel. (**D**) As a positive control for lysosomal targeting, a chimera in which the TMEM106B ICD was replaced with the ICD from TMEM192, which contains known lysosomal targeting motifs, was generated (FLAG-TMEM192-ICD/TMEM106B-TM-lumenal domain). As expected, this chimera localized strongly to lysosomes as shown by co-localization with LAMP1. This chimera appeared to localize more potently and specifically to lysosomes than WT FLAG-TMEM106B.

actually targeted to the lysosomes with an even higher efficiency than WT TMEM106B as shown in Figure C.2D. This chimera was almost totally restricted to the lysosomes, with little to no staining at the cell surface, which is observed to some degree in most cells transfected with FLAG-TMEM106B. This is noteworthy, as it shows that specific lysosomal targeting motifs actually improve the localization of TMEM106B to the lysosomes, further strengthening the argument that TMEM106B lacks traditional YXXΦ or di-leucine trafficking motifs. Thus, TMEM106B lysosomal targeting may be represented by a novel trafficking mechanism, involving cooperation between the ICD and lumenal domains.

APPENDIX D

TMEM106B EXISTS AS A DIMER AND BINDS HOMOTYPICALLY THROUGH ITS INTRACELLULAR DOMAIN

D.1 Summary

In this series of co-immunoprecipitation (co-IP) experiments, I analyze the domain determinants governing TMEM106B's homodimerization and show that this interaction is mediated primarily through the ICD. Additionally, I show that TMEM106B is capable of forming heterodimers *in vitro* with its lysosomally localized paralog, TMEM106A.

D.2 Introduction

Western blots of TMEM106B reveal the presence of a heat sensitive species that runs at approximately twice the size of its monomeric ~43 kDa form, suggesting the presence of an SDS-resistant dimer (1,2). In order to determine the regions of TMEM106B that mediate this interaction, I performed co-IP experiments with various deletion constructs and chimeras. These experiments reveal that the ICD of TMEM106B is necessary and sufficient to bind to full length TMEM106B. TMEM106A, a highly conserved family member that also localizes to lysosomes is also shown to co-IP with TMEM106B, suggesting that heterodimers may exist *in vivo*.

D.3 Materials and Methods

Plasmids and constructs

Full-length TMEM106B and all N-terminal and C-terminal deletion constructs were sub-cloned into the pCMV3xFLAG7.1 vector. TMEM106B chimeras were generated as described in the previous appendix. GFP tagged TMEM106A and TMEM106B were used as prey proteins and were expressed in pEGFP-C1 (Clontech).

Co-immunoprecipitations

HEK293T cells in 6-well plates were co-transfected with the indicated constructs with PEI. 48 hours post-transfection, cells were washed with PBS and lysed in 500 µl IP-lysis buffer (50 mM Tris pH 7.5, 150 mM NaCl, 1% Triton X-100, 1 mM EDTA, 10 mM β-glycerophosphate, 5 mM sodium fluoride, and a Complete Mini protease inhibitor [Roche]). Lysates were cleared by centrifuging at 18,000 rcf for 20 minutes at 4º C. A fraction of the cleared supernatant was saved as input and the remaining supernatant was immunoprecipitated for four hours at 4º C with ANTI-FLAG M2 Magnetic Beads (Sigma) or GFP Magnetic beads (ChromoTek). Beads were washed four times with lysis buffer, eluted with 15 µl of 3xFLAG peptide 200 ng/µl (Sigma) or 1% SDS in 50 mM Tris pH 8.0 elution buffer, then mixed with 2x Lamelli's loading buffer and boiled two minutes.

Western blots

Inputs and eluates were run on 12% SDS-PAGE gels and transferred to PVDF membranes. Membranes were blocked with Odyssey blocking buffer (Li-Cor) for one hour. Mouse anti-FLAG M2 (Sigma) and homemade rabbit anti-GFP primary antibodies were added overnight at 4º C in Tris buffered saline pH 7.5 with 0.1%

Tween-20 (TBS-T). Membranes were washed three times with TBS-T, and incubated 90 minutes at room temperature with donkey anti-mouse/rabbit conjugated to AlexaFluor 680 (Invitrogen) or IR DYE 800 (Li-Cor). Membranes were washed three more times with TBS-T and imaged with an Odyssey infrared scanner (Li-Cor).

D.4 Results and Discussion

GFP-TMEM106B co-IPed with full length FLAG-tagged and a series of C-terminal TMEM106B deletion constructs as shown in Figure D.1 (A and B). Deletion constructs as short as the first 96 amino acids, corresponding to the ICD of TMEM106B maintained the ability to bind GFP-TMEM106B *in vitro*. N-terminal deletion constructs on the other hand, failed to bind GFP-TMEM106B. A TMEM106B lumenal domain construct (127-274) failed to significantly interact with GFP-TMEM106B. A very faint band could be seen under these conditions; however its levels were comparable to those seen in a vector control IP. A shorter N-terminal deletion construct (70-274), which contains the transmembrane region and part of the ICD of TMEM106B also failed to interact with GFP-TMEM106B, suggesting that an intact ICD is necessary for homodimerization. One feature of the N-terminal deletion constructs is their lower apparent stability, as shown by the weaker immunoreactive bands seen in the inputs. In an attempt to control for these lowered protein levels, I used a chimeric protein consisting of the ICD and TM regions of membrane bound TNF-α (1-55) fused to the lumenal domain of TMEM106B (127-274) described in Appendix C. A sub-population of this chimera localizes to lysosomes as shown in Figure C.2B, yet it still fails to bind to GFP-TMEM106B in these co-IP experiments,

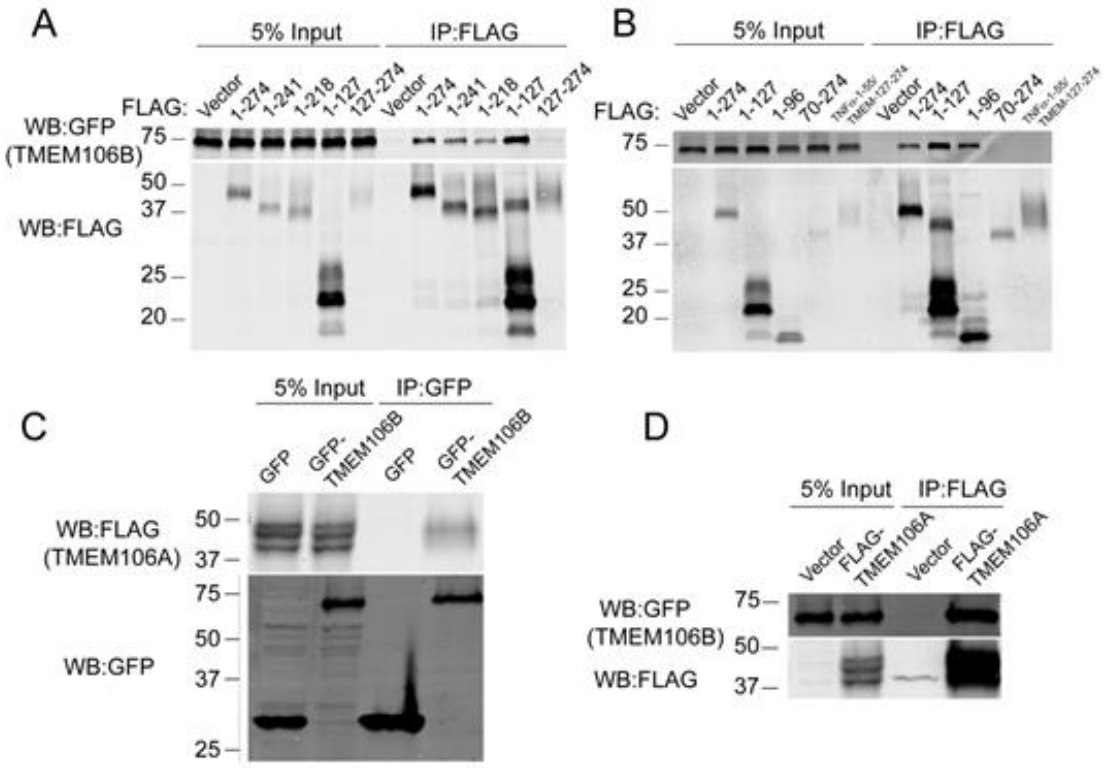

Figure D.1: TMEM106B homodimerizes through its ICD and can heterodimerize with TMEM106A. (**A**) Co-IPs from 293T cells transfected with GFP-TMEM106B and vector control or FLAG-TMEM106B and N- and C-terminal truncations. a chimera with its ICD from TNF-α (TNF-α 1-55/TMEM-127-274) (**B**) More TMEM106B co-IPs with additional truncation construts and a chimeric TMEM106B with its ICD replaced with one from TNF-α (TNF-α 1-55/TMEM-127-274) demonstrate that the TMEM106B ICD is required for dimerization. (**C**) GFP-TMEM106B co-IPs FLAG-TMEM106A and (**D**) FLAG-TMEM106A reciprocally co-IPs GFP-TMEM106B.

suggesting that the TMEM106B ICD contains specific structural features governing its homodimerization.

I have previously demonstrated that the TMEM106B paralog, TMEM106A also localizes primarily to lysosomes (Figure 4.4A and Figure C.1F). In order to test if TMEM106B could form heterodimers *in vitro*, I performed reciprocal co-IPs with GFP-TMEM106B and FLAG-TMEM106A as shown in Figure D.1 (C and D). TMEM106B and TMEM106A bound strongly and specifically in these experiments, raising the possibility that they may form functional heterodimers *in vivo*. Since the primary functions of these membrane proteins still remains unknown, the physiological implications of this interaction remain to be determined.

The results of these experiments confirm that TMEM106B likely exists as a dimer *in vivo* to some degree. An extremely large number of membrane proteins have been shown to be able to dimerize and/or oligomerize and these self-interactions are thought to likely regulate a multitude of physiologically relevant protein functions *in vivo*, ranging from signal transduction events, regulation of channel activity, and as scaffolds for the formation of supramolecular complexes, among other functions (11). These results also have important implications for the interpretation of the trafficking experiments described in Appendix C. Since the ICD of TMEM106B is required for homodimerization, this may explain why the lysosomal targeting motif mutants did not have defects in localization, but the 70-274 deletion mutant, which cannot homodimerize, did have defects. Future experiments will have to be performed to address this discrepancy, preferably in a TMEM106B knockout background. Another question that needs to be addressed is if this homodimerization occurs in cis or in

trans; that is within the same membrane, or between adjacent membranes, respectively. Since the ICDs of TMEM106B embedded in lysosome membranes face the cytosol, it is conceivable that adjacent vesicles could bind to each other through the homophilic interaction of their respective ICDs. Interestingly, TMEM106B puncta were observed to accumulate between tightly packed, enlarged lysosomes in the live imaging experiments described in Appendix A. It is tempting to speculate that these interactions may play a role in mediating homotypic or heterotypic fusion events between lysosomes and/or other vesicles such as late endosomes and autophagosomes. These ideas could be tested more systematically and in depth in future studies.

APPENDIX E

UBIQUITINATION OF TMEM106B ON ITS INTRACELLULAR DOMAIN CONTROLS ITS LEVELS

E.1 Summary

In this set of experiments I demonstrate that TMEM106B can be ubiquitinated *in vitro* with lysine residue 3, being particularly important. This ubiquitination event appears to modulate the levels of TMEM106B, but not its localization on lysosomes at steady state.

E.2 Introduction

Ubiquitin modifications to the cytosolic sides of membrane proteins provide a versatile way to regulate their trafficking and degradation (12). Because elevated levels of TMEM106B are strongly implicated as a risk factor for FTLD-TDP, identifying mechanisms by which its levels can be controlled will be critical for determining targets for therapeutic intervention.

E.3 Materials and Methods

Plasmids and constructs

HA-ubiquitin in the pCDNA3.1 vector (Addgene # 18712) was used for all ubiquitination assays. TMEM106B constructs in the pCDNA3xFLAG7.1 vector were used to determine ubiquitinated domains and were: full length (1-274), NTF (1-127), ICD (1-96), and ΔICD (70-274). For determining the contribution of individual ubiquitination sites, untagged TMEM106B in pCMV-Sport6 was subjected to site-

directed mutagenesis as described previously to generate K3R, K14R, and K3R/K14R double mutants.

Ubiquitination assay

HEK293T cells were co-transfected in 6-well plates with HA-ubiquitin and either FLAG-TMEM106B deletion constructs or pCMV-TMEM106B ubiquitination site mutants. Cells were washed with PBS and lysed in 500 µl RIPA buffer (50 mM Tris pH 7.5, 150 mM NaCl, 0.1% SDS, 0.05% sodium deoxycholate, 1% Triton X-100, and a Roche complete mini protease inhibitor). Lysates were cleared at 18,000 rcf for 20 minutes at 4ºC. Inputs were saved and supernatants immunoprecipitated with either ANTI-FLAG M2 Beads (Sigma) or homemade Rabbit anti-ICD or Rabbit IgG control antibodies conjugated to sepharose resin. Purified TMEM106B was eluted with either FLAG peptide of 1% SDS elution buffer.

Western blots

Western blots were performed as previously described. Primary antibodies used were mouse anti-HA.11 (Covance) and homemade rabbit anti-ICD.

Immunofluorescence

Immunofluorescence was performed as previously described.

E.4 Results and Discussion

In order to determine if TMEM106B can be ubiquitinated *in vitro* and if so, which domains are modified, I performed immunoprecipitations with FLAG-TMEM106B and several domain deletion constructs co-transfected with HA-ubiquitin. These experiments reveal that full length TMEM106B is robustly ubiquitinated, with three

clear ubiquitin modifications visible as ICD and HA immunoreactive bands, each spaced ~7 kDa apart as shown by arrows in Figure E.1A. A 1-127 amino acid TMEM106B construct, which we have dubbed the NTF and includes a short region of the lumenal domain, the transmembrane region, and ICD also showed robust ubiquitination in this assay. Interestingly, the ICD alone (1-96) revealed no detectable ubiquitination, despite the fact that the majority of the ubiquitinatable lysine residues in the previous NTF construct are located in the ICD. This suggests that membrane anchoring is essential for TMEM106B to be properly targeted for ubiquitination by the appropriate E3 ligase. As predicted, a construct lacking the majority of the ICD (70-274) failed to be ubiquitinated as well. Note, that this band does not appear on the western blot in Figure E.1A, as it was immunoprecipitated with FLAG-beads, but blotted with rabbit anti-ICD antibodies so as to be compatible with the mouse anti-HA antibodies used on the same membrane. I have previously shown that this construct is readily immunoprecipitated by FLAG-beads in Figure D.1B.

The previous experiment established that TMEM106B is most likely ubiquitinated somewhere in its ICD as long as it remains membrane bound. TMEM106B has three lysines in its ICD which can potentially be modified with ubiquitin at residues 3, 14, and 95 (K3, K14, and K95). K95 is directly adjacent to the start of the hydrophobic transmembrane helix and based on surrounding residues is likely a part of the type II signal anchor sequence (13). K3 and K14 appear to be prime targets for ubiquitination, and in fact TMEM106B ubiquitination at K14 has been detected as a ubiquitinated residue in a number of proteomic studies of global ubiquitination (14-17). The proteomic methods used in these studies involve trypsin

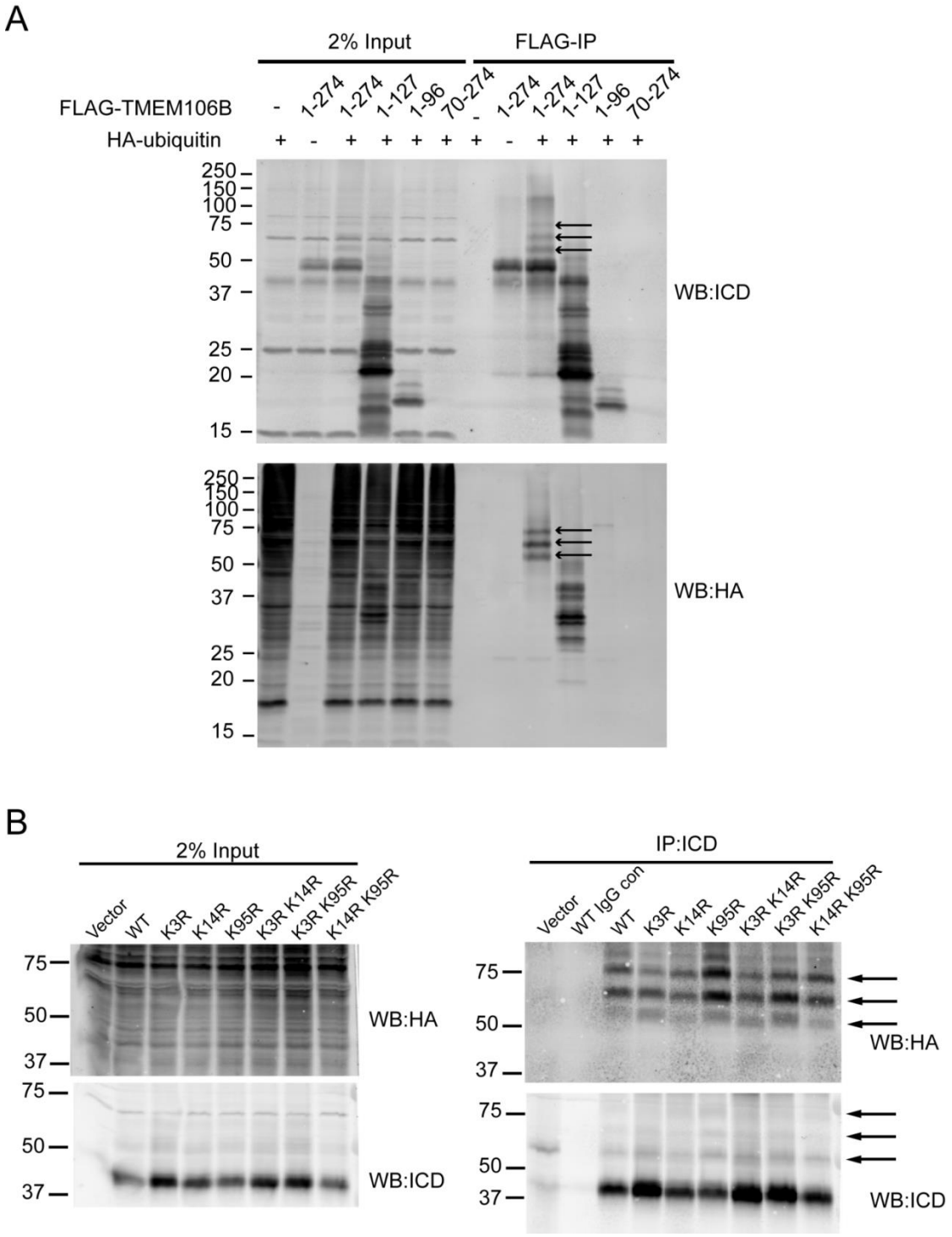
A
2% Input
FLAG-IP
FLAG-TMEM106B
HA-ubiquitin
-
1-274
1-274
1-127
1-96
70-274
250
150
100
75
50
37
25
20
15
WB:ICD
WB:HA
B
2% Input
IP:ICD
Vector
WT
IgG con
K3R
K14R
K95R
K3R K14R
K3R K95R
K14R K95R
WB:HA
WB:ICD

Figure E.1: TMEM106B is ubiquitinated *in vitro* to regulate its levels. (**A**) FLAG-TMEM106B and truncation constructs were immunoprecipitated from HEK293T cells co-expressing HA-ubiquitin. Full length (1-274) and a membrane bound NTF (1-127) show robust ubiquitination, but not the soluble ICD domain alone (1-96) or an ICD truncation (70-274). (**B**) Untagged TMEM106B and various ICD ubiquitination defective mutants were co-transfected with HA-ubiquitin and immunoprecipitated. Constructs with K3R mutated consistently reveal higher levels of TMEM106B, suggesting that ubiquitination at K3 may mediate degradation of TMEM106B.

digestion of target proteins. Since trypsin cuts after lysine and arginine residues, it is highly likely that the small three amino acid peptide containing K3 was lost during chromatographic separation of peptides and was not detected in these studies. K3, K14, and K95 were mutated to arginine residues, both individually and in pairs. Also, since the FLAG tag has several lysines which can potentially be ubiquitinated, the next immunoprecipitation was performed with untagged wild type and mutant TMEM106B. As before, immunoprecipitation of each of these species yielded the characteristic ubiquitin ladder separated by ~7 kDa each and reactive to both ICD and HA antibodies as shown in Figure E.1B. All TMEM106B species tested showed this pattern, albeit in differing degrees, suggesting that TMEM106B is ubiquitinated redundantly. In particular, K95R appeared to be more heavily ubiquitinated, despite slightly lower levels of full-length TMEM106B in this sample. It is also possible that TMEM106B is ubiquitinated at its N-terminal amine, which cannot be controlled for through mutagenesis. Of particular interest is the fact that all mutants containing a K3R mutation (K3R, K3R/K14R, and K3R/K95R) showed more full-length TMEM106B in both input and immunoprecipitation fractions, strongly suggesting that ubiquitination at K3 may be a critical ubiquitination site that serves as a mode of regulating TMEM106B levels *in vivo*.

In order to test if these ubiquitination mutants had any defects in lysosomal localization, or effects on size and distribution of lysosomes, they were transfected into N2a cells and stained with rabbit anti-ICD and rat anti-LAMP1 antibodies. To our surprise, none of the mutants appeared to significantly affect the size or morphology of lysosomes and none had any apparent defects in internalization into the lysosomal

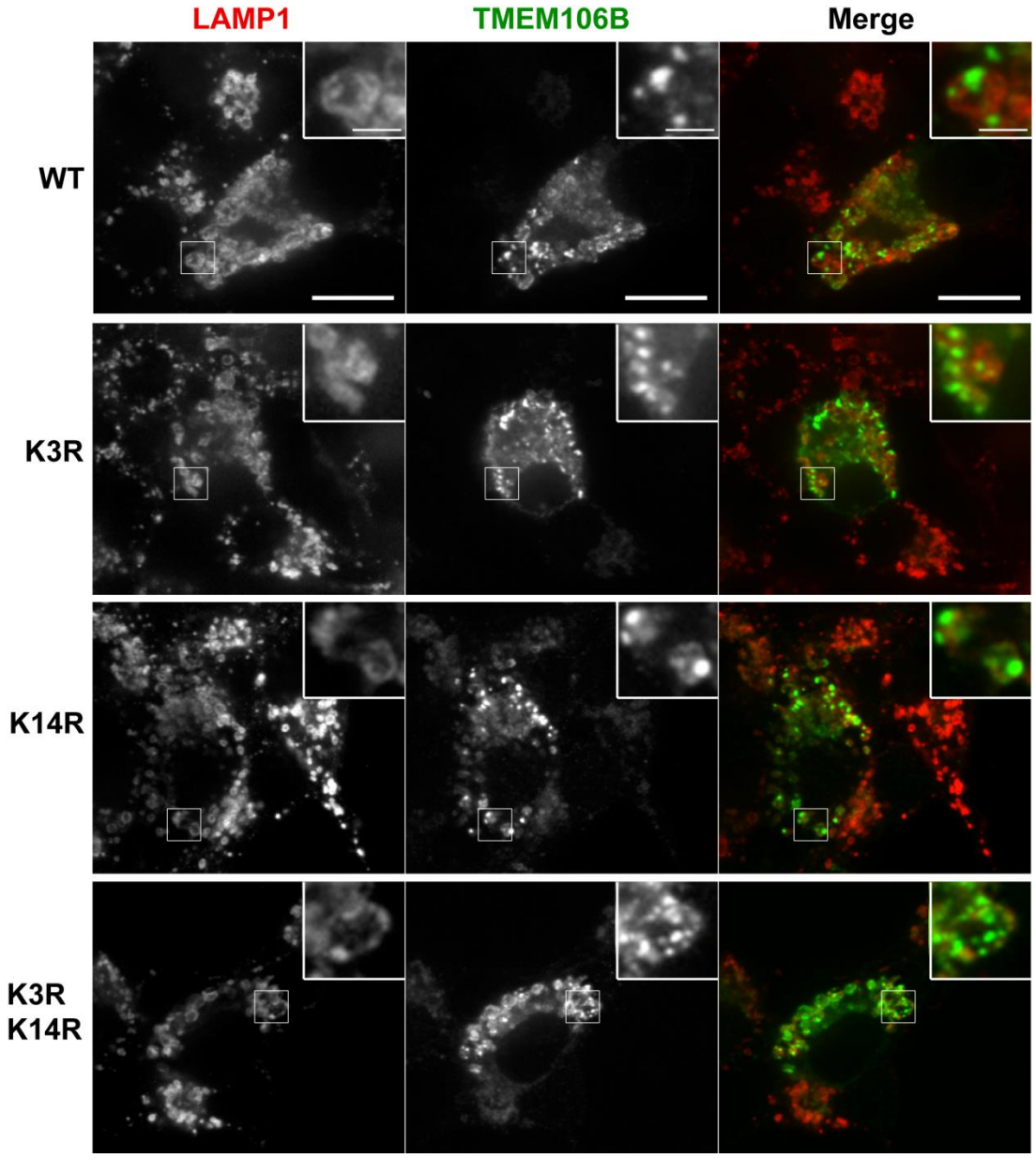
LAMP1
TMEM106B
Merge
WT
K3R
K14R
K3R
K14R

Figure E.2: TMEM106B ubiquitination mutants do not disrupt localization on lysosomes. N2a cells were transfected with WT TMEM106B and K3R TMEM106B, K14R TMEM106B, and K3R K14R TMEM106B ubiquitination defective mutants. No major differences in intracellular distribution on and within lysosomes were detected, suggesting that no single ubiquitination site is critical for internalization into lysosomes. (Scale bar = 10 µm, 2 µm in inset)

lumen, at least at steady state. Like most of these immunofluorescence experiments, the distribution of TMEM106B on and within lysosomes was somewhat heterogeneous, but no large scale differences could be detected (Figure E.2). Nonetheless, these results suggest that ubiquitination likely plays a major role in controlling TMEM106B levels and potentially its trafficking as well. As with the trafficking experiments described in Appendix C, one caveat is that TMEM106B is known to homo-dimerize, and it is possible that ubiquitination mutants such as K3R/K14R could bind to endogenous wild type TMEM106B, and be internalized into lysosomes through this interaction, rather than being solely dependent on ESCRT mediated internalization. These results warrant further investigation to more thoroughly characterize the causes and consequences of TMEM106B ubiquitination at the cellular level.

APPENDIX F

TMEM106B PROTEIN-PROTEIN INTERACTION PARTNERS IDENTIFIED USING SILAC

F.1 Summary

The proteomic technique, stable isotope labeling by amino acids in cell culture (SILAC), was used to identify potential protein-protein interaction partners of TMEM106B. Several candidates were identified and confirmed biochemically with co-IP assays. Additionally, the localization of these putative binding partners was examined via immunofluorescence.

F.2 Introduction

SILAC describes a proteomic technique in which cells are grown in parallel with different isotopically labeled amino acids in order to identify protein-protein interaction partners (18). Briefly, cells are grown for several generations to fully incorporate the light and heavy isotopically labeled amino acids. The protein of interest, TMEM106B, was then expressed and affinity purified from the heavy isotope labeled cells, while the light isotope labeled cells were mock purified. Fractions from both populations were then combined and subjected to analysis with mass spectrometry. By selecting peptides identified by the mass spectrometer that have a high abundance and high heavy peptide to light peptide ratio, it is possible to predict potential interacting partners. Likely candidates were selected for further biochemical analysis in order to identify bona fide TMEM106B interacting partners. From these

experiments, we were able to identify four likely TMEM106B protein interacting partners: Motile Sperm Domain-Containing Protein (MOSPD2), clusterin, neural cell adhesion molecule 1 (NCAM1), and calnexin. These interactions were confirmed via co-IP and further analyzed for localization with TMEM106B using immunofluorescence.

F.3 Materials and Methods

SILAC

NSC-34 cells were grown for a minimum of five generations in DMEM with 10% dialyzed FBS (Sigma) supplemented with either light (C^{12}, N^{14} arginine and lysine) or heavy (C^{13}, N^{15} arginine and lysine) amino acids. The heavy cells were transfected in two 15 cm dishes with GFP-TMEM106B while the light cells were transfected with pEGFP-C1 as a control. Cells were lysed in IP lysis buffer and clarified lysates were immunoprecipitated with GFP-beads (Chromo-Tek) as previously described.

The presence of GFP and GFP-TMEM106B in immunoprecipitated samples was confirmed by running SDS-PAGE and performing a silver stain. Samples were then mixed and boiled 5 minutes with 1% DTT followed by alkylation by treating samples with a final concentration of 28 mM iodoacetamide. Proteins were precipitated on ice for 30 minutes with a mixture of 50% acetone/49.9% ethanol/0.1% acetic acid. Protein was pelleted and washed with this buffer, re-precipitated on ice, and dissolved in 8M urea/50 mM Tris pH 8.0 followed by dilution with three volumes of 50 mM Tris pH 8.0/150 mM NaCl. Proteins were digested overnight at 37º C with 1 µg mass-spec grade Trypsin (Promega).

The resulting peptide samples were cleaned up for mass spectrometry by treatment with 10% formic acid and 10% trifluoroacetic acid (TFA) and washed twice with 0.1% acetic acid on pre-equilibrated Sep-Pak C18 cartridges (Waters). Samples were eluted with 80% acetonitrile (ACN)/0.1% acetic acid into silanized vials (National Scientific) and evaporated using a SpeedVac. Samples were re-dissolved in H_2O with ~1% formic acid and 70% ACN. Peptides were separated using hydrophilic interaction liquid chromatography (HILIC) on an Ultimate 300 LC (Dionex). Each fraction was evaporated with a SpeedVac and resuspended in 0.1% TFA with 0.1 pM angiotensin internal standard. Samples were run on a Thermo LTQ Orbitrap XL mass spectrometer and data analyzed using the SORCERER system (Sage-N research).

Co-immunoprecipitations

co-IPs were performed in HEK 293T cells as previously described. In the case of cross-linking co-IP, cells were treated with Dimethyl 3,3´-dithiobispropionimidate (DTBP) (Pierce). DTBP was applied to cells at a final concentration of 500 µg/ml in DMSO and PBS at 37º C for 2 minutes. DTBP cross-linking was quenched by washing cells three times with TBS prior to lysis.

Immunofluorescence

Cells were transfected, fixed, and imaged, as described previously. YFP-Golgi and YFP-Tgn38 plasmids were kindly provided by Dr. Volker Vogt.

F.4 Results and Discussion

The proteins MOSPD2, clusterin, NCAM1, and calnexin were considered likely candidates for interaction with TMEM106B based on the SILAC mass spectrometry

data which measured the number and abundance of unique peptides detected in the heavy versus light fractions. These interactions were confirmed by co-transfecting GFP and GFP-TMEM106B baits with the indicated prey proteins. GFP-TMEM106B, but not GFP control co-IPed with each of these proteins in HEK 293T cells. Both GFP-TMEM106B (data not shown) and FLAG-TMEM106B were able to co-IP with detectable levels of endogenous calnexin. In order to further demonstrate that these protein-protein interactions are not an artifact of the GFP-tag, I repeated them with FLAG-TMEM106B in HEK 293T cells treated with the reversible protein cross-linking reagent, DTBP (Pierce). These experiments revealed that FLAG-TMEM106B is also capable of binding MOSPD2, clusterin, and NCAM1 *in vitro*, albeit not as strongly as GFP-TMEM106B. The results of these co-IP experiments are summarized in Figure F.1. We have previously noted in Chapter 3 that GFP-TMEM106B appears to be expressed at higher levels compared to FLAG-TMEM106B, and this correlates with a more severe vacuolar phenotype in cell culture models of TMEM106B overexpression. We speculate that these differences in expression levels and their effect on lysosome morphology may partially explain the heightened binding between GFP-TMEM106B and these protein binding partners identified with SILAC.

The identities and distribution of these TMEM106B interacting partners may provide some insight towards the nature and function of these interactions. Calnexin is a membrane bound ER-resident chaperone that binds and facilitates the proper co-translational folding of nascent glycoproteins (19). Hence, it is unsurprising that TMEM106B is one of the many substrates whose folding and stability are maintained by calnexin when traversing the ER.

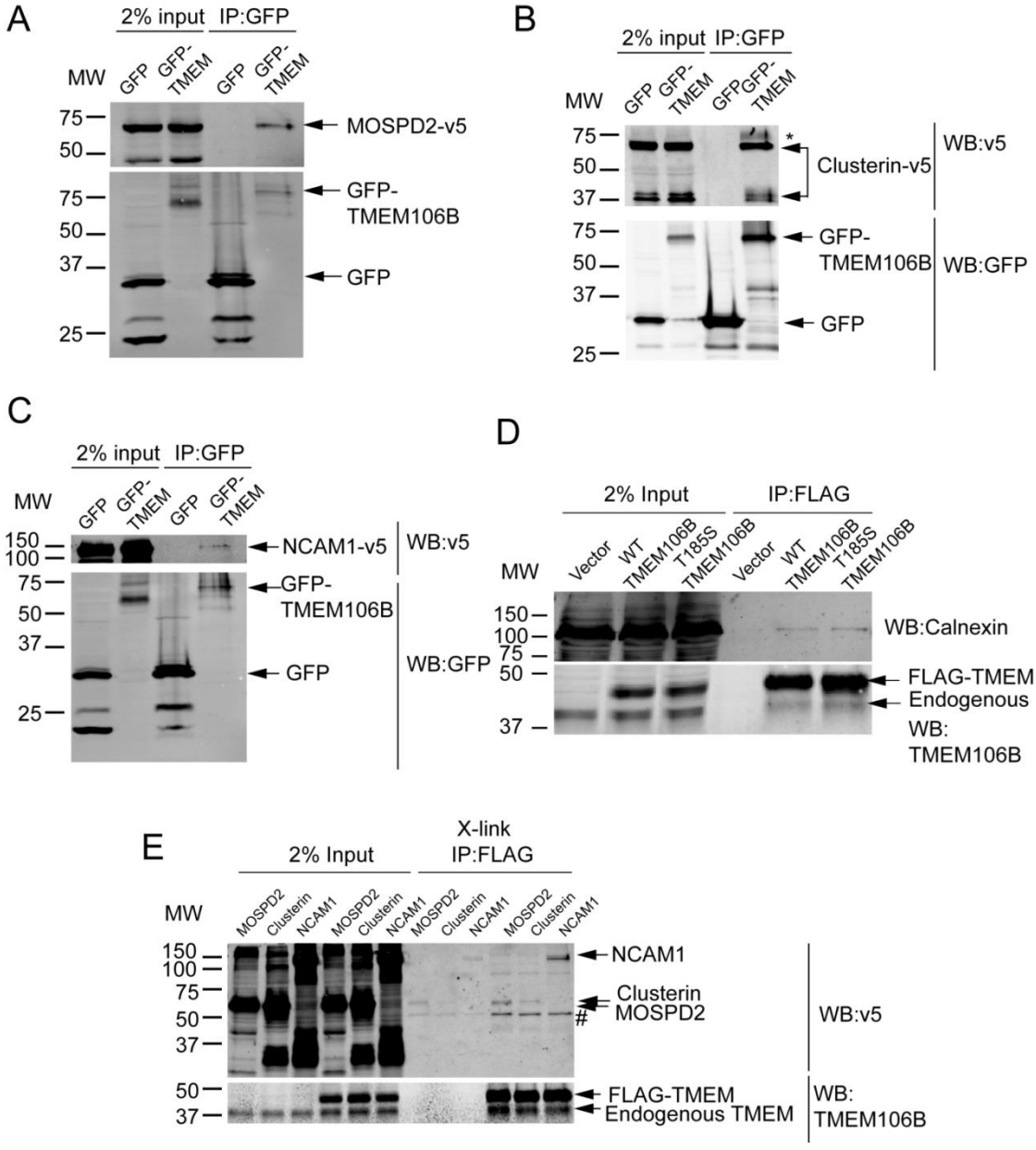
A
2% input
IP:GFP
MW
GFP
GFP-TMEM
GFP
GFP-TMEM
75
50
MOSPD2-v5
75
50
37
GFP-TMEM106B
GFP
25
B
2% input
IP:GFP
MW
GFP
GFP-TMEM
GFP
GFP-TMEM
75
50
37
*
Clusterin-v5
WB:v5
75
50
37
GFP-TMEM106B
GFP
WB:GFP
25
C
2% input
IP:GFP
MW
GFP
GFP-TMEM
GFP
GFP-TMEM
150
100
NCAM1-v5
WB:v5
75
50
37
GFP-TMEM106B
GFP
25
WB:GFP
D
2% Input
IP:FLAG
MW
Vector
WT TMEM106B
T185S TMEM106B
Vector
WT TMEM106B
T185S TMEM106B
150
100
75
50
WB:Calnexin
FLAG-TMEM
Endogenous
37
WB: TMEM106B
E
X-link
2% Input
IP:FLAG
MW
MOSPD2
Clusterin
NCAM1
MOSPD2
Clusterin
NCAM1
MOSPD2
Clusterin
NCAM1
MOSPD2
Clusterin
NCAM1
150
100
75
50
37
NCAM1
Clusterin
MOSPD2
#
WB:v5
50
37
FLAG-TMEM
Endogenous TMEM
WB: TMEM106B

Figure F.1: TMEM106B SILAC hits bind to TMEM106B *in vitro*. GFP-TMEM106B was co-transfected with (**A**) MOSPD2-v5, (**B**) clusterin-v5, or (**C**) NCAM1-v5 in HEK293T cells. GFP-TMEM106B potently co-IPs all of these proteins. Note, that in (**B**) GFP-TMEM106B also appears to pull down a higher MW band above the major clusterin band, indicated by *, suggesting potential enrichment of a post-translational modification. (**D**) FLAG-TMEM106B specifically co-IPs endogenous calnexin in HEK293T cells. (**E**) FLAG-TMEM106B co-IPs with MOSPD2, clusterin, and NCAM1 in HEK293T cells, albeit with lower efficiency than GFP-TMEM106B. These cells were treated with the cross-linking reagent DTBP, prior to immunoprecipitation.

Clusterin strongly co-localizes with GFP-TMEM106B in N2a cells as shown in Figure F.2A. Clusterin is a multi-functional protein that has been shown to play a role in the clearance of extracellular misfolded proteins and promote their trafficking to and degradation in lysosomes, partially explaining the high degree of co-localization with TMEM106B at lysosomes (20). Intriguingly, clusterin has recently been implicated as a modifying risk factor for Alzheimer's disease in several studies (21-23). Due to its role in extracellular proteostasis and its documented linkage to at least one neurodegenerative disease, it will be interesting to explore the functional relationship between clusterin and TMEM106B in future studies. One could speculate a potential function of TMEM106B as a lysosomal receptor for extracellularly derived complexes of clusterin and misfolded proteins, akin to the role of LAMP2 in chaperone mediated autophagy, another lysosomal degradation pathway used for a subset of cytosolic proteins (24).

NCAM1 has numerous isoforms that are highly expressed in the nervous system where its homophilic interactions at the cell surface are thought to play roles in processes ranging from neurite outgrowth, axon guidance, and cell migration to regulating synaptic plasticity and long term potentiation (25,26). NCAM1 is highly expressed at the plasma membrane, although a significant fraction was also seen on lysosome membranes along with TMEM106B in our immunofluorescence experiments shown in Figure F.2B. NCAM1 has been shown to be endocytosed in a mono-ubiquitin dependent manner, with a small fraction being degraded in lysosomes (27). As a resident lysosome membrane protein, it is difficult to say if TMEM106B plays a direct role in regulating NCAM1 trafficking or retention at the lysosome or if

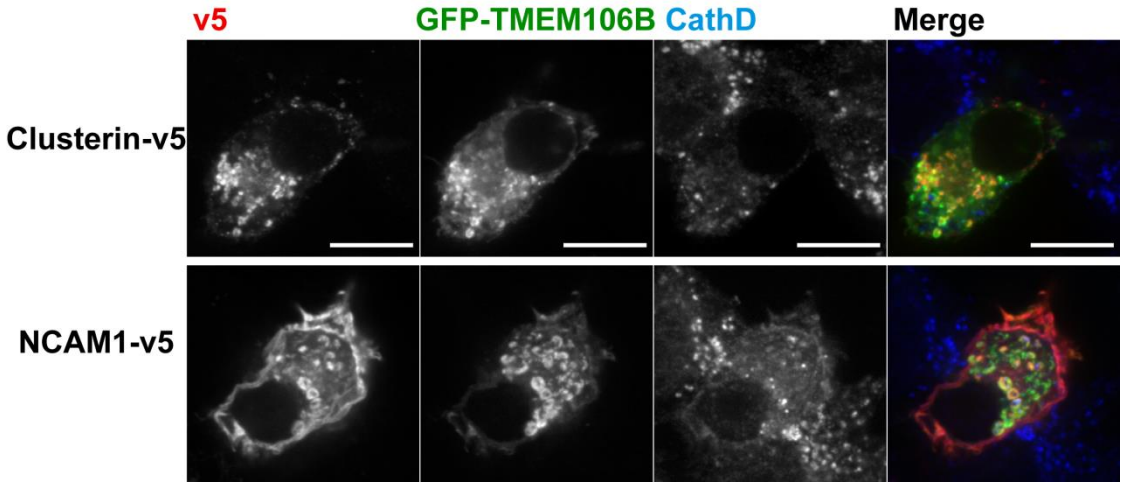

Figure F.2: GFP-TMEM106B co-localizes with clusterin and NCAM1. N2a cells were transfected with GFP-TMEM106B and clusterin-v5 (top panel) or NCAM1-v5 (bottom panel) (scale bar = 10 µm, 2 µm in inset). Clusterin localizes very well with GFP-TMEM106B positive vesicles. NCAM1 is primarily expressed at the cell surface, but a portion localizes to the membranes of GFP-TMEM106B positive vesicles. Cathepsin D staining used to indicate lysosomes.

this interaction is simply a byproduct of the normal endocytic delivery of excess NCAM1 to lysosomes for degradation. Nevertheless, as a critical player in a number of essential neuronal processes, it would be of interest if it can be shown that TMEM106B plays a role in regulating NCAM1 degradation *in vivo*.

The final verified SILAC hit to be discussed here is MOSPD2, a poorly characterized protein with an MSP (major sperm protein) domain, a Sec14 domain, and a small C-terminal transmembrane region, as inferred from UniProtKB-KW. MSP domain proteins, named for the MSP protein in *C. elegans* are thought to be protein-protein interaction domains capable of polymerizing into self-associating helical filaments (28). Sec14 domains from different proteins are known to bind to an array of different phospholipids, suggesting MOSPD2 may play a role dependent on membrane binding (29). MOSPD2 localizes strongly to GFP-TMEM106B positive membranes; however, the major pool appears to originate from the Golgi as evidenced by near perfect co-localization with the Golgi markers YFP-Golgi and YFP-Tgn38 shown in Figure F.3A. To our surprise, very little MOSPD2 co-localizes with untagged TMEM106B at lysosome membranes at steady state as shown in Figure F.3B. These differences in co-localization between the different forms of TMEM106B expressed may also explain the much higher affinity between GFP-TMEM106B and MOSPD2 in our co-IP assays, with the GFP-TMEM106B form potentially dominantly binding to MOSPD2. Despite the much lower co-localization overall, small amounts of MOSPD2 still localized with TMEM106B at steady state. Interestingly, when cells were treated over night with the lysosomotropic agent chloroquine, MOSPD2 was redistributed from the Golgi to lysosomes and showed a near perfect co-localization with

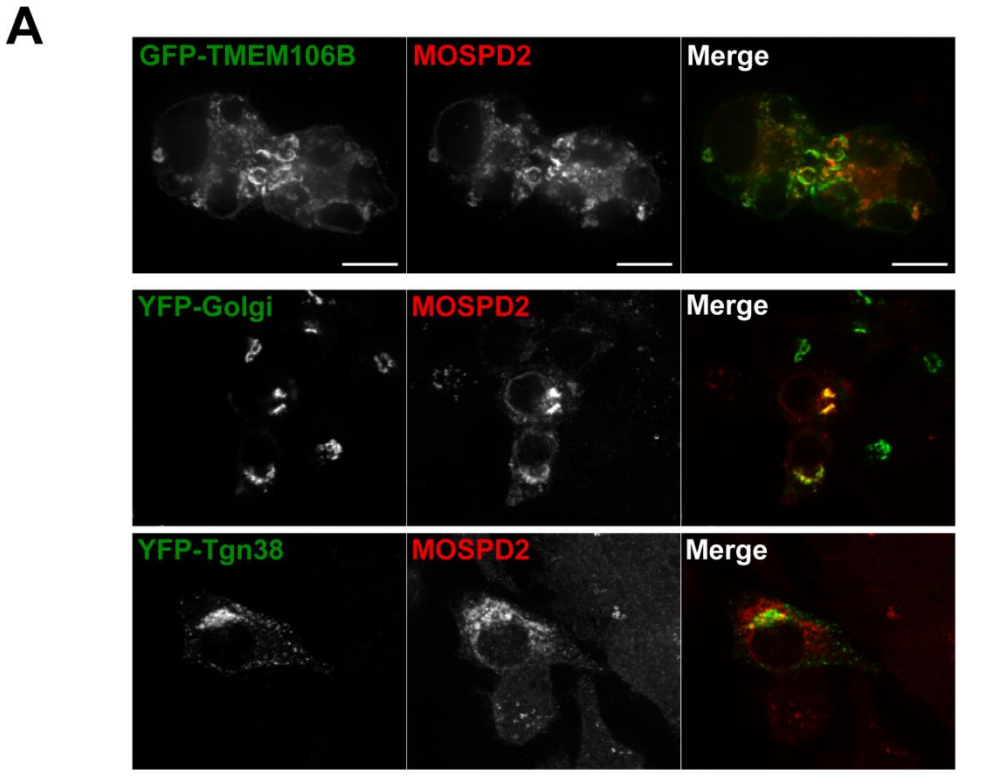
A
GFP-TMEM106B
MOSPD2
Merge
YFP-Golgi
MOSPD2
Merge
YFP-Tgn38
MOSPD2
Merge
B
LAMP1
MOSPD2
TMEM106B
Merge
Untreated
Chlor.
C
5% Input
IP:V5
BafA1
- - + - - +
MW
75
WB:V5
(MOSPD2)
WB:TMEM106B
37

Figure F.3: MOSPD2 is primarily localized to the Golgi, but re-distributes to TMEM106B positive lysosomes under alkalizing conditions. (**A**) GFP-TMEM106B localizes somewhat well with MOSPD2-v5 in N2a cells (top panel). MOSPD2-v5 is located mainly within the Golgi at steady state, as shown by co-localization with YFP-Golgi (middle panel) and YFP-Tgn38 (bottom panel) (scale bar = 10 µm). (**B**) Only a small amount of MOSD2-v5 localizes to untagged TMEM106B positive lysosomes at steady state (top panel). Upon treatment with the lysosome alkalizing agent, chloroquine, MOSPD2-v5 completely relocalizes to swollen, TMEM106B positive lysosomes (bottom panel). (**C**) Treatment with 100 nM Bafilomycin for 14 hours results in co-immunoprecipitation of untagged TMEM106B and MOSPD2.

TMEM106B as shown in the lower panel of Figure F.3B. Similar results were obtained with another inhibitor of lysosome acidification, bafilomycin A1 (BafA1) (data not shown). Consistent with this re-loacalization of MOSPD2 to TMEM106B positive lysosomes under alkalizing conditions, we see a physical interaction between MOSPD2 and TMEM106B when cells are treated with BafA1, but not under untreated conditions as seen in Figure F.3C. These data suggests that MOSPD may shuttle back and forth between the Golgi and lysosomes and that elevated expression of TMEM106B, or inhibition of lysosome acidification may trap MOSPD2 at lysosomal membranes. MOSPD2 contains a putative phospholipid binding Sec14 domain and appears to be able to move back and forth between the Golgi and lysosomes, suggesting a potential role in regulating post-golgi membrane trafficking events. Further biochemical and live imaging experiments may help uncover a possible role for MOSPD2 that involves TMEM106B.

Taken together, these SILAC hits shed some light on potential roles of TMEM106B in lysosomal degradation of extracellular and membrane bound proteins as well as involvement in membrane trafficking. Nonetheless, it is difficult to tell the significance of some of these interactions. For example, calnexin is an ER-resident chaperone that binds a large variety of glycoprotein substrates. Clusterin also has well documented roles as a molecular chaperone and it is unclear if its binding to TMEM106B reflects a non-specific chaperone function or as a specific ligand-receptor interaction. Similarly, NCAM1 has been shown to be degraded in lysosomes and its appearance in our hits may reflect this normal turnover process. Finally, MOSPD2, while potentially interesting due to its domain structure, is completely uncharacterized

functionally, and any functional interaction with TMEM106B so far remains a mystery. Future SILAC experiments could be optimized to find more potential binding partners to give a clue towards TMEM106B function. Stable cell lines expressing closer to endogenous levels of TMEM106B could be used in conjunction with cross-linking reagents in order to sensitively detect interactions with transient or low-abundance binding partners. Additionally, lysosomal fractions could be purified prior to immunoprecipitation of TMEM106B in order to eliminate much of the non-specific binding and enrich the sample with lower abundance lysosomal proteins. These experiments have provided some insight into TMEM106B's potential roles in the cell and should be followed up in order to more accurately determine TMEM106B's physiological functions.

APPENDIX G

TMEM106B IS A COMPONENT OF AUTOLYSOSOMES AND A SUBSTRATE FOR AUTOPHAGIC DEGRADATION

G.1 Summary

TMEM106B has been demonstrated to be a component of the membranes of late endosomes/lysosomes meaning it has the potential to be form hybrid organelles with autophagosomes. In this set of experiments, I demonstrate that TMEM106B is a component of autolysosome membranes and is turned over in response to starvation induced autophagy.

G.2 Introduction

Because TMEM106B has been shown to be a component of late endosome/lysosome membranes, I sought to determine if TMEM106B was incorporated into hybrid organelles such as amphisomes or autolysosomes, the formation of which are essential for neuronal health (30). The fate of membrane proteins incorporated into these hybrid organelles generally follows one of two patterns: intralysosomal degradation or membrane recycling in a process known as autophagic lysosome reformation (4). LC3-II, which decorates the double membrane of autophagic vacuoles is a prototypical example of a membrane bound protein which undergoes intralysosomal degradation while the lysosomal membrane protein LAMP1, typifies a membrane protein that is preferentially recycled from hybrid organelles into nascent protolysosomes (5,31).

In the following experiments, I demonstrate that TMEM106B is indeed a component of starvation induced autolysosomes and that its levels appear to decrease concomitant with increased autophagy. This supports a model in which TMEM106B is at least partially degraded intralysosomally following autophagy. TMEM106B overexpression still allowed for the formation of autolysosomes, suggesting that elevated TMEM106B does not prevent lysosome-autophagosome fusion, as has been proposed to be the case for some FTLD causative proteins like mutant VCP and CHMP2B.

G.3 Materials and Methods

Cell culture and transfections

N2a cells were transfected with GFP-TMEM106B, mCherry-LC3 as described in (32), and LAMP1-iRFP in which LAMP1 was sub-cloned into the piRFP vector (Addgene #31857) (33). For serum starvation conditions, cells were washed with PBS and grown in DMEM without FBS for the indicated time points. For amino acid starvation conditions, cells were washed with PBS and grown in Hank's balanced salt solution (HBSS) for the indicated time period. All cells were kept at 37ºC in a 5% CO_2 incubator.

Western blots

Western blots were performed as previously described.

G.4 Results and Discussion

We have previously shown that endogenous TMEM106B levels increase when cells are treated with the autophagy inhibitor, 3-MA, or with lysosomal alkalizing agents such as BafA1 (1). In order to further confirm that TMEM106B levels are regulated via autophagic turnover, N2a cells were serum starved for up to 10 hours and the levels of TMEM106B assayed at two hour intervals. TMEM106B levels were noticeably reduced and continued to decline throughout the time course. The most notable reduction occurred starting at ~4 hours and coincided with the beginning of the most prominent increase in autophagy as indicated by the levels of LC3-II relative to LC3-I. These results are displayed in Figure G.1A.

Since membrane proteins can be turned over through other mechanisms, including ERAD and in primary lysosomes that have not fused with autophagosomes, I sought to confirm that TMEM106B was indeed present on autolysosomes. Autophagy was rapidly induced by amino acid starvation of N2a cells expressing mCherry-LC3 and GFP-TMEM106B. In this assay mCherry-LC3 puncta are formed as LC3-I is converted to LC3-II and this is used as a readout for autophagosome formation. After one hour of amino acid starvation, numerous LC3 puncta could be detected, with a subset of them also positive for GFP-TMEM106B and cathepsin D, suggesting that even under overexpression conditions, TMEM106B can still be incorporated into autolysosomes. Treatment with BafA1 increases endogenous TMEM106B levels and is known to inhibit LC3-II turnover in autolysosomes. Based on this knowledge, I tested if it is possible to enhance the visualization of TMEM106B positive autolysosomes by treating amino acid starved cells with 50 nM BafA1 for 16

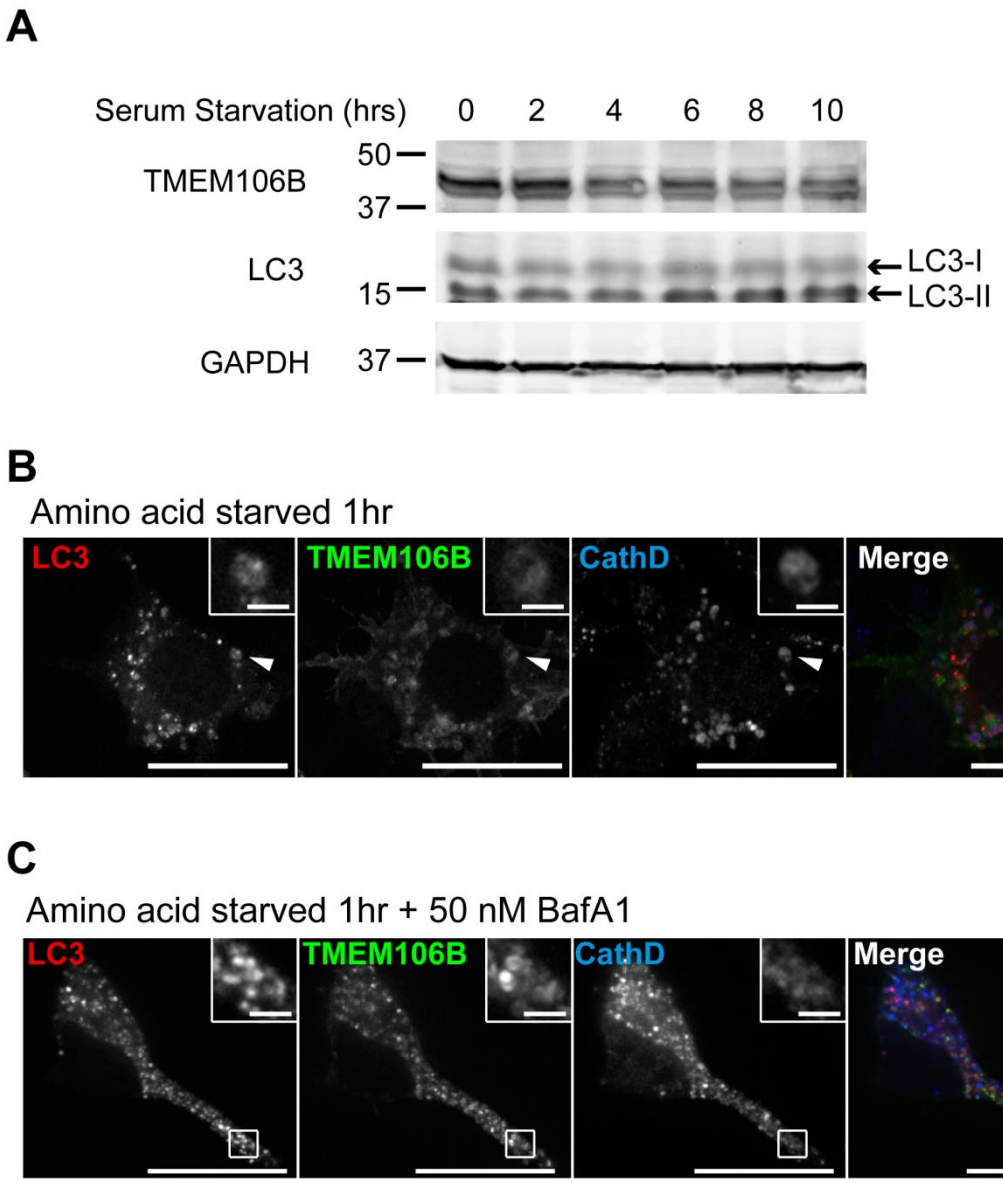
A
Serum Starvation (hrs) 0 2 4 6 8 10
TMEM106B
50
37
LC3
15
LC3-I
LC3-II
GAPDH
37
B
Amino acid starved 1hr
LC3
TMEM106B
CathD
Merge
C
Amino acid starved 1hr + 50 nM BafA1
LC3
TMEM106B
CathD
Merge

Figure G.1: TMEM106B is turned over via autophagy and is present on autolysosomes. (**A**) Western blot from N2a cells serum starved for the indicated times. Levels of endogenous TMEM106B decrease concomitant with starvation along with conversion of LC3-I to LC3-II which becomes most apparent from 6 hours and beyond. (**B**) N2a cells expressing mCherry-LC3 and GFP-TMEM106B were amino acid starved for 1 hour and stained for cathepsin D. GFP-TMEM106B appears on the same vesicles as mCherry-LC3 that stain for Cathepsin D in the lumen, indicating that TMEM106B is a component of autolysosomes. A single autolysosome is indicated with an arrowhead and highlighted in the inset. (**C**) The same population of cells from (**B**) was amino acid starved and co-treated with BafA1 to inhibit the degradation of mCherry-LC3 and GFP-TMEM106B in autolysosomes. These conditions allow the visualization of numerous autolysosomes simultaneously. Several clustered autolysosomes are highlighted in the inset. Scale bars = 10 μm, 1 μm in inset.

hours. As expected, TMEM106B, LC3-II, and cathepsin positive vesicles were readily apparent, lending further support to the idea that TMEM106B is turned over in autolysosomes similarly to LC3-II. These results are shown in Figure G.1B.

These results confirm that TMEM106B is indeed a component of hybrid organelles and that it is at least partially degraded via autophagy. Collectively, the data argue against a model in which elevated TMEM106B causes defects in autophagosome-lysosome fusion. Nevertheless, at this point, it cannot be ruled out that subtle differences in the kinetics or efficiency of these fusion events may be affected until more carefully controlled experiments are performed which compare endogenous to overexpressed TMEM106B.

APPENDIX H

TMEM106B mRNA IS UPREGULATED IN THE MICROGLIA OF PGRN KNOCKOUT MICE

H.1 Summary

TMEM106B mRNA levels have been reported to be elevated in FTLD-TDP, particularly those caused by *GRN* mutations, however these results have been controversial due to reproducibility issues and the reliance on post-mortem brain tissue. Here, we sought to compare the levels of TMEM106B and other lysosomal gene mRNAs in different populations of CNS cells from WT and PGRN knockout mice. In cells from newborn mice, TMEM106B mRNAs appears unaffected by *Grn* genotype status in neurons and astrocytes, whereas TMEM106B mRNA is significantly upregulated in microglia from $Grn^{-/-}$ mice.

H.2 Introduction

Mounting evidence indicates that TMEM106B mRNA and protein levels are elevated in the brains of FTLD-TDP patients with *GRN* mutations; however some of these results are confounded by a reliance on post-mortem brain tissue, which can suffer from poor mRNA quality, as well as difficulties in reproducibility (2,34-36).

Using quantitative real-time PCR (qPCR), we sought to determine if PGRN knockout mice had elevated TMEM106B mRNA levels and if any effects were specific to any of the three major cell classes of the CNS: neurons, astrocytes, and microglia. To our surprise, mouse TMEM106B mRNA levels were unaffected in the

neurons and astrocytes of PGRN knockout mice; however levels were significantly upregulated in cells of microglial lineage.

H.3 Materials and Methods

Primary cell preparation

Wild type C57BL/6 and *Grn*$^{-/-}$ mice (Jackson Laboratory) were used for these experiments. For cortical neuron preparation, cortexes were rapidly dissected from the brains of postnatal day 1 (P1) mice in HBSS supplemented with B27 and 0.5 mM L-glutamine (Invitrogen) on ice. Separated cortexes were digested with papain (Worthington) and DNase I (Sigma) at 37º C with gentle agitation. Neurons were separated by trituration and passage through a flame polished glass pipette. The supernatant was then centrifuged at 225 rcf for 5 minutes and pellets washed with Neurobasal A medium (Invitrogen). Cells were separated through a 70 µm cell strainer and plated at a concentration of 1.0 x 10^6 cells/ml on poly D-lysine coated cell culture plates (BD Biosciences). Cells were grown in Neurobasal A medium supplemented with B27, sodium pyruvate, and L-glutamine. After day 3, cells were treated with 1 µM cytosine arabinoside (Sigma) to limit mitotic growth and to enrich for neurons.

Microglia and astrocytes were prepared by dissecting forebrains from P1 mice in PBS-5% FCS on ice. Cells were separated by trituration and passage through a flame polished pipette followed by separation with a cell strainer. Cells were pelleted and resuspended in DMEM with 10% FBS and penicillin-streptomycin (Sigma). Cells were seeded in 75 cm flasks and grown at 37º C and 5% CO_2. After 4 days, culture medium was supplemented with 5 ng/ml GM-CSF (Sigma) and media changed every

4 days. At DIV12, flasks were shaken at 125 rpm at 37º C for 4-5 hours. Floating microglial cells were separated, pelleted, and re-plated on poly D-lysine coated cell culture plates while the remaining cells in the flask were comprised primarily of astrocytes.

RT-PCR

mRNA was collected and reverse transcribed followed by quantitative RT-PCR (qPCR) as described (1). All transcripts were normalized to the geometric mean of two reference genes, *Tbp*, and the 18S rRNA gene. Statistical significance between WT and PGRN-/- samples was determined with Student's t-test.

H.4 Results and Discussion

Mouse TMEM106B mRNA levels from cortical neurons, astrocytes, and microglia from WT and $PGRN^{-/-}$ mice were compared using qPCR. Surprisingly, TMEM106B mRNA levels were virtually unchanged in the neurons and astrocytes from WT versus $Grn^{-/-}$ mice. Interestingly, microglia from $Grn^{-/-}$ mice had a statistically significant >1.5 fold increase in TMEM106B mRNA compared to WT controls as shown in Figure H.1A. This is intriguing because along with neurons, microglia, are one of the major cellular sources of PGRN in the CNS, particularly in response to injury (37,38). When comparing PGRN between these three cell classes, microglia consistently showed the highest levels with virtually no PGRN mRNA detected in samples from PGRN knockout mice, confirming the specificity of our assay (data not shown). This may indicate that the effect of PGRN loss on transcription of targets such as TMEM106B is most acutely seen in cells with high basal PGRN expression.

A

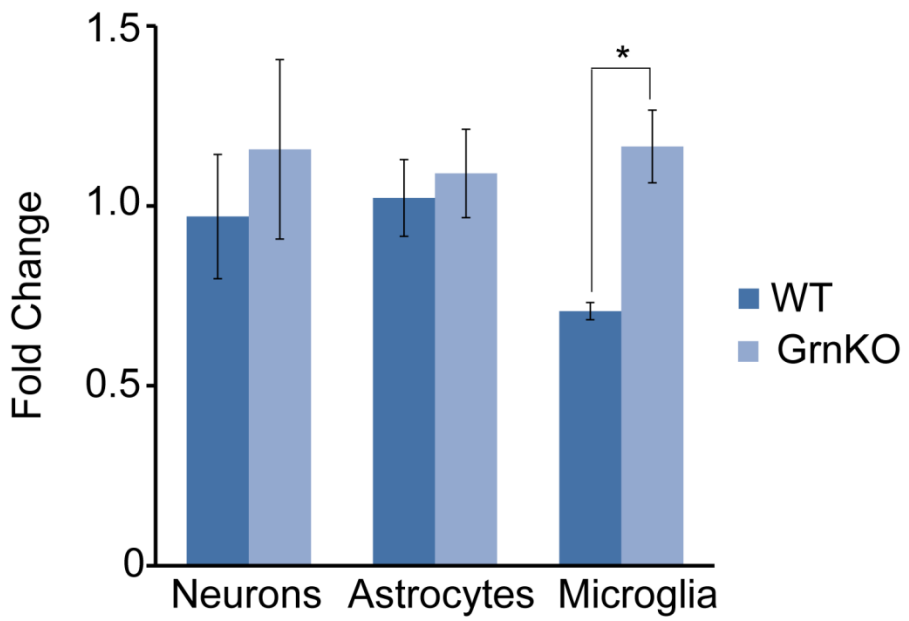
TMEM106B mRNA Levels
Fold Change
1.5
1.0
0.5
0
*
Neurons
Astrocytes
Microglia
WT
GrnKO

B

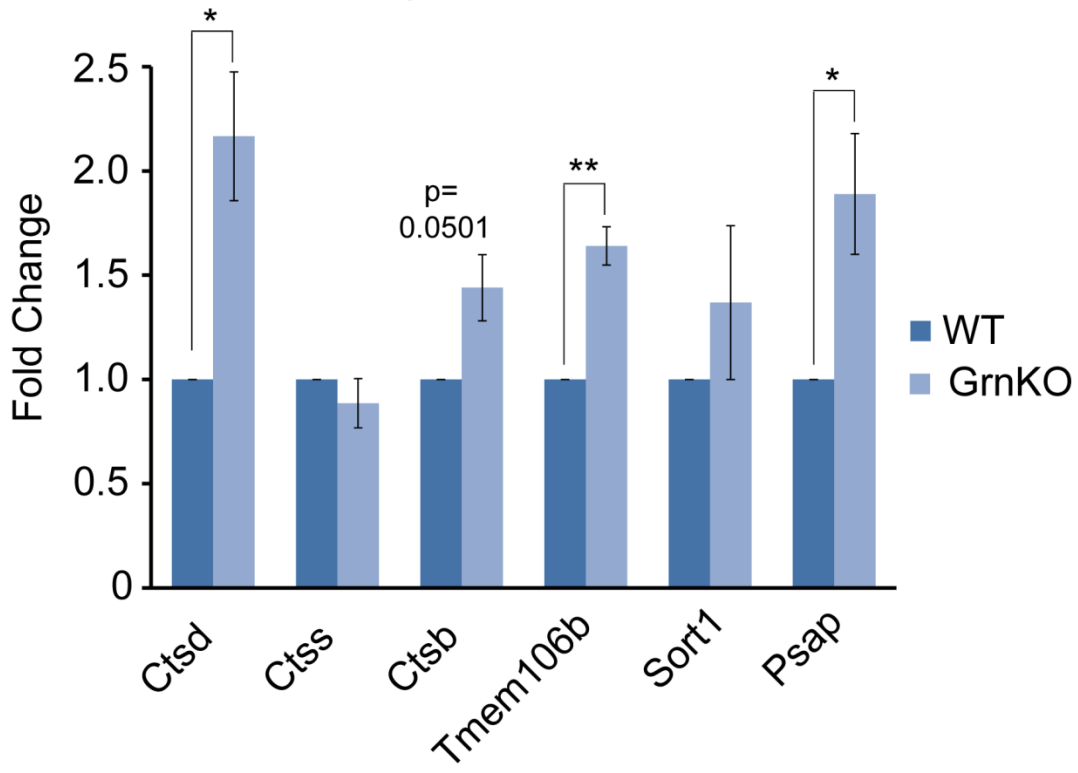
Microglia mRNA Levels
Fold Change
2.5
2.0
1.5
1.0
0.5
0
*
p=
0.0501
**
*
Ctsd
Ctss
Ctsb
Tmem106b
Sort1
Psap
WT
GrnKO

Figure H.1: Microglia from *Grn*$^{-/-}$ mice exhibit increased *Tmem106b* mRNA. (**A**) Cortical neurons, astrocytes, and microglia from WT and *Grn*$^{-/-}$ newborn mice were analyzed using qPCR. Microglia, but not neurons or astrocytes, from *Grn*$^{-/-}$ mice showed >1.5 fold increase over WT mice. (**B**) Microglia from *Grn*$^{-/-}$ mice show upregulation of a number of lysosomal genes in addition to *Tmem106b*, including *Ctsd* and *Psap*. Not all lysosome genes were affected the same way as *Ctss* was not upregulated. Values represent mean +/-SEM (neurons and microglia n=3, astrocytes n=5, *$p < 0.05$, **$p < 0.01$ paired Student's t-test).

Strikingly, in a microglia specific conditional PGRN knockout mouse model, neuroinflammation is increased and neuronal loss in response to injury is exaggerated, suggesting that neuronal loss in FTLD-TDP may occur in a cell non-autonomous manner (38). Based on this model, elevated TMEM106B in PGRN deficient microglia may potentially also exhibit effects on neurons *in vivo*. It should be noted that cortical neurons were selected for these experiments based on the types of neurons most affected in FTLD-TDP; however other populations of neurons may exhibit differing responses to loss of PGRN. Additionally, while microglia clearly showed a robust increase in TMEM106B mRNA due to PGRN loss, there was a slight upward trend in TMEM106B mRNA in our cortical neuron samples and it is possible that these data may be limited by small sample size. Finally, as an age-related dementia, FTLD-TPD typically manifests at middle age or later and this age-dependence is recapitulated in mouse models of FTLD caused by loss of PGRN (39-41). Hence, it is possible that we failed to see an increase in TMEM106B mRNA in neurons since they were cultured from newborn mice. Due to technical limitations, we did not analyze neuronal mRNA from aged mice, but future experiments could explore the effect of aging on levels of TMEM106B mRNA in the brains of WT and PGRN knockout mice.

During the course of these experiments, we also looked at the mRNA levels of a number of other lysosomal genes. Interestingly, many of these lysosomal genes behaved similarly to TMEM106B, with levels being upregulated ~1.5-2 fold in PGRN knockout mice. As before, this effect was by far the most prominent in microglia. Besides TMEM106B, lysosomal genes which were upregulated in *Grn*$^{-/-}$ mice included *Psap*, which encodes the sphingolipid activator protein prosaposin, and *Ctsd*, which

encodes the lysosomal hydrolase cathepsin D. Another lysosomal hydrolase, cathepsin B (*Ctsb*) was upregulated and approached significance with a p-value = 0.501 and would likely become significant with a larger sample size. Interestingly, not all lysosomal genes were upregulated, with some completely unaffected, including another hydrolase, cathepsin S (*Ctss*), suggesting that there is some specificity in the lysosomal genes that are upregulated, and loss of PGRN does not result in a global upregulation of all lysosomal genes. Additionally mRNA levels of the PGRN receptor, sortilin (*Sort1*), which is responsible for delivering PGRN to lysosomes, were unaffected. The results from these experiments appear in Figure H.1B.

As discussed in previous chapters, PGRN appears intimately involved in lysosomal function and is one of the major transcriptional targets of the lysosomal master regulator, TFEB (42,43). A recent report supports the notion that PGRN suppresses at least some lysosomal gene expression, with PGRN knockout microglia exhibiting increased activation and increased transcription of many lysosomal genes in response to injury (44). This report and our data suggest that the increased TMEM106B mRNA levels seen in PGRN deficient backgrounds may represent a somewhat large scale perturbation of lysosome associated transcription. Furthermore, this may indicate that PGRN, itself a target of TFEB, acts in a negative feedback loop to suppress TFEB transcriptional events. The nature of this interaction still remains elusive and further research should investigate the signaling pathways and mechanistic aspects of PGRN and TFEB function and why certain subsets of lysosomal genes appear to be differentially affected.

REFERENCES

1. Brady, O. A., Zheng, Y., Murphy, K., Huang, M., and Hu, F. (2013) The frontotemporal lobar degeneration risk factor, TMEM106B, regulates lysosomal morphology and function. *Hum Mol Genet* 22, 685-695
2. Chen-Plotkin, A. S., Unger, T. L., Gallagher, M. D., Bill, E., Kwong, L. K., Volpicelli-Daley, L., Busch, J. I., Akle, S., Grossman, M., Van Deerlin, V., Trojanowski, J. Q., and Lee, V. M. (2012) TMEM106B, the risk gene for frontotemporal dementia, is regulated by the microRNA-132/212 cluster and affects progranulin pathways. *J Neurosci* 32, 11213-11227
3. Luzio, J. P., Pryor, P. R., and Bright, N. A. (2007) Lysosomes: fusion and function. *Nat Rev Mol Cell Biol* 8, 622-632
4. Chen, Y., and Yu, L. (2013) Autophagic lysosome reformation. *Exp Cell Res* 319, 142-146
5. Rong, Y., Liu, M., Ma, L., Du, W., Zhang, H., Tian, Y., Cao, Z., Li, Y., Ren, H., Zhang, C., Li, L., Chen, S., Xi, J., and Yu, L. (2012) Clathrin and phosphatidylinositol-4,5-bisphosphate regulate autophagic lysosome reformation. *Nat Cell Biol* 14, 924-934
6. Wraith, J. E., Baumgartner, M. R., Bembi, B., Covanis, A., Levade, T., Mengel, E., Pineda, M., Sedel, F., Topcu, M., Vanier, M. T., Widner, H., Wijburg, F. A., and Patterson, M. C. (2009) Recommendations on the diagnosis and management of Niemann-Pick disease type C. *Mol Genet Metab* 98, 152-165
7. Pearse, B. R., and Hebert, D. N. (2010) Lectin chaperones help direct the maturation of glycoproteins in the endoplasmic reticulum. *Biochim Biophys Acta* 1803, 684-693
8. Lang, C. M., Fellerer, K., Schwenk, B. M., Kuhn, P. H., Kremmer, E., Edbauer, D., Capell, A., and Haass, C. (2012) Membrane orientation and subcellular localization of transmembrane protein 106B (TMEM106B), a major risk factor for frontotemporal lobar degeneration. *J Biol Chem* 287, 19355-19365
9. Bonifacino, J. S., and Traub, L. M. (2003) Signals for sorting of transmembrane proteins to endosomes and lysosomes. *Annu Rev Biochem* 72, 395-447
10. Behnke, J., Eskelinen, E. L., Saftig, P., and Schroder, B. (2011) Two dileucine motifs mediate late endosomal/lysosomal targeting of transmembrane protein 192 (TMEM192) and a C-terminal cysteine residue is responsible for disulfide bond formation in TMEM192 homodimers. *Biochem J* 434, 219-231
11. Woolf, P. J., and Linderman, J. J. (2003) Self organization of membrane proteins via dimerization. *Biophys Chem* 104, 217-227
12. MacGurn, J. A., Hsu, P. C., and Emr, S. D. (2012) Ubiquitin and membrane protein turnover: from cradle to grave. *Annu Rev Biochem* 81, 231-259
13. Parks, G. D., and Lamb, R. A. (1991) Topology of eukaryotic type II membrane proteins: importance of N-terminal positively charged residues flanking the hydrophobic domain. *Cell* 64, 777-787

14. Kim, W., Bennett, E. J., Huttlin, E. L., Guo, A., Li, J., Possemato, A., Sowa, M. E., Rad, R., Rush, J., Comb, M. J., Harper, J. W., and Gygi, S. P. (2011) Systematic and quantitative assessment of the ubiquitin-modified proteome. *Mol Cell* 44, 325-340
15. Lee, K. A., Hammerle, L. P., Andrews, P. S., Stokes, M. P., Mustelin, T., Silva, J. C., Black, R. A., and Doedens, J. R. (2011) Ubiquitin ligase substrate identification through quantitative proteomics at both the protein and peptide levels. *J Biol Chem* 286, 41530-41538
16. Udeshi, N. D., Mani, D. R., Eisenhaure, T., Mertins, P., Jaffe, J. D., Clauser, K. R., Hacohen, N., and Carr, S. A. (2012) Methods for quantification of in vivo changes in protein ubiquitination following proteasome and deubiquitinase inhibition. *Mol Cell Proteomics* 11, 148-159
17. Wagner, S. A., Beli, P., Weinert, B. T., Nielsen, M. L., Cox, J., Mann, M., and Choudhary, C. (2011) A proteome-wide, quantitative survey of in vivo ubiquitylation sites reveals widespread regulatory roles. *Mol Cell Proteomics* 10, M111 013284
18. Westermarck, J., Ivaska, J., and Corthals, G. L. (2013) Identification of protein interactions involved in cellular signaling. *Mol Cell Proteomics* 12, 1752-1763
19. Kleizen, B., and Braakman, I. (2004) Protein folding and quality control in the endoplasmic reticulum. *Curr Opin Cell Biol* 16, 343-349
20. Wyatt, A. R., Yerbury, J. J., Berghofer, P., Greguric, I., Katsifis, A., Dobson, C. M., and Wilson, M. R. (2011) Clusterin facilitates in vivo clearance of extracellular misfolded proteins. *Cell Mol Life Sci* 68, 3919-3931
21. Corneveaux, J. J., Myers, A. J., Allen, A. N., Pruzin, J. J., Ramirez, M., Engel, A., Nalls, M. A., Chen, K., Lee, W., Chewning, K., Villa, S. E., Meechoovet, H. B., Gerber, J. D., Frost, D., Benson, H. L., O'Reilly, S., Chibnik, L. B., Shulman, J. M., Singleton, A. B., Craig, D. W., Van Keuren-Jensen, K. R., Dunckley, T., Bennett, D. A., De Jager, P. L., Heward, C., Hardy, J., Reiman, E. M., and Huentelman, M. J. (2010) Association of CR1, CLU and PICALM with Alzheimer's disease in a cohort of clinically characterized and neuropathologically verified individuals. *Hum Mol Genet* 19, 3295-3301
22. Kok, E. H., Luoto, T., Haikonen, S., Goebeler, S., Haapasalo, H., and Karhunen, P. J. (2011) CLU, CR1 and PICALM genes associate with Alzheimer's-related senile plaques. *Alzheimers Res Ther* 3, 12
23. Lambert, J. C., Heath, S., Even, G., Campion, D., Sleegers, K., Hiltunen, M., Combarros, O., Zelenika, D., Bullido, M. J., Tavernier, B., Letenneur, L., Bettens, K., Berr, C., Pasquier, F., Fievet, N., Barberger-Gateau, P., Engelborghs, S., De Deyn, P., Mateo, I., Franck, A., Helisalmi, S., Porcellini, E., Hanon, O., de Pancorbo, M. M., Lendon, C., Dufouil, C., Jaillard, C., Leveillard, T., Alvarez, V., Bosco, P., Mancuso, M., Panza, F., Nacmias, B., Bossu, P., Piccardi, P., Annoni, G., Seripa, D., Galimberti, D., Hannequin, D., Licastro, F., Soininen, H., Ritchie, K., Blanche, H., Dartigues, J. F., Tzourio, C., Gut, I., Van Broeckhoven, C., Alperovitch, A., Lathrop, M., and Amouyel, P. (2009) Genome-wide association study identifies variants at CLU and CR1 associated with Alzheimer's disease. *Nat Genet* 41, 1094-1099

24. Cuervo, A. M., and Dice, J. F. (2000) Unique properties of lamp2a compared to other lamp2 isoforms. *J Cell Sci* 113 Pt 24, 4441-4450
25. Arai, M., Itokawa, M., Yamada, K., Toyota, T., Haga, S., Ujike, H., Sora, I., Ikeda, K., and Yoshikawa, T. (2004) Association of neural cell adhesion molecule 1 gene polymorphisms with bipolar affective disorder in Japanese individuals. *Biol Psychiatry* 55, 804-810
26. Senkov, O., Sun, M., Weinhold, B., Gerardy-Schahn, R., Schachner, M., and Dityatev, A. (2006) Polysialylated neural cell adhesion molecule is involved in induction of long-term potentiation and memory acquisition and consolidation in a fear-conditioning paradigm. *J Neurosci* 26, 10888-109898
27. Diestel, S., Schaefer, D., Cremer, H., and Schmitz, B. (2007) NCAM is ubiquitylated, endocytosed and recycled in neurons. *J Cell Sci* 120, 4035-4049
28. Tarr, D. E., and Scott, A. L. (2005) MSP domain proteins. *Trends Parasitol* 21, 224-231
29. Saito, K., Tautz, L., and Mustelin, T. (2007) The lipid-binding SEC14 domain. *Biochim Biophys Acta* 1771, 719-726
30. Nixon, R. A. (2013) The role of autophagy in neurodegenerative disease. *Nat Med* 19, 983-997
31. Tanida, I., Minematsu-Ikeguchi, N., Ueno, T., and Kominami, E. (2005) Lysosomal turnover, but not a cellular level, of endogenous LC3 is a marker for autophagy. *Autophagy* 1, 84-91
32. Brady, O. A., Meng, P., Zheng, Y., Mao, Y., and Hu, F. (2011) Regulation of TDP-43 aggregation by phosphorylation and p62/SQSTM1. *J Neurochem* 116, 248-259
33. Filonov, G. S., Piatkevich, K. D., Ting, L. M., Zhang, J., Kim, K., and Verkhusha, V. V. (2011) Bright and stable near-infrared fluorescent protein for in vivo imaging. *Nat Biotechnol* 29, 757-761
34. Finch, N., Carrasquillo, M. M., Baker, M., Rutherford, N. J., Coppola, G., Dejesus-Hernandez, M., Crook, R., Hunter, T., Ghidoni, R., Benussi, L., Crook, J., Finger, E., Hantanpaa, K. J., Karydas, A. M., Sengdy, P., Gonzalez, J., Seeley, W. W., Johnson, N., Beach, T. G., Mesulam, M., Forloni, G., Kertesz, A., Knopman, D. S., Uitti, R., White, C. L., 3rd, Caselli, R., Lippa, C., Bigio, E. H., Wszolek, Z. K., Binetti, G., Mackenzie, I. R., Miller, B. L., Boeve, B. F., Younkin, S. G., Dickson, D. W., Petersen, R. C., Graff-Radford, N. R., Geschwind, D. H., and Rademakers, R. (2011) TMEM106B regulates progranulin levels and the penetrance of FTLD in GRN mutation carriers. *Neurology* 76, 467-474
35. Van Deerlin, V. M., Sleiman, P. M., Martinez-Lage, M., Chen-Plotkin, A., Wang, L. S., Graff-Radford, N. R., Dickson, D. W., Rademakers, R., Boeve, B. F., Grossman, M., Arnold, S. E., Mann, D. M., Pickering-Brown, S. M., Seelaar, H., Heutink, P., van Swieten, J. C., Murrell, J. R., Ghetti, B., Spina, S., Grafman, J., Hodges, J., Spillantini, M. G., Gilman, S., Lieberman, A. P., Kaye, J. A., Woltjer, R. L., Bigio, E. H., Mesulam, M., Al-Sarraj, S., Troakes, C., Rosenberg, R. N., White, C. L., 3rd, Ferrer, I., Llado, A., Neumann, M., Kretzschmar, H. A., Hulette, C. M., Welsh-Bohmer, K. A., Miller, B. L.,

Alzualde, A., Lopez de Munain, A., McKee, A. C., Gearing, M., Levey, A. I., Lah, J. J., Hardy, J., Rohrer, J. D., Lashley, T., Mackenzie, I. R., Feldman, H. H., Hamilton, R. L., Dekosky, S. T., van der Zee, J., Kumar-Singh, S., Van Broeckhoven, C., Mayeux, R., Vonsattel, J. P., Troncoso, J. C., Kril, J. J., Kwok, J. B., Halliday, G. M., Bird, T. D., Ince, P. G., Shaw, P. J., Cairns, N. J., Morris, J. C., McLean, C. A., DeCarli, C., Ellis, W. G., Freeman, S. H., Frosch, M. P., Growdon, J. H., Perl, D. P., Sano, M., Bennett, D. A., Schneider, J. A., Beach, T. G., Reiman, E. M., Woodruff, B. K., Cummings, J., Vinters, H. V., Miller, C. A., Chui, H. C., Alafuzoff, I., Hartikainen, P., Seilhean, D., Galasko, D., Masliah, E., Cotman, C. W., Tunon, M. T., Martinez, M. C., Munoz, D. G., Carroll, S. L., Marson, D., Riederer, P. F., Bogdanovic, N., Schellenberg, G. D., Hakonarson, H., Trojanowski, J. Q., and Lee, V. M. (2010) Common variants at 7p21 are associated with frontotemporal lobar degeneration with TDP-43 inclusions. *Nat Genet* 42, 234-239

36. van der Zee, J., Van Langenhove, T., Kleinberger, G., Sleegers, K., Engelborghs, S., Vandenberghe, R., Santens, P., Van den Broeck, M., Joris, G., Brys, J., Mattheijssens, M., Peeters, K., Cras, P., De Deyn, P. P., Cruts, M., and Van Broeckhoven, C. (2011) TMEM106B is associated with frontotemporal lobar degeneration in a clinically diagnosed patient cohort. *Brain* 134, 808-815
37. Yin, F., Banerjee, R., Thomas, B., Zhou, P., Qian, L., Jia, T., Ma, X., Ma, Y., Iadecola, C., Beal, M. F., Nathan, C., and Ding, A. (2010) Exaggerated inflammation, impaired host defense, and neuropathology in progranulin-deficient mice. *J Exp Med* 207, 117-128
38. Martens, L. H., Zhang, J., Barmada, S. J., Zhou, P., Kamiya, S., Sun, B., Min, S. W., Gan, L., Finkbeiner, S., Huang, E. J., and Farese, R. V., Jr. (2012) Progranulin deficiency promotes neuroinflammation and neuron loss following toxin-induced injury. *J Clin Invest* 122, 3955-3959
39. Ahmed, Z., Sheng, H., Xu, Y. F., Lin, W. L., Innes, A. E., Gass, J., Yu, X., Wuertzer, C. A., Hou, H., Chiba, S., Yamanouchi, K., Leissring, M., Petrucelli, L., Nishihara, M., Hutton, M. L., McGowan, E., Dickson, D. W., and Lewis, J. (2010) Accelerated lipofuscinosis and ubiquitination in granulin knockout mice suggest a role for progranulin in successful aging. *Am J Pathol* 177, 311-324
40. Filiano, A. J., Martens, L. H., Young, A. H., Warmus, B. A., Zhou, P., Diaz-Ramirez, G., Jiao, J., Zhang, Z., Huang, E. J., Gao, F. B., Farese, R. V., Jr., and Roberson, E. D. (2013) Dissociation of frontotemporal dementia-related deficits and neuroinflammation in progranulin haploinsufficient mice. *J Neurosci* 33, 5352-5361
41. Ghoshal, N., Dearborn, J. T., Wozniak, D. F., and Cairns, N. J. (2012) Core features of frontotemporal dementia recapitulated in progranulin knockout mice. *Neurobiol Dis* 45, 395-408
42. Sardiello, M., Palmieri, M., di Ronza, A., Medina, D. L., Valenza, M., Gennarino, V. A., Di Malta, C., Donaudy, F., Embrione, V., Polishchuk, R. S.,

Banfi, S., Parenti, G., Cattaneo, E., and Ballabio, A. (2009) A gene network regulating lysosomal biogenesis and function. *Science* 325, 473-477

43. Belcastro, V., Siciliano, V., Gregoretti, F., Mithbaokar, P., Dharmalingam, G., Berlingieri, S., Iorio, F., Oliva, G., Polishchuck, R., Brunetti-Pierri, N., and di Bernardo, D. (2011) Transcriptional gene network inference from a massive dataset elucidates transcriptome organization and gene function. *Nucleic Acids Res* 39, 8677-8688
44. Tanaka, Y., Matsuwaki, T., Yamanouchi, K., and Nishihara, M. (2013) Increased lysosomal biogenesis in activated microglia and exacerbated neuronal damage after traumatic brain injury in progranulin-deficient mice. *Neuroscience* 250, 8-19